MATHEMATICAL MODELING AND EXPERIMENTAL STUDY OF AIR GAP MEMBRANE DISTILLATION FOR SEPARATION OF HCl/WATER AZEOTROPE

Ph.D. Thesis

Sarita Kalla

ID No. 2015RCH9022

DEPARTMENT OF CHEMICAL ENGINEERING

MALAVIYA NATIONAL INSTITUTE OF TECHNOLOGY JAIPUR

May, 2019

MATHEMATICAL MODELING AND EXPERIMENTAL STUDY OF AIR GAP MEMBRANE DISTILLATION FOR SEPARATION OF HCl/WATER AZEOTROPE

Submitted in

fulfillment of the requirements for the degree of

Doctor of Philosophy

by

Sarita Kalla
ID: 2015RCH9022

Under the Supervision of

Dr. Sushant Upadhyaya

Prof. Kailash Singh

DEPARTMENT OF CHEMICAL ENGINEERING

MALAVIYA NATIONAL INSTITUTE OF TECHNOLOGY JAIPUR

May, 2019

DECLARATION

I, **Sarita Kalla**, declare that this thesis titled, "**Mathematical Modeling and Experimental Study of Air Gap Membrane Distillation for Separation of HCl/Water Azeotrope**" and the work presented in it, are my own. I confirm that:

- This work was done wholly or mainly while in candidature for a research degree at this university.
- Where any part of this thesis has previously been submitted for a degree or any other qualification at this university or any other institution, this has been clearly stated.
- Where I have consulted the published work of others, this is always clearly attributed.
- Where I have quoted from the work of others, the source is always given. With the exception of such quotations, this thesis is entirely my own work.
- I have acknowledged all main sources of help.
- Where the thesis is based on work done by myself, jointly with others, I have made clear exactly what was done by others and what I have contributed myself.

Date:

Sarita Kalla

(2015RCH9022)

CERTIFICATE

This is to certify that the thesis entitled **"Mathematical Modeling and Experimental Study of Air Gap Membrane Distillation for Separation of HCl/Water Azeotrope"** being submitted by **Sarita Kalla (2015RCH9022)** is a bonafide research work carried out under my supervision and guidance in fulfillment of the requirement for the award of the degree of **Doctor of Philosophy** in the Department of Chemical Engineering, Malaviya National Institute of Technology, Jaipur, India. The matter embodied in this thesis is original and has not been submitted to any other University or Institute for the award of any other degree.

Place: Jaipur
Date:

Dr. Kailash Singh
Professor
Joint-Supervisor
Dept. of Chemical Engineering
MNIT Jaipur

Dr. Sushant Upadhyaya
Associate Professor
Supervisor
Dept. of Chemical Engineering
MNIT Jaipur

ACKNOWLEDGEMENT

I would like to thank everybody who has helped me directly or indirectly during this research work. First and foremost, I would like to express my deep gratitude to my supervisor, **Dr. Sushant Upadhyaya**, Associate Professor, Department of Chemical Engineering, for his invaluable support, constant motivation and confidence that he has shown in me. His contribution to this thesis goes well beyond his role as an academic supervisor and includes constant support on a personal level without which this journey might not have been completed. I am truly amazed by the liberty that he gave to me to just fearlessly walk-in his room any time during working hours. His cooperation and valuable knowledge helped me in understanding the phenomena during thesis work.

Next, I would like to express my sincere gratitude to my joint-supervisor, **Prof. Kailash Singh**, Head, Department of Chemical Engineering, for invaluable support, constant motivation, and persistent follow-up always kept me on my toes that indeed helped me in producing current work. Their constant encouragement and valuable suggestion for my improvement have been of great help in preparing this report.

I sincerely express my thanks to the members of Doctoral Research Committee (DRC) **Prof. S.P. Chaurasia**, Department of Chemical Engineering and **Dr. Rajeev Dohare**, Department of Chemical Engineering for their valuable suggestions and guidance.

I pay thanks to **Mr. Ramesh Sharma**, Technician, Chemical Engineering Department, MNIT Jaipur for his efforts in the installation and fabrication of the experimental set-up in the laboratory round the clock. In addition, I would also like to thank **Mr. Rakesh Baghel**, Research Scholar, Department of Chemical Engineering, MNIT, for their help and encouragement during my research work.

Although obvious but still I would like to acknowledge the ever ending support from my family during every stage of my education. Specially, my husband, **Dr. Anshuman Kalla** who endures me during all ups and down. Last but the most important, I do realize the grace of "**Gururaya**" almighty God in accomplishing this task. It is he who gives me strength to work and shows me the way to proceed.

Sarita Kalla

(2015RCH9022)

ABSTRACT

In the present work, experimental and mathematical modeling has been carried out for the separation of HCl/Water azeotrope using air gap membrane distillation. The main purpose of this study is to eliminate the azeotropic point in both retentate and permeate and find out the operating conditions at which it will achieve. Consequently, a mathematical model of AGMD for HCl-water mixture at azeotropic feed composition has been developed and solved in MATLAB to determine trans-membrane flux and the effect of several operating parameters. Two-Dimensional (2-D) numerical simulation has also been performed to determine the temperature profile at the membrane surface and inside the AGMD module by using COMSOL multiphysics simulation software. The trans-membrane flux has also been calculated by using the membrane surface temperature estimated by CFD simulation and compared it with the value obtained by MATLAB programming. The effects of the operating parameters on permeate flux and both retentate and permeate composition were also studied.

The HCl selectivity in permeate was obtained lower than 1, which indicates that permeate flux is leveraged with water and higher HCl concentration in retentate was achieved as compared to permeate. The permeate flux decreased from 36 kg/m^2·h to 17 kg/m^2·h upon increasing the air gap from 3 mm to 11 mm at 50 ^{o}C feed temperature. The permeate flux increased from 4 kg/m^2·h to 28.5 kg/m^2·h upon increasing the feed temperature from 30 ^{o}C to 50 ^{o}C at 5 mm air gap. With azeotropic feed, the maximum concentration of HCl in retentate was achieved to 30.8 mass% HCl, i.e., hyperazeotropic solution and maximum concentration of HCl in permeate was found to be 15.29 mass% HCl, i.e., hypoazeotropic solution. Taguchi's design of experiment is applied to determine the optimum conditions for higher permeate flux and to find out which parameter is more statistical significant. The best combination for the highest permeate flux was found as bulk feed temperature 50 ^{o}C, air gap width 3 mm, feed flow rate 10 L/min and cooling water temperature 5 ^{o}C by Taguchi method. It was also observed that the separation of HCl/Water mixture is independent of the cooling water flow rate.

The effect of operating time on permeate flux and selectivity has been analysed by continuously running the AGMD setup for 50 h. There was no reduction in permeate flux and selectivity was found for the continuous run of 50 h at 45 ^{o}C bulk feed input

temperature, 15 ^{o}C cooling water temperature 1 L/min feed flow rate, 1 L/min cooling water flow rate and 3 mm air gap thickness at azeotropic feed concentration. The permeate flux at above mentioned operating conditions was observed as 25.2 kg/m^2·h, and it remained nearly constant for 50 h of operation due to the volatile nature of feed components which causes no deposition on the membrane surface. No membrane wetting was observed due to the hydrophobic nature of PTFE membrane. FESEM (Field Emission Scanning Electron Microscopy) and AFM analysis also confirms the no deposition on membrane surface.

Heat and mass transfer correlations were developed by varying the feed flow rate from 0.5 to 2.5 L/min and feed temperature from 30 to 50 ^{o}C at azeotropic feed concentration. The heat transfer correlation was found as $Nu = 4.67\, Re^{0.75} Pr^{0.33}$ and mass transfer correlation obtained as $Sh = 10.13\, Re^{0.62} Sc^{0.33}$.

The experimental recovery was estimated at feed flow rate 1 L/min, cooling water temperature 15 ^{o}C, cooling water flow rate 1 L/min and air gap width 5 mm and was observed to be 42% at 45 ^{o}C temperature by running the AGMD setup for 80 h. The effects of different process parameters on permeate flux, selectivity, and azeotropic breaking point has been compared for argon and air as inert gases and found that argon gas gives better separation regarding selectivity.

The artificial neural network (ANN) model has also been developed, using 5 input and 1 output data, to compare the effect of operating parameters with mathematical model and experimental data and found that ANN model best fitted with the experimental data. The AGMD process compares with the extractive distillation (ED) to analyse the unit product cost and energy consumption and found production cost by AGMD process lower than ED process.

TABLE OF CONTENTS

Declaration i

Certificate ii

Acknowledgement iii

Abstract iv

Table of Contents vi

List of Figures xi

List of Tables xv

List of Notations xvii

List of Publications xix

CHAPTER 1 INTRODUCTION 1

1.1 Membrane Separation Processes 1

1.2 Membrane Distillation 2

1.3 Different Membrane Distillation Configurations 3

1.3.1 Direct Contact Membrane Distillation (DCMD) 3

1.3.2 Vacuum Membrane Distillation (VMD) 5

1.3.3 Sweeping Gas Membrane Distillation (SGMD) 6

1.3.4 Air Gap Membrane Distillation (AGMD) 7

1.4 Principles and Applications of AGMD 8

1.5 Azeotrope 11

1.6 Azeotropic Separation by Conventional and Membrane Technology 12

1.6.1 Azeotropic Distillation 12

1.6.2 Extractive Distillation 12

1.6.3 Pervaporation 13

1.6.4 Stumbling Blocks of Distillation and Membrane Separation Methods 13

1.7 HCl-Water Azeotrope 13

1.7.1 Source of HCl-Water Azeotrope 14

1.8 Research Gaps and Objectives 15
1.9 Thesis Organization 16
CHAPTER 2 REVIEW OF LITERATURE 18
2.1 Membranes Used in AGMD 18
2.1.1 Commercial Available Membranes 18
2.1.2 Fabricated and Modified Membranes 21
2.2 AGMD Membrane Modules 21
2.2.1 Plate and Frame Module 21
2.2.2 Tubular Membrane Module 22
2.2.3 Hollow Fiber Membrane Module 22
2.2.4 Spiral Wound Membrane Module 22
2.3 Transport Mechanism of AGMD 23
2.3.1 Heat Transfer 23
2.3.2 Mass Transfer 25
2.4 Process and Membrane Parameters affecting AGMD Flux 26
2.4.1 Feed Temperature 27
2.4.2 Feed Concentration 29
2.4.3 Air Gap Thickness 29
2.4.4 Feed Flow Rate 32
2.4.5 Cooling Water Temperature 32
2.4.6 Cooling Water Flow Rate 32
2.4.7 Non-Condensable Inert Gases 34
2.4.8 Membrane Thickness 34
2.4.9 Membrane Thermal Conductivity 35
2.4.10 Membrane Porosity 35
2.4.11 Membrane Pore Size 35
2.5 Membrane Fouling and Wetting 38
2.6 Energy and Economic Analysis of AGMD 39

2.7 Advancement in AGMD Process 41
2.7.1 Heat integration and Renewable/Waste Energy Driven AGMD process 44
2.8 Artificial Neural Network (ANN) 45
CHAPTER 3 THEORETICAL CONSIDERATIONS 49
3.1 Mathematical Modeling 49
3.2 COMSOL Modeling for Interfacial Membrane Temperature Estimation 57
3.2.1 Model Equations 58
3.3 Model for Recovery Calculation 59
3.4 ANN Modeling 61
CHAPTER 4 EXPERIMENTAL 64
4.1 Materials Used For Experiments 64
4.1.1 Distilled Water 64
4.1.2 Hydrochloric Acid 64
4.1.3 Inert Gas (Argon) 65
4.1.4 Membrane 66
4.1.5 Instruments and Sensors 66
4.2 Experimental Setup 67
4.3 Experimental Procedure 70
4.4 Testing Conditions and Evaluation Parameters 71
4.4.1 Testing Conditions 71
4.4.2 Evaluation Parameters 71
4.5 Feed and Product Concentration Analysis 72
4.6 Membrane Characterization Methods 73
4.6.1 Field Emission Scanning Electronic Microscopy (FE-SEM) 73
4.6.2 Atomic Force Microscopy (AFM) 73
CHAPTER 5 RESULTS AND DISCUSSION 74
5.1 Taguchi's Optimization 74
5.2 Membrane Interfacial Temperature Estimation using COMSOL Multiphysics© 80

5.2.1 Comparison of Modeling and Experimental Results 82
5.3 Effects of Operating Variables on Total permeate Flux, HCl Selectivity and Azeotrope Breaking Point 83
5.3.1 Effect of Feed Bulk Inlet Temperature 83
5.3.2 Effect of Feed Flow Rate 87
5.3.3 Effect of Air Gap Thickness 89
5.3.4 Effect of Cooling Water Temperature 92
5.3.5 Effect of Cooling Water Flow Rate 94
5.4 Effects of Operating Time on Total permeate Flux and HCl Selectivity 96
5.5 Membrane Morphology Study Before and After Use 97
5.5.1 SEM and AFM Analysis 97
5.5.2 Pore Size Distribution 100
5.6 Recovery Calculation 102
5.7 Heat Transfer Correlation Development 104
5.8 Mass Transfer Correlation Development 106
5.9 Effect of Inert Gas (Argon) Analysis 108
5.9.1 Effect of argon gas on total permeate flux, HCl selectivity and azeotrope breaking point at different feed bulk inlet temperature 109
5.9.2 Effect of argon gas on total permeate flux, HCl selectivity and azeotrope breaking point at different feed flow rate 112
5.9.3 Effect of argon gas on total permeate flux, HCl selectivity and azeotrope breaking point at different air gap thickness 114
5.9.4 Effect of argon gas on total permeate flux, HCl selectivity and azeotrope breaking point at different cooling water temperature 117
5.10 Flux Calculation by ANN Model 119
CHAPTER 6 ECONOMIC EVALUATION 127
6.1 Cost Model Development for AGMD 127
6.1.1 Capital Cost 127
6.1.2 Annual Operating Cost 128

6.1.3 Total Annual Cost 130
6.1.4 Unit Product Cost 131
6.2 Cost Model Development for Extractive Distillation 131
6.2.1 Heat Exchanger Cost Estimation 134
6.2.2 Column Shell Cost 134
6.2.3 Column Tray Cost 134
6.2.4 Operating Cost 135
6.2.5 Unit Product Cost 135
6.3 Results and Discussion 135
CHAPTER 7 CONCLUSIONS AND FUTURE WORK 137
7.1 Conclusions 137
7.2 Contribution to Knowledge 139
7.3 Scope for Future Work 139
References 140
Appendices 160
Appendix A 160
Appendix B 161

LIST OF FIGURES

Figure 1.1 : Schematic Representation of Direct Contact Membrane Distillation (DCMD) Configuration 4
Figure 1.2 : Schematic Representation of Vacuum Membrane Distillation (VMD) 5
Figure 1.3 : Schematic Representation of Sweeping Gas Membrane Distillation (SGMD).... 7
Figure 1.4 : Schematic Representation of Air Gap Membrane Distillation (AGMD) 8
Figure 1.5 : Schematic View of Mass Transfer Steps in AGMD 9
Figure 1.6 : HCl Vapor-Liquid Equilibrium 14
Figure 2.1 : Schematic Representation of Heat Transfer in AGMD 24
Figure 2.2 : Schematic Representation of Temperature Profile in AGMD 24
Figure 2.3 : Schematic Representation of Different Resistance in AGMD process 25
Figure 2.4 : Schematic Representation of Concentration Profile in AGMD 26
Figure 2.5: Artificial Neuron Design 46
Figure 2.6 : Basic Neural Network Structure (One hidden layer) 47
Figure 3.1: Schematic Representation of (a) Knudsen Diffusion (b) Molecular Diffusion, through the Membrane Pores 50
Figure 3.2 : Module Domain Used for AGMD Modeling..... 58
Figure 3.3: A Block Diagram of AGMD Setup for Recovery Calculation..... 60
Figure 3.4: Network/Data Manager GUI of NNTOOL..... 62
Figure 3.5: Generated Network GUI..... 62
Figure 3.6: ANN Architecture Used for ANN Modeling..... 63
Figure 4.1 : A Schematic Diagram of AGMD Module 68
Figure 4.2 : Fabricated AGMD Module 68
Figure 4.3 : Argon Gap Rings of Different Thicknesses with Permeate Collector and Gas Supply Connector 69
Figure 4.4 : Schematic Diagram of AGMD Experimental Setup 69
Figure 4.5 : Fabricated Setup Used for the Experimental Study. 70
Figure 5.1 : Flow Chart for Taguchi Procedure 76
Figure 5.2: Main Effect Plot for AGMD Permeate Flux 78
Figure 5.3 : AGMD Main Effect Plot for S/N Ratios 79
Figure 5.4 : Normal Probability Plot 80
Figure 5.5 : Mesh Geometry of AGMD Module 81
Figure 5.6 : Temperature Profile within AGMD Module 82

Figure 5.7 : Comparison of Simulated Results (Mathematical and COMSOL Modeling) with Experimental Flux at Various Feed Temperatures 83
Figure 5.8 : Effect of Bulk Feed Temperature on Total Permeate Flux for Different Air Gap Widths 84
Figure 5.9 : Effect of Temperature on Vapour Pressure of HCl and Water 84
Figure 5.10 : Effect of Temperature on HCl Selectivity for Different Air Gap Widths 85
Figure 5.11 : Change in Permeate and Retentate HCl Concentration for Different Air Gap Widths 86
Figure 5.12 : Effect of Bulk Feed Temperature 87
Figure 5.13 : Effect of Feed Flow Rate on Total Permeates Flux at Different Air Gap 88
Figure 5.14 : Effect of Feed Flow Rate on HCl Selectivity for Different Air Gap Widths ... 88
Figure 5.15 : Change in Permeate and Retentate HCl Concentration for Different Air Gap Widths 89
Figure 5.16 : Effect of Air Gap Width on Total Permeate Flux at Various Feed Flow Rates 90
Figure 5.17 : Effect of Air Gap Width on Selectivity at Various Feed Flow Rates 91
Figure 5.18 : Change in Permeate and Retentate HCl Concentration for Various Feed Flow Rates 91
Figure 5.19 : Effect of Cooling Water Temperature on Total Permeate Flux for Various Air Gap Widths 92
Figure 5.20 : Effect of Cooling Water Temperature on Selectivity for Various Air Gap Widths 93
Figure 5.21 : Change in Permeate and Retentate HCl Concentration for Various Air Gap Widths 93
Figure 5.22 : Effect of Cooling Water Flow Rate on Total Permeate Flux for Various Cooling Water Temperatures 95
Figure 5.23 : Effect of Cooling Water Flow Rate on HCl Selectivity for Various Cooling Water Temperatures 95
Figure 5.24 : Change in Permeate and Retentate HCl Concentration for Different Cooling Water Temperature 96
Figure 5.25 : Effect of Operating Time on Flux 97
Figure 5.26 : Effect of Operating Time on Selectivity 97
Figure 5.27 : SEM Micrograph of (a) Fresh Membrane (b) Used Membrane 98
Figure 5.28 : AFM Image of Fresh Membrane 99
Figure 5.29 : AFM Image of Used Membrane 99

Figure 5.30 : Pore Size Distribution of Fresh Membrane Surface (a) Bar Graph (b) Probability Density Curve.....101
Figure 5.31 : Pore Size Distribution of Used Membrane (a) Bar Graphs (b) Probability Density Curve 101
Figure 5.32 : Change in Concentration of HCl in Feed Tank with Time at 45 ^{o}C.....102
Figure 5.33 : Change in HCl Recovery with Time at 45 ^{o}C 103
Figure 5.34 : Theoretical Variation in Concentration in Feed Tank at Different Temperature 103
Figure 5.35 : Theoretical Variation in Recovery at Different Temperature 104
Figure 5.36 : Effect of Feed Bulk Temperature on Heat Transfer Coefficient at Different Feed Flow Rate 105
Figure 5.37 : Heat Transfer Correlation Fitting 106
Figure 5.38 : Effect of Feed Bulk Temperature on Mass Transfer Coefficient at Different Feed Flow Rate 107
Figure 5.39 : Mass Transfer Correlation Fitting 108
Figure 5.40 : Effect of Bulk Feed Temperature on Total Permeate Flux for Different Inert Gases 110
Figure 5.41 : Effect of Temperature on HCl Selectivity for Different Inert Gases 110
Figure 5.42 : Change in Permeate HCl Concentration for Different Inert Gases with Bulk Feed Temperature 111
Figure 5.43 : Change in Retentate HCl Concentration for Different Inert Gases with Bulk Feed Temperature 111
Figure 5.44 : Effect of Feed Flow Rate on Total Permeate Flux for Different Inert Gases.112
Figure 5.45 : Effect of Feed Flow Rate on HCl Selectivity for Different Inert Gases 113
Figure 5.46 : Change in Permeate HCl Concentration for Different Inert Gases with Feed Flow Rate 113
Figure 5.47 : Change in Retentate HCl Concentration for Different Inert Gases with Feed Flow Rate 114
Figure 5.48 : Effect of Air Gap Width on Total Permeate Flux for Different Inert Gases..115
Figure 5.49 : Effect of Air Gap Width on HCl Selectivity for Different Inert Gases.....115
Figure 5.50 : Change in Permeate HCl Concentration for Different Inert Gases with Air Gap Width.....116
Figure 5.51 : Change in Retentate HCl Concentration for Different Inert Gases with Air Gap Width.....116

Figure 5.52 : Effect of Cooling Water Temperature on Total Permeate Flux for Different Inert Gases 117
Figure 5.53 : Effect of Cooling Water Temperature on HCl Selectivity for Different Inert Gases 118
Figure 5.54 : Change in Permeate HCl Concentration for Different Inert Gases with Cooling Water Temperature 118
Figure 5.55 : Change in Retentate HCl Concentration for Different Inert Gases with Cooling Water Temperature 119
Figure 5.56 : Neural Network Model Training 120
Figure 5.57 : Comparison of AGMD Experimental Data and ANN Predicted One for Independently Training, Validation and Testing Subsets and for Combined Data Set (Training + Validation + Testing) 122
Figure 5.58 : Effect of Feed Input Temperature on Total Permeate Flux 125
Figure 5.59: Effect of Air Gap Width on Total Permeate Flux 126
Figure 6.1 : Redfrac Column 132

LIST OF TABLES

Table 1.1 : Different Types of Membrane Separation Processes....1
Table 1.2: Various Applications of AGMD....10
Table 1.3 : Pure Component and Azeotrope Boiling Point for HCl/Water Mixture at 1 atm 14
Table 2.1 : Some Commercial Membranes Used by Different Researcher with their Properties....19
Table 2.2 : Effect of Feed Temperature on AGMD Permeate flux....28
Table 2.3 : Effect of Feed Concentration on Permeate Flux....30
Table 2.4 : Effect of Air Gap Thickness on Permeate Flux....31
Table 2.5 : Effect of Feed Flow Rate on Permeate Flux....33
Table 2.6 : Effect of Cooling Water Temperature on Permeate Flux....33
Table 2.7 : Effect of Cooling Water Flow Rate on Permeate Flux....36
Table 2.8 : Effect of Non-Condensable Gases on Permeate Flux....36
Table 2.9 : Effect of Membrane Thickness on Permeate Flux....36
Table 2.10 : Effect of Membrane Thermal Conductivity....37
Table 2.11 : Effect of Membrane Porosity....37
Table 2.12 : Different Types of Fouling Observed in AGMD Process....39
Table 2.13 : Different Renewable Energy Resources....45
Table 3.1: Module Dimensions....57
Table 3.2 : Operational Parameters Used for the Simulation Study....57
Table 4.1: Physical and Chemical Properties of Water....64
Table 4.2 : Properties of Hydrochloric Acid....65
Table 4.3 : Physical and Chemical Properties of Argon Gas....66
Table 4.4 : Membrane Properties....66
Table 4.5 : Specifications of Different Instruments Used in the Experimental Setup....67
Table 4.6 : Operating Variables....71
Table 5.1 : L_{27} Orthogonal Array....77
Table 5.2 : Analysis of Variance for Permeate Flux (ANOVA Table)....79
Table 5.3 : Mesh Statistics....81
Table 5.4 : Comparison between Predicted and Experimental Data in terms of R^2 and MAPE for Feed Temperature 30-50 °C....86
Table 5.5 : Comparison between Predicted and Experimental Data in terms of R^2 and MAPE for Feed Flow Rate 2-6 L/min....89

Table 5.6 : R^2 and MAPE Values for Various Air Gap Widths (3-11 mm) 92
Table 5.7 : R^2 and MAPE Values for Cooling Water Temperature Variation in the Range of 5-25 °C 94
Table 5.8 : R^2 and MAPE Values for Various Cooling Water Temperatures 96
Table 5.9: ANN Specifications 120
Table 5.10 : Optimal Value of Network Weights and Biases Gained after NN training 121
Table 5.11 : Comparative Study of ANN Modeling and Mathematical Modeling 123
Table 5.12: Comparison of ANN and Mathematical Model in terms of Effect of Bulk Feed Input Temperature 125
Table 5.13 : Comparison of ANN and Mathematical Model in terms of Effect of Air Gap Width 126
Table 6.1 : Different Equipment's Investment Cost 128
Table 6.2 : Column Design Parameters 132
Table 6.3 : Simulation Operating Parameters 133
Table 6.4 : Simulation Results 133
Table 6.5: Comparison between AGMD and ED Processes 136

LIST OF NOTATIONS

Symbols

b	Air gap width (m)
b'	Total thickness for mass transfer ($\delta\tau + b$) (m)
C_p	Specific heat (J/kg·K)
d_p	Membrane pore diameter (m)
d_h	Hydraulic diameter (m)
D	Diffusion coefficient (m^2/s)
g	Gravitational acceleration (m/s^2)
h_{hot}	Heat transfer coefficient in the feed boundary layer ($W/m^2 \cdot K$)
h_{cold}	Total heat transfer coefficient from vapor liquid interface to cooling water ($W/m^2 \cdot K$)
h_d	Film condensation heat transfer coefficient ($W/m^2 \cdot K$)
h_{cf}	Coolant film heat transfer coefficient ($W/m^2 \cdot K$)
h_a	Heat transfer coefficient in the gaseous phase ($W/m^2 \cdot K$)
ΔH	Latent heat of vaporization (J/mol)
k	Thermal conductivity of cooling plate (W/m·K)
k_p	Fluid thermal conductivity at the condensate film temperature (W/m·K)
k_B	Boltzman Constant, $1.3805*10^{-23}$ (J/K)
L	Height of air gap (m)
l	Cooling plate thickness (m)
M	Molecular weight (kg/kmol)
N	Total transmembrane flux ($mol/m^2 \cdot s$)
P	Pressure (Pa)
$\lvert P_a \rvert_{ln}$	Log mean partial pressure difference of stagnant component i.e. Air (Pa)
Pr	Prandtl number (-)
R	Universal gas constant (J/mol·K)
Re	Reynolds number (-)
T	Temperature (K)
ΔT	Bulk temperature difference between the feed and permeate (K)
U_t	Overall heat transfer coefficient ($W/m^2 \cdot K$)
v	Fluid velocity (m/s)

x	Mole fraction (-)

Subscripts

a	Air
b	Bulk side
c	Cold side
mf	Feed side membrane surface
i	Index for component number
ia	Diffusivity of component i in air
$K-d$	Knudsen- diffusion
$M-d$	Molecular- diffusion
pg	Cooling plate side

Greek Letters

α	Selectivity (-)
ε	Membrane porosity (-)
τ	Membrane tortuosity (-)
θ	Heat transfer rate factor (-)
ρ_p	Fluid density at the condensate film temperature (kg/m^3)
ρ	Fluid density evaluated at the bulk temperature (kg/m^3)
μ_p	Dynamic viscosity at the condensate film temperature (N·s/m^2)
μ	Fluid viscosity evaluated at the bulk temperature (N·s/m^2)
μ_m	Fluid viscosity evaluated at the membrane interface temperature (N·s/m^2)
λ	Latent heat of component at the absolute temperature (J/mol)
δ	Membrane thickness (m)
β	Coefficient of thermal expansion (/^{o}C)
ν	Kinematic viscosity (m^2/s)
κ	Thermal diffusivity (m^2/s)
σ	Collision diameter (m)

LIST OF PUBLICATIONS

Paper Published in SCI/Scopus/International Journals (04)

1. **Sarita Kalla**, Sushant Upadhyaya, Kailash Singh, Rakesh Baghel, "Development of Heat and Mass Transfer Correlations and Recovery Calculation for HCl - Water Azeotropic Separation using Air Gap Membrane Distillation", *Chemical Papers*, 2019. doi: 10.1007/s11696-019-00795-w. **(**Impact Factor: 0.963)

2. **Sarita Kalla**, Sushant Upadhyaya, Kailash Singh, Rakesh Baghel, "Experimental and mathematical study of air gap membrane distillation for aqueous HCl azeotropic separation", *Journal of Chemical Technology & Biotechnology* 94, no. 1 (2019): 63-78. doi: 10.1002/jctb.5766. (Impact Factor: 2.587) ***(One of the figures along with the affiliation of the paper has been selected as the cover page of the journal)***

3. **Sarita Kalla**, Sushant Upadhyaya, Kailash Singh, "Principles and Advancements of Air Gap Membrane Distillation - A Review", *Reviews in Chemical Engineering*, 2018. doi: 10.1515/revce-2017-0112. (Impact Factor: 4.49)

4. **Sarita Kalla**, Sushant Upadhyaya, Kailash Singh, Rajeev Kumar Dohare and Madhu Agarwal, "A case study on separation of IPA-water mixture by extractive distillation using aspen plus" published in *International Journal of Advanced Technology and Engineering Exploration*, Volume 3(24), November, 2016. doi: 10.19101/IJATEE.2016.324004

Allied Publications in SCI/Scopus/International Journals (02)

1. Rakesh Baghel, Sushant Upadhyaya, S. P. Chaurasia, Kailash Singh, and **Sarita Kalla**, "Optimization of process variables by the application of response surface methodology for naphthol blue black dye removal in vacuum membrane distillation." *Journal of Cleaner Production*, Volume 199, pp. 900-915, 2018. (Impact Factor: 5.651)

2. Rakesh Baghel, **Sarita Kalla**, Sushant Upadhyaya, S.P. Chaurasia, Jitendra Kumar Singh, "Treatment of Sudan III Dye from wastewater using Vacuum Membrane Distillation" published in *International Journal of Basic Science and Applied Engineering Research*, vol.4(3), pp. 237-241, 2017.

Papers Presented/Published in International/National Conferences Proceedings (04)

1. **Sarita Kalla**, Sushant Upadhyaya, Kailash Singh, Rakesh Baghel, "Taguchi Optimization Approach for Azeotropic Mixture Separation using Air Gap Membrane Distillation" accepted for oral presentation in 71th annual session of IIChE *Chemcon'18* organised by Department of Chemical Engineering, Dr. B. R. Ambedkar National Institute of Technology Jalandhar**,** (India), December 27-30, 2018.

2. **Sarita Kalla**, Rakesh Baghel, Sushant Upadhyaya, Kailash Singh, "Effects of Operating Parameters and Development of Heat Transfer Correlation in Air Gap Membrane Distillation for Azeotropic Mixture Separation", accepted for oral presentation in *International Conference on Desalination (Inda-2018)* organised by NIT, trichy and Indian Desalination Association (InDA) at Trichy , Tamil Nadu (India), April 20-21, 2018.

3. **Sarita Kalla**, Kailash Singh, Sushant Upadhyaya , "Concentration of Hydrochloric Acid using Membrane Distillation," accepted for oral presentation in 70th annual session of IIChE *Chemcon'17* organised by Haldia Regional Center of IIChE and Department of Chemical Engineering, Haldia Institute of Technology, Haldia, West Bengal (India), December 27-30, 2017.

4. **Sarita Kalla**, Sushant Upadhyaya, Kailash Singh , "Theoretical Assessment of the separation of HCl-Water azeotrope using Air-Gap Membrane Distillation", presented in 69th annual session of IIChE *Chemcon'16* organised by Chennai Regional Center of IIChE and Department of Chemical Engineering, AC Tech., Anna University, Chennai (India), December 27-30, 2016.

Allied Papers Presented/Published in International/National Conferences Proceedings (02)

1. Rakesh Baghel, **Sarita Kalla**, Sushant Upadhyaya, S.P. Chaurasia. **"**Removal of Basic Red 9 Azo Dye by using Flat Sheet PVDF Membrane in Vacuum Membrane Distillation" accepted for oral presentation in 71th annual session of IIChE Chemcon'18 organised by Department of Chemical Engineering, Dr. B. R. Ambedkar National Institute of Technology Jalandhar**,** (India), December 27-30, 2018.

2. Rakesh Baghel, **Sarita Kalla**, Sushant Upadhyaya, S.P. Chaurasia, "Treatment of Sudan III Dye from waste water using Vacuum Membrane Distillation" presented in International conference on Recent Trends in "Chemical, Environmental, Bioprocess, Textile, Mining, Material and Metallurgical Engineering" in 2017.

Book Chapter Publication (01)

1. Sushant Upadhyaya, Kailash Singh, S.P. Chaurasia, Rakesh Baghel and **Sarita Kalla**. "Vacuum Membrane Distillation for Water Desalination" In "Membrane Processes: Pervaporation, Vapor Permeation and Membrane Distillation for Industrial Scale Separations". S.Sridhar, Siddhartha Moulik (Editors) Published by Wiley (2018) pp.399 - 430

CHAPTER 1
INTRODUCTION

1.1 **Membrane Separation Processes**

Membrane separation processes are mainly used to separate the mixture of components partially or wholly by using membrane. Membrane separation processes are classified into different types depending on the driving force applied. The various driving forces used in the membrane separation process are concentration difference, vapor pressure difference, pressure difference, temperature difference etc. Membranes are generally semipermeable in nature through which one component passes and other confines due to any of the above mentioned driving force (Mulder, 1991). Different membrane separation processes along with some applications are mentioned in the Table 1.1.

Table 1.1 : Different Types of Membrane Separation Processes

Driving Force	Types	Applications
Pressure Difference	Reverse Osmosis Nano-Filtration Ultra-Filtration Micro-Filtration	Wastewater Treatment, Food Industry, Pharmaceutical Industries, Textile Industries etc.
Concentration Difference	Gas Separation Pervaporation Dialysis Diffusion Dialysis	Purification of Flue Gases, Azeotropic Mixture Separation, In Pharmaceutical Application, In Haemodialysis, Pulp And Paper Industries, Metallurgy Industries etc.
Electrical Potential Difference	Electrodialysis Electro-osmosis	Semiconductor Industries, Desalination, Waste Water Treatment etc.
Temperature Difference	Thermo-Osmosis	In Biological System, For Water and Methanol Separation etc.
Vapour pressure Difference	Membrane Distillation	Desalination, Breaking of Azeotrope Point, Concentration of Fruit Juices, Extraction of Volatile Organic Compound, Treatment Of Textile Water etc.

1.2 **Membrane Distillation**

The membrane distillation process finds its roots in the desalination process primarily being used to fulfil the drinking water requirement. On the earth, about 97% of water reservoirs are saline since the oceans are the source and only remaining 3% is available as fresh water from the other natural sources (Shiklomanov, 1993). Consequently, the desalination techniques became popular to provide drinkable water. There are different methods for desalination like Multiple-Effect Distillation (MED) (Raach and Mitrovic, 2007; Sharaf et al., 2011; Zhao *et al.*, 2011; de la Calle *et al.*, 2015), , Reverse Osmosis (RO) (Li *et al.*, 2004; Manolakos *et al.*, 2007; Zhu *et al.*, 2015), Multi-stage Flash (MSF) (Hamed *et al.*, 2000; Alsehli et al., 2017) , Pervaporation (PV) (Komgold et al., 1996; Korin et al., 1996; Zwijnenberg et al., 2005; Xie *et al.*, 2011; Wang *et al.*, 2016; Nigiz, 2017), Forward Osmosis (FO) (McCutcheo et al., 2006; Li *et al.*, 2012; McGinnis *et al.*, 2013), Capacitive Deionization (CD) (Kim and Choi, 2010; Porada *et al.*, 2012; Jande and Kim, 2013) , Membrane Distillation (MD) (Al-Obaidani *et al.*, 2008; Winter et al., 2011; Fang *et al.*, 2012) etc. Among them membrane distillation is the most suitable for desalination as it removes almost 100% of salt, requires low energy (as it operates at low operating temperature (40 – 80 ^{o}C) and low pressure) and is able to make use of use of waste heat or low graded thermal energy like solar energy, geothermal energy (El-Bourawi *et al.*, 2006; Khayet and Matsuura, 2011), etc. Membrane distillation is a thermal process and is used for very high saline feed water of concentration 70-300 g-salt/kg-solution (Swaminathan *et al.*, 2018). For such saltier stream, conventional RO (Reverse Osmosis) process cannot be applied directly because conventional spiral wound reverse osmosis process usually operates below 70 bar pressure (Fritzmann *et al.*, 2007) however for such a high concentration salt solution, the osmotic pressure required is around 300 bar (Thiel *et al.*, 2015). For such an application, AGMD turns out to be highly energy efficient process. Although high energy is required for MD commercialization yet MD has been considered as the most suitable for desalination of sea water, brackish ground water and other waste streams. The earliest uses of MD have been credited to Bodell (Bodell, 1963) for water treatment and converting contaminated water into potable by using hydrophobic membrane. First paper based on membrane distillation was published by Findley in 1967 (Findley, 1967). This technology became popular in 80's and various researchers started working on it for different applications like pharmaceutical wastewater treatment, textile wastewater treatment, for extraction of volatile organic compounds, concentration of different organic solutions (like

H_2SO_4, HCl etc.), breaking of azeotropic mixtures, food processing, etc. (Khayet and Matsuura, 2011).

The name and associated terminology used in the membrane distillation process were first decided in the membrane distillation workshop conducted on May 5, 1987 in Rome (Smolders and Franken, 1989). The main characteristics of membrane distillation process are (Smolders and Franken, 1989; Lawson and Lloyd, 1997; Anezi *et al.*, 2013):

1. Membrane should have high hydrophobicity and porosity.
2. Only vapors can pass through the membrane.
3. No capillary condensation should happen in the pores of the membrane.
4. Membrane only acts as the barrier which implies that it does not change the vapor-liquid equilibria.
5. At least one side of the transfer medium would be in physical contact with the working fluid.
6. The driving force is the vapor pressure difference.

1.3 **Different Membrane Distillation Configurations**

Membrane distillation process is defined as the thermally driven separation process in which the membrane act as the wall and only volatiles are permitted to escape from the membrane. The membrane used must be hydrophobic in nature. Depending on the means by which the driving force (i.e. transmembrane vapor pressure difference) is maintained across the membrane and somewhat on techniques used for permeate vapor collection, the membrane distillation has been classified into four different configurations; Direct Contact Membrane Distillation (DCMD), Vacuum Membrane Distillation (VMD), Air Gap Membrane Distillation (AGMD) and Sweeping Gas Membrane Distillation (SGMD). In addition to these four configurations, other MD configurations that resemble to air gap MD by simply filling different filler in the gap are Permeate Gap Membrane Distillation (PGMD), Conductive Gap Membrane Distillation (CGMD), Material Gap Membrane Distillation (MGMD) etc.

1.3.1 Direct Contact Membrane Distillation (DCMD)

The simplest arrangement of membrane distillation is direct contact membrane distillation (DCMD) as shown in Figure 1.1. The Figure 1.1 shows schematic view of DCMD module configured with the hydrophobic membrane. The module comprises of two sections; the feed section and the permeate section. These sections are separated by the hydrophobic membrane. In the feed section, feed flows and gets vaporised at the membrane surface while

in the permeate section an aqueous solution which is comparatively at lower temperature than the feed solution passes through and enables the condensations of vapour molecules that passes through the membrane.

In DCMD configuration, the feed is kept in immediate contact with upstream side of the hydrophobic membrane. The vapor passes due to vapor pressure difference and condensate is collected in the permeate section of the membrane module. DCMD is extensively studied MD configuration as it has comparatively simple module design and has adequately high flux rate. The main disadvantage of DCMD over other configurations is that it leads to more conductive heat loss because of the membrane which works as the only separating barrier between feed solution and permeate (Lei et al., 2005). Another drawback of DCMD configuration is the difficulty faced in detection of membrane wetting or leakage due to the mixing of condensate directly into fluid in the cooling section (Lei et al., 2005). DCMD is mainly used in desalination (Lawson and Lloyd, 1996; Godino *et al.*, 1997; Burgone, A. and Vahdati M.M, 2000; Martinez-Diaz, L. and Florido-Diaz F.J., 2001; Cath et al., 2004; Gunko *et al.*, 2006; García-Fernández et al., 2017b; Khalifa *et al.*, 2017) and concentration of aqueous solutions for example apple juice, orange juice, etc. (Calabrb and Drioli, 1994; Alves and Coelhoso, 2006; Gunko *et al.*, 2006).

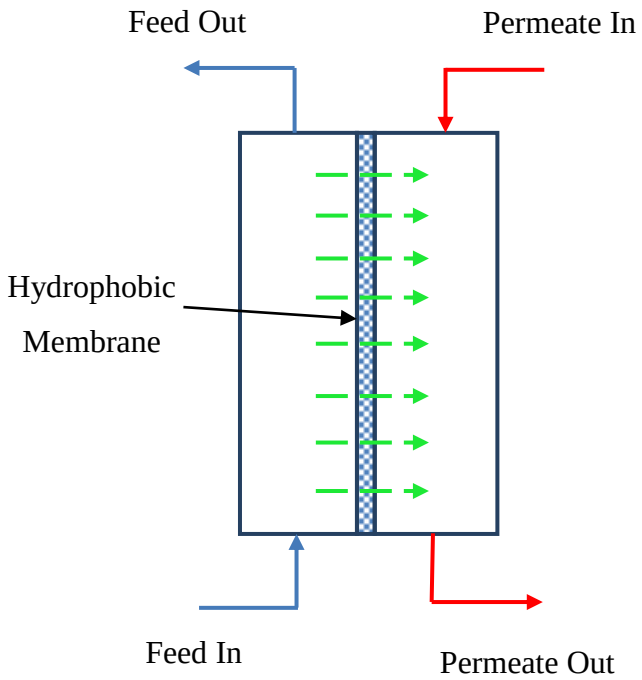

Figure 1.1 : Schematic Representation of Direct Contact Membrane Distillation (DCMD) Configuration

1.3.2 Vacuum Membrane Distillation (VMD)

The schematic representation of VMD module configured with the hydrophobic membrane and equipped with vacuum pump is illustrated in Figure 1.2. In this configuration, the vacuum pump is used to generate the vacuum and the condensation of vapours takes place outside the membrane module. The permeate pressure created by applied vacuum is generally maintained below the saturation pressure of vapours to create the driving force (El-Bourawi *et al.*, 2006). In VMD, the hydrostatic pressure across the membrane must be lower than the Liquid Entry Pressure (LEP) to prevent the entry of feed liquid into the membrane pores. This creates a liquid-vapour interface at the feed side membrane surface and bulk feed evaporates due to applied lower pressure at the permeate side and get condensed in the external condenser by passing through the membrane pores (Khayet and Matsuura, 2011). In this configuration, the heat loss is reduced due to very low heat conduction through the membrane because of applied vacuum (Lei et al., 2005). This is one of the main advantages of VMD which ultimately leads to high thermal efficiency. In VMD, mass flux is generally higher than the other MD configurations because of higher partial pressure gradient. The drawback associated with the VMD is the higher probability of wetting of membrane pore due to applied vacuum in the permeate side. VMD is mainly used for separation of volatile organic compounds from aqueous solution (Sarti et al., 1993; Banat and Simandl, 1996; Couffin et al., 1998; Urtiaga at al., 2000; Urtiaga *et al.*, 2001; Jin *et al.*, 2007) and for desalination or water purification (Upadhyaya *et al.*, 2011; Upadhyaya *et al.*, 2015; Upadhyaya *et al.*, 2016; Baghel *et al.*, 2017; Huang *et al.*, 2017).

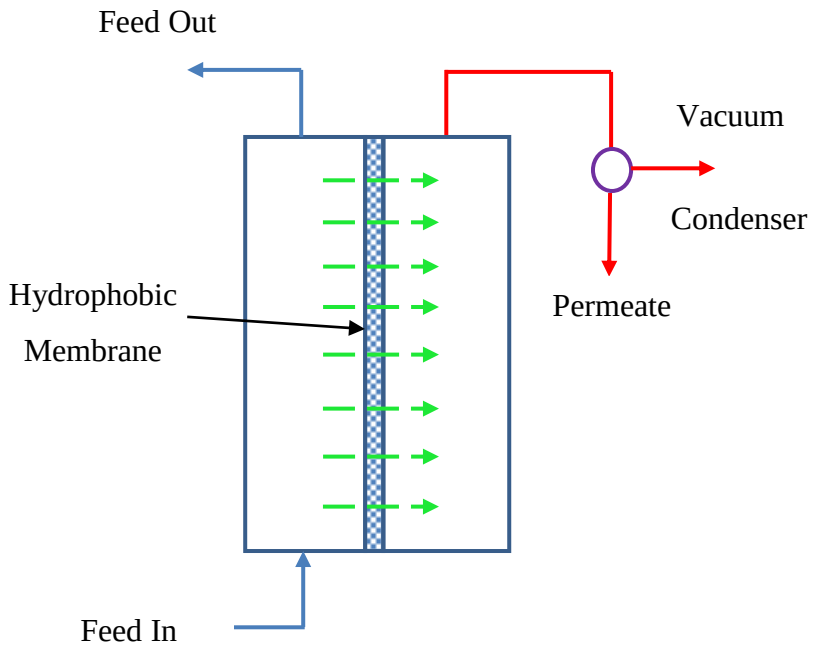

Figure 1.2 : Schematic Representation of Vacuum Membrane Distillation (VMD)

1.3.3 Sweeping Gas Membrane Distillation (SGMD)

Figure 1.3 depicts the Sweeping Gas Membrane Distillation (SGMD) module in which vapour condensation occurs outside the module like in VMD. In this configuration, a cold inert gas is used to carry the vapours, coming from the feed side, outside the module for condensation as shown in Figure 1.3. In SGMD, a large external condenser is required since the small amount of vapours diffuse into the large volume of inert gas. This ultimately increases the cost of equipment and complicates the system design (Khayet et al., 2000). SGMD is generally considers as the combination of AGMD and DCMD processes as it has low conductive heat loss property of AGMD and low mass transfer resistance property of DCMD. The gas used in SGMD moves in the cooling chamber and sweeps the membrane which results in increase in the mass transfer rate and higher permeate flux than AGMD (as AGMD uses stationary gas barrier) (El-Bourawi *et al.*, 2006). In addition SGMD exhibits higher flux and lower heat loss due to conduction when compared to the DCMD under the same operating conditions while using same membrane module (Khayet et al., 2003). The main drawback of SGMD configuration is that the heat recovery becomes complicated since an external heat exchanger or an internal system for heat recovery is required (Koschikowski et al., 2003). Other disadvantages associated with SGMD are large amount of gas flow required to achieve desired permeate and high transfer cost of the sweeping gas (Khayet et al., 2000; Lei et al., 2005). As compared to other configurations, less research work has been carried out in SGMD configuration.

SGMD is mainly used for removing volatile organic compounds from aqueous solution (Lee and Hong, 2001; García-Payo *et al.*, 2002; Rivier *et al.*, 2002; Boi et al., 2005; Ding *et al.*, 2006; Xie *et al.*, 2009). SGMD has been also successfully applied to desalination (Khayet et al., 2003; Charfi et al., 2010; Khayet and Cojocaru, 2013; Karanikola *et al.*, 2015) and is used to concentrate sucrose aqueous solution (Cojocaru and Khayet, 2011), to concentrate dilute glycerol waste water (Shirazi *et al.*, 2014), to recover volatile fruit juice aroma compounds (Bagger-Jørgensen *et al.*, 2011), etc.

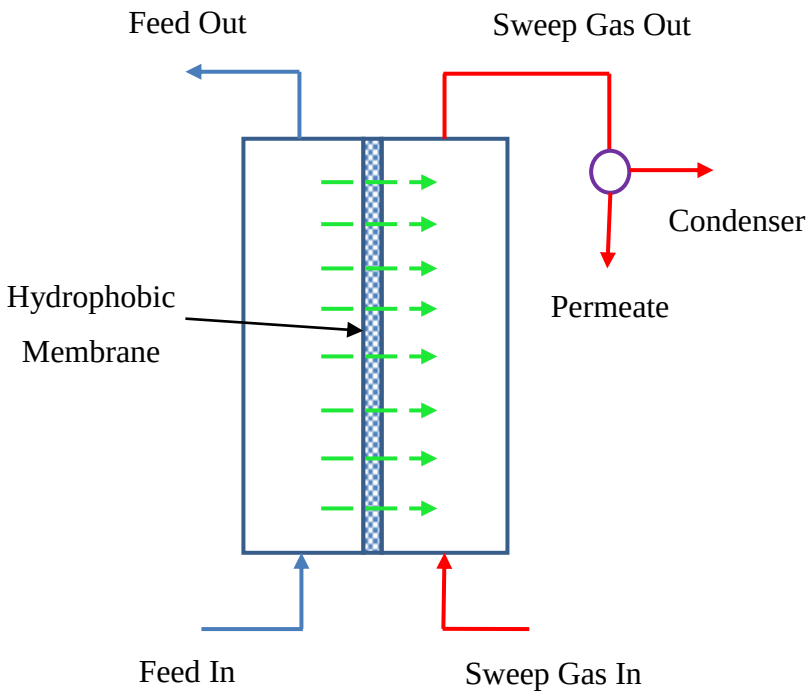

Figure 1.3 : Schematic Representation of Sweeping Gas Membrane Distillation (SGMD)

1.3.4 Air Gap Membrane Distillation (AGMD)

In Air Gap Membrane Distillation (AGMD) as shown in Figure 1.4, an air gap is maintained between the membrane and the condensing plate. Figure 1.4 shows schematic view of AGMD module configured with the hydrophobic membrane and condensing plate. The module comprises three sections: feed section, air gap or permeate section and cooling section. The coolant flows on the other side of the cooling plate i.e. cooling section. The vapours coming from the feed section diffuse in the air gap and get condensed on the cooling plate and are finally drained out. The main advantage of the AGMD is less conductive heat loss and temperature polarization due to stagnant air gap (because air has low heat conductivity) but simultaneously an additional mass transfer resistance is also developed. This additional mass transfer resistance results into lower permeate flux. The developed resistance is directly proportional to the air gap width i.e. larger is the air gap thickness, higher is the resistance and consequently the lower is the permeate flux (Alklaibi and Lior, 2005; Matheswaran and Kwon, 2007; Pangarkar et al., 2011; Khalifa, 2015). In AGMD, the condensate is directly obtained from the air gap without any physical separation (as in DCMD and SGMD) thus it is easy to detect membrane leakage or wetting. The AGMD is mainly used for desalination along with solar energy (Banat *et al.*, 2007a, 2007b; Koschikowski *et al.*, 2009; Guillén-Burrieza *et al.*, 2011; Zaragoza et al., 2014) and for

concentration of aqueous solutions (Banat and Simandl, 1999; Banat et al., 1999a; Garcia-Payo et al., 2000).

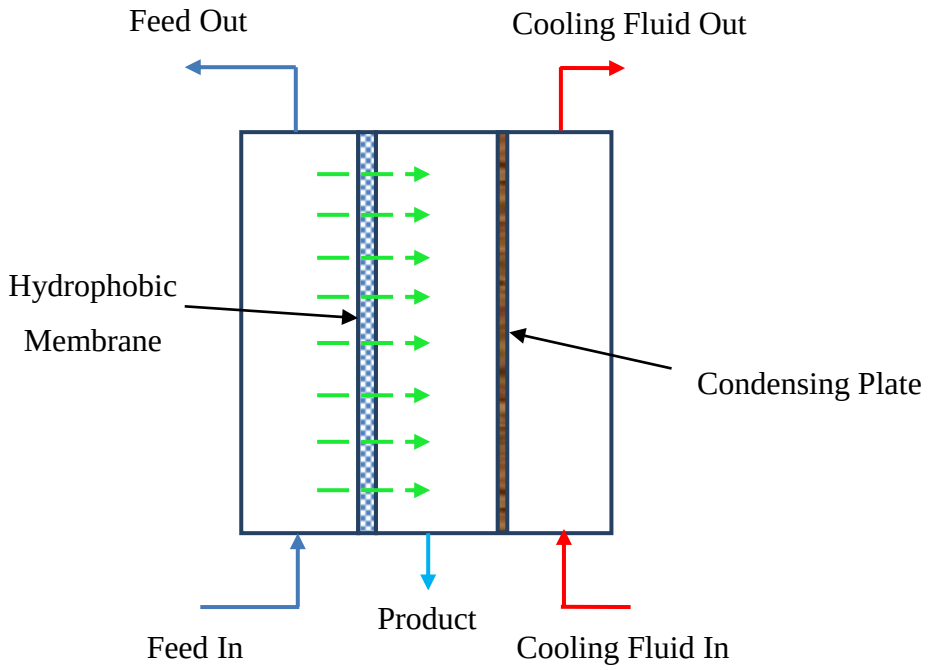

Figure 1.4 : Schematic Representation of Air Gap Membrane Distillation (AGMD)

1.4 **Principles and Applications of AGMD**

In Air Gap Membrane Distillation (AGMD), the temperature difference maintained between hot feed solution and cooling surface is the driving force for mass transfer. The vapour passes through the air gap and condenses on the cooling plate. The air gap is introduced in AGMD configuration to reduce the heat transfer resistance which is the prime cause of the low thermal efficiency of MD process. However, the presence of this air gap increases the mass transfer resistance which leads to the reduction in permeate flux. Therefore an optimized value of air gap thickness needs to be used. Since in this configuration there is no direct contact between the membrane surface and the cooling surface, therefore the AGMD process is more suitable for the separation of compounds which are not separated by DCMD configuration such as Volatile Organic Compounds (VOCs) (Khayet and Matsuura, 2011).

Mass transfer in AGMD process consists of four steps:

1. Flow of liquid/vapors from bulk towards the membrane surface.
2. Vaporization at the membrane surface.
3. Diffusion of vapours through the membrane and the air gap.
4. Condensation at the cooling plate.

The schematic view of these mass transfer steps is shown in Figure 1.5. In step 1 and step 4, the direction of arrows corresponds to the flow of species i.e. bulk fluid and cooling water. The circles in the Figure (specifically in step 2 and step 3) indicate vapour molecules. In step 2, the feed gets vaporised near the membrane surface and in step 3 these molecules get condensed at the cooling plate in order to form the liquid condensate film.

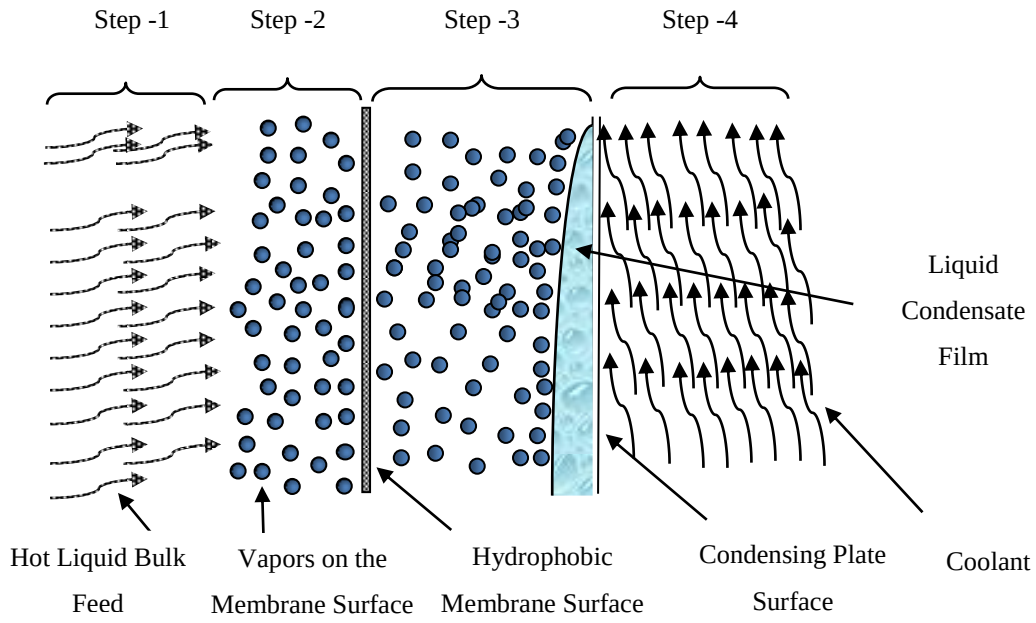

Figure 1.5 : Schematic View of Mass Transfer Steps in AGMD

AGMD has been successfully applied at laboratory scale to different applications including desalination, food processing, concentration of aqueous solution, removal of Volatile Organic compounds (VOCs), concentration of acid solution, water purification etc. Limited amount of work has also been done at pilot plant scale for applying AGMD for desalination with solar energy as source. Liu *et al.* (1998) examined the separation of pure water from five different solution namely tap water, solution of dyed (eosin Y dye), aqueous solution containing salt (NaCl solution of concentrations 0.1 wt%, 0.5 wt%, 3 wt%), acid aqueous solution (acetic acid glacial) and alkali aqueous solution (Sodium bicarbonate) using air gap membrane distillation. Alkhudhiri et al., (2012b) performed an experimental study for the separation of four different salts NaCl (Sodium Chloride), $MgCl_2$ (Magnesium Chloride), Na_2SO_4 (Sodium Sulphate), Na_2CO_3 (Sodium Carbonate) by air gap membrane distillation. Khan and Martin (2014) studied the feasibility of AGMD for arsenic infected water purification. The authors used three different feeds for the study namely medium concentration of arsenic contaminated ground water; arsenic spiked tap water of high and medium concentration. They found that when using feed water of arsenic concentration

1800 µg/l, arsenic level in the permeate flux was only 10 µg/l, which is even lower than the accepted limit by WHO. Khalifa *et al.* (2015) theoretically and experimentally investigated the purification of saline water using air gap membrane distillation. Flux was increased by 550% to 750% on increasing the temperature from 40 ^{o}C to 80 ^{o}C and on the other hand decreasing the air gap width from 7 mm to 3 mm resulted in the maximum rise of flux by 130%. The authors found AGMD to be the best for desalination as the salt rejection was 99.9%. Various authors also worked on AGMD in combination with solar energy. Guillen-Burrieza *et al.* (2014) worked on solar driven air gap membrane distillation pilot plant located at Spain for desalination. Banat *et al.* (2007a) established a small scale desalination plant at Jordan University campus at Irbid, Jordan and operated by solar energy and Photovoltaic (PV) energy and named it 'compact SMADES'. Later on, Banat *et al.* (2007b) , build up a 'large SMADES' system to produce good quality potable water installed at Marine Science Station (MSS) of Aqaba, Jordan. Bouguecha, Hamrouni and Dhahbi (2005) worked on air gap membrane distillation by using geothermal water (MD-GW) energy source. T and Martin (2014) performed an experimental analysis by using solar air gap membrane and also developed a pilot plant with Solar Domestic Hot Water (SDHW) system for producing drinking water and household hot water. In addition to desalination, other uses of (AGMD) process along with feed solution are listed in Table 1.2.

Table 1.2: Various Applications of AGMD

Applications	Feed	References
Desalination	Sea Water, Salt Solutions (NaCl, $MgCl_2$, Na_2SO_4, Na_2SO_3)	(El Amali et al., 2004; Guijt *et al.*, 2005a; Alklaibi and Lior, 2005; Gazagnes *et al.*, 2007; Feng *et al.*, 2008; Alkhudhir et al., 2012b, 2013a, Khayet and Cojocaru, 2012a, 2012b; Singh and Sirkar, 2012; Alkhudhiri et al., 2013b; Chang *et al.*, 2012; Alsaadi *et al.*, 2013; Harianto *et al.*, 2014; He *et al.*, 2014; Khalifa and Lawal, 2015; Khalifa *et al.*, 2015; Vazirnejad *et al.*, 2016; García-fernández *et al.*, 2017)

Applications	Feed	References
Food Processing	Mandarin Orange Juice, Sugar (Sucrose) Solution	(Kimura et al., 1987; Izquierdo-Gil et al., 1999)
Breaking of Azeotropic Mixture	HCl/water, Propionic acid/water, Formic acid/water	(Udriot, Araque and von Stockar, 1994; Fawzi A Banat *et al.*, 1999; Fawzi A. Banat, Abu Al-Rub, *et al.*, 1999; Fawzi A. Banat, Al-Rub, *et al.*, 1999; Kalla *et al.*, 2018)
Concentration of Aqueous Solutions	Ethanol/Water, Acetone Solution, Methanol/Water, Isopropanol/Water, Acetone-Butanol-Ethanol Solution	(Banat and Simandl, 1999; Banat et al., 1999d; Garcia-Payo et al., 2000; Chang *et al.*, 2012)
Concentration of acid solutions	Nitric Acid/Water, HCl/Water, H_2SO_4/Water	(Kurokawa *et al.*, 1990; Thiruvenkatachari *et al.*, 2006b; Liu *et al.*, 2012)
Removal of VOCs	Ethanol, Butanol, Propanone, Acetone-Butanol-Ethanol	(Banat and Simandl, 1999, 2000; Kujawska *et al.*, 2016; Woldemariam *et al.*, 2017)
Isotopes Separation from aqueous Solutions	^{18}O isotopic water	(Kim *et al.*, 2004)

1.5 **Azeotrope**

Work on azeotropic mixture separation is an important, practical and industrial important topic for research. There are a number of organic compounds that forms non-ideal solution in its aqueous form. Azeotropes are liquid mixtures which have same liquid and vapor composition when boiling (Swietoslawski, 1963) or a constant boiling mixture. There are mainly two types of azeotrope exists:

(i) Minimum Boiling Azeotrope or Positive Azeotrope

(ii) Maximum Boiling Azeotrope or Negative Azeotrope.

Minimum boiling azeotrope boils at a temperature lowers than the boiling point of its individual components. Most common example of minimum boiling azeotrope is ethanol/water mixture (95.63 mass% ethanol + 4.37 mass% water). In ethanol/water system

ethanol boils at 78.4 ^{o}C and water boils at 100 ^{o}C while the ethanol/water azeotrope boils at 78.2 ^{o}C and 101.3 kPa pressure (Seader & Henley, 2006). Similarly, maximum boiling azeotrope boils at a temperature higher than the boiling point of its individual components. Such as hydrochloric acid/water system (20.2 mass% HCl + 79.8 mass% H_2O), in this case hydrogen chloride boils at -85 ^{o}C and water boils at 100 ^{o}C but the HCl/water azeotrope boils at 108.58 ^{o}C and 760 mmHg pressure (Bonner & Wallace, 1930).

Relative volatility is the common term used to represent the degree of separation between two components. Higher the relative volatility of the mixture, more easy the separation will possible. The relative volatility of azeotropic mixture is always 1; hence the azeotrope mixture cannot be separated by ordinary distillation. The separation of different azeotropes is a vital assignment in process industries and considerable research has been carried out for azeotropic separation methods.

1.6 **Azeotropic Separation by Conventional and Membrane Technology**

The azeotropic mixture are mainly separated by two technologies i.e. distillation and membrane separation processes. In distillation process, azeotropic distillation and extractive distillation are the two main process used for the azeotrope separation by introducing third component named as entrainer. In membrane separation processes, pervaporation has been considered as most promising technology for azeotrope mixture separation. In addition to the above mention two broadly classified categories, process intensification technology that includes divided wall column, ultrasonic enhance and microwave enhance process has been also a fast developing approach (Mahdi *et al.*, 2014).

1.6.1 Azeotropic Distillation

In azeotropic distillation method, a third component, called entrainer, added in the azeotropic mixture that forms an azeotrope with one of the component of the original azeotrope mixture. Generally, in azeotropic distillation the entrainer is recovered from distillate in the distillation column (Brignole and Pereda, 2013). The entrainer which forms binary azeotrope with one of the component has been separated by different separation methods after collecting as distillate.

1.6.2 Extractive Distillation

In extractive distillation a relatively non-volatile and high boiling component, entrainer, is added to the azeotropic mixture that creates the volatility difference between the individual components of azeotropic mixture. The entrainer and the less volatile component are

collected from the bottom and high volatile or non-extracted component is collected from the top of distillation column. The main differences between the azeotropic and extractive distillation are that, in extractive distillation the entrainer does not form azeotrope with any of the original component of the azeotrope while in azeotrope distillation the entrainer forms azeotrope and in extractive distillation the entrainer fed continuously in the column at different locations while in azeotropic distillation entrainer added with the feed solution and then fed to distillation tower (Gerbaud and Rodriguez-Donis, 2014; Mahdi *et al.*, 2014).

1.6.3 Pervaporation

Pervaporation is a membrane separation process in which the liquid feed solution is allowed to pass through the dense nonporous oliophilic membrane and separation occurs due to partial vaporization. The driving force for the pervaporation is the transmembrane partial pressure difference. The liquid feed is in direct contact of the feed side of membrane and vapor permeate get condensed on the other side of membrane. The thick dense membranes used in pervaporation make mass transfer through the membrane a slow process. This membrane property is one of the limitations of pervaporation and restricted the pervaporation process to break the azeotrope mixture (Mahdi *et al.*, 2014).

1.6.4 Stumbling Blocks of Distillation and Membrane Separation Methods

- Extractive and azeotropic distillation requires very high energy.
- Limited numbers of entrainers are present so choice for entrainer's selection is limited.
- The desirable key component recovered by another separation process, which increases the overall production cost.
- Pervaporation is a slow process because of thick dense polymer membrane.
- Pervaporation is not suitable for breaking aqueous azeotrope.
- Pervaporation is yet need to be implemented at industrial scale.

1.7 **HCl-Water Azeotrope**

Aqueous solution of hydrogen chloride gas is known as hydrochloric acid. Hydrochloric acid (HCl) is an important chemical used in many industries like petroleum, chemical, food, metal, etc. (Shreve, 1956). HCl forms an azeotrope with water at 20.2 mass% HCl concentration having boiling point at 108.58 ^{o}C (H.L.Horsley, 1973). Concentration of HCl above 20.2 mass% is not possible by conventional distillation because of its azeotrope

formation as shown in Figure 1.6 (Vega and Vera, 1976). Azeotropic boiling point and composition for HCl/Water system are mentioned in Table 1.3.

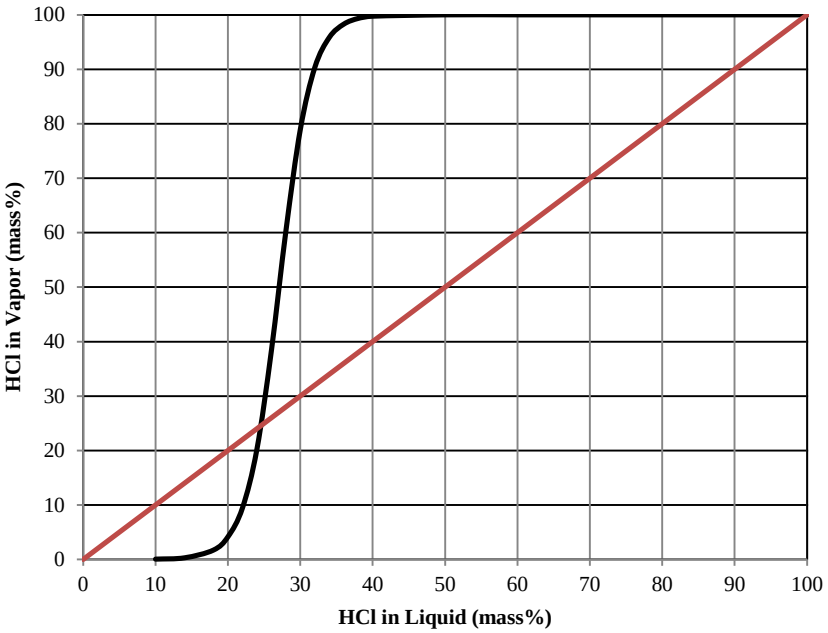

Figure 1.6 : HCl Vapor-Liquid Equilibrium

Table 1.3 : Pure Component and Azeotrope Boiling Point for HCl/Water Mixture at 1 atm

Components	Boiling Point (^{o}C)	Azeotropic Point Composition (mass%)
Hydrogen Chloride	-84	-
Water	100	-
HCl/Water Azeotrope	108.58	20.2 / 79.8

1.7.1 Source of HCl-Water Azeotrope

HCl-Water azeotrope can be taken directly from the intermediate stage of concentrating HCl from 5% to 35%. In spite of this the different sources for HCl/water azeotrope are given below –

- Spent HCl discharging from the various sources. Spent HCl (1-5 mass%) coming from different chemical industries such as rare earth processing is corrosive, harmful and polluting in nature. So instead of discharging it directly to the environment, the spent hydrochloric acid could be concentrated up to azeotropic concentration by simple distillation. (Tomaszewska et al. 2001, Tomaszewska et al. 2000).

- The HCl/Water azeotrope generated during the production of anhydrous hydrogen chloride gas (AHCl). AHCl gas is mainly used in the pharmaceutical industries and chemical industries where moisture content is not allowed.
- HCl/water azeotrope forms in the intermediate stage of Copper-Chlorine (Cu-Cl) thermochemical water splitting cycle for the production of clean hydrogen (Masin et al., 2006).

1.8 **Research Gaps and Objectives**

From the literature study, following research gap has been identified-

1. Only one experimental study has been carried out to check the feasibility of breaking the HCl-H_2O azeotropic mixture by air gap membrane distillation (Udriot et al., 1994).
2. Mathematical model for azeotropic system separation by using air gap membrane distillation to determine the permeate flux has not been developed yet as per my best knowledge.
3. The effect of different operating parameters inclusive of feed temperature, concentration of HCl in feed, feed flow rate, cooling water temperature and air gap width on the total permeate flux have not been explored yet, neither by mathematical modeling nor by experimental method.
4. Only one theoretical study has been carried out to study the effect of inert gases on breaking the azeotropic mixture by air gap membrane distillation. (Banat et al. 1999b). No experimental and theoretical studies have been carried out till now to study the effects of inert gases on breaking the HCl-Water azeotrope mixture by air gap membrane distillation.
5. Comparison of AGMD with extractive distillation in terms of cost and energy consumption has not been studied yet.

Based on the gaps in existing literature, the broad objectives of present work are-

1. To develop a mathematical model incorporating various process base parameters namely feed temperature, feed flow rate, feed concentration, cooling water temperature, air gap width, and on permeate flux in separation of HCl/Water azeotrope and validation with the experimental data.
2. To study the effects of various inert gases on the extent of separation of HCl/Water azeotrope and membrane characterization.
3. Development of heat and mass transfer correlations from experimental data.

4. Recovery calculations and its comparison with experimental data
5. Comparison of AGMD with other azeotropic separation technique (Extractive distillation) for the HCl/Water system.
6. Use of Taguchi's optimization technique to determine optimum parameters using Design of Experiment (DOE) tool in MINITAB.
7. To develop COMSOL Multiphysics model for the interfacial temperature calculations.
8. To develop ANN Model and compares the effect of operating parameters with mathematical model and experimental data using MATLAB Software.

1.9 **Thesis Organization**

The above mentioned objectives are attained by performing different experimental, theoretical and simulated work and the complete research work is organized into seven chapters. A brief outline of each chapter is given as follows –

Chapter 1 Introduction

This chapter covers the short introduction part of membrane separation processes, membrane distillation, azeotrope, different separation methods of azeotrope mixture, HCl/water azeotrope followed by the research gap exists in the current working topic and research objectives to be accomplished.

Chapter 2 Review of Literature

This chapter comprises a literature review about the state-of-the-art of air gap membrane distillation.

Chapter 3 Theoretical Considerations

The objective of the chapter 3 is to develop a mathematical and computational fluid dynamics (CFD) model for interfacial temperature calculation, recovery model and artificial neural network (ANN) model.

Chapter 4 Experimental

This Chapter comprises of all the experimental materials, AGMD setup and experimental procedure along with brief overview of membrane characterization tools.

Chapter 5 Results and Discussion

The Chapter 5 covers the all results and following discussion of all the experimental and theoretical studies carried out in chapter 3 and chapter 4.

Chapter 6 Economic Evaluation

The main aim covers in this chapter is to estimation of cost of the production of HCl of desired concentration and comparison of AGMD with the extractive distillation method regarding cost analysis.

Chapter 7 Conclusions and Future Work

This chapter summarized all the work carried out to study the breaking of azeotropic mixture in the forms of conclusions along with recommendations for future work.

At the end of chapter 7 list of reference followed by appendices have been given.

CHAPTER 2

REVIEW OF LITERATURE

2.1 **Membranes Used in AGMD**

In membrane distillation techniques, the separation is directly related to membrane characteristics. The membranes used in MD process make certain the high process efficiency and must be hydrophobic in nature. The membrane used in MD must be composed of polymers or inorganic materials and should be in the form of hollow fiber or flat sheet and capillary. In general, the characteristics of membrane required in MD should have good chemical and thermal stability, high liquid entry pressure (LEP), low thermal conductivity and low mass transfer resistance. In AGMD system the membranes used are both commercially available and fabricated (Alkhudhiri et al., 2012a). Commercial hydrophobic membranes made of PP, PTFE and PVDF were used initially for MD applications. Recently, researchers have proposed novel materials like polyethylene chlorinetrifluoroethylene (ECTFE) (Gryta, 2016), Poly(tetrafluoroethylene-co-hexafluoropropylene)(FEP) (Chen *et al.*, 2015), poly (vinylidene fluoride-co-chlorotri-fluoroethylene) (PVDF-CTFE) (Zheng *et al.*, 2016), etc. for the formation of hydrophobic membrane used in the different MD configurations.

2.1.1 Commercial Available Membranes

In AGMD, most of researchers carried out experiments using commercial membrane rather than using fabricated membrane due to easy availability of the former. The commercial membranes are made up of PolyPropylene (PP), PolyEthylene (PE), Poly-Tetra-Fluoro-Ethylene (PTFE) and Poly-VinyliDene-Fluoride (PVDF) (Lawson and Lloyd, 1997; El-Bourawi *et al.*, 2006). These available membranes have the characteristic according to the requirement of AGMD process which are high permeate flux and higher separating factors at the given operating conditions. Table 2.1 reviews the kinds of commercial membranes and their properties used by different authors for experimental work. From the different studies as mentioned in Table 2.1, it is concluded that most of the commercial membranes, generally used by researchers are flat sheet and hollow fiber membranes. These membrane are made up of PTFE, PVDF and PP materials with porosity range 60-85 %, membrane thickness range 60-200 µm, membrane pore size varying between 0.1-1 µm and minimum value of LEP as 0.31 bar. There are no commercial membranes that have been optimized for MD operation, which is an important area to work on.

Table 2.1 : Some Commercial Membranes Used by Different Researcher with their Properties

Reference	Manufacturer	Membrane Type	Membrane Material	Porosity (%)	Thickness (µm)	Mean Pore Size (µm)	LEP (bar) (≈)
(Gostoli and Sarti, 1989)	Gelman Instruments Inc. as TF200	Flat Sheet	PTFE	60	60	0.2	2.7
(Banat and Simandl, 1994)	Millipore	Flat Sheet	Durapore - PVDF	75	110	0.45	-
		Flat Sheet	Fluropore – PTFE	75	175	0.50	-
(Liu *et al.*, 1998)	Millipore	Flat Sheet	PTFE -FALP	85	150	1	-
(Zhu *et al.*, 1999)	Millipore	Flat Sheet	PTFE	85	150	1	-
(Banat and Al-Shannag, 2000)	-	Flat Sheet	PVDF	75	110	0.45	-
(Kim *et al.*, 2004)	Millipore FGLP	-	PTFE	~70	~150	0.2	-
(Guijt *et al.*, 2005b)	Mitsubishi	Hollow fiber	PolyEhtylene – PE VA12[a]	77	90	0.18	-
	Mitsubishi		PolyEhtylene – PE FA16[a]	70	55	0.21	
	Millipore		UPE test[a]	57	250	0.26	
(Thiruvenkatachari *et al.*, 2006a)	Millipore	Flat Sheet	PTFE	~70	-	0.20	-

Reference	Manufacturer	Membrane Type	Membrane Material	Porosity (%)	Thickness (µm)	Mean Pore Size (µm)	LEP (bar) (≈)
(Singh and Sirkar, 2012)	Membrana, Charlotte, NC	Hollow fiber Membrane	PP[b]	65	150	0.6-0.8	-
	Arkema Inc., King of Prussia, PA		PVDF E	54	117	0.2	
	Hyflux-Filtech (Singapore) Pte Ltd. Burnaby, BC, Canada		PVDF H	52	350	0.69	
(Eziyi *et al.*, 2013)	-	Flat Sheet	PTFE	80	200	0.20	-
(Alsaadi *et al.*, 2013)	Sterlitech Corporation	Flat Sheet	PTFE	80	100	0.20 0.45	-
(Khan and Martin, 2014)	Gore	-	PTFE	80	200	-	-
(Geng *et al.*, 2014)	Tianjin Chemical Separation Technologies Co. Ltd	Hollow Fiber Membrane	Isotactic PolyPropylene (iPP) polymer	68	-	0.2	-
(Khalifa, 2015)	Tisch Scientific	Flat Sheet	PTFE	80	153.9±13.6	0.45	2.4±0.1
(Cai and Guo, 2017)	Membrane Solutions, LLC	Flat Sheet	PTFE	-	-	0.22 0.45	-
(Perves Bappy *et al.*, 2017)	Merck Millipore	Flat Sheet	PTFE	85	150	0.50	-
(Lies *et al.*, 2017)	Lydall	Flat Sheet	PE	76	99	0.30	3.9

[a] Abbreviated form used by authors

[b] Porous PolyPropylene (PP) hollow fiber membrane with fluorosilicone coating manufactured by Applied Membrane Technology Inc.

2.1.2 Fabricated and Modified Membranes

Due to increasing popularity of MD in different separation applications, membrane fabrication and modification is the hottest area of research. Different authors have worked on improving membrane morphology (Krajewski *et al.*, 2006; Feng *et al.*, 2008), pore size (Gazagnes *et al.*, 2007), porosities (Kimura et al., 1987) , thickness of membrane (Rosalam et al., 2016) in order to carry out different MD studies for improving the permeate flux and for achieving better separation factors or selectivity. Different fabrication methods generally used are phase inversion for flat and tubular hydrophobic membrane, dry/wet & melt spinning method for hollow fiber membrane and electro spinning for nanofiber membrane. Different surface modification methods of MD membrane are radiation graft polymerization including chemical grafting, plasma grafting, photo grafting, thermal grafting etc. (Krajewski *et al.*, 2006; Gazagnes *et al.*, 2007; Cerneaux *et al.*, 2009) , plasma polymerization (Wei *et al.*, 2012), surface coating (Eykens *et al.*, 2017), surface modification by surface modifying macromolecules (SMMs) (Khayet and Matsuura, 2003; Suk *et al.*, 2010; Essalhi and Khayet, 2012), co-extrusion spinning (Bonyadi and Chung, 2007) etc. Grafting (Krajewski *et al.*, 2006) and surface coating (Eykens *et al.*, 2017) are commonly used membrane modification techniques (Khayet and Matsura,2011).

2.2 **AGMD Membrane Modules**

In membrane distillation, the different types of modules used are plate and frame, tubular module having capillary or hollow fiber membrane and spiral wound module. Amongst these, the plate and frame module is the most commonly studied due to its easy applicability, simple fabrication methods, uncomplicated cleaning and can be used repeatedly to test the different membrane. In contrast, in the spiral wound and tubular module, the membrane is fitted in the module and is not easily changeable. The membrane module selected for the specific condition depends on its economic and operating conditions, competent control over the concentration & temperature polarization effects and membrane fouling. For AGMD process both commercial and laboratory scale membrane module have been prepared and tested by various researchers (Guijt *et al.*, 2005b; Thiruvenkatachari *et al.*, 2006a; Singh and Sirkar, 2012; Alsaadi *et al.*, 2013; Eziyi *et al.*, 2013; Khan and Martin, 2014).

2.2.1 Plate and Frame Module

These types of module consist of two holding plates between which membrane, the support plates and the spacers are arranged. The packing density of this type of module is

approximately 100 - 400 m^2/m^3 or varying with the number of membrane surface used (Curcio and Drioli, 2005). The only drawback of this module is the requirement of support for holding the membrane surface. The support selected should have characteristics of low heat and low mass transfer resistance and at the same time should be strong enough to avoid damage and to hold firmly the membrane at its place. Different researchers used plate and frame module in AGMD system of different dimensions (Liu *et al.*, 1998; Alsaadi *et al.*, 2013; Eziyi *et al.*, 2013; Harianto *et al.*, 2014; Khalifa, 2015).

2.2.2 Tubular Membrane Module

The use of tubular membrane is advantageous over plate and frame module for the reason that former supplies large membrane surface area to volume ratio hence the module is mainly used for treatment of high viscous liquids. It also provides less fouling, easy cleaning and low temperature polarization. The packing density of this module is relatively low i.e. 300 m^2/m^3 (Curcio and Drioli, 2005). Due to low packing density it exhibits high cost per module.

2.2.3 Hollow Fiber Membrane Module

In hollow fiber module, a membrane is installed in the shell and tube type assembly made up of glass, stainless steel or plastic. The hollow fiber module turns out to be advantageous in MD because of its high packing density (~3000 m^2/m^3), which in turn provides high membrane surface area (Curcio and Drioli, 2005). In this module the membrane is an intrinsic element of the module therefore cleaning and maintenance is difficult and membrane cannot be easily replaced.

2.2.4 Spiral Wound Membrane Module

In spiral wound membrane module, the membrane, the feed channel spacer, the permeate channel spa and the porous support are covered and wound in the region of perforated central tube. The direction of feed flow is axial and that of permeate flow is radial across the membrane. The packing density of these modules varies with packing height and ranges from 300-1000 m^2/m^3. These modules generally provide the large area in a small volume.

The Memstill® technology for MD module has been licenced to Aquastill for commercial production of MD module**.** Aquastill® module is spiral wound configuration module used for both AGMD and DCMD application by various researchers for different applications. Duong *et al.*, (2016) used pilot AGMD module for seawater desalination (Aquastill, The

Netherlands). Process efficiency was measured in terms of distillate production rate and electrical and thermal energy consumption and it was found that specific energy consumption was lower than all other AGMD pilot plants studied so far. Hitsov *et al.*, (2017) used AGMD module (Aquastill) to validate the developed model and found that flux and outlet temperature can be predicted with good accuracy.

2.3 **Transport Mechanism of AGMD**

The air gap membrane distillation is a non-isothermal process thus heat transfer plays an important role and due to multi-phase system the mass transfer between the phase boundaries also plays a crucial role in determining the AGMD permeate flux and permeate concentration. The different mathematical modelling has been done by different researchers to determine the heat transfer and the mass transfer rate along with corresponding transfer coefficients (Kimura et al., 1987; Gostoli and Sarti, 1989; Banat and Simandl, 1998; Izquierdo-Gil et al., 1999; Garcia-Payo et al., 2000; Alklaibi and Lior, 2005; Guijt *et al.*, 2005a; Abu *et al.*, 2012; Kujawska *et al.*, 2016).

2.3.1 Heat Transfer

In all MD configurations, heat transfer is an important step because it is considered to be the rate controlling step. The mathematical modelling equations include the transfer of volatile component in terms of heat transfer and mass transfer from feed section to permeate section. (Banat and Simandl, 1998). In AGMD, the feed component is vaporized at the point of entry in the membrane, and then the vapours of volatile components pass through two static air layer resistances: one provided by the air inside the membrane pores and the other provided by the air between membrane and condensing plate. This air gap makes the AGMD quite complicated as compared to others MD process in terms of operations and modelling. Figure 2.1 and Figure 2.2 represent the heat transfer and temperature profile in AGMD process, respectively.

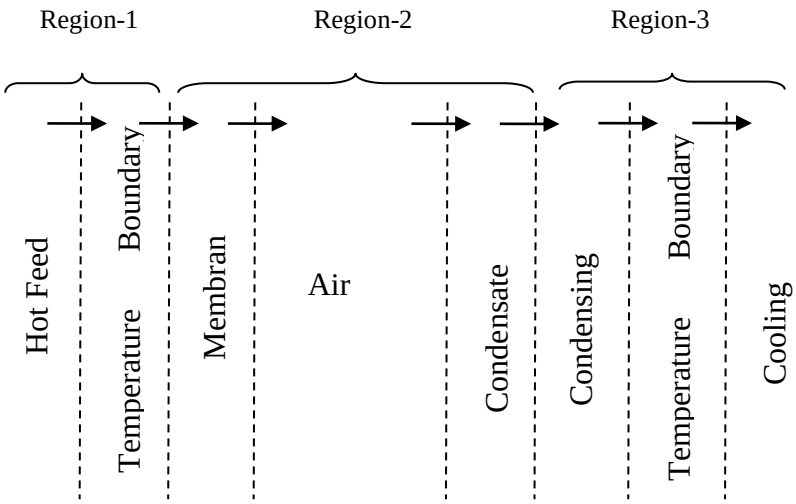

Figure 2.1 : Schematic Representation of Heat Transfer in AGMD

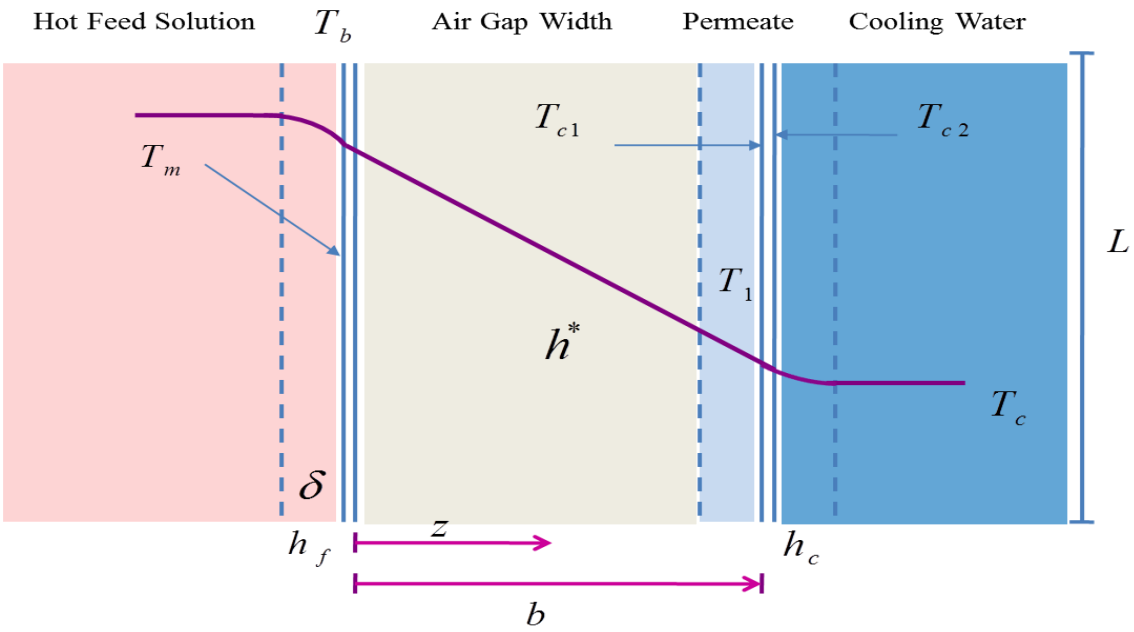

Figure 2.2 : Schematic Representation of Temperature Profile in AGMD

For calculating permeate compositions, the interfacial temperatures at membrane and condensation surface must be known. These interfacial temperatures are not experimentally accessible (and are thus unmeasurable) but can be estimated by applying conservation of enthalpy equation over the measurable temperature in different regions. Since in MD, both heat and mass transfer occur simultaneously therefore an enthalpy flux prevailed across the membrane and the condensing plate (Banat and Simandl, 1998, 2000). In AGMD the heated

fluid passes through the following heat transfer steps connected in series (Khayet and Matsuura, 2011) -

1. Heat transports from the hot feed to the membrane surface.
2. Heat transports from the feed side temperature boundary layer to the condensate liquid.
3. Heat transports from the condensate liquid through the condensing plate to the permeate side temperature boundary layer and finally to the cooling fluid.

2.3.2 Mass Transfer

In AGMD, the heated fluid passes through the following mass transfer regions connected in series -

1. Mass Transfer of liquid/vapour from the bulk to the membrane surface.
2. Evaporation of liquid feed over the membrane surface and transfer through the membrane and air gap.
3. Finally condensation of vapours of volatile component over condensing plate.

Figure 2.3 and Figure 2.4 shows the different resistances in AGMD processes and concentration profile in AGMD, respectively.

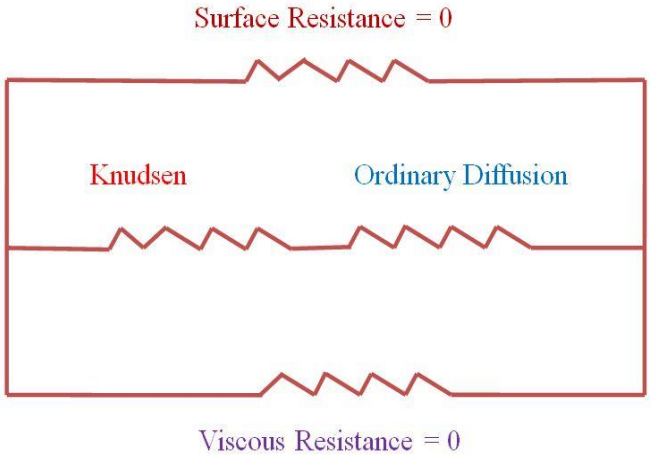

Figure 2.3 : Schematic Representation of Different Resistance in AGMD process

Since, the membrane used in MD process is highly porous to provide efficient mass transfer of vapours through the membrane pores. The general range of membrane porosity used in MD is 40-90 % (Lei et al., 2005). Consequently, surface diffusion in AGMD is considered negligible. The solubility of stagnant component, generally air, in water or in other volatile components is very low therefore it can be considered as stagnant film and viscous resistance can be considered negligible. Therefore, dominating mass transfer resistance in AGMD is due to molecular diffusion and Knudsen diffusion. Nevertheless, certain researcher worked on all diffusion resistances to determine the dependency of mass transfer

on various mechanisms (Liu *et al.*, 2017).

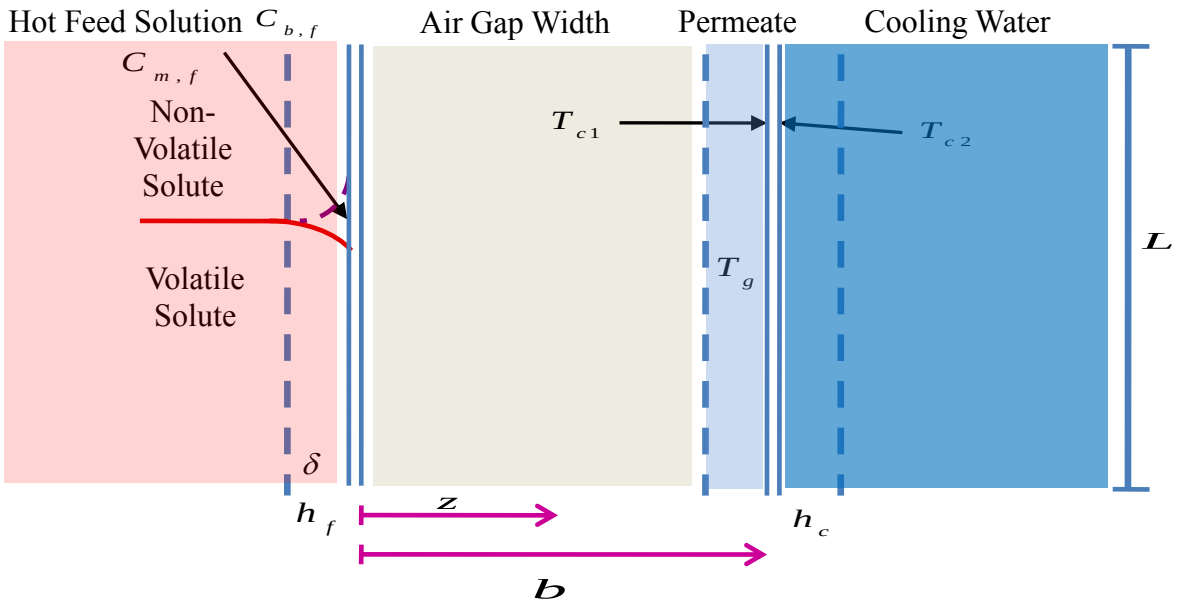

Figure 2.4 : Schematic Representation of Concentration Profile in AGMD

Generally, the mass transport in AGMD is described using molecular diffusion principles by researchers. Fickian approach is one of the approaches used for mathematical modeling in AGMD (Gostoli et al., 1987; Kimura et al., 1987; Udriot et al., 1994; Banat and Simandl, 1998, 1999, 2000; Abu et al., 2003; Guijt *et al.*, 2005a; Abu *et al.*, 2012; Alsaadi *et al.*, 2013; Cai and Guo, 2017).

Another approach for mass transfer is the Stefan-Maxwell model for multi-component system. The main difference between Fickian approach and Maxwell approach is that in the later the diffusional interaction between the components is also considered therefore it will give more accurate result as compare to the former. Various authors used this approach for AGMD modelling (Gostoli and Sarti, 1989; Banat et al., 1999b; Banat *et al.*, 1999c; Banat *et al.*, 1999d; Banat *et al.*, 1999e; Abu *et al.*, 2012).

2.4 **Process and Membrane Parameters affecting AGMD Flux**

The performance of AGMD is mainly measured by the permeate flux and the permeate flux is primarily affected by the process parameters like feed inlet temperature, feed concentration, solution nature, feed flow rate, cooling water temperature, cooling water flow rate, air gap thickness, non-condensable gases and recirculation rate. In this section the effects of the above process parameters on performance of AGMD has been reviewed and major findings have been discussed.

2.4.1 Feed Temperature

Feed inlet temperature has a key effect on AGMD permeate flux. The permeate flux increases exponentially with the increase in the feed temperature. This fact is manifested by the Antoine equation in which the vapor pressure increases exponentially with increase in temperature which in turn increases the driving force for mass transfer that ultimately results in increase in total permeate flux and partial permeate flux of both water and volatile solutes (Khayet and Matsuura, 2011). Sometimes a linear trend between permeate flux and vapor pressure difference has been also observed. This is mainly due to the membrane characteristics, types of permeating compounds, module design and feed flow rate (Kurokawa *et al.*, 1990; Banat and Simandl, 1994, 1998). The increase in feed temperature should increase the heat loss. However the increase in thermal efficiency is due to the increase in the useful heat relative to the conductive heat loss as the feed temperature increases (Alklaibi and Lior, 2005). From Table 2.2 it can be seen that feed temperature has major effect on permeate flux. Most of the researchers worked on temperature range between 40-90 ^{o}C (kept below the boiling point of the feed solution) to determine its effect on permeate flux while kept all other parameters constant. From Table 2.2, it is concluded that permeate flux increased by 9-10 folds on increasing the temperature from 40-90 ^{o}C.

Table 2.2 : Effect of Feed Temperature on AGMD Permeate flux

References	Membrane Type	Feed Solution	Feed Flow Rate (L/min)	Air Gap Thickness (mm)	Feed Temperature Range (^oC)	Permeate Flux ($kg/m^2 \cdot h$) (≈)
(Banat and Simandl, 1994)	PVDF	Tap water	-	8	25-80	1.8-28.8
(Banat and Simandl, 1998)	PVDF	Simulated Seawater	5.5	3.5	40-70	1-7
(Banat and Simandl, 1999)	PVDF	Ethanol-Water Solution	5	-	40-70	0.9-8.4
(Matheswaran and Kwon, 2007)	PTFE	Nitric Acid/ Water	0.05	-	60-90	6.5-13.8 $l/m^2 \cdot h$
(Pangarkar et al., 2011)	PTFE	Ground Water	≈ 0.92	1.2	40-60	20-38
(He et al., 2011)	PTFE	NaCl Solution	0.25	1	50-80	2.5-12.5 $l/m^2 \cdot h$
(Eziyi *et al.*, 2013)	PTFE	Solution of Distilled water and sea salt	22.73	1	ΔT = 20-65	0.9-5.3
(Alkhudhiri et al., 2013a)	PTFE	Produced water from oil field	1.5	-	40-80	3.6-16.2
(Khalifa *et al.*, 2015)	PTFE	Raw Seawater	2	3	40-80	10-70
(Khalifa, 2015)	PTFE	Laboratory prepared salty water	1.5	4	50-90	5-30
(Xu *et al.*, 2016)	PTFE	Simulated Seawater	0.12 m/s[#]	10	50-80	0.5-4

[#]The reference papers have used unit m/s and since the membrane area is not exactly known therefore it cannot be converted into L/min and hence the same unit is used.

2.4.2 Feed Concentration

The permeate flux of AGMD process is influenced by both volatile and non-volatile solute concentration in the feed. The drop in AGMD permeate flux has been observed on increasing the non-volatile solute concentration in feed owing to the decrement in vapor pressure driving force and also due to concentration polarization effect. For volatile solute present in the feed, the partial and the total permeate flux varied in different way with feed concentration than the non-volatile solute. Both the partial flux of volatile solute and the total flux increase with the increase in volatile solute concentration while the partial flux of water decreases marginally with the feed concentration. This is mainly attributed to the effect of concentration of different components on their partial pressures and on their activity coefficient (Banat and Simandl, 1999; Banat et al., 1999c). Table 2.3 shows the effect of feed concentration on the permeate flux studied by numerous researchers. It can be inferred from the Table 2.3 that by increasing feed concentration, permeate flux decreases in the case of non-volatile solute like salt solution (Xu *et al.*, 2016) while volatile component flux like ethanol increases and water flux decreases on increasing the concentration of volatile solute in the feed (Kujawska *et al.*, 2016). Also the thermal efficiency slightly decreases on increasing the feed concentration (Alklaibi and Lior, 2005).

2.4.3 Air Gap Thickness

Air gap thickness is the one of the most important factors that affects the AGMD performance. This air gap width along with the membrane thickness constitutes the diffusion path for the transfer of diffusing species in air gap membrane distillation. By increasing the air gap between the condensing plate and membrane, the permeate flux decreases due to high mass transfer resistance provided by the large air gap. Therefore, it can be inferred that permeate flux in AGMD is inversely proportional to the air gap thickness. The main purpose of using variable air gap thickness is to decrease the heat transfer resistance but it simultaneously increases the mass transfer resistance. Therefore an optimum value of air gap thickness must be used to get the maximum permeate flux. This thickness can be maintained by using gaskets of different thickness. By reducing the air gap thickness, the heat loss by conduction increased and this results in decreasing thermal efficiency (Alklaibi and Lior, 2005). Different studies have been done to determine the effect of air gap thickness on AGMD permeate flux. Air gap width employed by most of the researchers ranges from 2 mm to 10 mm and found large change in the flux value. Some of these studies are mentioned in Table 2.4.

Table 2.3 : Effect of Feed Concentration on Permeate Flux

Reference	Membrane	Pore size (µm)	Feed Flow Rate (L/min)	Feed Temperature (^oC)	Feed Solution	Concentration (g/l)	Permeate Flux ($kg/m^2 \cdot h$) (≈)
(Banat and Simandl, 1999)	PVDF	0.45	5	50	Ethanol/Water	6.6-80.6 or 0.83-10.2 wt%	1.9-3.1
(Garcia-Payo et al., 2000)	PVDF	0.22	2.01	50	Methanol/Water	≈30-200	3.9-4.5 (Methanol)
					Ethanol/Water	≈30-150	3.9-5 (Ethanol)
					Isopropanol/Water	≈10-95	4-5 (Isopropanol)
(Matheswaran and Kwon, 2007)	PTFE	0.22	0.05	80	HNO_3/ Water	≈ 126-378 or 2-6 M	0.9-2.11 $l/m^2 \cdot h$*
(He at al., 2011)	PTFE	0.45	0.25	80	NaCl/Water	0-100 or 0-10 wt%	12.5-10 $l/m^2 \cdot h$*
(Alkhudhiril et al., 2013b)	PTFE	0.20	1.5	50	NaCl/Water	46.4-84.4	10.8-0.9
(Khalifa, 2015)	PTFE	0.45	1.5	70 80	Saline Solution	0.145-60	18-5 17-15
(Khalifa *et al.*, 2015)	PTFE	0.45	2	70	NaCl/Water	0-60	42-38
(Xu *et al.*, 2016)	PP	0.2	0.12 m/s[#]	80	Salt Solution	40-120	5.2-4.5
(Kujawska *et al.*, 2016)	PP	0.10	-	63	Ethanol/Water	0-31.6 or 0-4 wt%	0-0.6 (Ethanol) 8.9-8.7 (Water)

*****The reference papers have used unit l/m^2h and since the density of solution is not exactly known therefore it cannot be converted into $kg/m^2 h$ and hence the same unit is used.

[#]The reference papers have used unit m/s and since the membrane area is not exactly known therefore it cannot be converted into L/min and hence the same unit is used.

Table 2.4 : Effect of Air Gap Thickness on Permeate Flux

Reference	Membrane Type	Feed Solution	Feed Temperature (^oC)	Cooling Water Temperature (^oC)	Feed Flow Rate (L/min)	Air Gap Thickness (mm)	Permeate Flux ($kg/m^2 \cdot h$) (≈)
(Kimura et al.,1987)	PTFE	NaCl-Water	60	20	-	0.3-9.0	19-1.5
(Udriot et al., 1994)	PTFE	HCl/Water	60	30	-	4-7	3.7-2.4
(Udriot et al., 1994)	PTFE	Propionic Acid/ Water	60	30	-	4-7	7.4-4.6
(Banat and Simandl, 1998)	PVDF	Artificial Sea Water	60	20	5.5	1.9-9.9	5-2.1
(Izquierdo-Gil et al., 1999)	PVDF	Sucrose Aqueous Solution	25.8	3.2	0.8	1-4	1.7-0.8 $l/m^2 \cdot h$
(Garcia-Payo et al., 2000)	PTFE	Isopropanol-Water	50	-	2.0	0.55-1.62	6.3-5.2
(Alklaibi and Lior, 2005)	NaCl/ Water	Saline Water	70	20	Re = 464	1-5	11.5-4.5
(Matheswaran and Kwon, 2007)	PTFE	HNO_3/Water	80	15	0.05	0.3-2.0	5.3-4.1 $l/m^2 \cdot h$
(Pangarkar et al., 2011)	PTFE	Natural Ground Water	60	15	0.9	1.2-3.2	40-22.5
(Khalifa et al., 2014)	PTFE	Saline Water	70	18	2.3	2-5	60-20
(Khalifa, 2015)	PTFE	Saline Water	50	24	1.5	4-8	5-15

2.4.4 Feed Flow Rate

In AGMD, by increasing the feed flow rate, the concentration and the temperature polarization effects are reduced due to turbulent flow and finally results in higher permeate flux. The significance of high Reynolds number due to turbulent flow is the declination in boundary layer width and resulting into high vapor pressure difference and large permeate flux.

In AGMD, the feed flow rate increment affects slightly the thermal efficiency because of simultaneous increment in permeate flux, conductive heat transfer and heat flow due to mass transfer (Alklaibi and Lior, 2005). Table 2.5 shows that permeate flux increases by increasing the feed flow rate or velocity while keeping all other parameters constant.

2.4.5 Cooling Water Temperature

In AGMD, the permeate flux is minutely influenced by the coolant temperature relative to the feed temperature. As the coolant temperature increases, the AGMD flux decreases due to decrease in the vapor pressure gradient. The low sensitivity of AGMD flux towards the cooling temperature is due to the air gap heat transfer coefficient that governs the overall heat transfer coefficient and at lower temperature the water vapour pressure is slightly affected (Banat and Simandl, 1998).

By reducing the cooling water temperature, the permeate flux increases slightly and simultaneously the thermal efficiency decreases to some extent. While by enhancing the feed water temperature, both the AGMD flux and thermal efficiency increase. For this reason, it is better to enhance the feed temperature than to decrease the cooling temperature. In general the coolant temperature in AGMD varies within 5-30 ^{o}C. Table 2.6 shows the effect of cooling water temperature on AGMD performance at different operating conditions.

2.4.6 Cooling Water Flow Rate

In AGMD, the cooling water flow rate shows negligible effect on permeate flux. The reason for this is the air gap heat transfer coefficient is much smaller than the hot feed side heat transfer coefficient and cold side heat transfer coefficient. The overall heat transfer coefficient, which consists of hot feed side heat transfer coefficient, cold side heat transfer coefficient and air gap heat transfer coefficient, is mainly dominated by air-gap heat transfer coefficient because of its low value. Therefore, cooling water flow rate affects slightly the AGMD permeate flux. The effect of cooling water on permeate flux is primarily controlled

Table 2.5 : Effect of Feed Flow Rate on Permeate Flux

Reference	Membrane Type	Pore Size (μm)	Feed Solution	Feed Temperature (^oC)	Feed Flow Rate Range (L/min)	Permeate Flux ($kg/m^2 \cdot h$) (≈)
(Banat and Simandl, 1998)	PVDF	0.45	Simulated Seawater	60	≈ 1-5.5	2.7-3.5
(Banat and Simandl, 1999)	PVDF	0.45	Ethanol-Water	60	≈ 2-5	4.5-4.8
(Garcia-Payo et al., 2000)	PVDF	0.22	Isopropanol /Water	50	≈ $1.5*10^{-2}$ -$8*10^{-2}$ m/s	1.6-2.2
(Matheswaran and Kwon, 2007)	PTFE	0.22	HNO_3/Water	80	≈ 0.05-0.2	2-5.4 $l/m^2 \cdot h$
(Alkhudhiri et al., 2013b)	PTFE	0.20	Na_2SO_4/Water	50	0.5-1.89	9-11.5
(Rosalam et al., 2016)	PP	0.1-1	NaCl/Water	80	≈ 0.2-0.5	3.8-6
(Xu *et al.*, 2016)	PTFE	0.20	Salt Solution	80	≈ 0.03-0.18 m/s	3.2-4.2

Table 2.6 : Effect of Cooling Water Temperature on Permeate Flux

Reference	Feed Type	Feed Temperature (^oC)	Cooling Water Range(^oC)	Permeate flux ($kg/m^2 \cdot h$) (≈)
(Banat and Simandl, 1998)	Simulated Seawater	60	7-30	4-3
(Banat et al., 1999e)	Ethanol/Water	50	5-30	0.5-0.3 (Modeling)
(Alklaibi and Lior, 2005)	NaCl/Water	70	5-45	10-5 (Modeling)
(Matheswaran and Kwon, 2007)	HNO_3/Water	80	10-25	2.5-1.8 $l/m^2 \cdot h$
(Abu *et al.*, 2012)	Acetone/Water	50	5-30	2.3-0.8 (Modeling)
(Alkhudhiri et al., 2013b)	$MgCl_2$/Water	50	5-25	12.0-8.2
	Na_2SO_4/Water			12.0-8.2
	NaCl/Water			9.7-6.5
(Khalifa *et al.*, 2015)	Saline Water	70	15-30	45-40
(Kujawska *et al.*, 2016)	Pure Water	63	≈ 5-25	10-8.2

by module geometry. Thermal efficiency of process also remain unchanged by changing cooling water velocity (Alklaibi and Lior, 2005)

Due to negligible or very small effect of cooling water flow rate on permeate flux, limited research work has been done on this parameter. Table 2.7 depicts the effect of cooling water flow rate on the permeate flux. From the different study indicated in Table 2.7, it is concluded that permeate flux is slightly affected by the cooling water flow velocity.

2.4.7 Non-Condensable Inert Gases

Non condensable gases are used in AGMD to fill the membrane pores as well as the gap between the membrane and cooling plate. Non condensable gases, such as air, are those gases which are not easily condensed by cooling and are chemically inert to the other species present in the AGMD module. These gases mainly increase the mass transfer resistance, reduce the condensation rate and ultimately decrease the permeate flux. Removing the air or deaerating the air gap will reduce the pressure between the air gap and condensing plate and will lead to decreasing the mass transfer resistance and increasing the permeate flux. Guijt *et al.* (2005b) compared the permeate flux obtained at atmospheric pressure and below atmospheric pressure and found that AGMD permeate flux is 2.5 to 3 times higher than the value obtained at atmospheric pressure.

Table 2.8 shows the work done by Banat et al. (1999b) to determine the effect of inert gases on breaking the formic acid-water azeotrope mixture. The authors concluded that heavy inert gas such as sulphur hexafluoride gives the best selectivity and favours in breaking the azeotropic point but at the cost of flux reduction. This is mainly due to the dependency of the both the flux and the selectivity on the vapor-liquid equilibrium and diffusivities on the inert gas.

2.4.8 Membrane Thickness

In general, the permeate flux in membrane distillation processes is inversely proportional to the membrane thickness, that is on increasing the membrane thickness, the permeate flux decreases. This is because of mass transfer resistance provided by the membrane. But in AGMD the membrane thickness does not have an appreciable effect on the permeate flux because of high mass transfer resistance offered by the air width. Therefore the resistance provided by the membrane is considered to be negligible. Table 2.9 depicts the effect of membrane thickness on the permeate flux. However, in the case of fabricated membrane, the effect of membrane thickness depends on the membrane material and its fabrication method.

2.4.9 Membrane Thermal Conductivity

On increasing the membrane thermal conductivity, the permeate flux decreases in AGMD. This behaviour is mainly due to the reason that the heat transfer resistance gets decreased and subsequent increases of the heat transfer flux because of conduction, and it ultimately leads to less heat availability for vaporization. Table 2.10 gives the effect of the membrane thermal conductivity on the permeate flux. Same behaviour was observed by authors on using membrane with 74% membrane porosity as mentioned in Table 2.10.

2.4.10 Membrane Porosity

In AGMD process, the permeate flux increases on increasing the membrane porosity due to decrease in thermal conductivity, as a result, the permeate flux increases. Table 2.11 depicts the effect of membrane porosity.

2.4.11 Membrane Pore Size

In general, AGMD flux increases on increasing the membrane pore size. In MD process, the pore diameter is selected such that it must satisfy the condition of both high permeate flux (fulfil by high pore diameter) and prevent the chances of membrane wetting (caused by high pore diameter). Therefore an optimum value of pore diameter should be selected to fulfil the above mentioned requirements. In mathematical modeling of the AGMD process, both Fick's molecular diffusion and Stefan-Maxwell modeling approach does not take into account the effect of membrane pore size on the permeate flux. Therefore, effect of membrane pore size could only be analysed by an experimental study.

Table 2.7 : Effect of Cooling Water Flow Rate on Permeate Flux

Reference	Feed Type	Feed Temperature (^oC)	Cooling Water Temperature, (^oC)	Cooling Water Flow Rate, L/min	Permeate Flux, ($kg/m^2 \cdot h$) (≈)
(Banat and Simandl, 1998)	Simulated Seawater	60	20	1-5.5	3.3-3.4
(Banat and Simandl, 1999)	Ethanol/Water	60	20	1.5-5.5	5.3-5.4
(Banat et al.,1999)	Ethanol/Water	50	20	Re = 500 -2000	0.7-0.8
(Alklaibi and Lior, 2005)	NaCl/Water	70	20	0.10-0.30 m/s[#]	8.2-8.5
(Abu *et al.*, 2012)	Acetone/Water	50	20	Re = 500-2000	1.4-2.2
(Khalifa, 2015)	Saline Water	80	24	1-4	23-25

[#]The reference papers have used unit m/s and since the membrane area is not exactly known therefore it cannot be converted into L/min and hence the same unit is used.

Table 2.8 : Effect of Non-Condensable Gases on Permeate Flux

Reference	Membrane Type	Feed Temperature (^oC)	Cooling Water Temperature (^oC)	Air Gap Thickness (mm)	Feed Composition (Wt %)	Type of Inert Gas	Permeate Flux ($kg/m^2 \cdot h$) (≈)
(Banat *et al.*, 1999)	PTFE	60	10	4	60 - 100	SF_6	1.5-2
						Air	3.1-4.2
						He	10-14

Table 2.9 : Effect of Membrane Thickness on Permeate Flux

Reference	Feed Type	Feed Temperature (^oC)	Cooling Water Temperature (^oC)	Cooling Water Flow Rate, L/min	Permeate Flux, ($kg/m^2 \cdot h$) (≈)
(Banat and Simandl, 1998)	Simulated Seawater	60	20	1-5.5	3.3-3.4
(Banat and Simandl, 1999)	Ethanol/Water	60	20	1.5-5.5	5.3-5.4
(Banat et al., 1999)	Ethanol/Water	50	20	Re = 500 -2000	0.7-0.8
(Alklaibi and Lior, 2005)	NaCl/Water	70	20	0.10-0.30 m/s[#]	8.2-8.5
(Khalifa, 2015)	Saline Water	80	24	1-4	23-25

Table 2.10 : Effect of Membrane Thermal Conductivity

Reference	Feed Solution	Feed Temperature (^oC)	Cooling Water Temperature (^oC)	Membrane Thickness (µm)	Membrane Porosity	Membrane Thermal Conductivity, W/m·K	Permeate Flux ($kg/m^2 \cdot h$) (≈)
(Alklaibi and Lior, 2005)	NaCl/Water	70	20	400	0.74	0.05-0.3	11.8-6
					0.84		13.1-8.1
(Alklaibi and Lior, 2007)	Saline Solution	70	20	400	0.78	0.05-0.3	11.5-6

Table 2.11 : Effect of Membrane Porosity

Reference	Membrane Type	Feed Solution	Feed Temperature (^oC)	Membrane Thickness (mm)	Membrane Thermal Conductivity, W/m K	Air Gap Thickness, (µm)	Membrane Porosity	Permeate Flux ($kg/m^2 \cdot h$) (≈)
(Jonsson et al., 1985)	PTFE	Salt Solution	60	0.2	0.22	200	≈ 0-1	0-37
						1000		0-11
						5000		0-2
(Kimura et al., 1987)	PTFE	Pure Water	60	20	-	-	≈ 0.6-0.9	13-16.1

2.5 **Membrane Fouling and Wetting**

Fouling is the deposition of the inorganic/organic macromolecules, retained particles, surfactants and colloid matters on or in the membrane surface. The fouling causes blockage of the membrane pores and results in low permeate flux. Fouling is comparatively less studied parameter in the air gap membrane distillation. The fouling can be classified on the basis of type of material deposited. The scale formation on the surface of membrane due to concentrated salts or mineral solutions is the most general form of membrane fouling (Chan *et al.*, 2005). The biological fouling is mainly due to the growth of bacteria or microorganism on the membrane surface. This type of fouling mainly occurs in food and waste water industries (Krivorot *et al.*, 2011; Baghel et al., 2017). The organic fouling is mainly due to the Natural Organic Matter composed of proteins, polysaccharides, organic acids etc. (Srisurichan, Jiraratananon and Fane, 2005). The inorganic fouling is mainly caused by alkaline salts, non-alkaline salts and uncharged molecules or particulate matter like silica (Gryta, 2007a).

Membrane distillation process is only possible with hydrophobic porous membranes which means pores of membrane do not get wet by liquid feed. To avoid the chances of membrane wetting in MD, different types of hydrophobic membranes (as mentioned in section 5.1) of high contact angle with very small pore and medium pore size distribution are used (Franken *et al.*, 1987). Liquid Entry Pressure (LEP) is the minimum pressure required to allow liquid to enter into membrane pores. Pore wetting gets started when hydrostatic pressure exceeds the LEP of the feed solution. Therefore high LEP is required for good MD performance and for reducing the chances of membrane wetting (Tijing *et al.*, 2015). Deposition of suspended and corrosive particles, biological growth, presence of surfactant in the solution and water abundant in oil or organics components are the main causes of scale formation and consequently increases the possibility of membrane wetting. Vapor condensation inside the membrane pores is also one of the possible reasons of membrane wetting (El-Bourawi *et al.*, 2006). Sometimes operational conditions such as temperature and flow rate also cause the wetting problems (Guillen-Burrieza *et al.*, 2016). Table 2.12 shows the different types of fouling observed in the AGMD process.

Table 2.12 : Different Types of Fouling Observed in AGMD Process

Reference	Feed Solution	Membrane	Fouling Type
(Guillen-Burrieza *et al.*, 2014)	NaCl/Water	Flat Sheet PTFE	Inorganic Fouling
(Kimura et al., 1987)	3.8 % NaCl Solution	PTFE	Organic Fouling
(Kullab and Martin, 2011)	Municipal Water and Flue Gas Condensate	PTFE flat Sheet	Scale Formation by Ca and Mg Salts
(Yang *et al.*, 2011)	Brackish Water	PTFE	Inorganic Fouling – $CaCO_3$ Precipitation
(Meindersma et al., 2006)	Pond Water	Memstill® Technology	Biofouling
(Phattaranawik *et al.*, 2008)	Synthetic Waste Water	MDBR* – Tubular PVDF	Biological Fouling – Sludge

* Membrane Distillation – Bioreactor

2.6 **Energy and Economic Analysis of AGMD**

Since, Membrane Distillation (MD) is an energy intensive process therefore energy analysis is an essential for MD study. The MD process requires both thermal energy and electrical energy: thermal energy is required for heating feed and condensing flux, while electrical energy is required to operate the fluid flow pumps. The contribution of heat energy in total energy requirement is generally more than 90%. The membrane distillation system is characterized by energy efficiency which is defined as:

$$\eta_E = \frac{Effective\ heat\ used\ for\ evaporation}{Energy\ input} \tag{2.1}$$

Here, the energy input considers both electrical energy and thermal energy (Khayet and Matsuura, 2011). Energy efficiency η_E often turns out to be the best in AGMD as compared with the other configurations and approaches the ideal value of 1 (realistically AGMD is capable of $\eta > 0.90$).

The energy efficiency of solar system integrated with heat recovery system is characterized by Gained Output Ratio (GOR). The GOR is defined as the ratio of the latent heat of evaporation to and the total input energy (Koschikowski et al., 2003):

$$GOR = \frac{\Delta h_{evap} m_{permeate}}{Q_{input}} \tag{2.2}$$

The process heat requirement can be reduced by recovering the heat from the retentate and reuse it in heating the feed solution thus reducing the total heat requirement. The heat recovery system adds to the initial cost but reduces the operating cost. Therefore research studies in this area revolve around getting an optimized value. The cost of membrane distillation process is indirectly proportional to the specific energy consumption i.e. lower value of specific energy consumption leads to higher economical MD process.

Another energy efficiency parameter of MD system is given by heat exchanger effectiveness ε. Based on traditional heat exchanger for heat transfer between cold stream and hot stream, ε compares the actual change in enthalpy to maximum change in enthalpy of cold stream. ε is therefore given as (Swaminathan *et al.*, 2016):

$$\varepsilon = \frac{\text{Energy Transfer between Two Streams}}{Total\ Energy\ Transfer} \tag{2.3}$$

The effectiveness in terms of temperature difference is given as:

$$\varepsilon = \frac{T_{cold,out} - T_{cold,in}}{T_{feed,in} - T_{feed,out}} \tag{2.4}$$

The GOR of AGMD process in terms of effectiveness ε and energy η_E is given as (Swaminathan *et al.*, 2016) –

$$GOR = \eta_E \frac{\varepsilon}{1 - \varepsilon} \tag{2.5}$$

Change in GOR with η_E is linear and with ε is non-linear.

The economics of membrane distillation process is an important criterion which makes it different from other separation process. The total MD cost at laboratory scale must include its installation cost, operational cost, electrical and thermal energy consumption cost, membrane and membrane module cost, maintenance cost and pre-treatment cost. At industrial level the annual operating cost, capital cost and amortization cost is also included. Amortization cost includes interest on the borrowed money and operating and maintenance cost includes the salary paid to the labour and staff workers.

2.7 **Advancement in AGMD Process**

Material Gap Membrane Distillation – In AGMD the primary reasons of low AGMD flux is an additional mass transfer resistance provided by the air gap and the limited condensation surface area. To overcome this problem and to analyse the effect of different material fill in air gap, Francis *et al.* (2013) developed a novel module known as Material Gap Membrane Distillation (MGMD). The module was examined and tested for desalination process. To increase the water vapor permeates flux as compare to the AGMD, the air gap was filled by certain material like sand, deionised water, polyurethane and polypropylene mesh. The polyurethane and polypropylene material cause reduction in heat transfer due to their insulating nature and this effect dominates the effect of air gap thickness reduction, consequently the water vapor flux decreases as compared to AGMD. While with the sand and DI water, the permeate flux increased by 200-800%. A maximum increase of 820% was observed with Water Gap Membrane Distillation (WGMD) as compared to AGMD. This is due to enhancement in the condensation surface and increase in heat transfer rate along with air gap width reduction. In AGMD, the water permeate flux obtained was 4.77 kg/m^2.h with salt rejection of 99.99%, but in WGMD the permeate flux increased up to 20.45 kg/m^2.h. Effect of feed temperature, feed flow rate and types of membrane on different material gap MD was also analysed.

Double Stage AGMD Unit - Lawal and Khalifa (2015) developed a double stage air gap membrane distillation unit for the desalination application and studied the effect of feed flow rate, cooling water flow rate, feed temperature, cooling water temperature and air gap thickness on AGMD performance. Experimental results showed the maximum value of cumulative permeate flux (sum of flux gained from stage 1 and stage 2) 128.46 kg/m^2h, total flux (average of flux gained from stage 1 (F_1) and stage 2 (F_2) i.e. ((F_1+F_2)/2) 64.23 kg/m^2h and flux from single stage 65.81 kg/m^2h. The important benefit of using this design is that two feed chambers are commonly cooled by one cooling chamber and it reduced the total capital cost, maintenance and energy consumption cost. The authors also developed a model for calculating permeate flux and validated it with experimental results and found less than 13% error. Depending on the working conditions the module can be used as single stage AGMD unit or double stage AGMD unit.

Conductive Gap Membrane Distillation - Swaminathan *et al.* (2015), developed a new configuration called Conductive Gap Membrane Distillation (CGMD) to increase the

thermal efficiency of conventional air gap membrane distillation process. The authors used a material of higher thermal conductivity and filled it in the air gap to increase the air thermal conductivity. The authors claimed that the energy efficiency increased by two times than conventional process. By using simple copper woven mesh in the air gap increased the 40% to 60% higher Gained Output Ratio (GOR) for air gap membrane distillation process. The authors experimentally compared Air Gap Membrane Distillation (AGMD), Conductive Gap Membrane Distillation (CGMD) and Permeate Gap Membrane Distillation (PGMD) for the same operating conditions and the same membrane area, and found that CGMD and PGMD gave higher GOR due to low transfer resistance.

Superhydrophobic Condenser Surface - Warsinger *et al. (*2015)**,** worked on the superhydrophobic condenser surface to increase the vapor condensation rate that will ultimately increase the permeate flux and the thermal efficiency of the AGMD process. The superhydrophobic surface used was a silanized copper oxide (CuO) nanoscale surface. As compared to conventional copper surface, this surface gives 30% higher heat transfer coefficient and 25% more heat flux (Miljkovic et al., 2012). The permeate flux production was found with an increase of 60% as compared to the standard AGMD. However, the use of superhydrophobic membrane at high heat transfer rate was not important as its effect was negligible.

Multi-Stage and Multi-Effect Membrane Distillation (MEMD) - The Memstill Technology is an ideal counter current air gap membrane distillation configuration which was used in desalination application for highly competent heat recovery (Hanemaaijer, 2004). Due to recovery of heat feature, the desalination can be carried out at minimum heat input or can be run by using waste heat. Memstill technology was developed by Keppel Seghers in three pilot plants; one has been situated at Singapore, Straits of Johor (M28) and another two at Netherlands, Port of Rotterdam (M32 and M33). Each pilot study has different module with different material. The pilot study showed the absolute flux of 0.25, 2.5 and 3 l/m^2 h with internal heat recovery of 30%, 50% and 90% and heat consumption 1000-2000, 400 and 350 – 400 MJ/m^3 from M28, M32 and M33 plants respectively. In Memstill process, a single unit composed of a condenser array and a hydrophobic membrane array were kept parallel to each other. In the condenser array, the output flow through a heating phase and then enter into the membrane array. A continuum of membrane array and condenser array with a permeate channel in between them is arranged in alternating mode (Dotremont *et al.*, 2010).

Modified Air Gap Membrane Distillation (MAGMD) - Chouikh *et al.* (2005) developed a mathematical model and performed an experiment for seawater desalination using a modified air gap membrane distillation. Instead of using the stagnant air between the condensing surface and membrane, the air was moved and heated by using electrical resistance. However, electrical driven MD processes have poor efficiency because it is highly inefficient to convert the high quality of electrical energy to low grade heat. Self-heating membranes using carbon nanotube (CNTs) resistive heating are capable to improve the energy efficiency of MD process (Boo & Elimelech, 2017; Dudchenko et al., 2017). By modifying the air movement the authors utilized both the benefits of low mass transfer resistance of DCMD configuration and low conductive heat loss of AGMD configuration. Due to air flow, the hydrodynamic conditions and the transport phenomena within the air gap ultimately there is increase in permeate flux. The experimental results show that MAGMD produced higher permeate flux relative to the AGMD flux by increasing the feed flow rate at constant temperature of 333 K, air gap 2 mm and at feed concentration of 30,000 ppm. The authors also studied the effect of air gap on AGMD flux. In AGMD the permeate flux decreases with the increase in the air gap width whereas in MAGMD the flux increases with the increase in the air cavity due to enhanced mass transfer coefficient and reduced temperature polarization effect.

Enhancement using Tangent and Rotational Turbulent Inlet Flow –Tian *et al.* (2014) developed a novel technique for enhancement of permeate flux in air gap membrane distillation process. This was achieved by tangent directional and rotational flow of inlet turbulent hot feed and by providing partial contact between the membrane and the condensing plate. By experimental study, the optimum tangential angle was found to be 30^{o} and placement of inlet tubes were at d_i of 0.7d i.e. (inlet flow diameter is) 0.7 times of nominal diameter of the membrane. The optimum area ratio for partial contact was found to be 70-85% .This technique produced 119 kg/m^2h permeate flux for tap water using hot feed temperature at 77 ^{o}C and cold water temperature at 12 ^{o}C which was 2.5 times of conventional AGMD process operating at the same conditions. The reason behind the increase in the flux due to tangential and rotational flow is the increase in mass and heat transfer rates, which reduces the boundary layer thickness and washes the membrane so as to improve the heat and mass transfer efficiencies. The partial contact between the membrane and cooling plate reduces the resistance provided by the air gap and increases the permeate flux.

Different New Enhancement Techniques - Geng *et al.*, (2014) developed a new AGMD module for desalination application, by using hollow fiber membrane and hollow fiber for heat exchange. The effects of operating parameters mainly feed flow rate, feed temperature and feed composition were analysed. The declination in effective driving force as compared to the applied driving force (for mass transfer) was measured using vapour pressure polarization coefficient. The experimental results showed the maximum permeate flux of 5.30 kg/m^2h and 5.70 as GOR (Gained Output Ratio). The authors also developed a mathematical model to evaluate how the temperature and permeate flux change in membrane module. The results produced by the model showed that drop in temperature and permeate flux were much high at upper region of membrane module than the lower part at the feed side.

Warsinger *et al.*, (2014) studied the effect of changing the module inclination angle on AGMD performance under fully developed heat and mass transfer conditions. A flat sheet AGMD module was used for experimental work. The authors found that high module inclination angle have significant effect on the permeate flux. Flux increased by more than 40% when angle was changed by $\pm 90^o$ and increase by less than 5% when the change in the module angle was within $\pm 15^o$. The authors work also indicates two important results i.e. flooding and thermal bridging. Flooding mainly occurred due to large positive or negative angles and when the permeate production rate was very high. Thermal bridging happens due to high negative angle and at this condition condensate gets attach to the membrane surface. Tan *et al.*, (2017) studied numerically and experimentally effects of module orientation and module geometry on the DCMD process permeate flux and concluded that the change in module orientation and geometry improves the DCMD performance.

2.7.1 Heat integration and Renewable/Waste Energy Driven AGMD process

Since, the membrane distillation process is operated at the moderate temperature, neither very high nor very low; therefore it is better to utilize the renewable energy (solar and geothermal energy) and waste energy for the heating purpose. However, due to safety reason and waste disposal problem use of nuclear energy is limited. Osmotic energy or blue energy or salinity gradient energy is an energy obtained by mixing two solution of different salt concentration (Veerman *et al.*, 2010; Tedesco *et al.*, 2015). It is completely renewable and sustainable source of energy having energy potential of about 1.4 - 2.6 TW. From this huge amount of energy around 980 GW is extractable (Veerman *et al.*, 2008, 2010). This osmotic source of energy can be used in combination with MD process for different applications.

Table 2.13 illustrate energy potential and energy cost information about different renewable energy resources (Tomabechi, 2010; Ali *et al.*, 2018).

Table 2.13 : Different Renewable Energy Resources

Types of Renewable Energy	Solar Energy	Geothermal Energy	Blue Energy
Energy Potential (TW h/ year)	12,000 – 40,000	4000 – 40,000	8500
Levelizied Energy Cost ($/ MW h)	80 – 231	116	-

TW h/ year – Terawatt hour / year, $/ MW h - $/ Megawatt hour

The geothermal and solar energy have been successfully used for the MD or AGMD applications because of its thermal driven nature.

Different researchers have explored AGMD processe by utilizing the Solar energy (Banat *et al.*, 2007a; Guillén-Burrieza *et al.*, 2011, 2012; T and Martin, 2014), Geothermal energy (Bouguecha et al., 2005; Jaafar and Sarbatly, 2012) and Waste heat (Jansen *et al.*, 2013; Woldemariam et al., 2017). T and Martin, (2014) performed an experimental analysis for producing drinking water and household hot water by using solar air gap membrane distillation process; 1.5-2 l/h distillate was produced. A pilot plant was also designed in combination of Solar Domestic Hot Water (SDHW) arrangement and membrane distillation system. This plant produced 15 - 40 l/day of pure water beside hot water that is sufficient for five membered family in Middle East and North Africa region (MENA). This plant was specially designed for MENA regions where there are the limited resources of fresh water. In experimental setup of air gap membrane distillation, for the optimum conditions for permeate flux, there was large difference between cold and hot side temperature.

2.8 **Artificial Neural Network (ANN)**

An artificial neural network is a mathematical model or a type of artificial intelligence techniques which is used to solve the linear and non-linear regression problems. The ANN technique based on the working of human brain whose basic building block is neurons, similarly the fundamental part of ANN architecture is artificial neuron (i.e. hidden unit). The ANN generally considered as “Black-Box” model because it does not require understanding of what is happening physically inside the process. Figure 2.5 shows the schematic diagram of artificial neuron.

The ANN model mainly flow the information by 3 steps: First, multiplication in which all the inputs are individually weighted by multiplying with some weight; second, summation in which all the weighted inputs and bias are added; third, activation in which all the combined weighted inputs and bias are allow to pass through the transfer function (i.e. activation function). Liner, threshold function, sigmoid etc. are the some examples of activation functions.

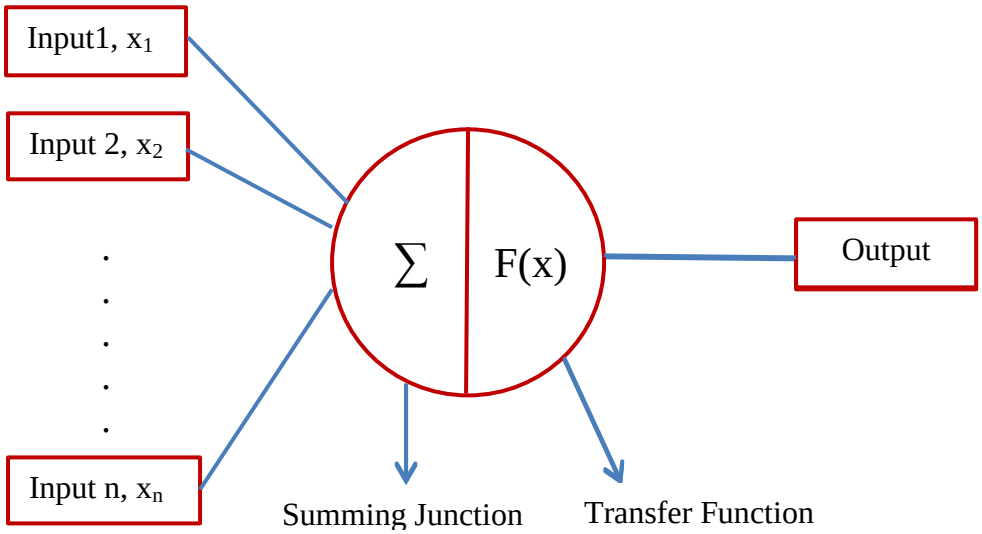

Figure 2.5: Artificial Neuron Design

The summing junction operator consists of external input, weights and bias and it converts all these three parameters into an argument λ which is given as (Khayet and Cojocaru, 2012b) –

$$\lambda = \sum_{i=1}^{n} x_i \cdot w_i + b \qquad (2.6)$$

where w_i are the connection weights, x_i are the input variables and b is the bias. Here i is the index whose value ranges from 1 to n and n is the number of input variables. The activation function or transfer function receives the argument and produces the output.

Figure 2.6 shows the basic neural network structure in which neurons are band together to form the different layers for describing the neurons mathematically (Krenker, Bester and Kos, 2009). These layers are input layer, hidden layer and output layer. The input layer consist of neurons collected from external source, the hidden layer which is situated

between input and output layer and stored the intermediate output, the output layer consist of neurons in the form of final result that to be finally supply to the user.

The ANN architecture or topology depicts that how the individual's neurons are interconnected. Based on the ANN topology, the ANN is primarily classified into two classes; Feed-forward network and Feedback Network or Recurrent Network. In feed-forward network the flow of information is unidirectional i.e. from the input to the output direction while in feedback or recurrent network the flow is bidirectional means the information is flowing not only input to output but also from output to input to vary the input data (Vinícius Gonçalves Maltarollo, 2013).

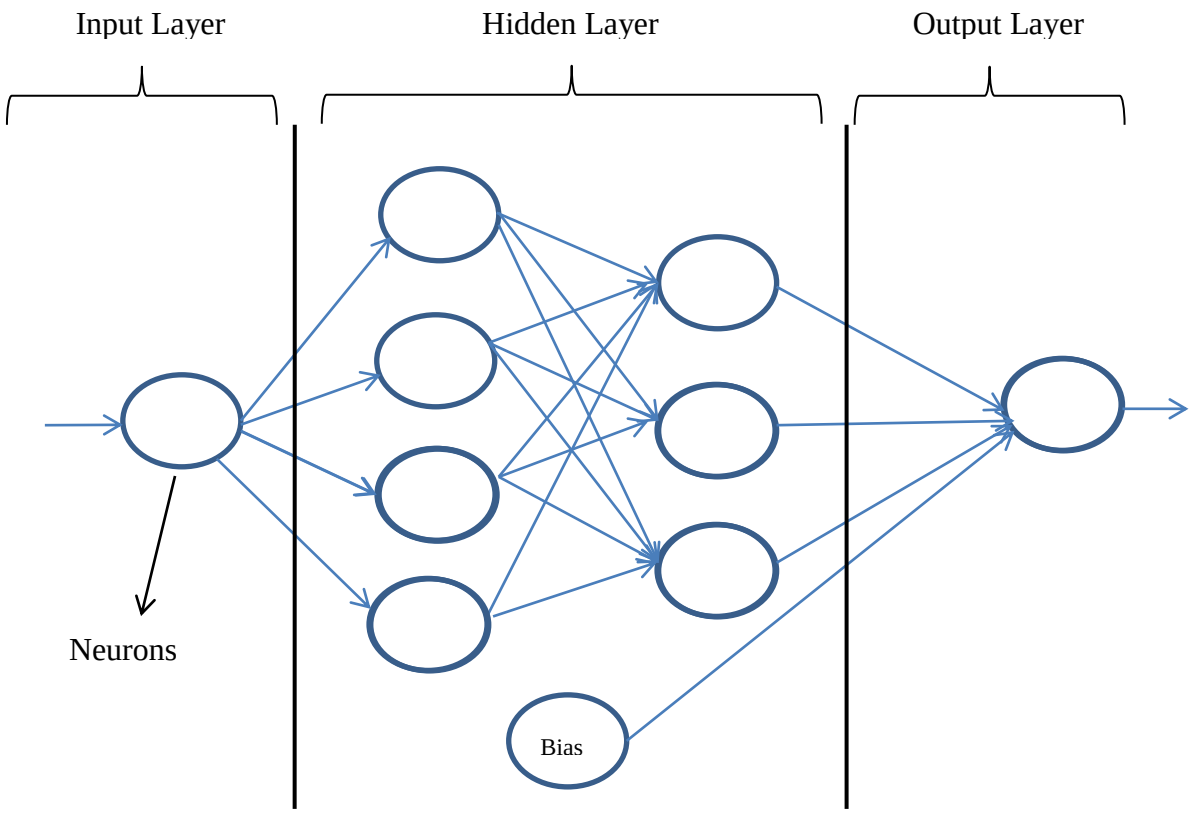

Figure 2.6 : Basic Neural Network Structure (One hidden layer)

Learning

In ANN, the neurons are connected and their strength of connection is presented by weight-value. However, there is no analytical method available to calculate the weight-value, therefore, the training of network must be carried out. The training of network is carried out by an algorithm called as "learning algorithm", in which the optimized value of weight is calculated and network architecture created (Himmelblau, 2000). After learning, the trained neural network should produce the desired result according to the input arrangement. There are mainly three learning methods –

Supervised learning means something directed or guided by a teacher. This learning method consists of different input vector along with the target vector. Different supervised learning systems are feed-forward, functional link, recurrent etc.

Unsupervised learning means learns from the data by recognizing the data pattern without the help of teacher. It is based on Hebb's rule which helps the neural network to remember the specific pattern.

Reinforced learning is a machine learning technique that based on the reinforcement from the external environment. Reinforced learning also requires the teacher as in the case of supervised learning. But teacher in this learning does not give the right answer but only point out that the computed output is correct or not.

Applications

ANN can be used in wide range of fields including medicinal chemistry, biochemistry, food research, pharmaceutical research, military application, financial system, power system, oil and gas exploration, artificial intelligence, etc. (Himmelblau, 2000; Marini *et al.*, 2008). In addition to the above mentioned field the ANN was also used in different areas of membrane technology like microfiltration, nanofiltration, reverse osmosis, membrane distillation, etc. (Khayet and Cojocaru, 2012b).

CHAPTER 3
THEORETICAL CONSIDERATIONS

3.1 **Mathematical Modeling**

Mass transfer in AGMD process has been described mainly by two mathematical models, i.e. Fickian model based on binary diffusion (Banat and Simandl, 1998, 1999, 2000; Abu Al-Rub et al., 2003; Guijt *et al.*, 2005a; Abu *et al.*, 2012; Alsaadi *et al.*, 2013; Cai and Guo, 2017) and Stefan-Maxwell model based on multi component diffusion (Banat *et al.*, 1999c; Banat *et al.*, 1999a; Banat *et al.*, 1999b; Abu *et al.*, 2012). The Stefan-Maxwell model has two types of solution method: exact matrix solution (Krishna and Standart, 1976) and approximate solution (J. A. Wesselingh and R. Krishna, 1990). All these three solution methods have not considered the membrane pore size in modeling equation, but molecule-pore wall collision is as much important as molecule-molecule collision in membranes with very small pore size in the range of 0.20 - 0.30 µm. Therefore, it is important to consider the Knudsen diffusion in modeling equations describing mass transfer. Some authors considered dusty gas model (DGM), which describes molecular, Knudsen and viscous diffusion through the membrane by accounting all the membrane parameters including pore diameter (Guijt *et al.*, 2005a, 2005b). However, one problem associated with application of DGM in MD is that DGM model was initially developed for isothermal flux calculation (Clerk Maxwell., 1860) but MD is a non-isothermal process and DGM applied in MD process by considering certain terms such as thermal diffusion are easily negligible in MD (Lawson and Lloyd, 1997). Since air is insoluble in water, it can be considered as stagnant film and viscous flow can be neglected. Thus, in this work, a mathematical model has been developed by considering both molecular diffusion and Knudsen diffusion. Schofield et al. (1987) conducted a preliminary study to determine the mass transfer coefficient by combined molecular/Knudsen diffusion. But study of effect of different operating parameters was missing.

The mathematic model developed in this study considers the following assumptions:

(a) Feed side membrane surface temperature is different than the bulk feed temperature.
(b) Both the transport mechanisms, i.e. Knudsen diffusion and molecular diffusion have been considered for calculating the permeate flux.
(c) The electrolyte NRTL model has been considered as a thermodynamic model for flux calculation and tailoring NRTL parameters to activity coefficients

(d) Thermodynamic properties as function of temperature.

(e) Steady state heat transfer.

(f) Air is considered as stagnant.

Calculation of Knudsen Number

To decide the transport mechanism in the membrane pores, it is necessary to calculate the Knudsen number. Knudsen number is the decision parameter used to determine the mass transfer mechanism within the membrane pores given by:

$$N_{kn} = \frac{\lambda}{d_p} \tag{3.1}$$

Where, λ is the mean free path of volatile components in the vapor phase inside the membrane pores. The Schematic of Knudsen and molecular diffusion is presented in the Figure 3.1.

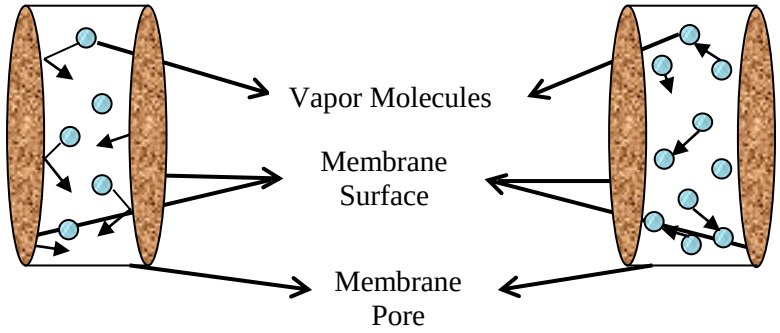

Figure 3.1: Schematic Representation of (a) Knudsen Diffusion (b) Molecular Diffusion, through the Membrane Pores

For binary component, λ is given by (Khayet and Matsuura, 2011) :

$$\lambda_{i/j} = \frac{k_B T_m}{\pi P_m \left(\frac{\sigma_i + \sigma_j}{2}\right)^2} \frac{1}{\sqrt{1 + \frac{M_j}{M_i}}} \tag{3.2}$$

Here, i and j denotes components HCl and Water and P_m is mean pressure in the membrane pores.

(i) If $Kn < 0.01$ or $d_p > 100\lambda$, the mass transfer mechanism within the membrane pores is mainly due to the molecular diffusion.

(ii) If $Kn > 10$ or $d_p < 0.1\lambda$, the mass transfer mechanism is due to Knudsen diffusion because the molecule-pore wall collisions govern the process than the molecule-molecule collisions.

(iii) In transition state, $0.01 < Kn < 10$ or $0.1\lambda < d_p < 100\lambda$, the mass transfer mechanism is governed by both molecular diffusion and Knudsen diffusion.

At 50 ^{o}C feed temperature and 3 mm air gap, the Knudsen number was found 1.6 i.e. 0.01 < 1.6 < 10, therefore mass transfer in membrane pores is due to both, molecular diffusion and Knudsen diffusion.

Calculation of Rayleigh Number

Mass transfer in the air gap may occur either due to molecular diffusion or due to convection. In most of the AGMD studies, the effect of natural convection through the air gap has been considered negligible. The convection direction is subject to the position of the air gap with reference of the gravity. The parameter which decides the transfer mechanism in the air gap is the Rayleigh number and the intensity of convection is directly proportional to this dimensionless number. The dimensionless Rayleigh number is given as (MacGregor, R. K., and Emery, 1969):

$$N_{Ra} = \frac{g\beta\Delta T_m b^3}{\nu_a k_a} \tag{3.3}$$

Here, ΔT_m is the temperature difference between membrane surface and cooling plate

For Ra < 1000, natural convection can be neglected as compared to the heat transfer by conduction (MacGregor, R. K., and Emery, 1969) . Alklaibi and Lior (2005) studied the transport analysis of AGMD and found that for Rayleigh number very less than its critical value (<<1000), the natural convection is negligible in all AGMD configurations. MacGregor and Emery,1969 concluded that for very high rayleigh number (Ra ≥ 1000), the dominate mechanism of heat transfer is convection. Bougecha, Chouikh and Dhahbi, (2002) carried out numerical study of coupled heat and mass transfer in AGMD processes and observed that for smaller air gaps (b < 5mm), the heat transfer by natural convection is negligible.

At 50 ^{o}C feed temperature and 3 mm air gap, Rayleigh Number was found 62.6 i.e. 62.6 < 1000, therefore mass transfer in in air gap occurs only by Molecular diffusion and mass transfer by natural convection can be overlooked (Khayet and Matsuura, 2011).

Thus, mass transfer in the membrane pores and in air gap is given by:

$$N_i = N_{i,K-d} + N_{i,M-d} \tag{3.4}$$

Mass transfer within the membrane pore by Knudsen diffusion is given by (Khayet and Matsuura, 2011):

$$N_{i,K-d} = \frac{4d_p\varepsilon}{3b\tau}\sqrt{\frac{1}{2\pi RM_iT_{fm}}}\left(P_{i,mf} - P_{i,pg}\right) \tag{3.5}$$

Mass transfer governed by the Molecular diffusion through the membrane pore is (Khayet and Matsuura, 2011):

$$N_{i,M-d} = \frac{\varepsilon D_{ia}P_{mf}}{RT_{fm}b'|P_a|_{ln}}\left(P_{i,mf} - P_{i,pg}\right) \tag{3.6}$$

Combining equations (3.4) – (3.6) results into:

$$N_i = \frac{\varepsilon D_{ia}P_{mf}}{RT_{fm}b'|P_a|_{ln}}\left(P_{i,mf} - P_{i,pg}\right) + \frac{4d_p\varepsilon}{3b\tau}\sqrt{\frac{1}{2\pi RM_iT_{fm}}}\left(P_{i,mf} - P_{i,pg}\right) \tag{3.7}$$

Here, since both the HCl and water are volatile in nature, therefore, flux is calculated separately for both the components and finally total flux is calculated as:

$$N_{Total} = N_{HCl} + N_{H_2O} \tag{3.8}$$

$p_{a_{lm}}$is the log mean partial pressure difference of stagnant component which is given as (Khayet and Matsuura, 2011):

$$p_{a_{lm}} = \frac{p_{a,2} - p_{a,1}}{ln\frac{p_{a,2}}{p_{a,1}}} \tag{3.9}$$

$p_{a,1}$ and $p_{a,2}$ are the air pressures at $z = 0$ and $z = b'$.

The partial pressure (P) of the HCl and water at the feed side membrane surface and permeate side membrane surface is computed by (Banat and Simandl, 1999):

$$P' = \gamma_i x_i P^o \tag{3.10}$$

The vapor pressure (P^o) of HCl and water is calculated by Antoine equation (Banat and Simandl, 1999):

$$ln\, P^o = A - \frac{B}{T + C} \tag{3.11}$$

Where, *A*, *B*, and *C* are Antoine constants.

Activity coefficients γ_i for binary mixture is computed from electrolyte NRTL (e-NRTL) thermodynamic model (Chen *et al.*, 1982).

$$ln\,(\gamma_c^*) = \frac{\tau_{c,s} x_s^2 G_{c,s}}{\left(x_a G_{c,s} + x_c G_{c,s} + x_s\right)^2} + \frac{\tau_{s,c} Z_c x_s G_{s,c}}{x_a + x_s G_{s,c}} - \frac{\tau_{s,c} Z_a x_a x_s G_{s,c}}{\left(x_c + x_s G_{s,c}\right)^2} - \tau_c G_{c,s} - \tau_{s,c} Z_c \tag{3.12}$$

$$ln\,(\gamma_a^*) = \frac{\tau_{c,s} x_s^2 G_{c,s}}{\left(x_a G_{c,s} + x_c G_{c,s} + x_s\right)^2} + \frac{\tau_{s,c} Z_a x_s G_a}{x_c + x_s G_{s,c}} - \frac{\tau_{s,c} Z_c x_c x_s G_{s,c}}{\left(x_a + x_s G_{s,c}\right)^2} - \tau_c G_{c,s} - \tau_{s,c} Z_a \tag{3.13}$$

$$G_{c,s} = exp\left(-\alpha \tau_{c,s}\right) \quad \& \quad G_{s,c} = exp\left(-\alpha \tau_{s,c}\right) \tag{3.14}$$

$$\tau_{s,c} = \frac{g_{s,c} - g_{a,c}}{RT} \quad \& \quad \tau_{s,c} = \frac{g_{a,s} - g_{s,s}}{RT} \tag{3.15}$$

Here, x_s, x_c and x_a are the mole fractions of solvent, cation, and anion species, respectively. α is a non-randomness factor and has fixed value of 0.2. $\tau_{c,s}$ and $\tau_{s,c}$ are NRTL parameters. $g_{s,c}$, $g_{a,c}$, and $g_{a,s}, g_{s,s}$ are interaction energies between a solvent molecule and cation, between anion and cation, between anion and solvent molecule and between solvent molecule and another solvent molecule, respectively.

The interfacial temperature at the membrane surface where evaporation occurs and at the condensing surface is calculated by executing energy balances on the different heat transfer region as mentioned in Figure 2.1.

Region 1 **–** At steady state condition, heat transfer through region 1 is given by Equation (3.16) (Banat and Simandl, 1999):

$$q_1 = h_{hot}(T_b - T_m) \tag{3.16}$$

where h_{hot} is film heat transfer coefficient at the feed side and could be estimated from various heat transfer correlation. T_b & T_m are the bulk feed temperature and the feed side membrane surface temperature, respectively. Heat flux is denoted by q.

Region 2 **–** In this region the total heat flux is made up of two parts (Bougecha, Chouikh and Dhahbi, 2002):

(i) Sensible heat flux, q_s and (ii) Heat flux due to liquid vaporization at the membrane surface or latent heat flux

Sensible heat flux mainly contains the following two components (Bagucha, 2000) -

(a) Sensible heat carried by conduction with no mass transfer.

(b) Sensible heat carried by vapors i.e. transferring species.

In equation (3.17) sensible heat flux denoted by q_s and $\sum N_i\lambda_i$ represents latent heat flux.

$$q_2 = q_s + \sum N_i\lambda_i \tag{3.17}$$

$$q_2 = h\left(T_m - T_p\right) + \sum N_i\lambda_i \tag{3.18}$$

Where N_i is the mass flux of the i^{th} component. λ_i is the latent heat of vaporization of component i, h is the film heat transfer coefficient and T_p is the permeate side membrane surface temperature. h can be calculated from equation no. (3.19):

$$h = h_a \frac{\theta}{1 - e^{-\theta}} \tag{3.19}$$

$$h_a = \frac{k}{b} \tag{3.20}$$

where, h_a is the heat transfer coefficient in the vapor phase, b is the air gap thickness, k is the gas phase thermal conductivity and θ is the dimensionless heat transfer factor and given as (Banat and Simandl, 1999) :

$$\theta = \frac{\sum N_i \, \Delta H_i}{h_a} \tag{3.21}$$

ΔH_i is the specific heat of component i in the gas phase. $\frac{\theta}{1-e^{-\theta}}$ is the Akerman correction factor accounts for sensible heat transferred by diffusing species. If there is no condensation, this factor becomes equal to 1 and increases from the value of 1 as evaporation rate increases.

Region 3 – Heat flux in region 3 is given by (Banat and Simandl, 1999):

$$q_3 = h_{cold} \left(T_p - T_c\right) \tag{3.22}$$

Here, T_c is the cooling water temperature. h_{cold} is the total heat transfer coefficient for region 3 and is calculated from given equation:

$$h_{cold} = \left(\frac{1}{h_d} + \frac{l}{k_c} + \frac{1}{h_{c,f}}\right)^{-1} \tag{3.23}$$

Where, $h_{c,f}$ is the coolant film heat transfer coefficient, l is the cooling plate thickness, k_c is the cooling plate thermal conductivity and h_d is the condensate liquid heat transfer coefficient and is calculated by equation below:

$$h_d = 0.943 \left[\frac{\rho^2 g \lambda k_l^3}{\mu L \Delta T}\right]^{1/4} \tag{3.24}$$

Where, g is the gravitational acceleration, k_l, ρ and μ are the fluid thermal conductivity, the density and the viscosity at the permeate side condensate temperature, respectively. L is the cooling plate height.

The interface temperature T_{fm} and T_p can be calculated from equations (3.16), (3.18) and (3.22) given as:

$$T_{fm} = T_b - \frac{U_t}{h_{hot}} \left\{ (T_b - T_c) + \frac{\sum N_i \lambda_i}{h} \right\} \tag{3.25}$$

$$T_p = T_c + \frac{U_t}{h_{cold}}\left\{(T_b - T_c) + \frac{\sum N_i \lambda_i}{h}\right\} \tag{3.26}$$

Where,

$$U_t = \left(\frac{1}{h_{hot}} + \frac{1}{h} + \frac{1}{h_{cold}}\right)^{-1} \tag{3.27}$$

$$Nu = 1.86 * (Re * Pr)^{1/3}(d_h/L)^{1/3}\,(\mu/\mu_m)^{0.14} \tag{3.28}$$

$$Re = \frac{\rho v d_h}{\mu}, \qquad Nu = \frac{h_{hf} d_h}{k}, \qquad Pr = \frac{C_p \mu}{k} \tag{3.29}$$

Here d_h is the hydraulic diameter defined as:

$$d_h = \frac{4A}{W}$$

Where A is the cross sectional area and W is the wetted perimeter.

Diffusion coefficient of components in air has been calculated by using Fuller correlation (Fuller et al., 1966). Use of this correlation was also recommended by Poling et al., (1987) and also by Banat *et al.*, (1999b) to study the effect of inert gases on breaking azeotropic point. According to Fuller correlation, the relation of diffusion coefficient to temperature and pressure can be elucidated by:

$$D_{ij(T_2,P_2)} = D_{ij(T_1,P_1)}\left(\frac{T^{1.75}}{T_1}\right)\left(\frac{P_1}{P}\right) \tag{3.30}$$

The value of different heat transfer coefficients i.e. h_{hot}, h_a and h_{cold} is computed to be 390 W/m^2·K, 36 W/m^2·K and 35 W/m^2·K, respectively at feed temperature 50 ^{o}C, feed flow rate 2 lpm, air gap width 5 mm, cooling water temperature 20 ^{o}C, cooling water flow rate 1 lpm. Eqs. (3.7) to (3.15), Eqs. (3.19) to (3.21) and Eqs. (3.23) to (3.29) were solved numerically in MATLAB to estimate the permeate flux and interfacial temperatures. It is assumed that there is well mixed layer at the membrane interface because concentration and temperature at the interface are unknown. The interfacial concentration, temperature and ultimately the permeate flux are calculated iteratively.

3.2 **COMSOL Modeling for Interfacial Membrane Temperature Estimation**

A complete 2-D model for AGMD process having HCl-Water as feed was simulated by using COMSOL Multiphysics® software. Figure 3.2 shows the module domain used for simulation study. The AGMD module dimension and operating parameters used for the simulation study are mentioned in Table 3.1 and Table 3.2, respectively.

Table 3.1: Module Dimensions

Domain	Dimensions (cm)
1	a =13
2	b = 150 (μm)
3	c = 0.5
4	d = 13

Table 3.2 : Operational Parameters Used for the Simulation Study

Parameter	Value
Hot feed inlet temperature	50 ^{o}C
Coolant inlet temperature	20 ^{o}C
Hot feed flow rate	2 L/min
Coolant flow rate	1 L/min
Membrane Material	PTFE
Thermal conductivity of membrane material	0.28 W/m·K
Membrane porosity	0.85
Diffusivity of HCl in air	3.6510×10^{-5} m^2/s
Diffusivity of water in air	5.3065×10^{-5} m^2/s

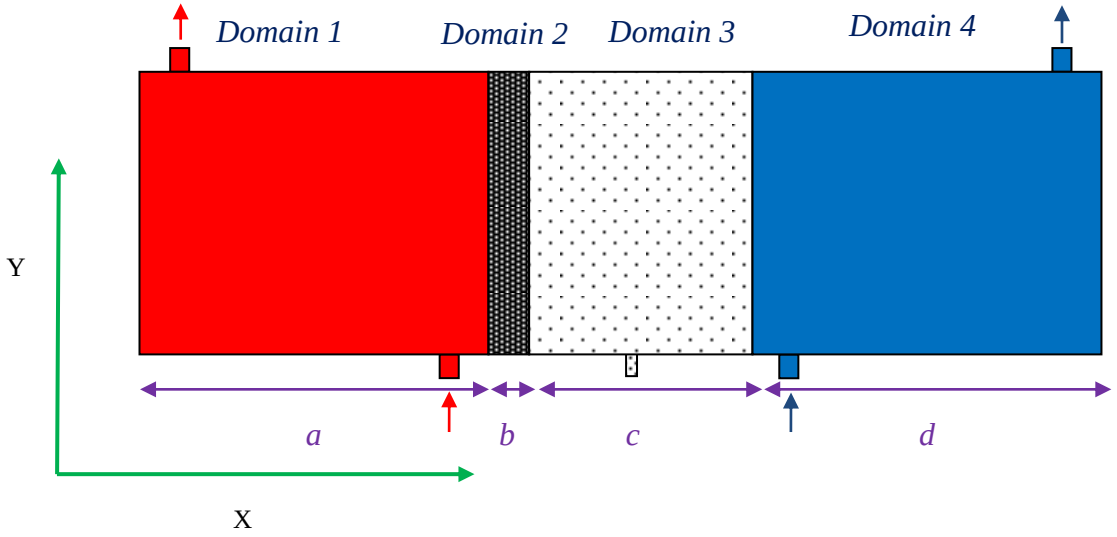

Figure 3.2 : Module Domain Used for AGMD Modeling
Domain 1 – Hot feed section with feed input and output sections, Domain 2 – Membrane, Domain 3 – Air gap, Domain 4 – Coolant flow Section with coolant input and output sections

3.2.1 Model Equations

The equation for heat transfer in both feed side and cooling water side is given by both conduction and convection mechanism.

The model equation for heat transfer in feed side is given by:

$$\rho_h C_{ph} u_h . \nabla T_h = \nabla . (k_h \nabla T_h) \tag{3.31}$$

Here , ρ_h, C_{ph} and k_h are the density, specific heat capacity at constant pressure and thermal conductivity of HCl feed solution at azeotropic composition, respectively. u and T_h are the velocity and temperature of the hot feed solution. Similarly, for the cooling side, the model equation is given by –

$$\rho_c C_{pc} u_c . \nabla T_c = \nabla . (k_c \nabla T_c) \tag{3.32}$$

Here, ρ_c, C_{pc} and k_c are the density, specific heat capacity at constant pressure and thermal conductivity liquid, respectively. u and T_c & are the velocity and temperature of the cooling liquid i.e. water, respectively. Velocity u has been calculated by the using Navier - Stokes equations at both feed side and cooling water section side:

$$\rho_h \frac{\partial u_h}{\partial t} + \rho_h (u_h . \nabla) u_h = -\nabla . p_h + \nabla . [\mu (\nabla u_h + (\nabla u_h)^{T_h})] + F \tag{3.33}$$

$$\rho_c \frac{\partial u_c}{\partial t} + \rho_c (u_c . \nabla) u_c = -\nabla . p_c + \nabla . [\mu (\nabla u_c + (\nabla u_c)^{T_c})] + F \tag{3.34}$$

$$\nabla . u_h = 0 \tag{3.35}$$

$$\nabla . u_c = 0 \tag{3.36}$$

Since there is no external force and time independent study was carried out so equation (3.33) and (3.34) reduced to:

$$\rho_h (u_h . \nabla) u_h = -\nabla . p_h + \nabla . [\mu_h (\nabla u_h + (\nabla u_h)^{T_h})] \tag{3.37}$$

$$\rho_c (u_c . \nabla) u_c = -\nabla . p_c + \nabla . [\mu_c (\nabla u_c + (\nabla u_c)^{T_c})] \tag{3.38}$$

Here p is the pressure and μ_h and μ_c are the viscosity of hot HCl feed solution and coolant, respectively.

The temperature profile through the membrane is estimated only by conduction mechanism. The heat transfer equation for the conduction is given by:

$$\nabla . (k_{mem} \nabla T_{mem}) = 0 \tag{3.39}$$

k_{mem} is the membrane thermal conductivity calculated by $k_m = \varepsilon k_p + (1 - \varepsilon) k_s$. Here, k_p and k_s is the thermal conductivity of HCl-Water vapor through the membrane pores and through the solid membrane surface, respectively. T_{mem} is the temperature within the membrane.

The diffusional equation for the mass transfer is obtained by the simplifying the continuity equation.

$$\nabla . (D_i \nabla C_i) = 0 \tag{3.40}$$

Here i denotes the component, i.e. HCl or Water vapour, which pass through the membrane pores. D_i is the diffusivity for i^{th} component and C_i is the concentration of i^{th} component inside the membrane.

3.3 **Model for Recovery Calculation**

A mathematical model developed by Upadhyaya *et al.*, (2015) was considered for the HCl recovery calculation. The block diagram for recovery calculation is shown in Figure 3.3.

Overall material balance in AGMD membrane module is given as:

$$Q_F = Q_R + Q_p \tag{3.41}$$

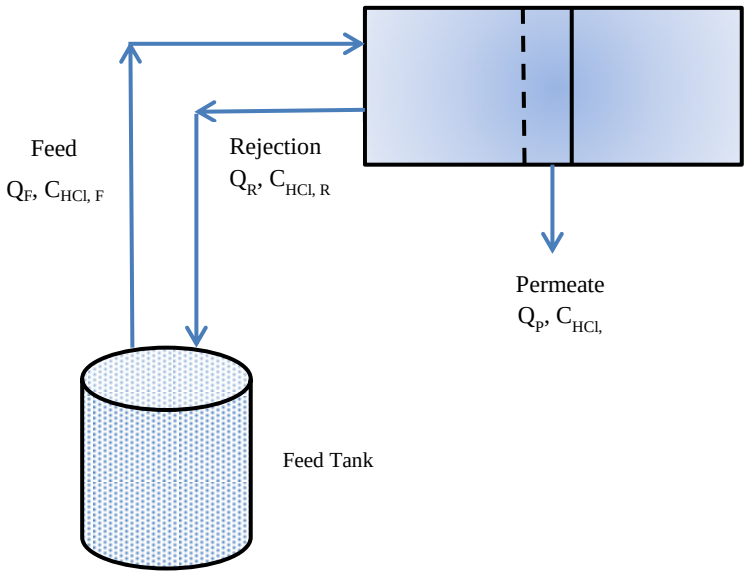

Figure 3.3: A Block Diagram of AGMD Setup for Recovery Calculation

Overall material balance in feed chamber written as:

$$dV/_{dt} = Q_R - Q_F \tag{3.42}$$

HCl material balance in feed chamber is given as:

$$\frac{dC_{HCl,F}}{dt} = \frac{(C_{HCl,R} - C_{HCl,F})Q_R}{V} \tag{3.43}$$

HCl material balance in membrane module:

$$\frac{d(C_{HCl,R}V_m)}{dt} = Q_F C_{HCl,F} - Q_R C_{HCl,R} - Q_p C_{HCl,p} \tag{3.44}$$

Where, Q_F, Q_R and Q_P are the feed, retentate and permeate volumetric flow rates (m^3/h), respectively. $C_{HCl,F}$, $C_{HCl,R}$ and $C_{HCl,p}$ are the mass concentration (kg/m^3) of HCl in feed, retentate and permeate, respectively.

The equation used for calculating Partial HCl flux and total flux is given as:

$$N_i = \frac{\varepsilon D_{ia} P_{mf}}{RT_{fm} b' |P_a|_{ln}} \left(P_{i,mf} - P_{i,pg}\right) + \frac{4 d_p \varepsilon}{3 b \tau} \sqrt{\frac{1}{2\pi R M_i T_{fm}}} \left(P_{i,mf} - P_{i,pg}\right) \tag{3.45}$$

In equation (3.44) Q_p and $C_{HCl,p}$ was calculated by the following equations:

$$Q_p = \frac{N_T M_{avg} A}{\rho_p} \tag{3.46}$$

$$C_{HCl,p} = \left(\frac{N_{HCl}}{N_T}\right)\left(\frac{M_{wt,HCl}}{M_{wt,Total}}\right)\rho_p \quad (3.47)$$

Where, i is the index for component HCl and Water, ε is membrane porosity, D_{ia} is the diffusivity of component i into air (m^2/s), d_p is membrane pore diameter (m), b is air gap thickness (m), τ is membrane tortuosity, R is universal gas constant (J/mol·K), M_i is molecular weight of component i, T_{fm} is feed side membrane surface temperature, $b' = \delta\tau + b$ is total thickness for mass transfer (m) , $P_{i,mf}$ and $P_{i,pg}$ are the partial pressures of component i at feed side membrane surface and cooling plate side (Pa), respectively, $|P_a|_{ln}$ is the log mean partial pressure difference of stagnant component air, ρ_m is the density of permeate solution (kg/m^3) , N_{HCl} and N_T are the HCl partial flux and total permeate flux ($kg/m^2 \cdot h$), respectively.

Ordinary Differential (OD) model equations number (3.42), (3.43) and (3.44) were solved in MATLAB using ODE solver to determine the change in retentate concentration with time and recovery at different feed bulk temperature 40 °C, 45 °C and 50 °C.

3.4 **ANN Modeling**

ANN model was developed using MATLAB software of version 8.4.0 (R2014b). MATLAB is a data mining tool which consists of NNTOOL for ANN modeling. NNTOOL used for training and testing the data by writing a script using back propagation algorithm. The script already consists of collection of hidden layer, number of neurons in hidden layers etc.

The performance function used for the ANN is Mean Squared Error (MSE) which is calculated by the given equation (Khayet and Cojocaru, 2012b):

$$MSE = \frac{1}{n}\sum_{i=1}^{n}\left(N_{exp} - N_{pred}\right)^2 \quad (3.48)$$

Here N_{exp} and N_{pred} are the permeate flux measured experimentally and permeate flux predicted by ANN model, respectively. n is the number of data points used for the modeling and i is the integer index. The neural networks are trained by using back propagation algorithm which used the gradient descent iterative method for modifying the weights and biases. The iteration for back propagation algorithm is given as (Khayet and Cojocaru, 2012b):

$$\boldsymbol{W}_{New} = \boldsymbol{W}_{old} - \eta.\ \boldsymbol{grad}(MSE) \quad (3.49)$$

Here, $\boldsymbol{W}$ is vector of weights and biases and η is learning rate.

NNTOOL mainly consist of 2 graphical user interfaces (GUIs), First; Network/Data Manager GUI, as shown in Figure 3.4, used to create the network and Second; Network GUI, as shown in Figure 3.5, used for the training the network data.

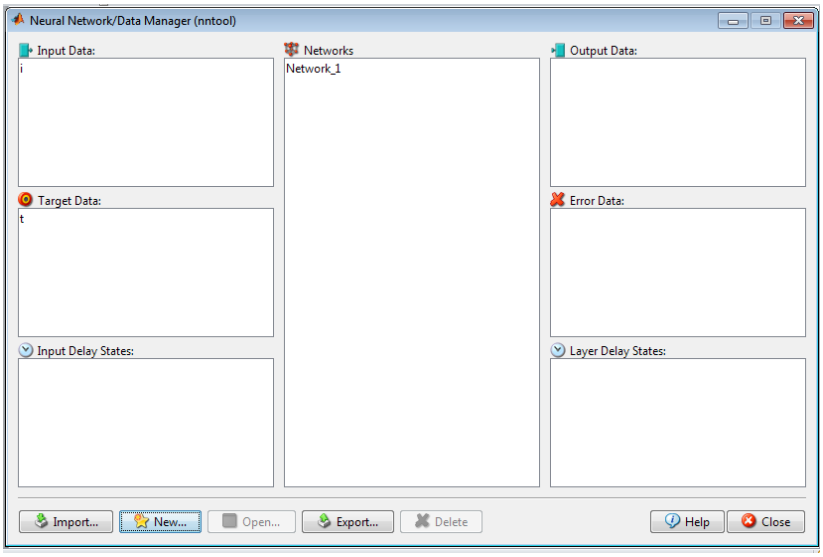

Figure 3.4: Network/Data Manager GUI of NNTOOL

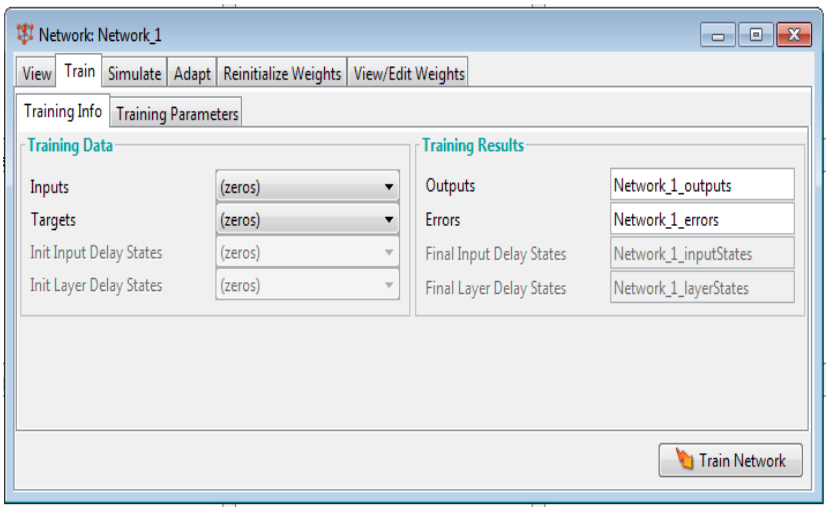

Figure 3.5: Generated Network GUI

Five inputs namely bulk feed input temperature, feed flow rate, air gap width, cooling water temperature and cooling water flow rate were selected for ANN modeling and permeate flux was set as target value.

The generated ANN architecture with hidden and output layer is shown in Figure 3.6.

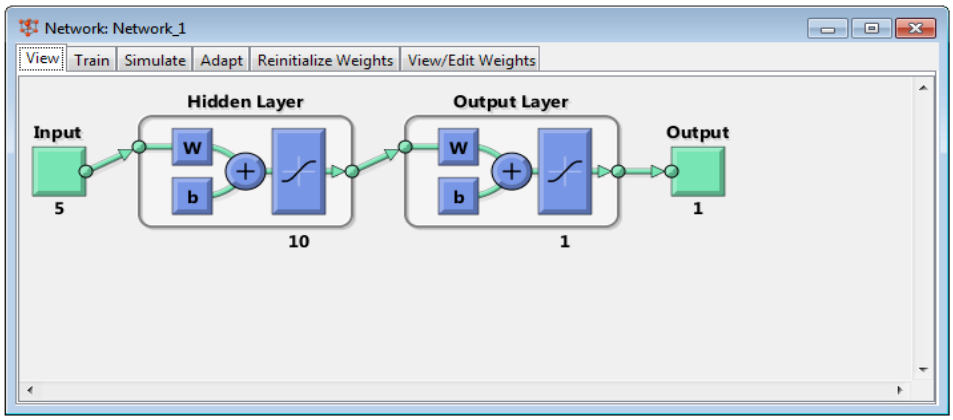

Figure 3.6: ANN Architecture Used for ANN Modeling

CHAPTER 4

EXPERIMENTAL

This chapter covers the thorough description of chemicals and equipment used for the study along with membrane characterization methods.

4.1 Materials Used For Experiments

4.1.1 Distilled Water

Distilled water produced in laboratory was used for the preparation of feed solution of HCl/Water. The main properties of water are listed in Table 4.1 (K.A. Sharp, 2001).

Table 4.1: Physical and Chemical Properties of Water

Properties	Specifications
Molar Mass	18.051 g/mol
Physical Appearance	White solid or almost colourless, transparent liquid
Density	1 gm/cm^3
Melting Point	0 ^{o}C or 273.15 K
Boiling Point	99.98 ^{o}C or 373.13 K
Viscosity	0.001 Pa·s at 20 ^{o}C

4.1.2 Hydrochloric Acid

Hydrochloric acid is an important chemical used in different applications. The major industrial use of hydrochloric acid is in steel industries to remove rust or scale from steel surface, in production of numerous organic and inorganic chemical, used as food additive in food industries, oil-field acidizing i.e. during oil production, the hard rocks are removed by pouring hydrochloric acid, in mining industries, used to regulate the pH of the solutions, leather tanning industries, used as cleaning agent for household items, production of drinking water, used in pharmaceutical industries as catalyst and as reduction agent, used in dye manufacturing etc.

Certified ACS grade HCl (Fisher Scientific, Mumbai, India) was used for the preparation of hydrochloric acid/water solution of 20.2 mass% azeotropic concentration. The physical properties of hydrochloric acid are mentioned in Table 4.2 (Shreve, 1956).

Table 4.2 : Properties of Hydrochloric Acid

Properties	Specifications
Chemical Formula	HCl
Molar Mass	36.47 g/mol
Physical Appearance	Clear, colourless or slightly yellowish corrosive liquid with highly pungent odour
Different Concentration Grade Available	Fuming Hydrochloric Acid - About 38% Industrial Grade - 30% to 35% Commercial Grade - 20% to 32% Household Grade - 10% to 12%
Boiling Point (B.P), Melting Point (M.P), Density and Viscosity	Since different concentration grade of HCl are available therefore its B.P, M.P, density and viscosity vary accordingly

4.1.3 Inert Gas (Argon)

The effects of inert gases on the azeotropic mixture separation have been studied by using argon as inert gas. Argon has been selected for the study because it is relatively cheap, easily available, can be used safely without distresses the environment and it is chemically inert for most of the materials. Argon gas is stored in high pressure cylinders in liquid form. The picture of argon cylinder along with pressure regulator used for the study is supplied by Green Checks Private Ltd., Jaipur, India. Argon gas used in different applications including metal fabrication processes such as arc welding, used as preservatives to increase the shelf-life of products, in air free laboratory equipment's such as gas chromatography and in Scanning Electron Microscopy (SEM) for sputter coating, in lightening industries to fill the bulbs and also used in combinations with other gases to create the neon lights etc. The physical and chemical properties of argon gas are shown in Table 4.3 (Sismanoglu *et al.*, 2013).

Table 4.3 : Physical and Chemical Properties of Argon Gas

Properties	Specifications
Chemical Formula	Ar
Molar Mass	39.948 g/mol
Physical Appearance	Colourless, odourless, nontoxic noble gas, heavier than air
Water Solubility	Approx. 40 mg/L (At 25 ^{o}C temperature and 1 bar pressure)
Boiling Point	87.302 K
Melting Point (M.P)	83.81 K
Density	1.784 g/L

4.1.4 Membrane

Hydrophobic, microporous, flat-sheet polytetrafluroethylene (PTFE) membrane supplied by Millipore was used for the test study. The membrane properties used for the investigation are given in Table 4.4. The values depicted in the table have been provided by the manufacturer i.e. Millipore.

Table 4.4 : Membrane Properties

Properties	Value
Material	PTFE
Membrane Diameter (mm)	90
Effective Membrane Diameter (mm)	55
Nominal Pore Size (µm)	0.22
Thickness (µm)	150
Porosity (%)	85
Maximum Operating Temperature	130 ^{o}C

4.1.5 Instruments and Sensors

The specifications of different instruments and sensors used for the fabrication of experimental setup along with their suppliers are stated in Table 4.5.

Table 4.5 : Specifications of Different Instruments Used in the Experimental Setup

Instruments	Specifications	Supplier/ Manufacturer
Acid Pump	Capacity: 10 L/min Head: 3-4 meter Motor : 0.5 HP, 2900 RPM, 220 v, Electric Motor Casing and Impeller Material: P.P (Inj- Moulded)	Leakless Pumps & Sealings Equipments, Mumbai, India
Cooling Pump	Capacity: 10 L/min Head: 3-4 meter Motor : 0.5 HP	Prasad Overseas, Jaipur, India
Chiller	Capacity – 30 lit Cooling Capacity – 5-25 ^{o}C Material – SS 316	Prasad Overseas, Jaipur, India
Rotameter	Range – 10 L/min	Starflow, India
Thermocouple	J-Type Digital Thermocouples , PT-100	Techno Instruments, Gujrat

4.2 **Experimental Setup**

The performance of AGMD process for HCl/Water azeotropic mixture separation under different operating conditions was assessed using a test-cell module. Figure 4.1 illustrates the schematic diagram of AGMD module and Figure 4.2 shows the picture of fabricated module that was installed in the experimental setup. The test cell module consists of three sections, *viz.*, feed section, air gap/permeate section and cooling section.

Hydrophobic membrane is fixed between feed section and air gap while the condensing plate is set between air gap and cooling section. The feed solution was circulated continuously using an acid pump from the feed tank to the feed section. The feed tank was persistently heated with a heater to maintain the desired feed temperature. Similarly, the cooling water from water chiller was pumped continuously to cooling section. Both feed and cooling water flow rates were maintained by monitoring rotameters. The feed solution

temperature and cooling water temperature at the module entrance were measured using J-Type digital thermocouples. The HCl and water vapors after passing through membrane and air gap get condensed on the condensing/cooling plate. The liquid permeate was collected in the glass receiver.

Argon Gap Rings of different thickness with permeate collector and gas supply connector are depicted in Figure 4.3. Figure 4.4 illustrates the schematic diagram of AGMD setup used for the investigation and Figure 4.5 shows the picture of fabricated setup used for the experimental study.

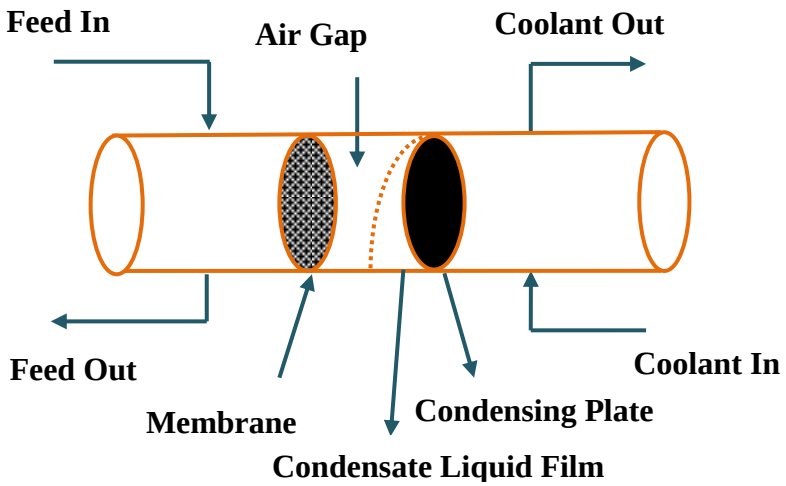

Figure 4.1 : A Schematic Diagram of AGMD Module

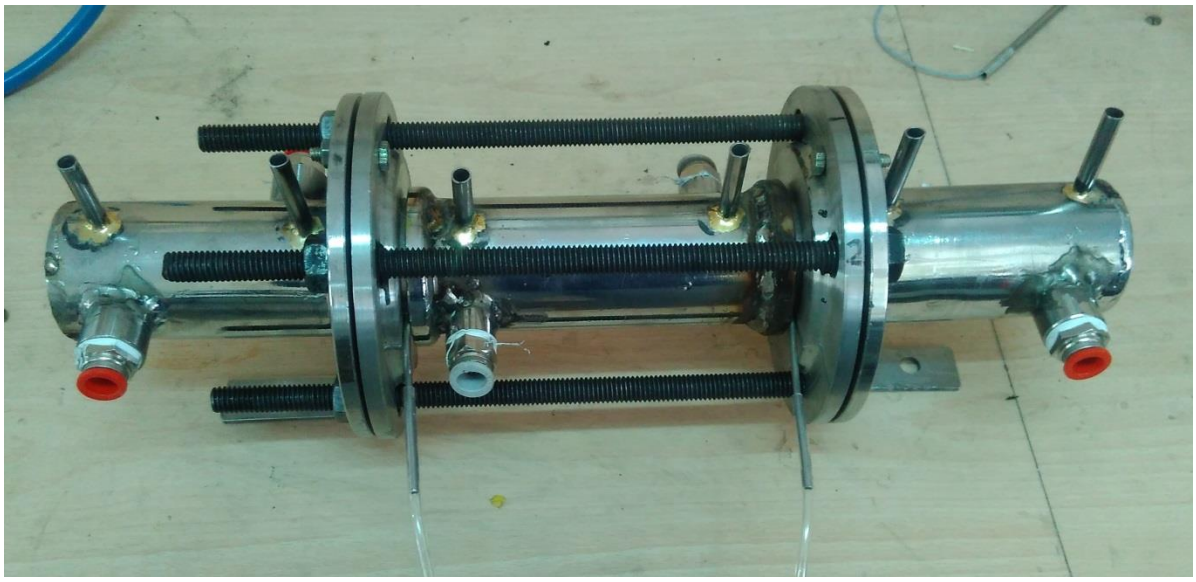

Figure 4.2 : Fabricated AGMD Module

Figure 4.3 : Argon Gap Rings of Different Thicknesses with Permeate Collector and Gas Supply Connector

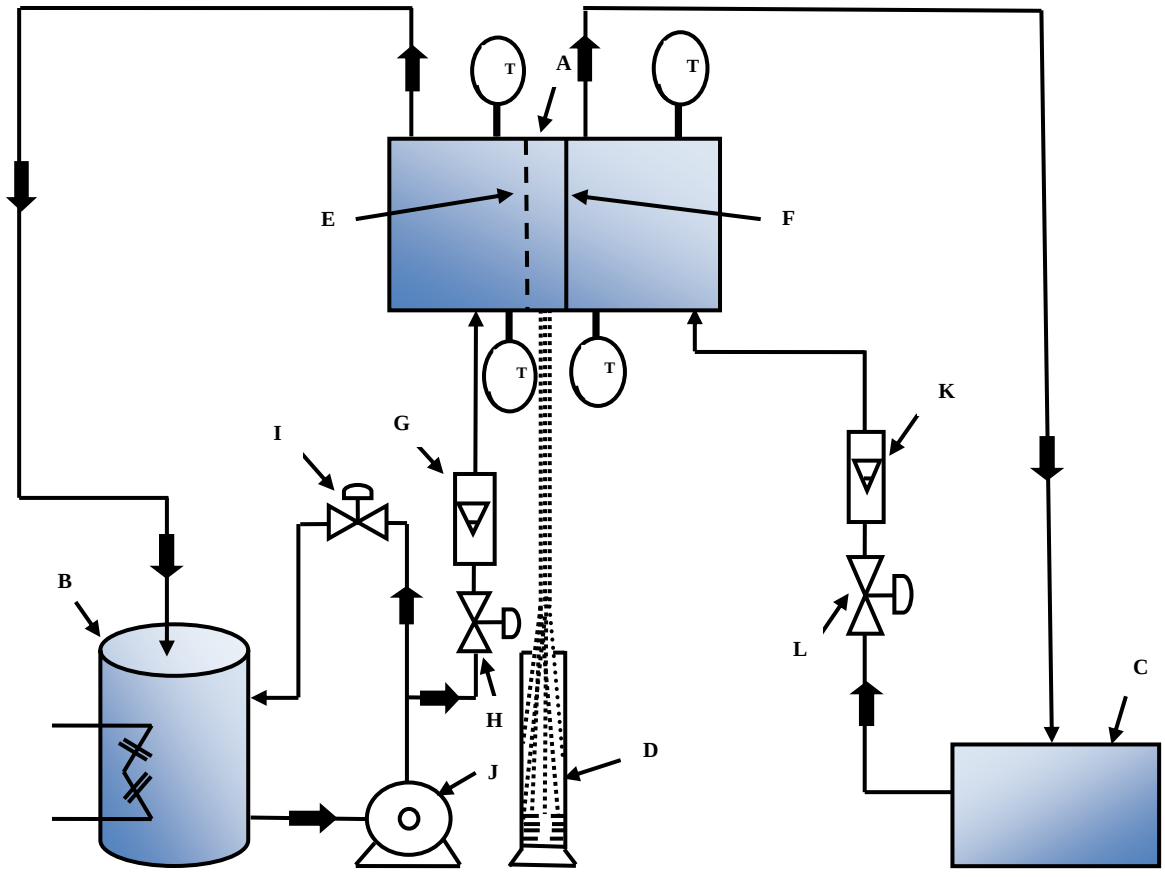

T = Temperature Measuring Instrument Indicator

Figure 4.4 : Schematic Diagram of AGMD Experimental Setup

A-AGMD Module, B-Feed Tank, C-Water Chiller, D-Permeate Receiver, E-Membrane, F-Cooling Plate, G-Feed Flow Rotameter, H-Feed Flow Valve, I- Bypass Valve, J-Acid Pump, K-Coolant Flow Rotameter, L-Coolant Flow Valve

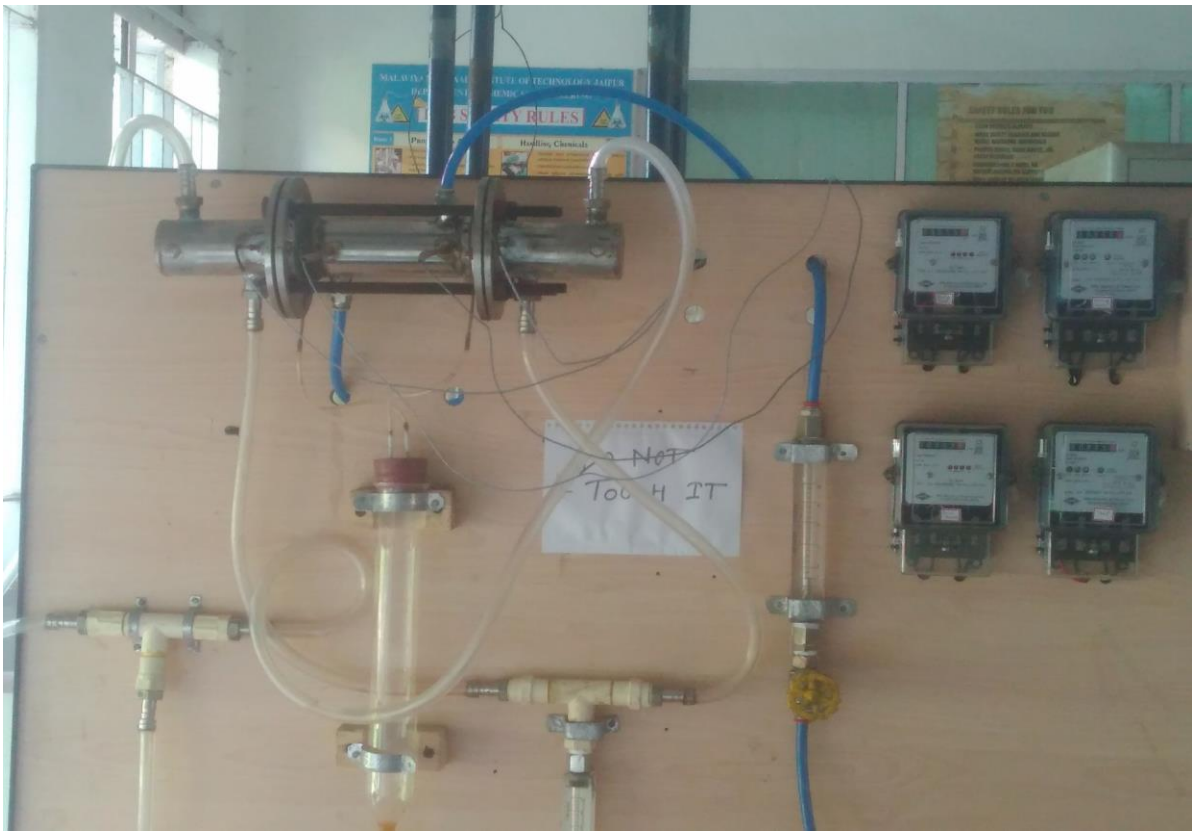

Figure 4.5 : Fabricated Setup Used for the Experimental Study.

4.3 **Experimental Procedure**

The start-up and operating procedure of AGMD process is relatively simple than other separation processes.

(1) Firstly, the feed tank and water chiller were filled up with the feed solution and water, respectively.

(2) The feed solution (HCl/water at azeotropic concentration) was continuously fed to feed section of membrane module using acid pump.

(3) Cooling water fed continuously to the cooling part of membrane module from the chiller using cooling pump.

(4) The rotameters continuously measure the flow rate of feed solution and water and controlled by the globe valves.

(5) The permeate vapors passes through air gap and get condensed when comes in contact with the cooling plate of cooling section.

(6) Permeate was collected in the graduating receiver to estimate the flux.

(7) The volume of permeate collected was measured using measuring cylinder or beaker.

(8) The permeate flux was calculated from the volume of permeate collected as:

$$J = \frac{\text{Permeate Collected in kg/h}}{\text{Membrane Area, } m^2}$$

Here, J= permeate flux measured in $kg/m^2 \cdot h$.

(9) The amount of HCl present in the collected permeate was estimated by the acid-base titration method of chemical analysis.

The experimental errors were determined by performing reproducibility test initially.

4.4 **Testing Conditions and Evaluation Parameters**

4.4.1 Testing Conditions

Table 4.6 elucidated the operating variables or testing conditions and their range used for the complete experimental study.

Table 4.6 : Operating Variables

S. No.	Operating Variable	Range/Type
1.	Feed Temperature	30-50 ^oC
2.	Air Gap Thickness	3-11 mm
3.	Feed Flow Rate	2-6 L/min
4.	Cooling Water Temperature	5-25 ^oC
5.	Cooling water Flow Rate	1- 5 L/min
6.	Inert Gases	Air, Argon
7.	Membrane Characterization	SEM & EDS analysis, Atomic Force Microscopy (AFM) analysis

4.4.2 Evaluation Parameters

The performance of the breaking of azeotropic point of HCl/ water system was measured in terms of permeate flux, HCl selectivity and concentration of HCl in permeate and retentate. The permeate flux calculated as:

$$J = \frac{\text{Permeate Collected in kg/h}}{\text{Membrane Area, } m^2}, \text{kg}/m^2 \cdot \text{h} \qquad (4.1)$$

The degree of separation of any component in MD when both the components are volatile is given by selectivity. Selectivity is defined by:

$$\alpha_{HCl} = \frac{y_{HCl}/1 - y_{HCl}}{x_{HCl}/1 - x_{HCl}} \quad (4.2)$$

Here y_{HCl} and x_{HCl} are mole fraction of HCl in permeate and feed, respectively.
HCl concentration in permeate and retentate was measured to determine whether the azeotrope break or not. Since the HCl/water azeotrope forms at 20.2 mass% HCl concentration therefore in permeate and retentate HCl concentration must be either lower or greater than the 20.2 mass% and measured by the titration method.

The specific energy consumption means total energy consumed in kWh to produce 1 kg of experimental flux and is computed by using equation (4.3) -

$$Specific\ Energy\ Consumption\ = \frac{Total\ Energy\ Consumed(kWh)}{Permeate\ Collected, kg} \quad (4.3)$$

4.5 **Feed and Product Concentration Analysis**

HCl concentration in permeate and retentate was analysed by titration method. Titration is an analytical method of determining the concentration of an unknown sample. In titration the unknown sample is allowed to react with the some standard solution. There are different types of titrations available but in this study acid-base titration was used to determine the HCl concentration. Since HCl is a strong acid therefore it was reacted with the strong base i.e. sodium hydroxide solution (NaOH). When HCl is mixed with the NaOH, they react until the number of moles of base added will be equal to the number of moles of acid. The point where the number of moles of HCl and NaOH becomes equal is known as equivalence point and this point during titration was observed by change in solution colour to pink due to added Phenolphthalein indicator. The neutralization reaction between hydrochloric acid and sodium hydroxide is given as-

$$HCl\ (aq.) + NaOH\ (aq.) \longrightarrow NaCl\ (aq.) + H_2O\ (liq.)$$

4.6 **Membrane Characterization Methods**

4.6.1 Field Emission Scanning Electronic Microscopy (FE-SEM)

In AGMD, the used and fresh membrane was characterized by an electron microscope named as Scanning Electron Microscope (SEM). Scanning Electron Microscope was used to get the topography and cross section of the sample by passing the electron beam through it at different accelerating voltage. The electron beam reacts with the atom of the sample and produce signal in the form of secondary electron, characteristics x-rays, back scattered electrons etc. Firstly, the membrane sample was required to dip into liquid nitrogen for very small time (10-15 sec) so that the sample remain sustain at high vacuum or does not losses water molecules or gases. Since the membrane sample is not electrically conductive so to make it conductive a thin layer of gold was applied on the membrane by sputter coater machine. This pre-treatment step of membrane surface is essential and care must be taken because the chances of membrane surface destruction are more in this step. After that, the membrane sample was cut by sharp scissors and put into the SEM Machine by pasting it on the sample holder using conductive tap.

At last, the membrane sample was examined and captured the SEM images at 10 kV accelerating voltage, at different magnifications and under high vacuum mode. The generated SEM inages was analysed by the Image Processing Software (ImageJ©) (Schneider et al., 2012) to estimate the pore size distribution. The SEM used for the membrane analysis is provided by Material Research Centre, MNIT, Jaipur.

4.6.2 Atomic Force Microscopy (AFM)

The atomic force microscope (AFM) is a scanning probe microscope technique used to characterize the membrane surfaces. The AFM works mainly in three steps; surface sensing, detection and finally imaging. The probe of the AFM which is attached to the cantilever moved on the surface of the sample and measures the force acting between the probe and sample. This force causes the deflection of lever operated by reflecting the laser beam and this reflected laser beam falls on the photo detector for obtaining image resolution. The AFM primarily managed in two ways either contact mode or non-contact mode depending on the type of material tested. In contact mode the tip of the probe is touch to the sample surface while in non-contact manner the tip is vibrate slightly above the sample. In this study the three dimensional (3D) topgraphical image of membrane was obtained by operating the AFM at tapping mode. AFM prefers over SEM analysis, due to no special sample preparation and no damage of membranes occurs as in the case of SEM due to metal coating (Khayet et al., 2004).

CHAPTER 5
RESULTS AND DISCUSSION

5.1 **Taguchi's Optimization**

Taguchi method is a statistical experimental design approach to optimize the process by using the best combination of different factors available at different levels. This approach of the design of the experiment not only determined the effect of various operating factors on process output but also analysed which factor influence the process more and which less. Thus by identifying the right and essential parameters which affects the process more, the operating time for experimental study can be reduced and simultaneously the process performance can be improved (Mohammadi and Safavi, 2009). Taguchi design used a set of the array called as Orthogonal Array (OA) which is the combinations of different controllable factors. The experiments are performed according to the orthogonal matrix because the orthogonal array designed such that, it reduces the effect of variations of uncontrollable factors. In Taguchi method, the controlled factor must be chosen such that it eliminates the effect of noise factor thus in this method the noise is an important factor of analysis. After predicting the optimum conditions, the confirmation experiments must be performed to approve the output and the Taguchi approach.

S/N Ratio

In Taguchi, the Signal to Noise Ratio (S/N Ratio) used as the performance characteristic which measures how the output varies from its target value under different noise factors. Signals are the design parameters or factors controlled by the designer and noise is the factors that are uncontrollable. The S/N Ratio consider both the mean and variations of experimental results. There are mainly three types of signal to noise ratios used as a quality characteristic in solving the problems that are; "Nominal is Best," "Larger is Better" and "smaller is better."

Nominal is Best

This case is used when the nominal value of specified output is desired means neither larger nor smaller value is required. For example, aerospace industries generally use this performance criterion.

$$SN_N = 10\ log\left(\frac{\bar{y}}{s^2}\right) \quad (5.1)$$

Here, $\bar{y}$ and s are the mean and standard deviation of the observed data, respectively.

Larger is Better

This case is used when the larger value of specified output is required. For example, to estimate the profit value, flux calculation etc.

$$SN_L = -10\ log\left(\frac{1}{n}\sum_{i=1}^{n}\frac{1}{y_i^2}\right) \quad (5.2)$$

Smaller is Better

This case is used when the smaller value of specified output is required. The cost estimation requires this criterion.

$$SN_s = -10\ log\ \left(\frac{1}{n}\sum_{i=1}^{n} y_i^2\right) \quad (5.3)$$

Here, n is the number of set of an orthogonal array and y_i is the output of each set of the array.

In this study, the L_{27} orthogonal array was used for the Taguchi's analysis. The five factors with three levels were chosen. The factors with the level are, Bulk Feed Input Temperature (30, 40, 50 ^{o}C), Air Gap Width (3, 7, 11 mm), Feed Flow Rate (2, 6, 10 L/min), Cooling Water Temperature (5, 15, 25 ^{o}C) and Cooling Water Flow Rate (1, 3, 5 L/min). The orthogonal array with different factors, their levels, and corresponding permeate flux is given in Table 5.1. The experiments were performed twice according to this set of experiments to study the effects of noise sources. The larger is better S/N ratio as mentioned is equation (5.2) was used because the value of permeate flux needs to be maximized. The analysis of variation (ANOVA) test was performed to check which process parameters are statistically significant.

The flow chart for Taguchi analysis is given in Figure 5.1 and set of L_{27} orthogonal array is mentioned in Table 5.1.

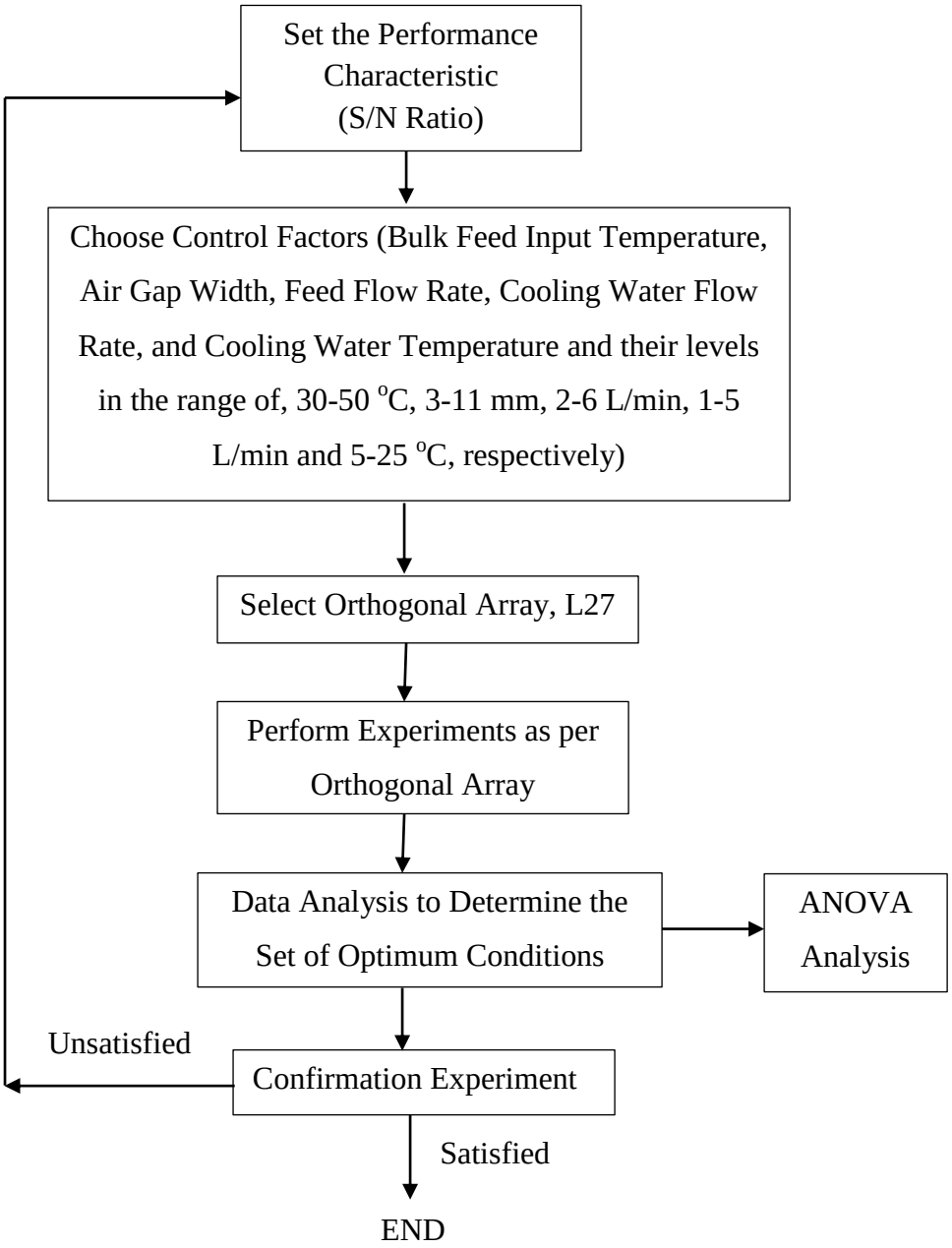

Figure 5.1 : Flow Chart for Taguchi Procedure

Table 5.1 : L_{27} Orthogonal Array

Run No.	Feed Temperature (^oC)	Feed Flow Rate (L/min)	Air Gap Width (mm)	Cooling Water Temperature (^oC)	Cooling Water Flow Rate (L/min)	Flux1	Flux2	SNRA1	Flux ($kg/m^2 \cdot h$)	
									Actual	Predicted
1	30	2	3	5	1	6.8	7.2	16.8913	7	7.0778
2	30	2	3	5	3	7.4	7.6	17.4989	7.5	7.35
3.	30	2	3	5	5	7	7.3	17.0804	7.15	7.22
4	30	6	7	15	1	4.2	4.3	12.566	4.25	3.97
5	30	6	7	15	3	3.8	3.9	11.707	3.85	4.25
6	30	6	7	15	5	4.4	4.1	12.5515	4.25	4.12
7	30	10	11	25	1	2	1.6	4.94426	1.8	1.82
8	30	10	11	25	3	1.5	2.2	4.87412	1.85	2.10
9	30	10	11	25	5	2.2	2.3	7.03722	2.25	1.97
10	40	2	7	25	1	7.8	8.2	18.0537	8	8.07
11	40	2	7	25	3	8.6	8.5	18.6389	8.55	8.35
12	40	2	7	25	5	8.2	8	18.1677	8.1	8.22
13	40	6	11	5	1	10	10.2	20.0852	10.1	9.91
14	40	6	11	5	3	10.5	10.6	20.4648	10.55	10.18
15	40	6	11	5	5	9.8	9.2	19.5415	9.5	10.05
16	40	10	3	15	1	15	14.8	23.4631	14.9	15.26
17	40	10	3	15	3	16.3	15.6	24.0489	15.95	15.53
18	40	10	3	15	5	15.2	15.5	23.7209	15.35	15.40
19	50	2	11	15	1	17.2	17.1	24.6852	17.15	17.11
20	50	2	11	15	3	17.4	17.5	24.8358	17.45	17.38
21	50	2	11	15	5	17	17.3	24.6843	17.15	17.25
22	50	6	3	25	1	23.9	23.5	27.494	23.7	23.42
23	50	6	3	25	3	23.4	23	27.3088	23.2	23.70
24	50	6	3	25	5	23.6	24	27.5306	23.8	23.57
25	50	10	7	5	1	24.4	24.5	27.7655	24.45	27.67
26	50	10	7	5	3	24.8	25	27.9238	24.9	24.95
27	50	10	7	5	5	25	25.2	27.9933	25.1	24.82

The main effect plot for permeate flux and for S/N ratio are shown in Figure 5.2 and Figure 5.3. It can be concluded from the main effect plot for permeate flux, that by increasing the feed temperature and feed flow rate the permeate flux and S/N ratio increases while by increasing the air gap width and cooling water temperature the mean response and S/N ration decreases. The mean response remains unaffected with the cooling water flow rate. The ANOVA results are depicted in the Table 5.2. The ANOVA analysis was performed at confidence level of 95 %. The feed temperature, feed flow rate, air gap width and cooling water temperature have the P-value < 0.0001, it indicates that these four parameters are the statistically significant at the confidence level of 95 % (level of significant $\alpha = 0.05$).

Similarly, the P-value of coolant flow rate i.e. 0.256 shows that this parameter is insignificant at the level of significant 0.05. The best combination for the highest permeate flux was found as bulk feed temperature 50 ^{o}C, air gap width 3 mm, feed flow rate 10 L/min and cooling water temperature 5 ^{o}C by Taguchi method. It was also observed that the separation of HCl/Water mixture is independent of the cooling water flow rate.

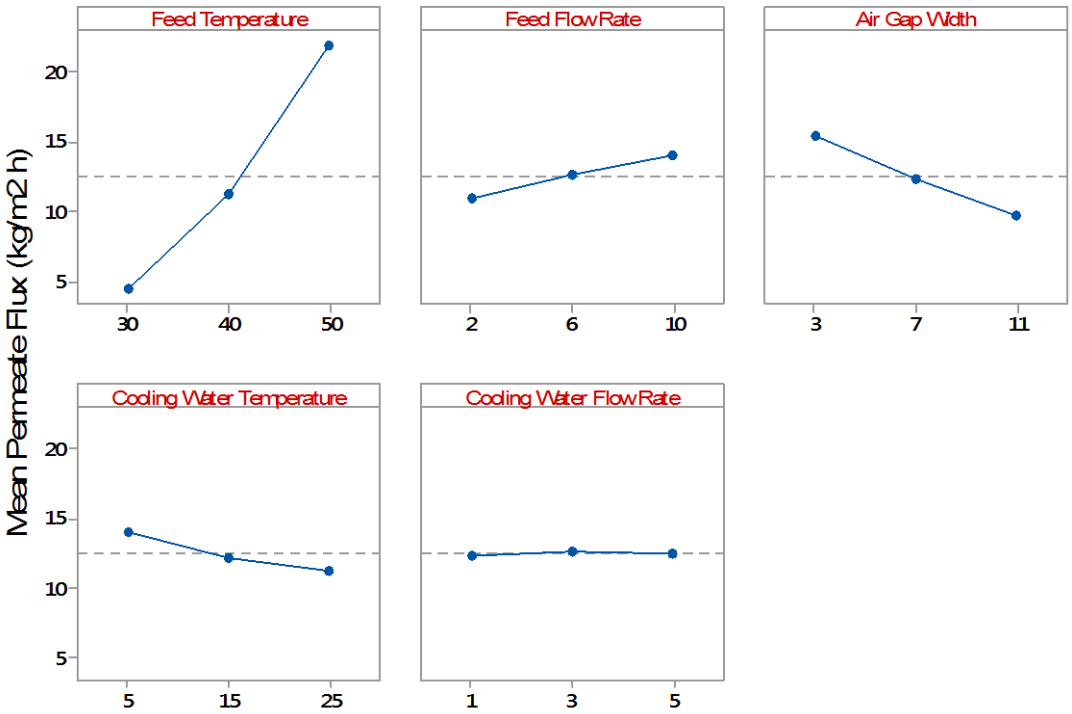

Figure 5.2: Main Effect Plot for AGMD Permeate Flux

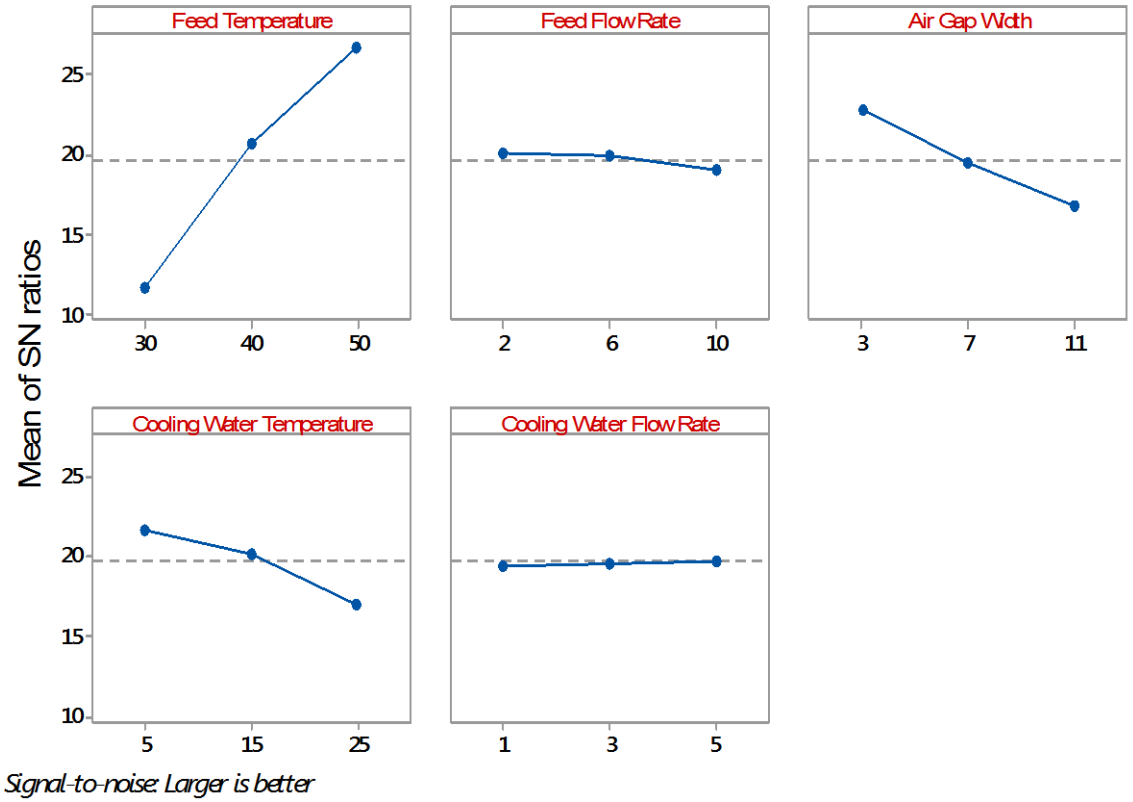

Figure 5.3 : AGMD Main Effect Plot for S/N Ratios

Table 5.2 : Analysis of Variance for Permeate Flux (ANOVA Table)

Source	DF	Adj. SS	Adj. MS	F-Value	P-Value
Feed Temperature	2	1391.82	695.908	6199.24	<0.0001
Feed Flow Rate	2	45.18	22.592	201.26	<0.0001
Air Gap Width	2	143.31	71.654	638.30	<0.0001
Cooling Water Temperature	2	35.60	17.802	158.58	<0.0001
Cooling Water Flow Rate	2	0.33	0.167	1.49	0.256
Error	16	1.80	0.112		
Total	26	1618.04			

S = 0.335048**,** R-Sq. = 99.89%, R-Sq. (adj.) = 99.82%, R-Sq. (pred.) =99.68%

The normal probability plot for the mean response is shown in Figure 5.4. From the Figure 5.4, it was detected that the most of the experimental data falls on the mean line or passes near to the mean line. It means the normal distribution is well suited model for the given system.

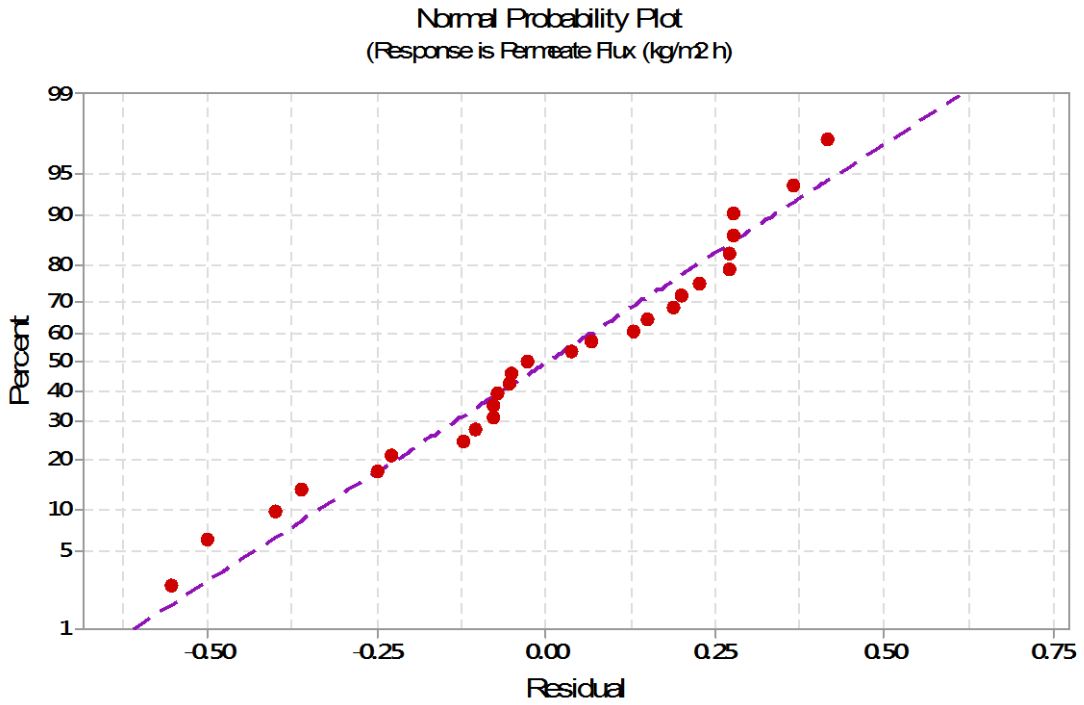

Figure 5.4 : Normal Probability Plot

5.2 Membrane Interfacial Temperature Estimation using COMSOL Multiphysics©

Time independent energy and mass balance equations from equation no. (3.31) to (3.40) were solved using PARDISO solver. Fine mesh element size was used to create the mesh in module geometry as shown in Figure 5.5. Mesh convergence study was performed to check how the solution converges with mesh refinement. The mesh statistics, detailed report of mesh elements, generated for AGMD module are shown in Table 5.3. The computational model was simulated in a computer having Intel core i5 processor, 2.40 GHz, 4 GB RAM, 64 bit and Windows 8 Operating System.

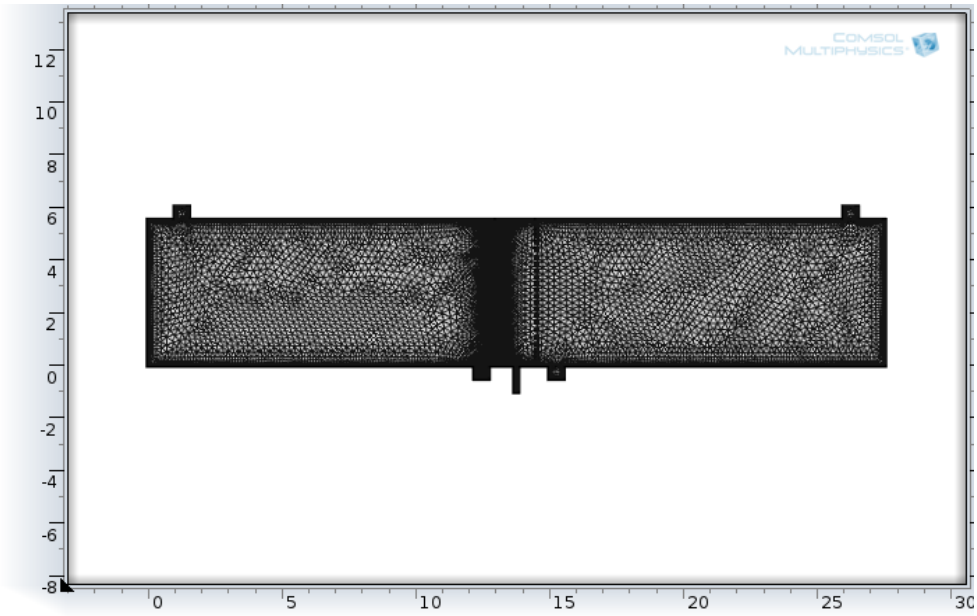

Figure 5.5 : Mesh Geometry of AGMD Module

Table 5.3 : Mesh Statistics

Property	Value
Minimum Element Quality	0.1136
Average Element Quality	0.9069
Total Elements	19009
Triangular Elements	18133
Quadrilateral Elements	876
Edge Elements	1061
Vertex Elements	30

From COMSOL simulation study, the temperature profile within the AGMD module was generated as shown in Figure 5.6. Average temperature at the feed side membrane surface and membrane side cooling plate surface were found 320.22 K and 307.53 K.

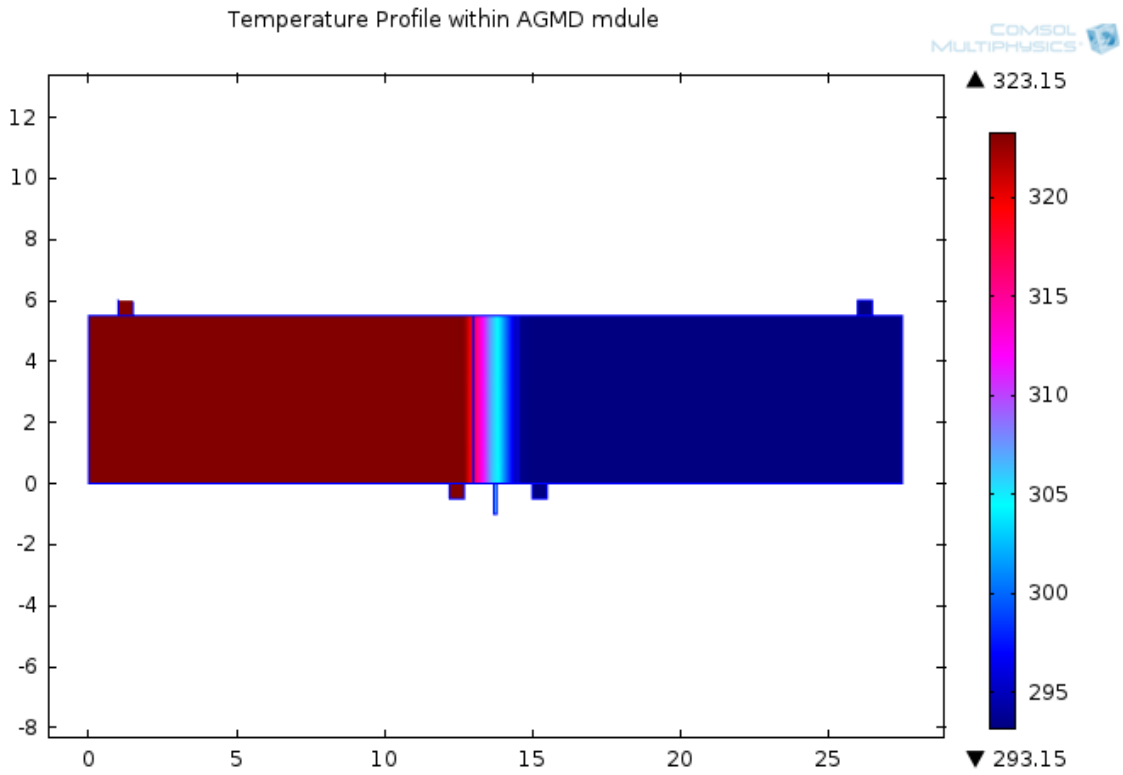

Figure 5.6 : Temperature Profile within AGMD Module

5.2.1 Comparison of Modeling and Experimental Results

The average temperature at the feed side membrane surface for the operating conditions as mentioned in Table 3 was computed to be 320.22 K using CFD modeling, while solving mathematical equations in MATLAB at the same operating conditions, it was obtained to be 321.7 K. Similarly, temperature at membrane side cooling surface obtained from CFD modeling and mathematical modeling was 307.53 K and 309.34 K, respectively. The simulated permeate flux was compared to the experimental results as shown in Figure 5.7. The operating conditions and membrane physical properties, as mentioned in Table 3.2 and Table 4.4 respectively, for all the three CFD, mathematical and experimental conditions were kept the same. The value of R^2 and MAPE values for comparison between CFD and experimental results were calculated to be 0.995 and 5.94%; and the same for mathematical model versus experimental results were computed to be 0.999 and 3.69%. R^2 and MAPE values indicate that model prediction by CFD is in good agreement with experimental results and therefore it can be applied for getting reliable and reasonable results.

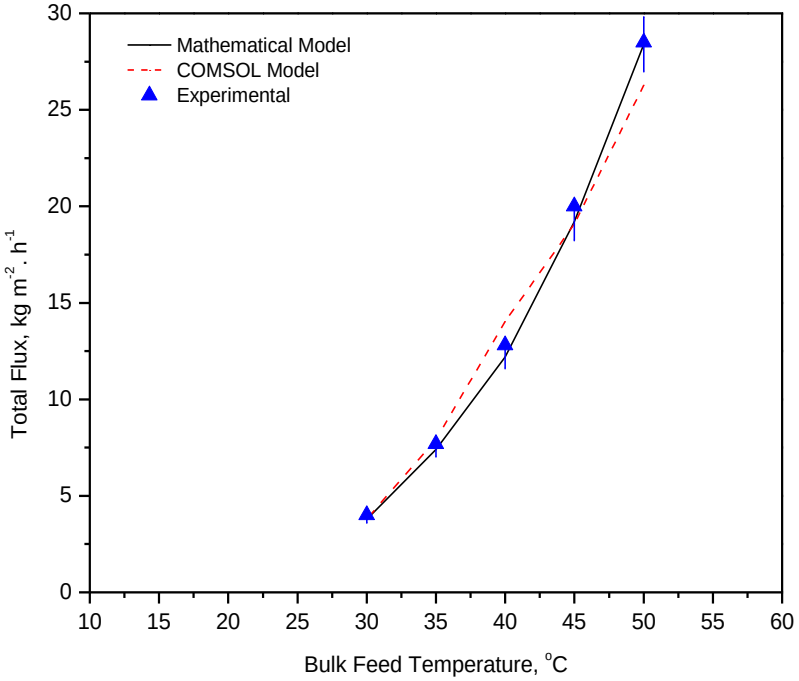

Figure 5.7 : Comparison of Simulated Results (Mathematical and COMSOL Modeling) with Experimental Flux at Various Feed Temperatures

5.3 Effects of Operating Variables on Total permeate Flux, HCl Selectivity and Azeotrope Breaking Point

5.3.1 Effect of Feed Bulk Inlet Temperature

Figure 5.8 illustrates the effect of bulk feed input temperature on total permeate flux for different air gap thicknesses by keeping all other parameters as constant. It was observed that for azeotropic feed concentration, total permeate flux increases exponentially on increasing feed temperature from 30 ^{o}C to 50 ^{o}C. This behaviour is due to the relationship of vapor pressure *versus* temperature for HCl and water (Fritz and Fuget, 1956) as shown in Figure 5.9. From Figure 5.9, it can be observed that there is increase in total vapor pressure with increasing temperature, which in turn results in increase in permeate flux. It can also be observed that no significant changes in HCl vapor pressure occur on changing the temperature while water vapor pressure changes exponentially with temperature. Therefore, It can be concluded that total permeate flux will be leveraged with water. In Figure 5.8, it can be seen that the increment ratio in the total flux for 7 mm air gap width is less than in 3 mm air gap width when the feed temperature increases from 30 ^{o}C to 50 ^{o}C. This behaviour is mainly because mass transfer resistance provided by the air gap. As air gap thickness increased, resistance to mass transfer increases therefore effect of temperature on permeate flux at low air gap is more significant as compared to large air gap width.

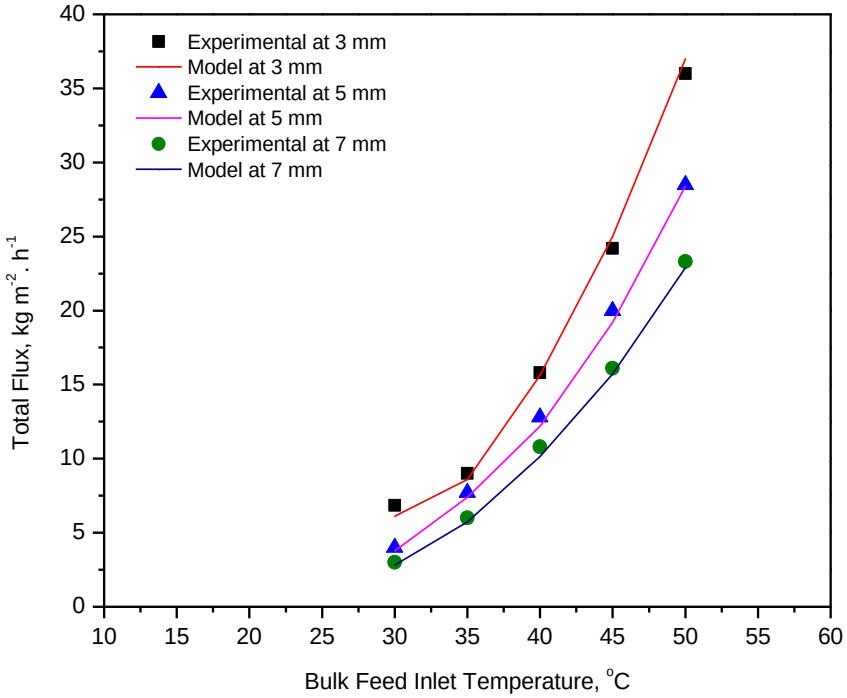

Figure 5.8 : Effect of Bulk Feed Temperature on Total Permeate Flux for Different Air Gap Widths
(T_c = 20 °C, feed flow rate = 2 L/min, cooling water flow rate = 1 L/min)

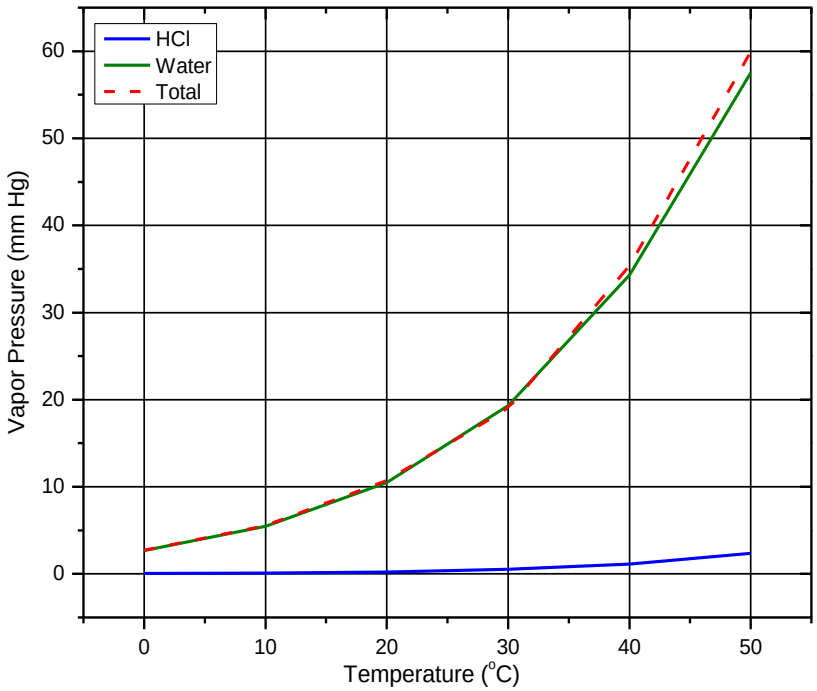

Figure 5.9 : Effect of Temperature on Vapour Pressure of HCl and Water

Figure 5.10 represents the change in HCl selectivity on varying feed temperature for various air gap widths. It can be observed from Figure 5.10 that selectivity of HCl is less than 1 for all the feed temperatures, which indicates selective permeation of water in permeate flux. A

temperature change not only affects the vapor pressure but also the diffusivity of HCl and water vapor. Change in diffusion coefficient with temperature was elaborated through equation 3.30, as Fuller correlation. The same behaviour was observed by (Banat *et al.*, 1999a; 1999b) for formic acid-water azeotropic mixture using AGMD process. A temperature increase leads to changes in the entropies of the constitute components and this entropy changes supply information about intermolecular differences therefore separation is more affected by diffusion phenomena. Heating HCl/Water mixture at azeotropic concentration forms the same composition of vapor but separation is possible due to higher diffusivity of water in air as compared to HCl, therefore concentration of HCl in permeate decreases to its azeotropic feed concentration and in retentate it is increased. The change in permeate and retentate HCl concentration on varying bulk feed temperature is shown in Figure 5.11. It can be observed that permeate HCl concentration decreases while retentate HCl concentration increases on increasing feed temperature due to lower selectivity of membrane to HCl vapor. The maximum concentration of HCl in retentate was found to be 30.8% and that in permeate was 15.29%. Thus, it is concluded that HCl/Water azeotrope breaks in both permeate and retentate. HCl at both lower and higher concentration could be used for different industrial applications. R^2 and MAPE values for total permeate flux and selectivity is given in Table 5.4 from which a good match between experimental and model results is found. Same pattern for effect of feed temperature on selectivity was observed by Banat *et al.* (1999b).

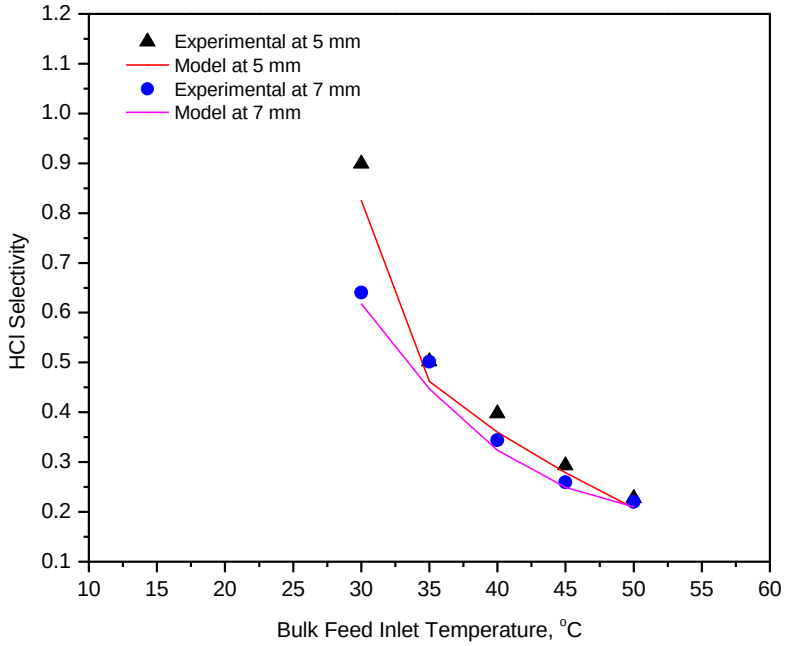

Figure 5.10 : Effect of Temperature on HCl Selectivity for Different Air Gap Widths (T_c = 20 °C, feed flow rate = 2 L/min, cooling water flow rate = 1 L/min)

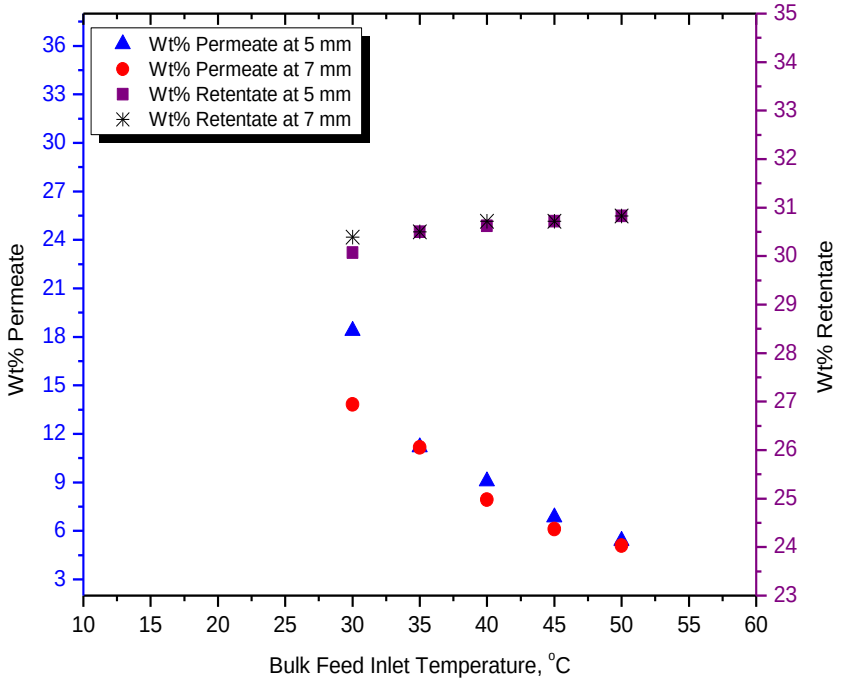

Figure 5.11 : Change in Permeate and Retentate HCl Concentration for Different Air Gap Widths
(T_c= 20 °C, feed flow rate = 2 L/min, cooling water flow rate = 1 L/min)

Table 5.4 : Comparison between Predicted and Experimental Data in terms of R^2 and MAPE for Feed Temperature 30-50 °C

Air Gap Width	Permeate Flux		HCl Selectivity	
	R^2	MAPE	R^2	MAPE
3 mm	0.99	4.49	-	-
5 mm	0.99	3.69	0.99	7.88
7 mm	0.99	4.16	0.99	5.70

For various feed inlet temperatures, total flux computed by present model was compared with that by Abu *et al.*, (2012) model and experimental data. Flux estimated by present model shows higher value than calculated by Abu *et al.*, (2012) because present model considers the Knudsen diffusion through the membrane pore for which contribution increases the total flux value. Figure 5.12 shows the trend of variation in simulated prediction and experimental data.

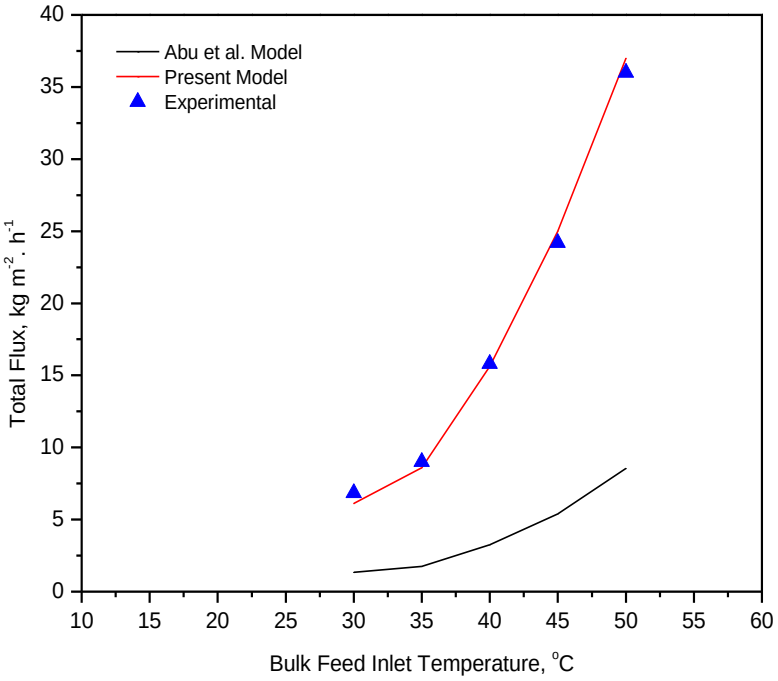

Figure 5.12 : Effect of Bulk Feed Temperature

5.3.2 Effect of Feed Flow Rate

The effect of feed flow rate on total flux and selectivity for various air gap widths is elucidated by Figure 5.13 and Figure 5.14, respectively while keeping feed temperature at 50 ^{o}C, cooling water temperature at 20 ^{o}C and cooling water flow rate 1 L/min. It can be observed that at azeotropic feed concentration, total permeate flux increases on increasing feed flow rate from 2 to 6 L/min. The effect of feed flow rate on flux dominates at low air gap width; as air gap increases, effect of flow rate becomes negligible. The reason for increase in flux with increasing flow rate is the decrement in thermal boundary layer due to increase in Reynolds number at small air gap. Simultaneously, turbulence, created due to large Reynolds number, lowers the HCl diffusional resistance through the membrane by decreasing the interfacial HCl concentration. Consequently, the selectivity of HCl increases on increasing feed flow rate as shown in Figure 5.13. The same dependency of selectivity of volatile solute on feed temperature was predicted by Thiruvenkatachari *et al.* (2006b). Since selectivity of HCl increases with flow rate therefore HCl concentration in permeate increases and in retentate it remains almost constant on increasing flow rate as shown in Figure 5.15. R^2 and MAPE value as shown in Table 5.5 indicates a good agreement between experimental measurements and model predictions.

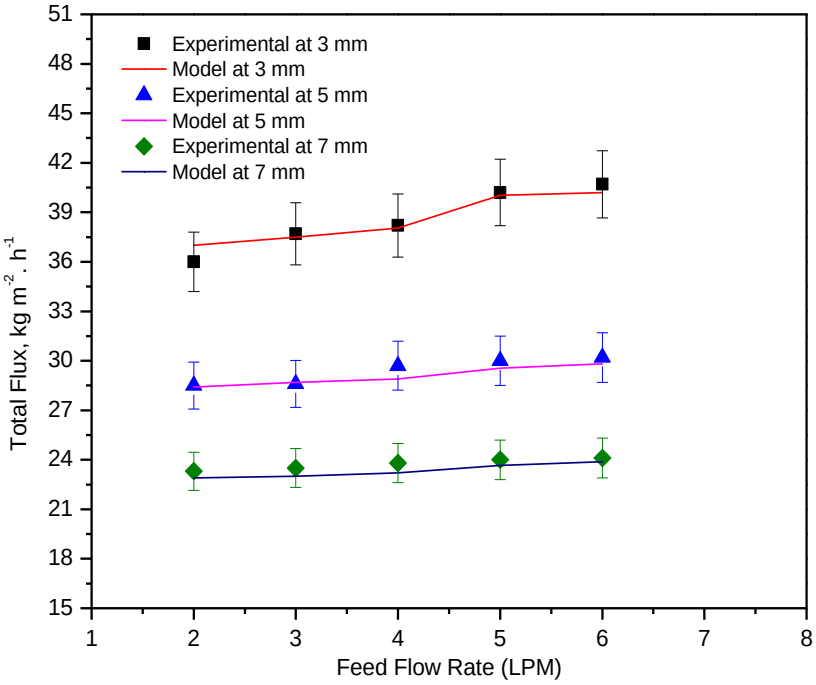

Figure 5.13 : Effect of Feed Flow Rate on Total Permeates Flux at Different Air Gap (T_b = 50 °C, T_c = 20 °C, cooling water flow rate = 1 L/min)

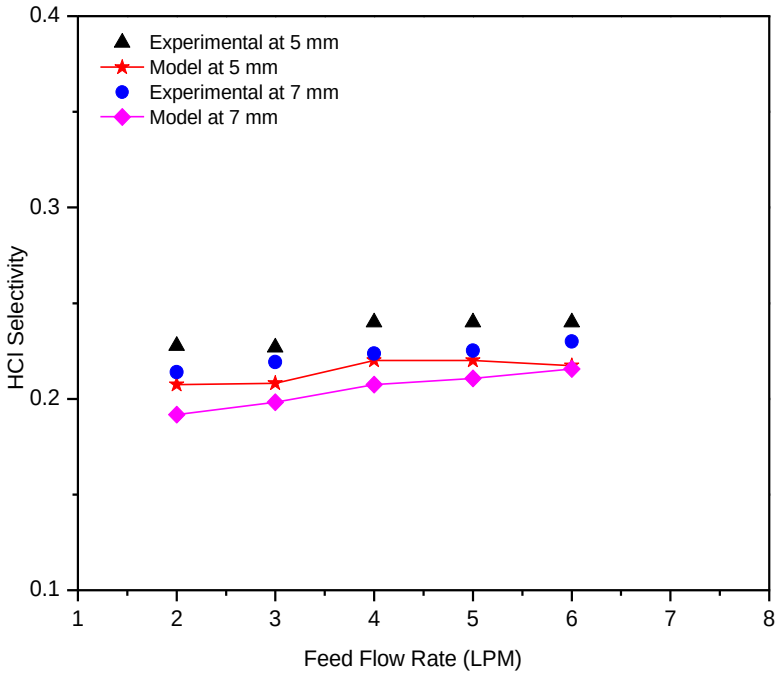

Figure 5.14 : Effect of Feed Flow Rate on HCl Selectivity for Different Air Gap Widths (T_b = 50 °C, T_c = 20 °C, cooling water flow rate = 1 L/min)

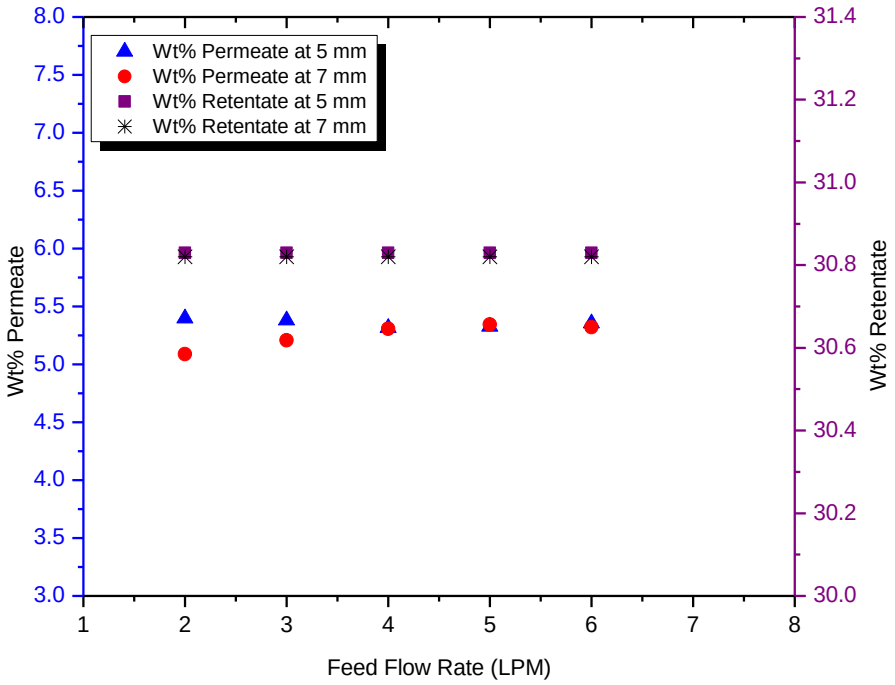

Figure 5.15 : Change in Permeate and Retentate HCl Concentration for Different Air Gap Widths
(T_b = 50 ^{o}C, T_c = 20 ^{o}C, cooling water flow rate = 1 L/min)

Table 5.5 : Comparison between Predicted and Experimental Data in terms of R^2 and MAPE for Feed Flow Rate 2-6 L/min

Air Gap Width	Permeate Flux		HCl Selectivity	
	R^2	MAPE	R^2	MAPE
3 mm	0.98	1.08	-	-
5 mm	0.94	1.36	0.98	9.59
7 mm	0.96	1.75	0.99	8.64

5.3.3 Effect of Air Gap Thickness

At azeotropic concentration of 20.2 mass% HCl, feed temperature of 50 ^{o}C, cooling water temperature of 20 ^{o}C and cooling water flow rate of 1 L/min, air gap width was varied for various feed flow rates. From Figure 5.16 it can be seen that by increasing air gap width, permeate flux decreases. This is mainly due to high mass transfer resistances provided by large air gap. The main drawback of heat loss by conduction in DCMD configuration can be overcome by using this variable air gap arrangement that varies the heat transfer resistance between membrane and cooling plate therefore an optimum value of air gap must be chosen for optimum results (Lawson and Lloyd, 1996). As shown in Figure 5.17, selectivity of HCl

varies inversely with the air gap width variation in the range, however, the rate of change is less significant beyond 7 mm. Same behavior was observed by Banat *et al.*, (1999b) and Udriot *et al.*, (1994) for the separation of formic acid/water and HCl/water azeotrope mixture, respectively. Since selectivity decreases with air gap width therefore permeate and retentate concentration of HCl varies inversely with air gap width as shown in Figure 5.18. A good match was found between experimental and mathematical model results as displayed in Table 5.6.

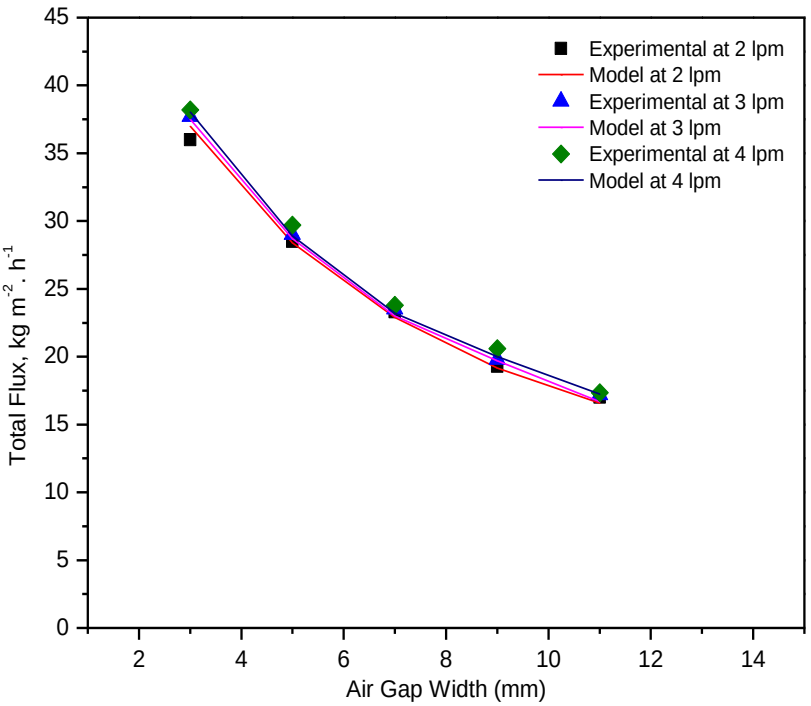

Figure 5.16 : Effect of Air Gap Width on Total Permeate Flux at Various Feed Flow Rates
(T_b = 50 ^{o}C, T_c = 20 ^{o}C, cooling water flow rate = 1 L/min)

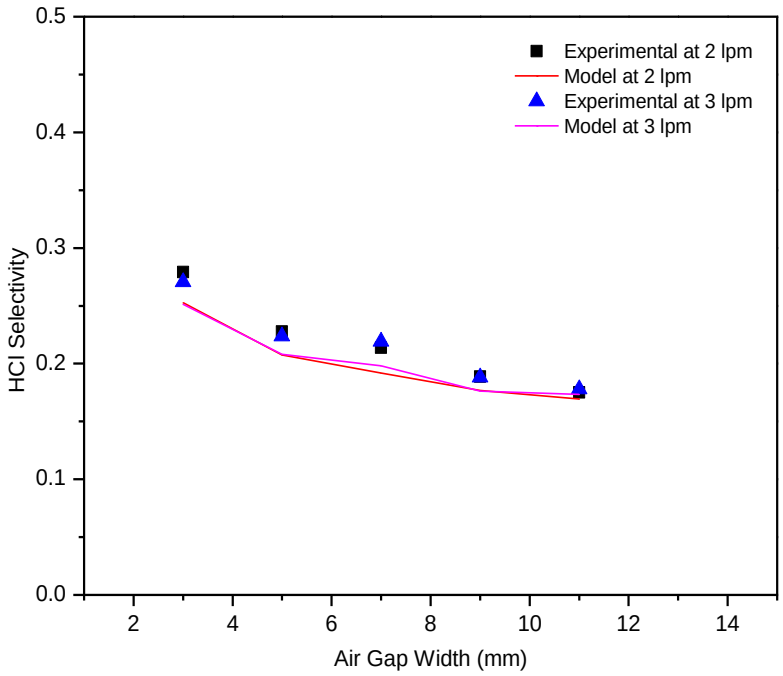

Figure 5.17 : Effect of Air Gap Width on Selectivity at Various Feed Flow Rates (T_b = 50 °C, T_c = 20 °C, cooling water flow rate = 1 L/min)

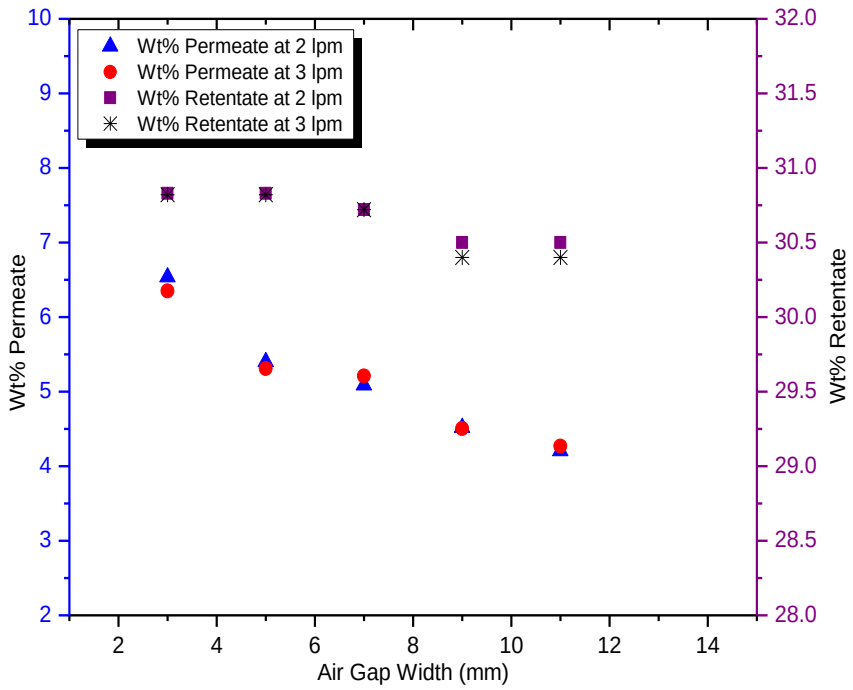

Figure 5.18 : Change in Permeate and Retentate HCl Concentration for Various Feed Flow Rates (T_b = 50 °C, T_c = 20 °C, cooling water flow rate = 1 L/min)

Table 5.6 : R^2 and MAPE Values for Various Air Gap Widths (3-11 mm)

Feed Flow Rate	Permeate Flux		HCl Selectivity	
	R^2	MAPE	R^2	MAPE
2 L/min	0.99	1.02	-	-
3 L/min	0.99	1.96	0.99	8.21
4 L/min	0.99	1.89	0.99	8.22

5.3.4 Effect of Cooling Water Temperature

Cooling water helps in condensing the vapors on permeate side. The effect of cooling water temperature on permeates flux and selectivity for several air gap widths is shown in Figure 5.19 and Figure 5.20, respectively. As evident, the permeate flux decreases on increasing the cooling water temperature from 10 ^{o}C to 25 ^{o}C as the temperature gradient gets reduced. However, on increasing the cooling water temperature, the selectivity of HCl in permeate increases. Banat *et al.*, (1999a,b) predicted the same effect of coolant temperature on formic acid-water azeotrope selectivity. The mathematical prediction shows the satisfactory results as evident from R^2 and MAPE values given in Table 5.7. Change in permeate and retentate HCl concentration with cooling water temperature is elucidated in Figure 5.21.

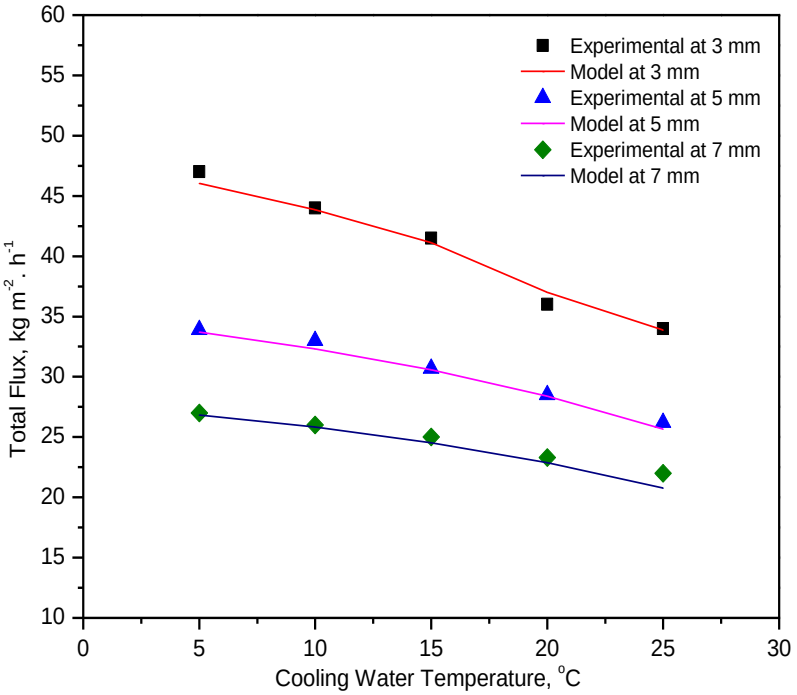

Figure 5.19 : Effect of Cooling Water Temperature on Total Permeate Flux for Various Air Gap Widths
(T_b = 50 ^{o}C, feed flow rate = 2 L/min, cooling water flow rate = 1 L/min)

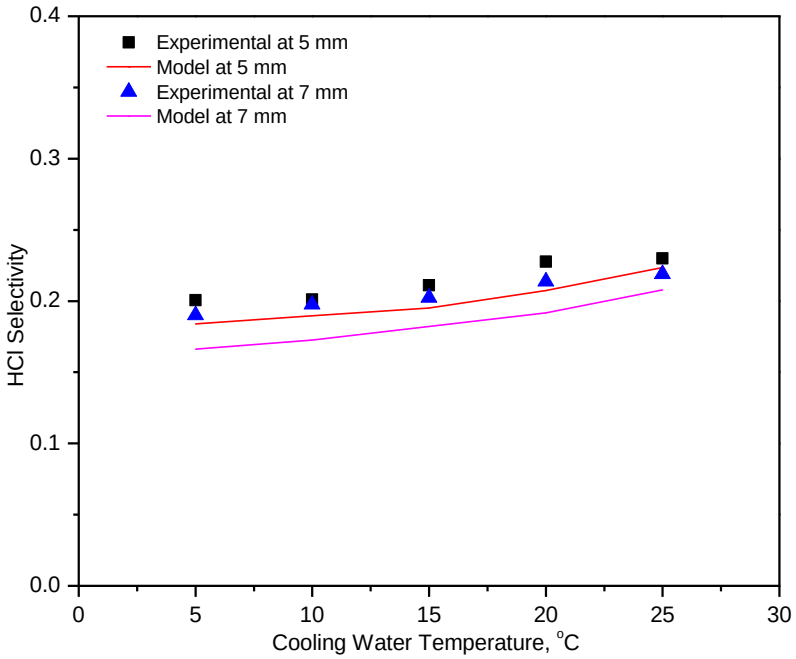

Figure 5.20 : Effect of Cooling Water Temperature on Selectivity for Various Air Gap Widths
(T_b = 50 °C, feed flow rate = 2 L/min, cooling water flow rate = 1 L/min)

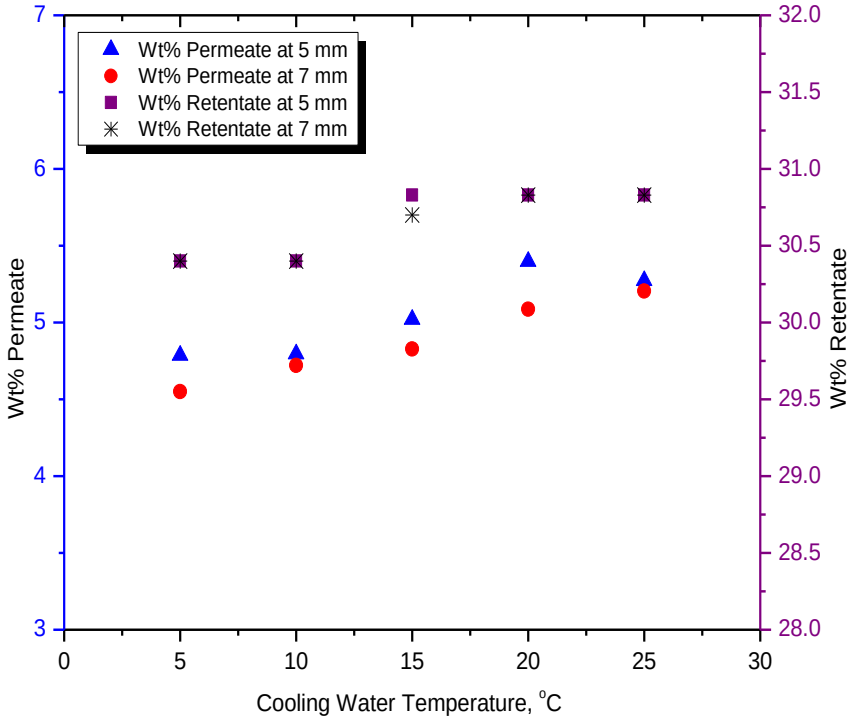

Figure 5.21 : Change in Permeate and Retentate HCl Concentration for Various Air Gap Widths
(T_b= 50 °C, feed flow rate = 2 L/min, cooling water flow rate = 1 L/min)

Table 5.7 : R^2 and MAPE Values for Cooling Water Temperature Variation in the Range of 5-25 °C

Air gap width	Permeate Flux		HCl Selectivity	
	R^2	MAPE	R^2	MAPE
3 mm	0.99	1.11	-	-
5 mm	0.99	1.30	0.95	9.26
7 mm	0.99	2.02	0.98	9.74

5.3.5 Effect of Cooling Water Flow Rate

Effect of cooling water was studied by varying cooling water flow rate from 1 L/min to 5 L/min at azeotropic feed concentration, feed temperature 50 ^{o}C, feed flow rate 2 L/min and variable cooling water temperature. It was observed that total permeate flux and selectivity were not affected significantly by changing the cooling water flow rate from 1 L/min to 5 L/min as shown in Figure 5.22 and Figure 5.23, respectively. This is attributed to the fact that overall heat transfer coefficient is mainly dominated by air gap heat transfer coefficient which is very much smaller than hot side heat transfer coefficient and cold side heat transfer coefficient. Another reason is small module length that keeps cooling water temperature at both inlet and outlet approximately constant. Minute change in permeate concentration and practically no change in retentate concentration with cooling water flow rate was observed as shown Figure 5.24. Due to negligible effect of cooling water flow rate on flux and selectivity, only a few studies have been carried out in this field (Banat and Simandl, 1999; Banat et al., 1999e; Abu *et al.*, 2012). A good fit between R^2 and MAPE value was found to validate the mathematical model prediction as shown in Table 5.8**.**

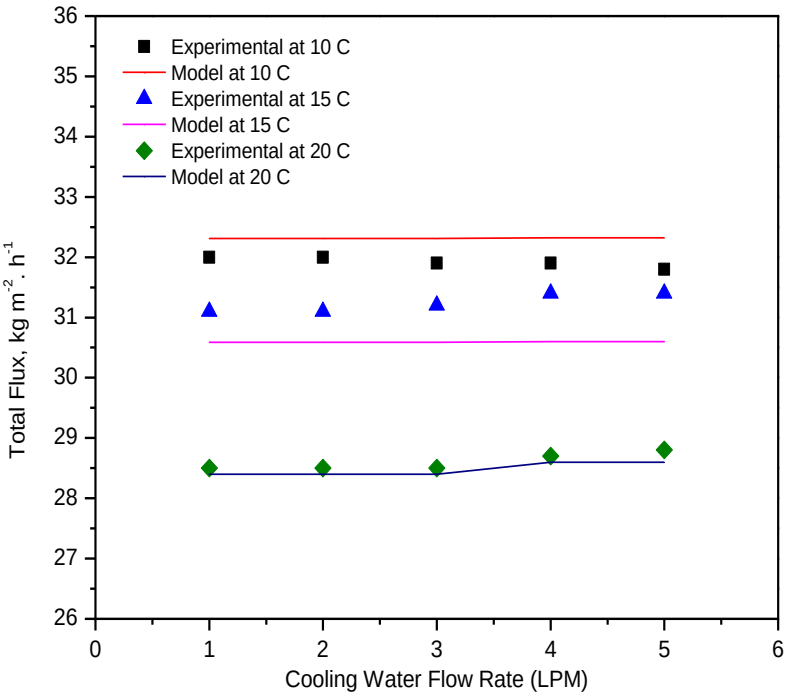

Figure 5.22 : Effect of Cooling Water Flow Rate on Total Permeate Flux for Various Cooling Water Temperatures
(T_b = 50 °C, cooling water flow rate = 1 L/min, air gap width = 5 mm)

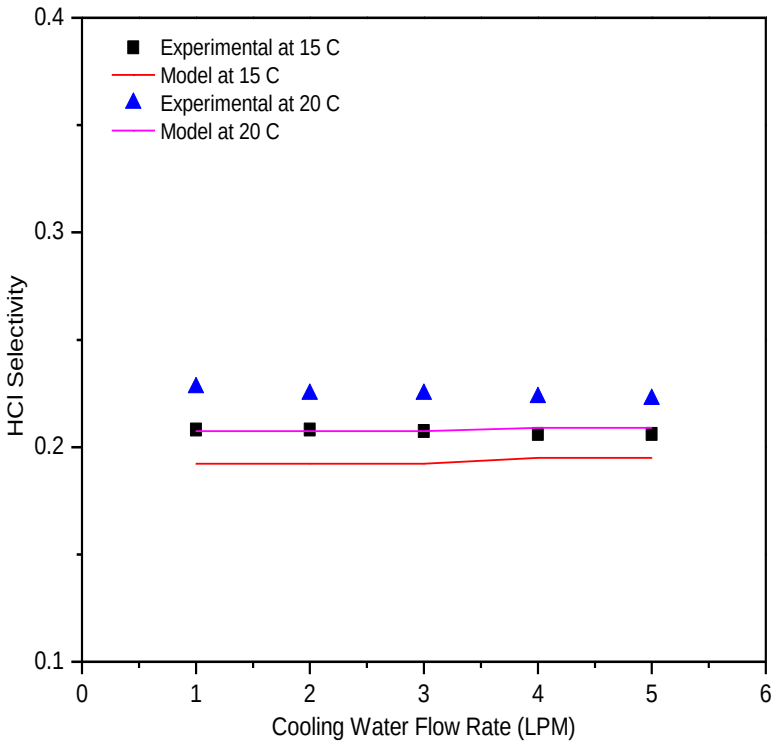

Figure 5.23 : Effect of Cooling Water Flow Rate on HCl Selectivity for Various Cooling Water Temperatures
(T_b = 50 °C, cooling water flow rate = 1 L/min, air gap width = 5 mm)

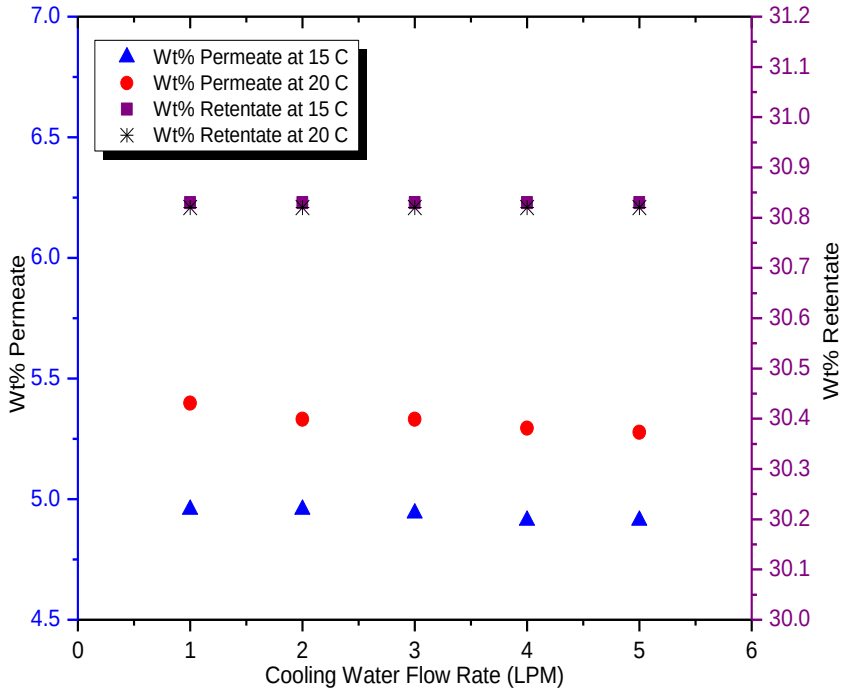

Figure 5.24 : Change in Permeate and Retentate HCl Concentration for Different Cooling Water Temperature
(T_b = 50 ^{o}C, cooling water flow rate = 1 L/min, air gap width = 5 mm)

Table 5.8 : R^2 and MAPE Values for Various Cooling Water Temperatures

Cooling Water Temperature	Permeate Flux		HCl Selectivity	
	R^2	MAPE	R^2	MAPE
15 °C	0.96	1.30	0.99	6.68
20 °C	0.97	2.02	0.98	7.30

5.4 Effects of Operating Time on Total permeate Flux and HCl Selectivity

To analyze the effect of operating time on permeate flux and selectivity, the AGMD setup was operated continuously for 50 h. From Figure 5.25 and Figure 5.26, it can be observed that there is no reduction in permeate flux and selectivity for a continuous run of 50 h at 45 ^{o}C bulk feed input temperature, 15 ^{o}C cooling water temperature, 1 L/min feed flow rate, 1 L/min cooling water flow rate and 3 mm air gap thickness at azeotropic feed concentration. The permeate flux and selectivity at above mentioned operating conditions were observed as 25.2 ± 0.1 kg/m^2·h and 0.33 ± 0.02, respectively for 50 h of continuous operation. The above mentioned results may be due to the volatile nature of feed components, which causes

no deposition on the membrane surface. No membrane wetting was observed due to the hydrophobic nature of PTFE membrane.

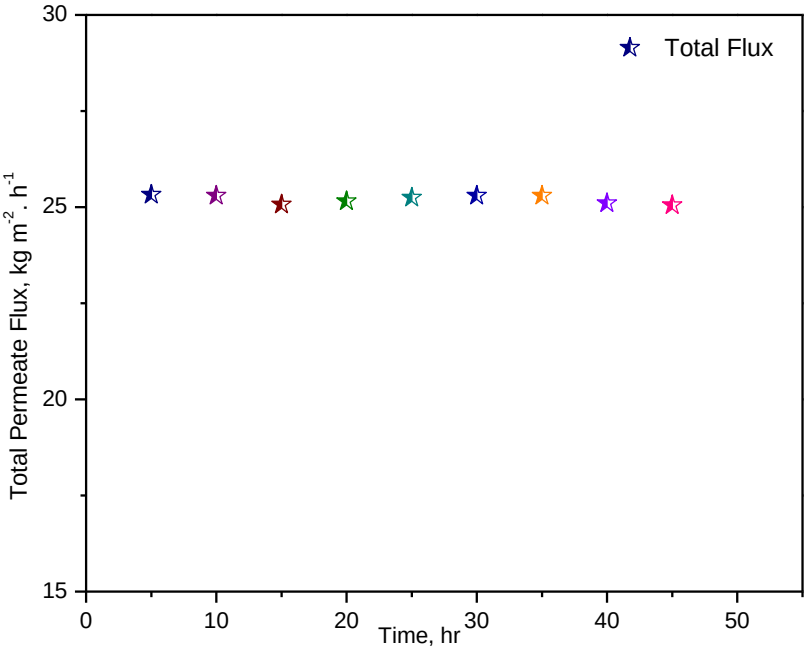

Figure 5.25 : Effect of Operating Time on Flux

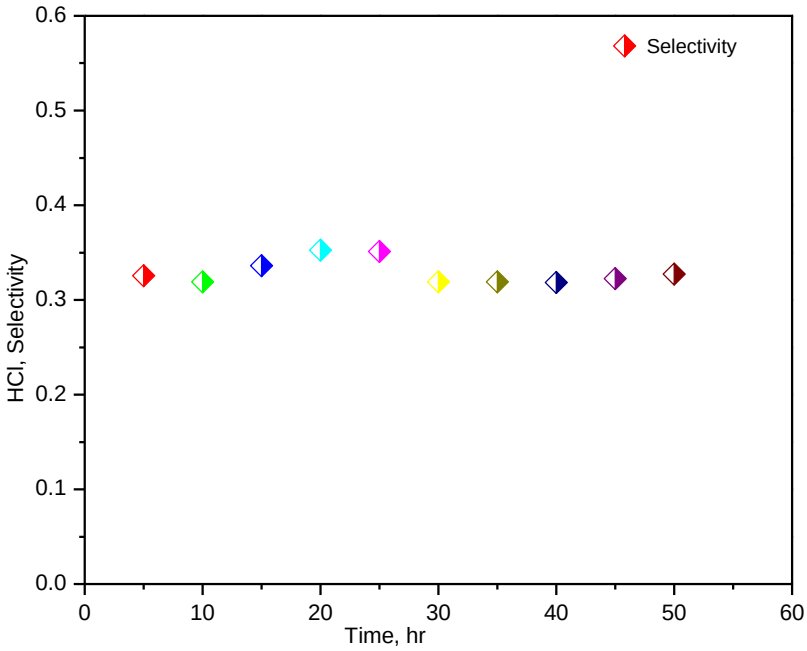

Figure 5.26 : Effect of Operating Time on Selectivity

5.5 Membrane Morphology Study Before and After Use

5.5.1 SEM and AFM Analysis

Change in membrane surface morphology before and after the run has been studied by FESEM and AFM analysis. Image analysis program analyzed pore size distribution of

membranes before and after the use. From the SEM images, as shown in Figure 5.27, it was observed that minimal fouling occurred on the membrane surface after 50 h of operation. The minimal membrane fouling is due to the fact of the volatile nature of feed components. It is the main reason for very small or almost no reduction of permeates flux after the continuous run of AGMD setup for 50 h. Three-dimensional topographical images of the used and new membrane have been studied by tapping mode AFM technique as shown in Figure 5.28 and Figure 5.29. AFM is preferred over SEM analysis, due to no special sample preparation and, no damage to membrane occurs as in the case of SEM due to metal coating (Khayet *et al.*, 2004). In Figure 5.28 (AFM image of the fresh membrane) and Figure 5.29 (AFM image of the used membrane), the nodules are seen as high bright elevations and pores as dark depressions. From Figure 5.29, it can be observed that no significant change in membrane topographical image has occurred.

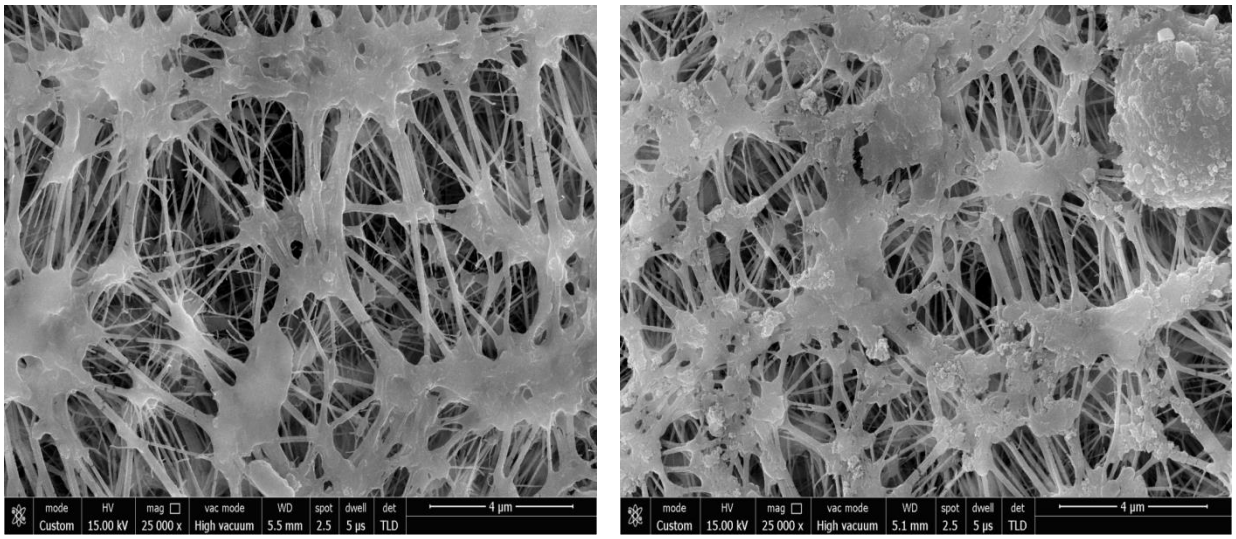

(a) (b)

Figure 5.27 : SEM Micrograph of (a) Fresh Membrane (b) Used Membrane

Also, HCl is most commonly used as the chemical cleaning agent in MD for the removal of inorganic scales from the membrane surface because the hydrophobicity and properties of membrane remain unchanged with strong or weak acids (Wang *et al.*, 2008; Tijing *et al.*, 2015). Marck Gryta (2007b) studied the effect of membrane porosity on the direct contact membrane distillation performance for tap water distillation. The $CaCO_3$ deposition on the membrane surface during MD operation was removed by washing the membrane surface with 2-5 mass% HCl. It has been reported by the Tomaszewska *et al.*, (1998) during the recovery of hydrochloric acid from salt content feed solution that the polypropylene membrane hydrophobicity and its properties remain unchanged for long-term MD operation

(above one year). SEM microscopic image of used PVDF membrane after washing with 2% (w/w) HCl acid showed the same characteristics as those of fresh membrane surface (Wang *et al.*, 2008). By points as mentioned above, it can be concluded that HCl solution at any feed concentration and also for long-term processes does not cause any membrane fouling or scale formation.

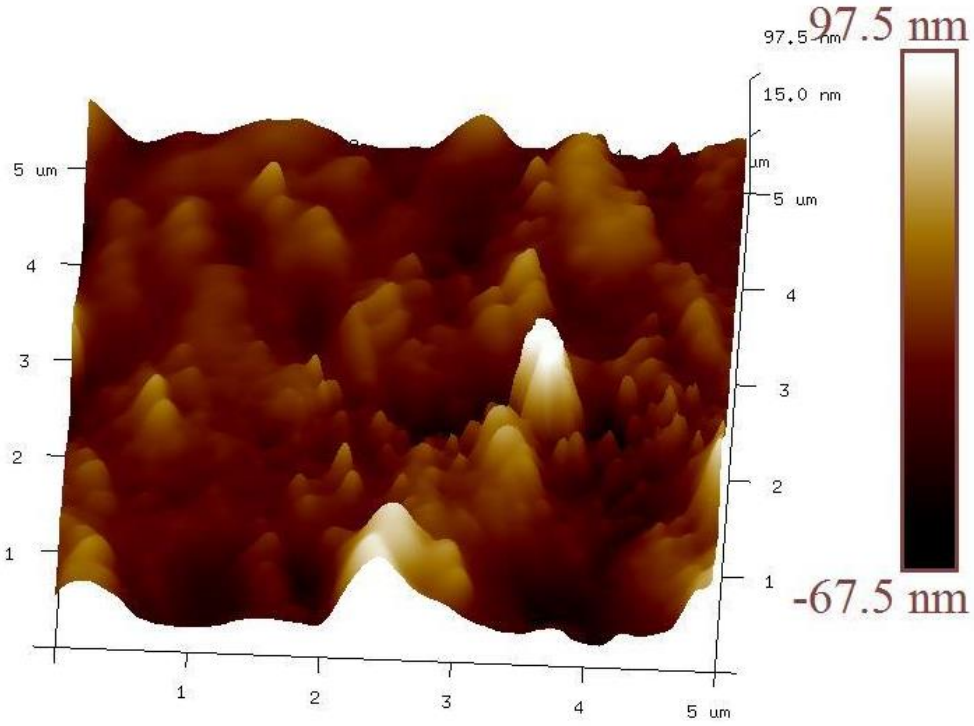

Figure 5.28 : AFM Image of Fresh Membrane

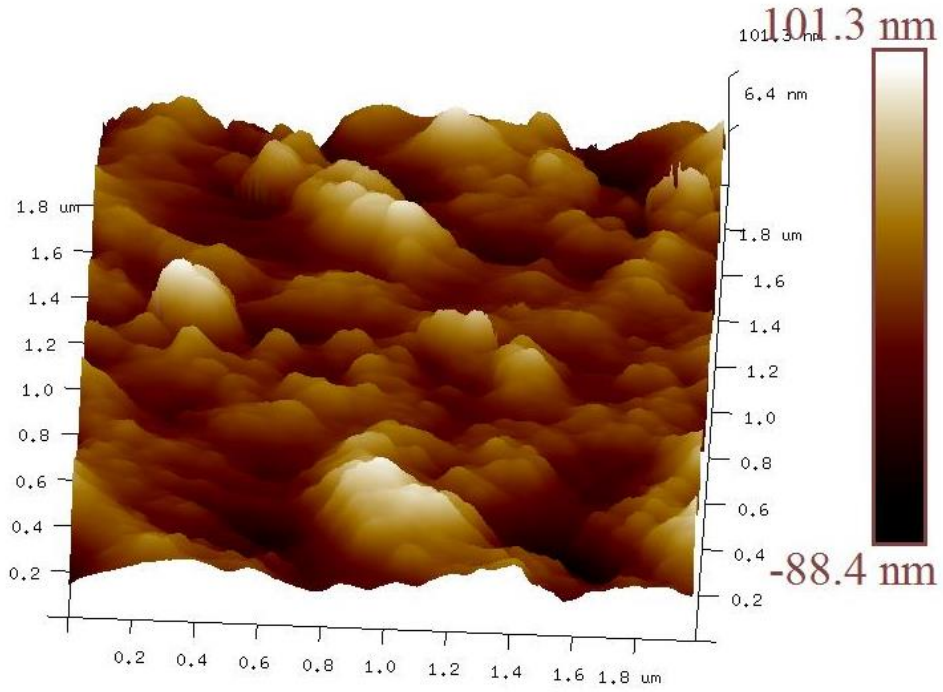

Figure 5.29 : AFM Image of Used Membrane

5.5.2 Pore Size Distribution

The field emission scanning electron microscopy (Nova NanoSEM™) generated image was used to study the membrane pore size distribution. For the generation of SEM image of 50,000 magnifications, electrons beam was accelerated under 15.0 kV in vacuum section. This generated SEM image was further analysed by Image processing software (ImageJ). The pore cross-sectional area was measured by the image processing software (Schneider et al., 2012). The equivalent diameter of membrane pore was calculated by considering the circular pore and measured by equation (5.4) (Phattaranawik et al., 2003):

$$d_{eq} = 2\sqrt{A/\pi} \tag{5.4}$$

The pore size distribution for fresh and used membrane was obtained in the form of a histogram and probability density function (pdf) as depicted in the Figures 5.30 and Figure 5.31, respectively. From these figures, it can be observed that there was approximately no remarkable change in pore size distribution of the membrane after 50 h run of AGMD setup for azeotropic mixture separation. Further, the same results have also been seen from the probability density function (Figure 5.30b and 5.31b) estimated by equation 5.5 (Khayet and Matsuura, 2011).

$$\frac{df(d_m)}{d(d_m)} = \frac{exp\left[\frac{-(ln\, d_m - ln\, \mu_m)^2}{2(ln\, \sigma_m)^2}\right]}{d_m ln\, \sigma_m \sqrt{2\pi}} \tag{5.5}$$

Where, d_m is the membrane pore size, σ_m is the geometric standard deviation and μ_m is mean pore size.

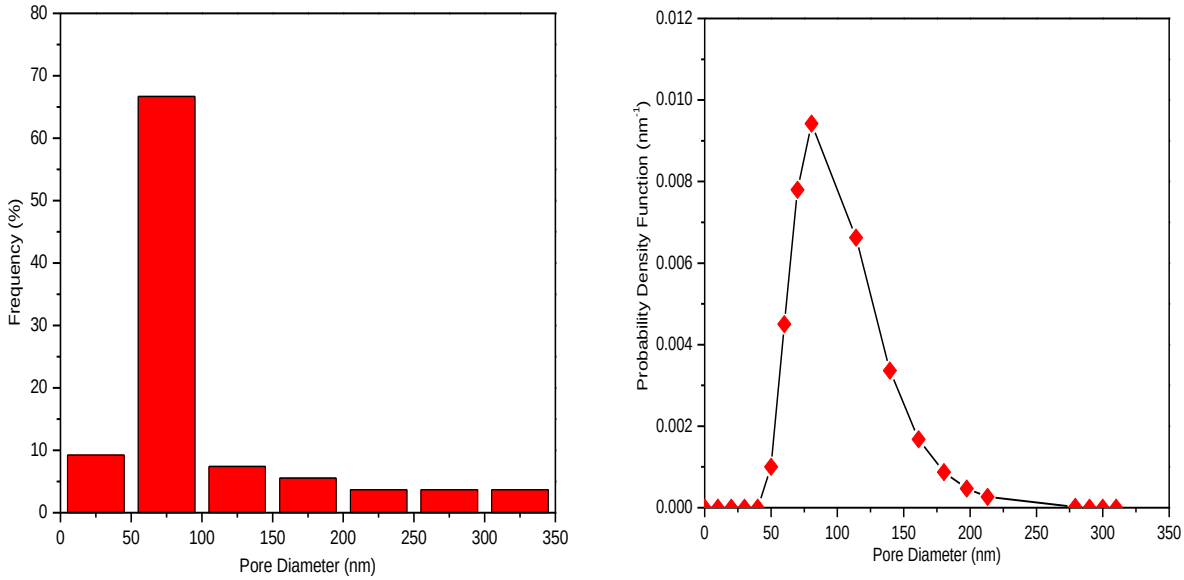

(a) (b)

Figure 5.30 : Pore Size Distribution of Fresh Membrane Surface (a) Bar Graph (b) Probability Density Curve

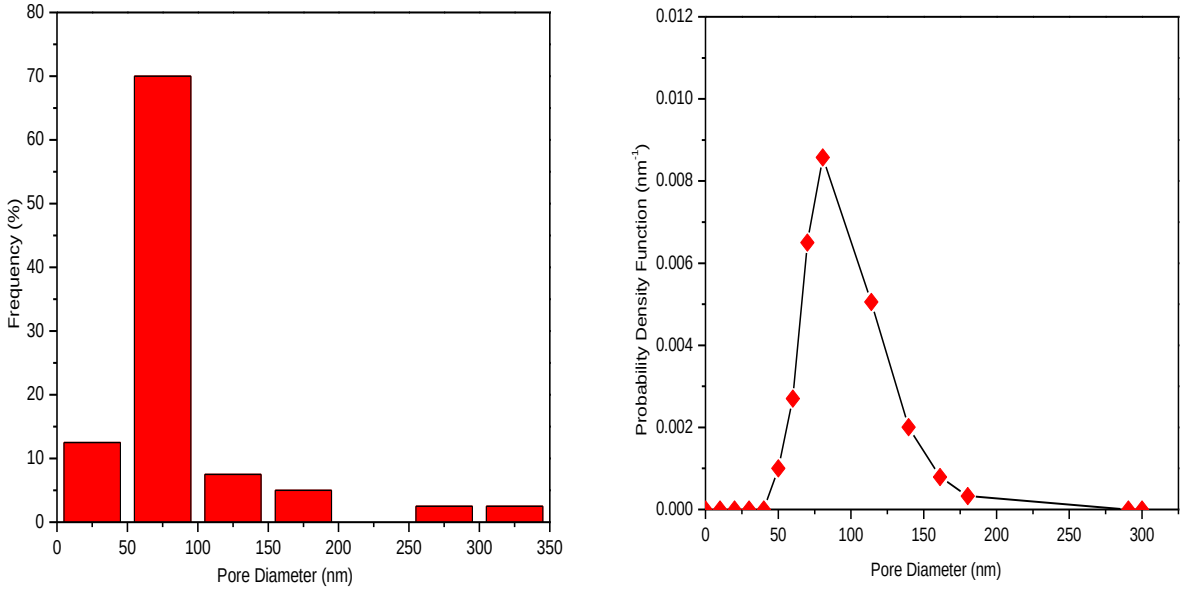

(a) (b)

Figure 5.31 : Pore Size Distribution of Used Membrane (a) Bar Graphs (b) Probability Density Curve
(For continuous run of 50 h at 45 ^{o}C bulk feed input temperature, 15 ^{o}C cooling water temperature, 1 L/min feed flow rate, 1 L/min cooling water flow rate and 3 mm air gap thickness at azeotropic feed concentration)

5.6 **Recovery Calculation**

For the estimation of the recovery of the HCl, an initial feed solution was taken at the azeotropic concentration in the feed tank. Other operating parameter namely feed flow rate, cooling water temperature, cooling water flow rate and air gap width were taken as 1 L/min, 15 ^{o}C, 1 L/min and 5 mm, respectively.

Since the maximum concentration of HCl desirable for commercial applications is 31 mass% so it was required to change the HCl concentration in feed tank from azeotropic concentration i.e. 20.2 mass% to hyperazeotropic concentration i.e., 31 mass%. Figure 5.32 depicts the variation of HCl concentration in the feed tank with time and Figure 5.33 shows the effect of time on recovery at 45 ^{o}C. It was observed that the percent recovery of HCl increases linearly and HCl concentration in the feed tank increases exponentially with time. It was observed that by running the experiment for 80 h at 45 ^{o}C, the maximum concentration level of HCl achieved in feed tank was 31 mass% (313.02 kg/m^{3}) with the recovery of 42%. It was not possible experimentally to determine the recovery at 50 ^{o}C due to the highly corrosive nature of HCl at such high temperature. As shown in Figure 5.34 and Figure 5.35, theoretically, 31 mass% feed concentration in the feed tank was achieved in 88.7 h with 26.6% recovery at 40 ^{o}C and in 79 h with 47.4% recovery at 50 ^{o}C. From recovery analysis, it can be concluded that HCl concentration in feed tank increases with increasing the temperature under fixed operating time.

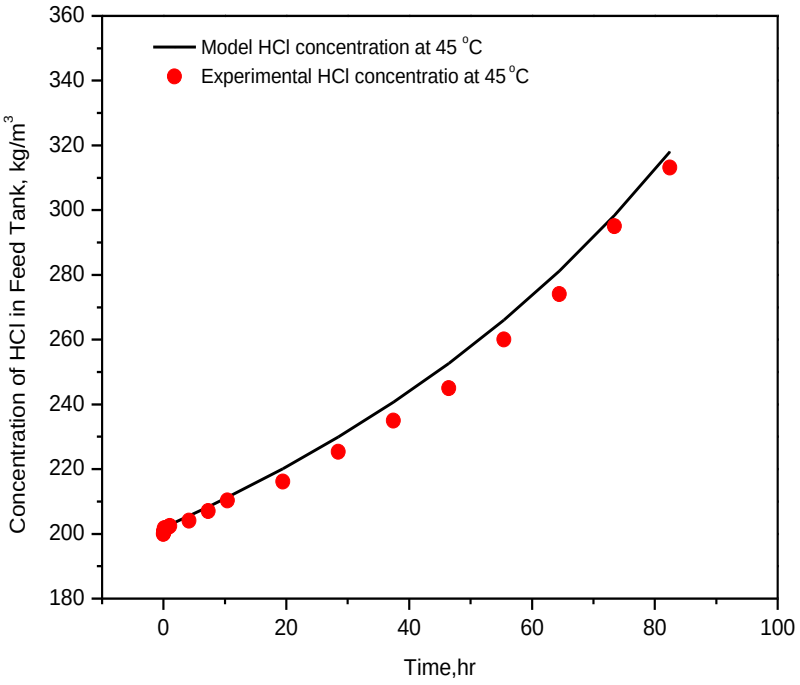

Figure 5.32 : Change in Concentration of HCl in Feed Tank with Time at 45 ^{o}C

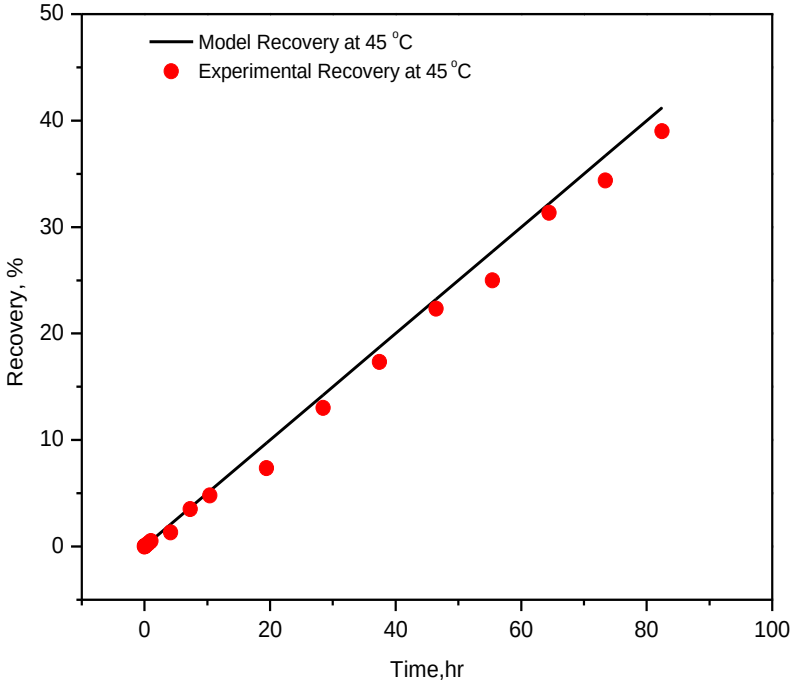

Figure 5.33 : Change in HCl Recovery with Time at 45 °C

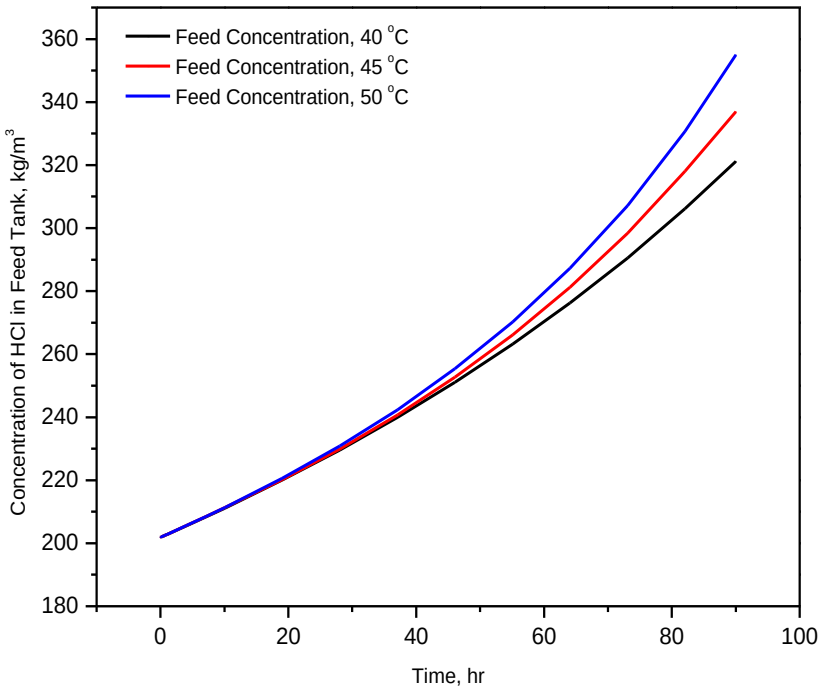

Figure 5.34 : Theoretical Variation in Concentration in Feed Tank at Different Temperature

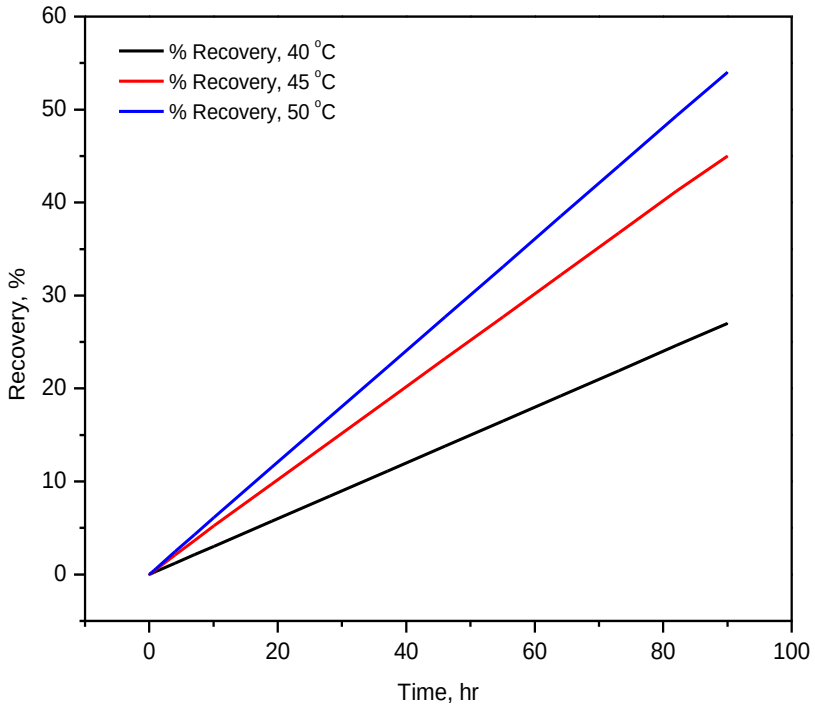

Figure 5.35 : Theoretical Variation in Recovery at Different Temperature

5.7 **Heat Transfer Correlation Development**

At steady state condition heat transport from the hot feed to membrane surface in terms of heat transfer coefficient h_f at feed side boundary layer is defined as –

$$q_1 = h_f(T_b - T_m) \tag{5.6}$$

Here, T_b and T_m are the bulk feed temperature and feed side membrane surface temperature.

Heat transports across the membrane is given by:

$$q_2 = h_m \left(T_m - T_g\right) + \sum N_i \lambda_i \tag{5.7}$$

Where, h_m is membrane heat transfer coefficient, N_i is the mass flux of component i calculated experimentally. λ_i is the latent heat of vaporization of component i. At steady state condition equation (5.6) is equivalent to the equation (5.7). The values of experimentally calculated heat transfer coefficient (h_f) were plotted against feed temperature at different feed flow rates as shown in Figure 5.36. It can be observed from the Figure 5.36 that by increasing the feed temperature and feed flow rate, the heat transfer coefficient increases. Since the heat transfer coefficient is inversely proportional to the viscosity of

fluid therefore by increasing the temperature, fluid viscosity decreases and that leads to rise in heat transfer coefficient.

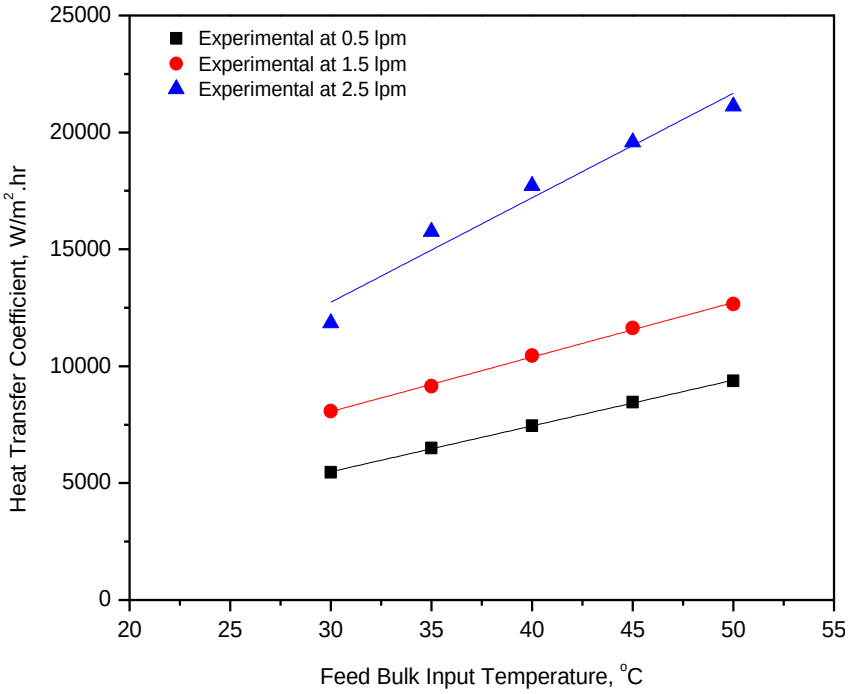

Figure 5.36 : Effect of Feed Bulk Temperature on Heat Transfer Coefficient at Different Feed Flow Rate

This may be attributed by decreasing the concentration and temperature polarization effect on membrane surface by increasing the feed temperature and also higher feed temperature increases vapour pressure on membrane surface leads to higher flux.

Theoretically, Nusselt number was estimated by $Nu = \frac{h_f d_h}{k}$, Reynolds number by $Re = \frac{\rho v d_h}{\mu}$ and Prandtl number by $Pr = \frac{C_p \mu}{k}$. The empirical correlation same as considered in heat exchanger heat transfer coefficient calculation written in simplified form as:

$$Nu = a\, Re^b Pr^c \tag{5.8}$$

Where a, b and c are the characteristic constant which depends on the module design, membrane properties and polarization effect. The empirical correlation given in equation (5.8) was fitted using non- linear regression analysis. The regression analysis gives the optimum value of a, b and c by minimizing the error between the experimental and estimated value of Nusselt number using GRG (Generalized Reduced Gradient) - nonlinear method. The empirical correlation established after fitting the data is as follows:

$$Nu = 4.67\, Re^{0.75} Pr^{0.33} \quad (5.9)$$

A graph between $\boldsymbol{log(Nu/Pr^{0.33})}$ and $\boldsymbol{log(Re)}$ was plotted for both theoretical and experimental values as shown in Figure 5.37. It can be observed from Figure 5.37 that theoretical model is in good agreement with experimental values with R^2 values of 0.938.

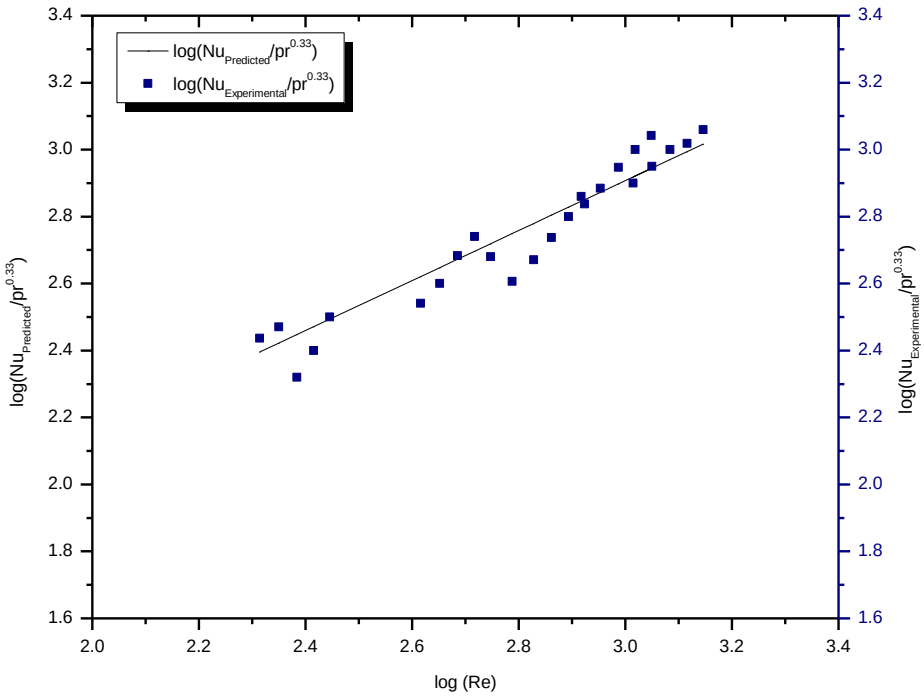

Figure 5.37 : Heat Transfer Correlation Fitting
[$\boldsymbol{log(Nu/Pr^{0.33})}$ *vs* $\boldsymbol{log(Re)}$]

5.8 Mass Transfer Correlation Development

Once the experimental heat transfer coefficient has been calculated, the experimental mass transfer coefficient has been estimated by:

$$k_f = \frac{NRT_{avg}}{M(P_{mf} - P_{pg})} \quad (5.10)$$

Here, N is the total permeate flux, R is the universal gas constant, T_{avg} is the mean of feed side membrane surface temperature and permeate side cooling surface temperature.

Theoretically, mass transfer coefficient was calculated in terms of Sherwood number which is the function of Schmidt number and Reynolds number. The correlation developed in the form of equation (5.11):

$$Sh = x\, Re^{y}\, Sc^{z} \quad (5.11)$$

Where $Sh = k_f d_h / D_{AB}$ and $Sc = \mu / \rho D_{AB}$. The mass transfer coefficient was calculated at different feed temperature ranging from 35 ^{o}C to 50 ^{o}C and feed flow rate varying from 0.5 L/min to 2.5 L/min. Figure 5.38 shows the graph plotted between experimental mass transfer coefficient and bulk feed temperature. From the Figure 5.38, it can be observed that the values of mass transfer coefficient increases by increasing the feed temperature. This effect is mainly credited to the fact that by increasing the temperature, the diffusivity of the volatile component in air increases and since mass transfer coefficient is directly proportional to the diffusivity therefore mass transfer coefficient increases by increasing the temperature. Also, this behaviour can be explained by the effect of temperature on concentration and temperature polarization. By increasing the temperature, concentration and temperature polarization effect decreases that leads to increasing in mass transfer coefficient.

The empirical mass transfer correlation was established by minimizing the error between experimental and theoretical values using newton's method described as:

$$Sh = 10.13\, Re^{0.62} Sc^{0.33} \quad (5.12)$$

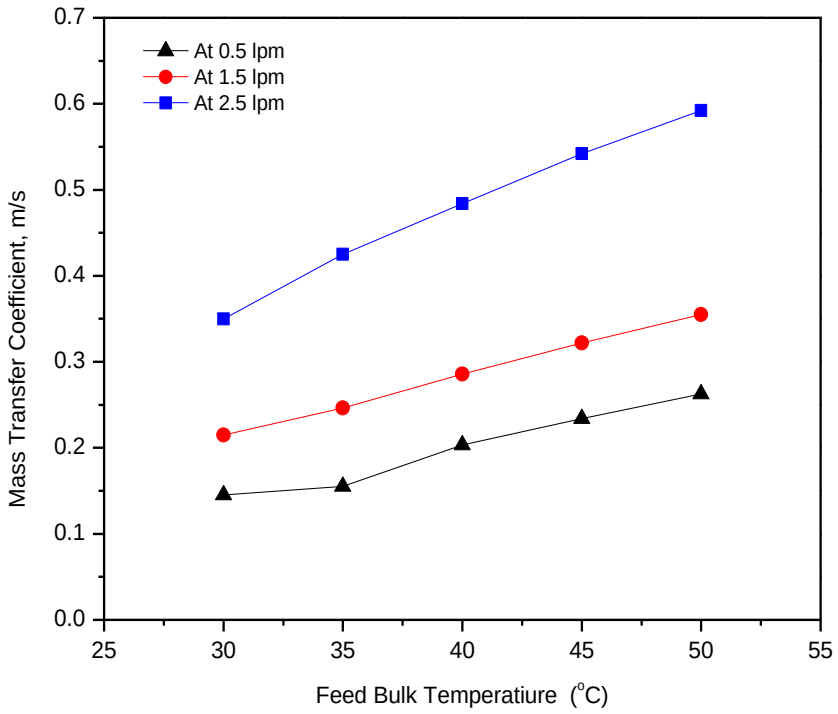

Figure 5.38 : Effect of Feed Bulk Temperature on Mass Transfer Coefficient at Different Feed Flow Rate

A graph between $\boldsymbol{log(Sh/Sc^{0.33})}$ and $\boldsymbol{log(Re)}$ was plotted for both theoretical and experimental values as shown in Figure 5.39. It can be observed from Figure 5.39 that theoretical model is in good agreement with experimental values with R^2 values of 0.973.

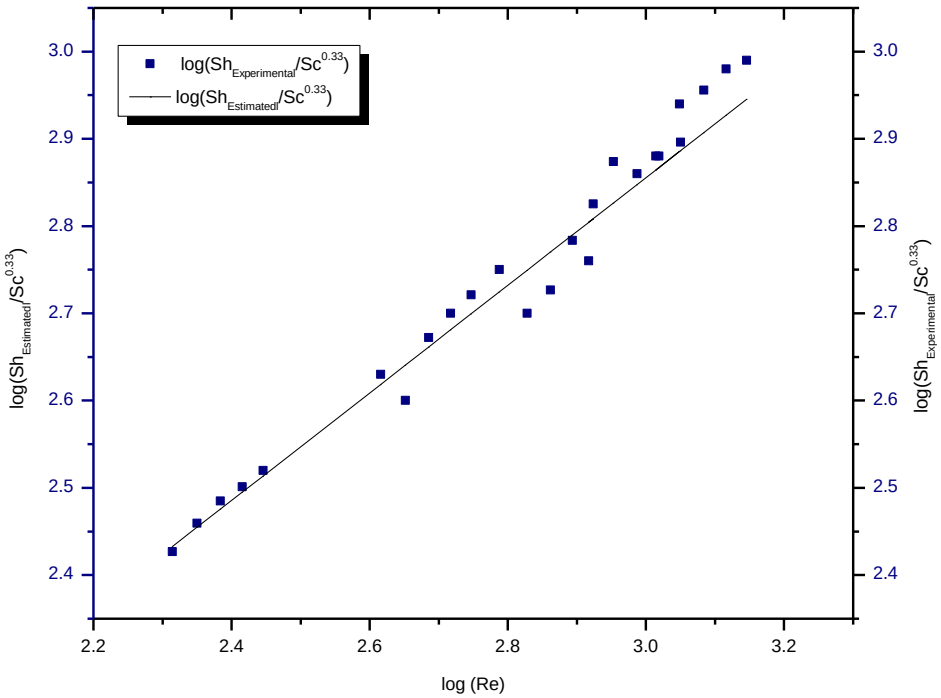

Figure 5.39 : Mass Transfer Correlation Fitting
[$\boldsymbol{log(Sh/Sc^{0.33})}$ *vs.* $\boldsymbol{log(Re)}$]

5.9 **Effect of Inert Gas (Argon) Analysis**

In the AGMD process, the volatile feed components are allowed to pass through the membrane pores and air gap by molecular diffusion to achieve the separation. Since breaking of azeotrope mixture is mainly depends on the diffusivity of volatile components into the air filled in the air gap and membrane pores, therefore, the inert gas used in AGMD play an essential role in breaking azeotrope. Heavy inert gases like argon (Ar), sulfur hexafluoride (SF_6) decelerate the diffusion rates while light gases like helium (He) accelerate the diffusion rate. Till now all the study for the braking of the azeotropic mixture has been studied by using air as an inert gas. Banat *et al.*, (1999b), theoretically predict the effect of inert gases namely helium, air and sulfur hexafluoride on the breaking of formic acid-water azeotrope mixture using the Stefan-Maxwell modeling approach. The authors found that using heaviest inert gas SF_6 azeotropic point was eliminated and gives the best selectivity at the cost of flux drop while keeping all other parameters viz. hot feed temperature, cold side temperature, air gap width and feed composition constant. The effect of different process parameters namely bulk feed input temperature, feed flow rate, air gap

width and cooling water temperature, at azeotropic feed composition, on permeate flux, selectivity, and azeotropic breaking point are compared for argon and air as inert gases.

5.9.1 Effect of argon gas on total permeate flux, HCl selectivity and azeotrope breaking point at different feed bulk inlet temperature

Figure 5.40 shows the effect of bulk feed input temperature on total permeate flux for two different gases argon and air. From Figure 5.40, it can be observed that for light gas such as air (density-1.204 kg/m^3) the total mass flux obtained was higher than the mass flux obtained using a dense gas such as argon (density-1.784 kg/m^3) and also in both cases the permeate flux increases by increasing the bulk feed input temperature from 30 ^oC to 50 ^oC. By increasing the feed temperature, the diffusivity of the HCl and water increases as per fuller correlation demonstrated in equation no. (3.30) (Fuller *et al.,* 1966). The high molecular size and collision frequency of argon gas molecules lower the diffusion rates of volatile feed components through the membrane and the gas gap medium therefore light gas such air increases the total permeate flux while heavy gas such as argon decreases it. Figure 5.41 shows the effect of feed temperature on selectivity at azeotropic concentration for argon and air gases. By increasing the feed temperature, the selectivity of HCl starts decreasing for heavy inert gas argon than the light gas air. At all the temperature range the selectivity of HCl in permeate less than one that means the membrane is more selective towards the water and permeate flux contains more water content as compared to retentate. From Figure 5.41 it can be observed that selectivity for heavy argon gas is shifted more from unity as compared to light gas air. It is well known that lower the selectivity from unity the better separation is, therefore, argon gives better separation in terms of selectivity but at the cost of flux reduction. Mass% permeate and retentate HCl concentration changes with temperature have been shown in Figure 5.42 and Figure 5.43, respectively. The lower selectivity of the membrane towards HCl vapor leads to the reduction of HCl concentration in permeates and rises of HCl concentration in retentate for both inert gases.

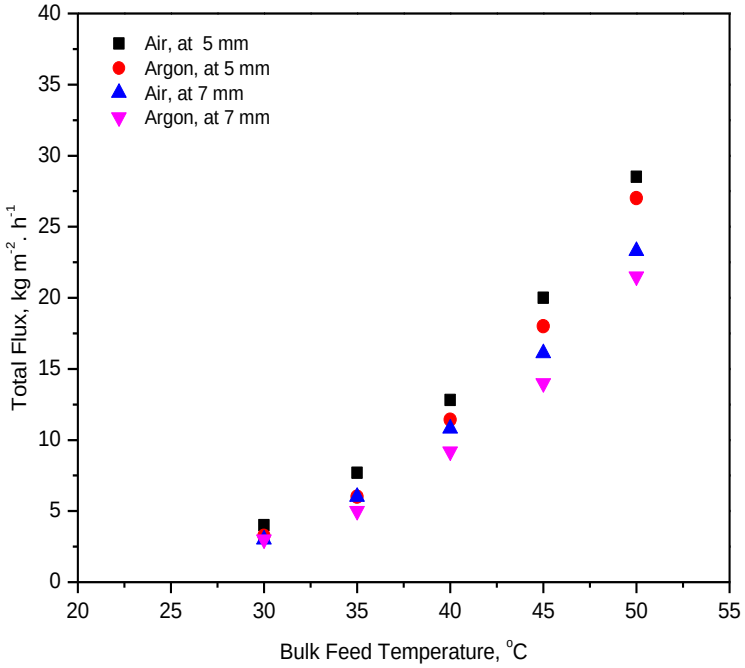

Figure 5.40 : Effect of Bulk Feed Temperature on Total Permeate Flux for Different Inert Gases
(T_c = 20 °C, feed flow rate = 2 L/min, cooling water flow rate = 1 L/min)

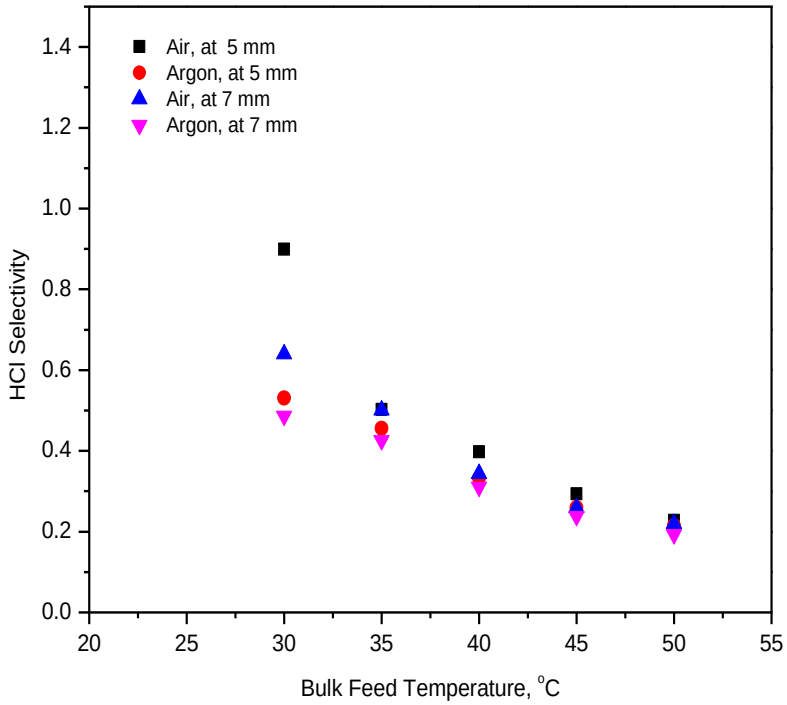

Figure 5.41 : Effect of Temperature on HCl Selectivity for Different Inert Gases
(T_c = 20 °C, feed flow rate = 2 L/min, cooling water flow rate = 1 L/min)

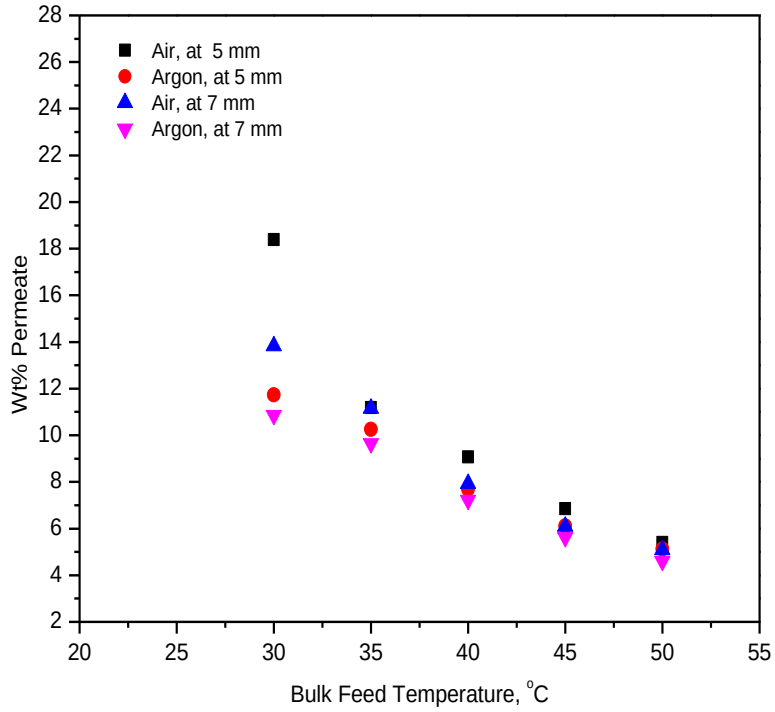

Figure 5.42 : Change in Permeate HCl Concentration for Different Inert Gases with Bulk Feed Temperature
(T_c= 20 °C, feed flow rate = 2 L/min, cooling water flow rate = 1 L/min)

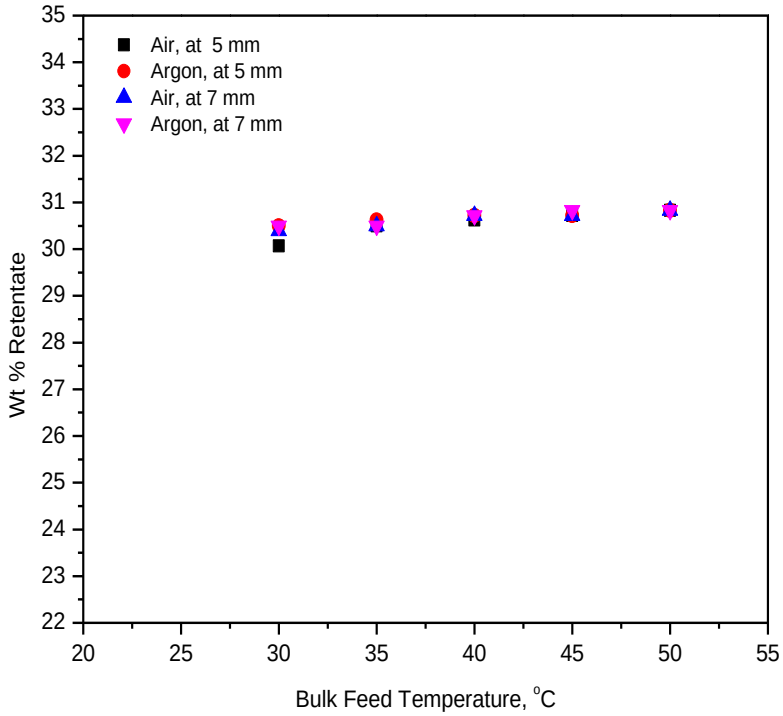

Figure 5.43 : Change in Retentate HCl Concentration for Different Inert Gases with Bulk Feed Temperature
(T_c = 20 °C, feed flow rate = 2 L/min, cooling water flow rate = 1 L/min)

5.9.2 Effect of argon gas on total permeate flux, HCl selectivity and azeotrope breaking point at different feed flow rate

The effect of feed flow rate on the total mass flux and selectivity is enlightened by the Figure 5.44 and Figure 5.45, respectively. As the flow rate increases, the flux starts increasing due to the reduction in the thermal boundary layer at large Reynolds number. The thermal boundary layer reduction in the case of heavy argon gas is small due to its large molecular size; therefore, flux growth for argon was more modest as compared to the light inert gas, i.e., air. Concurrently, the high flow rate decreases the HCl diffusional resistance through the membrane by reducing the interfacial concentration. Subsequently, the selectivity of HCl increases but this increment is almost constant, as shown in Figure 5.45, due to small HCl feed concentration. Since selectivity of HCl increases with flow rate, therefore, HCl concentration in permeate increases as shown in Figure 5.46 and in retentate it remains almost constant in increasing flow rate as shown in Figure 5.47.

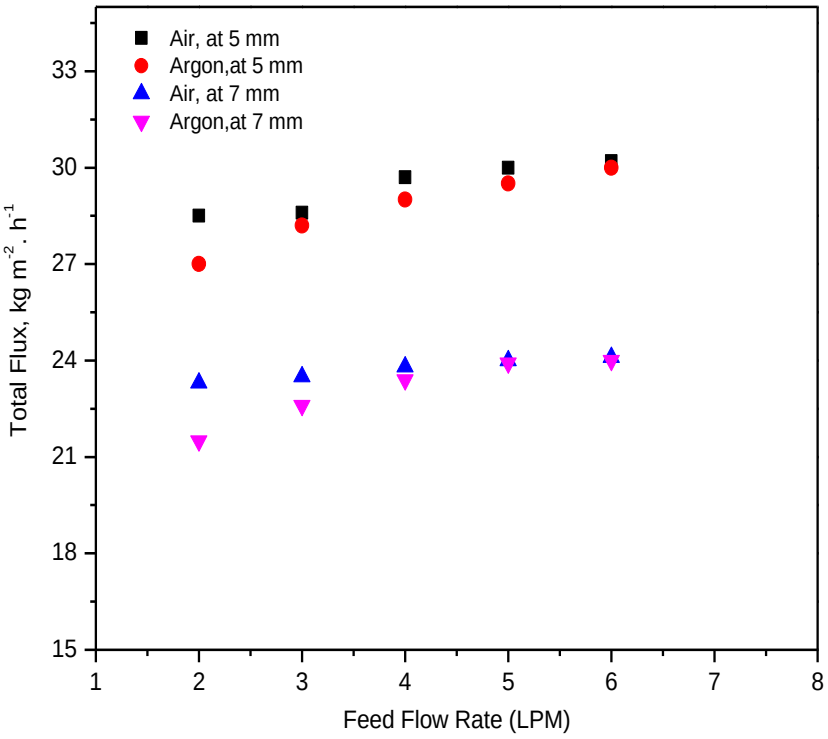

Figure 5.44 : Effect of Feed Flow Rate on Total Permeate Flux for Different Inert Gases
(T_b = 50 ^{o}C, T_c = 20 ^{o}C, cooling water flow rate = 1 L/min)

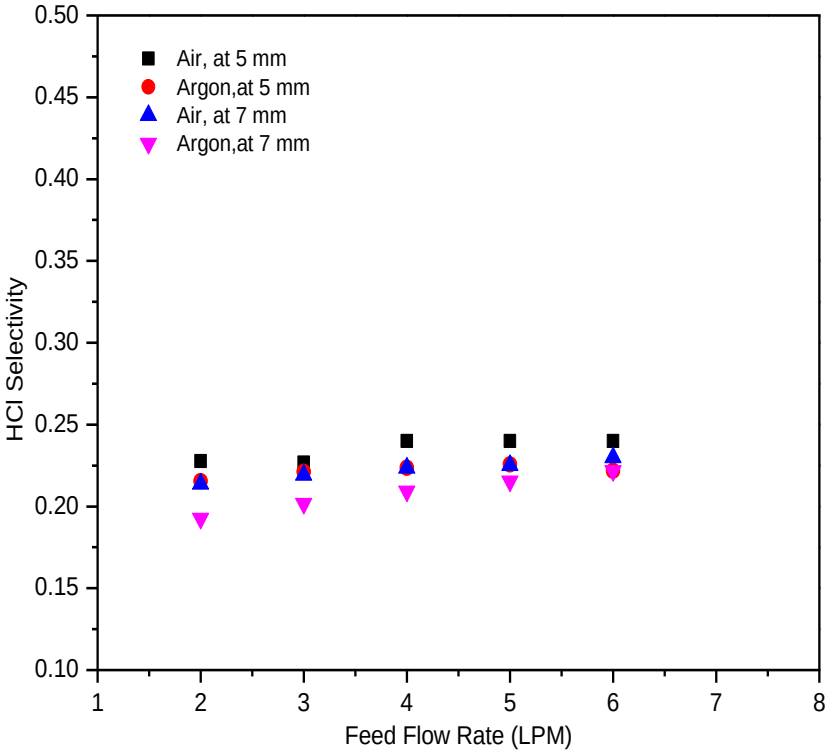

Figure 5.45 : Effect of Feed Flow Rate on HCl Selectivity for Different Inert Gases (T_b = 50 ^{o}C, T_c = 20 ^{o}C, cooling water flow rate = 1 L/min)

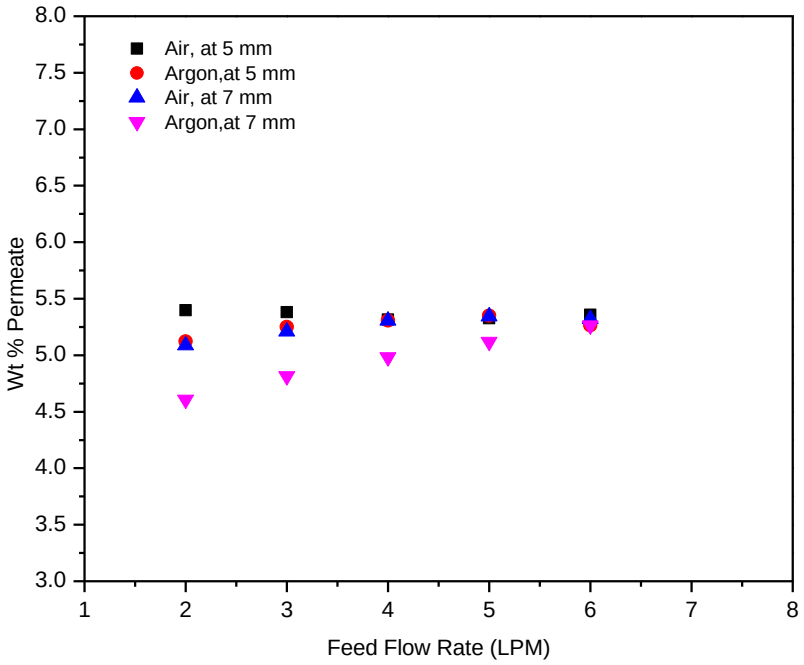

Figure 5.46 : Change in Permeate HCl Concentration for Different Inert Gases with Feed Flow Rate (T_b = 50 ^{o}C, T_c = 20 ^{o}C, cooling water flow rate = 1 L/min)

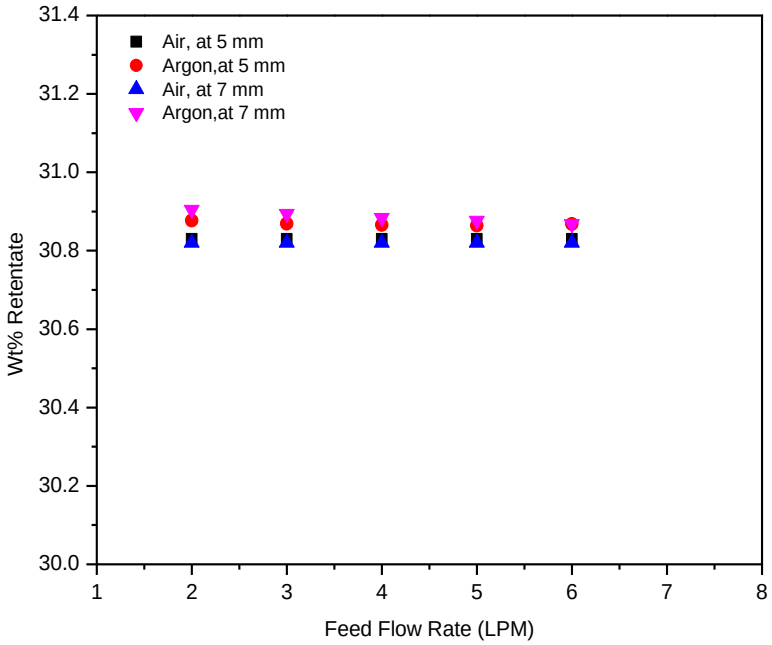

Figure 5.47 : Change in Retentate HCl Concentration for Different Inert Gases with Feed Flow Rate
(T_b = 50 ^{o}C, T_c = 20 ^{o}C, cooling water flow rate = 1 L/min)

5.9.3 Effect of argon gas on total permeate flux, HCl selectivity and azeotrope breaking point at different air gap thickness

Figure 5.8 shows the effect of air gap thickness on the total mass flux at different feed flow rate when argon and air used as inert gases and at the bulk feed temperature of 50 ^{o}C, cooling water temperature 20 ^{o}C, cooling water flow rate at 1 L/min and azeotropic feed concentration. It is depicted in Figure 5.48 that by increasing the air gap, the permeate flux decreases due to high mass transfer resistance provided by the air gap width. Mass transfer resistance supplied by the argon gas was higher than the resistance exerted by the air due to the large molecular size of heavy argon gas. That's the reason of obtaining lower permeate flux in the case of argon at different flow rate than achieved in the case of air. Change in selectivity with the air gap as shown in Figure 5.49. The selectivity starts decreasing with the air gap. This change of selectivity lies in the range 0.2 to 0.3. The shift in permeate and retentate concentration for the different inert gases was shown Figure 5.50 and Figure 5.51, respectively.

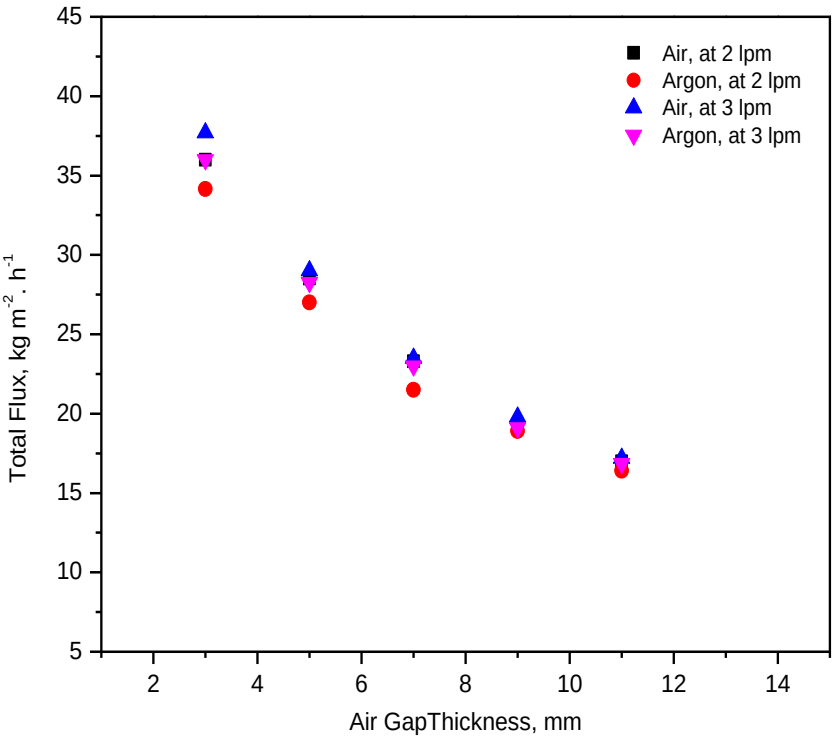

Figure 5.48 : Effect of Air Gap Width on Total Permeate Flux for Different Inert Gases
(T_b = 50 ^{o}C, T_c = 20 ^{o}C, cooling water flow rate = 1 L/min)

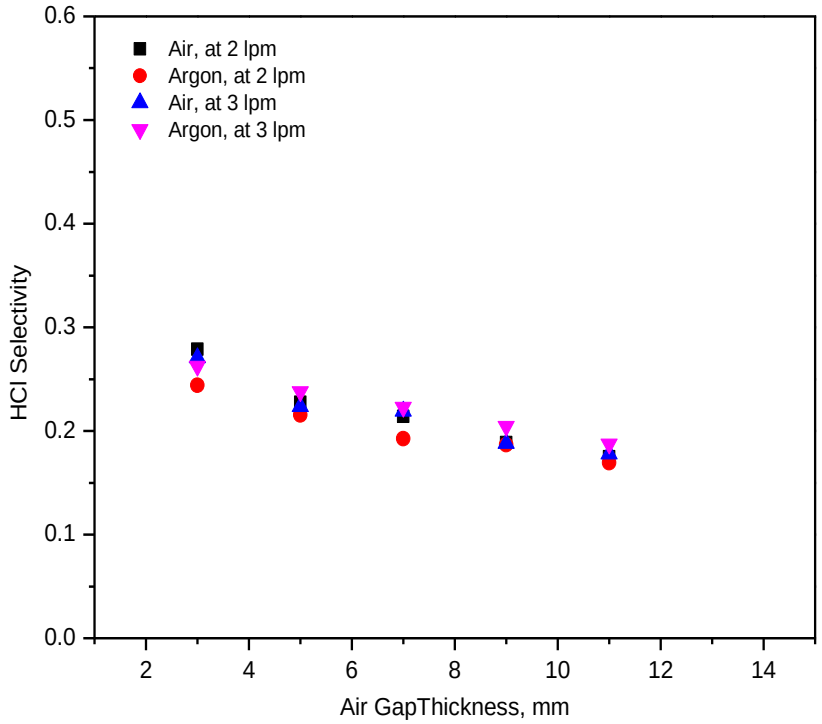

Figure 5.49 : Effect of Air Gap Width on HCl Selectivity for Different Inert Gases
(T_b = 50 ^{o}C, T_c = 20 ^{o}C, cooling water flow rate = 1 L/min)

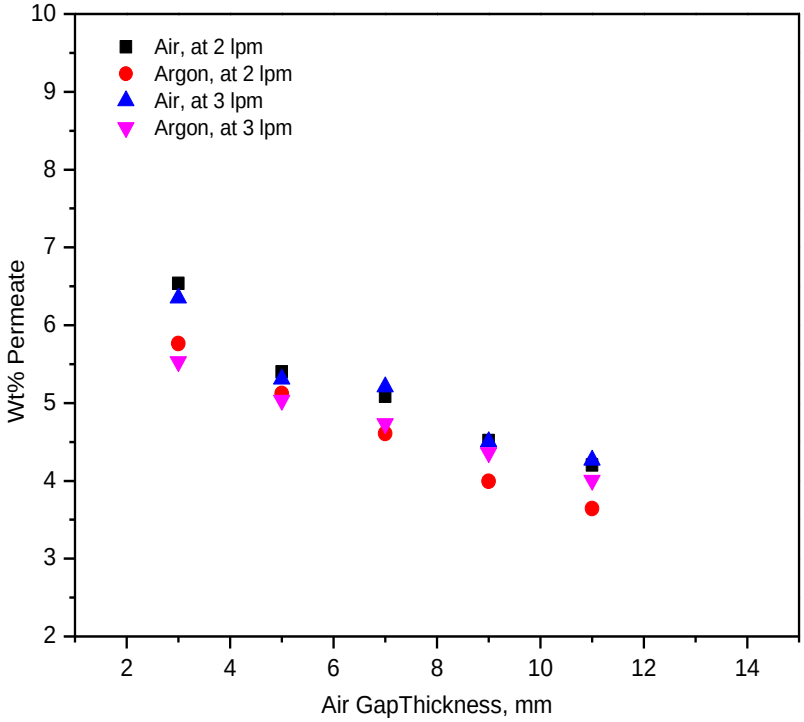

Figure 5.50 : Change in Permeate HCl Concentration for Different Inert Gases with Air Gap Width
(T_b = 50 ^{o}C, T_c = 20 ^{o}C, cooling water flow rate = 1 L/min)

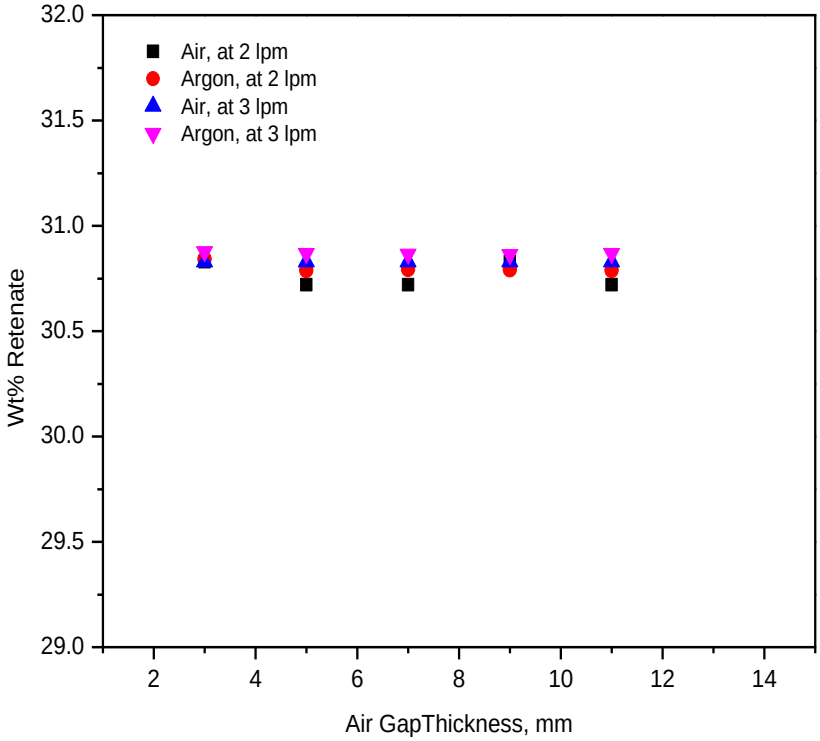

Figure 5.51 : Change in Retentate HCl Concentration for Different Inert Gases with Air Gap Width
(T_b = 50 ^{o}C, T_c = 20 ^{o}C, cooling water flow rate = 1 L/min)

5.9.4 Effect of argon gas on total permeate flux, HCl selectivity and azeotrope breaking point at different cooling water temperature

The effect of cooling water temperature on the flux at different air gap width for the argon and air as inert gases is explained by the Figure 5.52. The cooling water temperature change from 5 ^{o}C to 25 ^{o}C while keeping all other operation parameters constant. As evident, the permeate flux decreases on increasing the cooling water temperature because the temperature gradient gets reduced and that leads to the reduction in the driving force for the mass transfer. For heavy gas, i.e., argon this temperature gradient reduction is considerable as compared to light gas, i.e., air. Although no significant change in the selectivity was observed when the cooling water temperature changes in both cases of air and argon inert gases as depicted in Figure 5.53. This means increasing the cooling water temperature constantly modify the ratio of molecular interactions. Change in permeate and retentate HCl concentration with cooling water temperature is elucidated in Figure 5.54 and Figure 5.55, respectively.

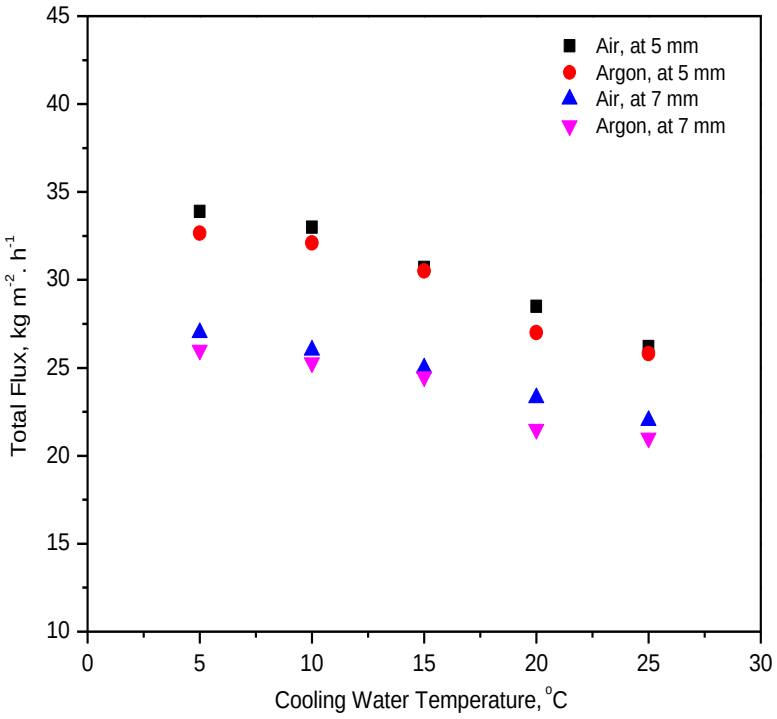

Figure 5.52 : Effect of Cooling Water Temperature on Total Permeate Flux for Different Inert Gases
(T_b = 50 ^{o}C, feed flow rate = 2 L/min, cooling water flow rate = 1 L/min)

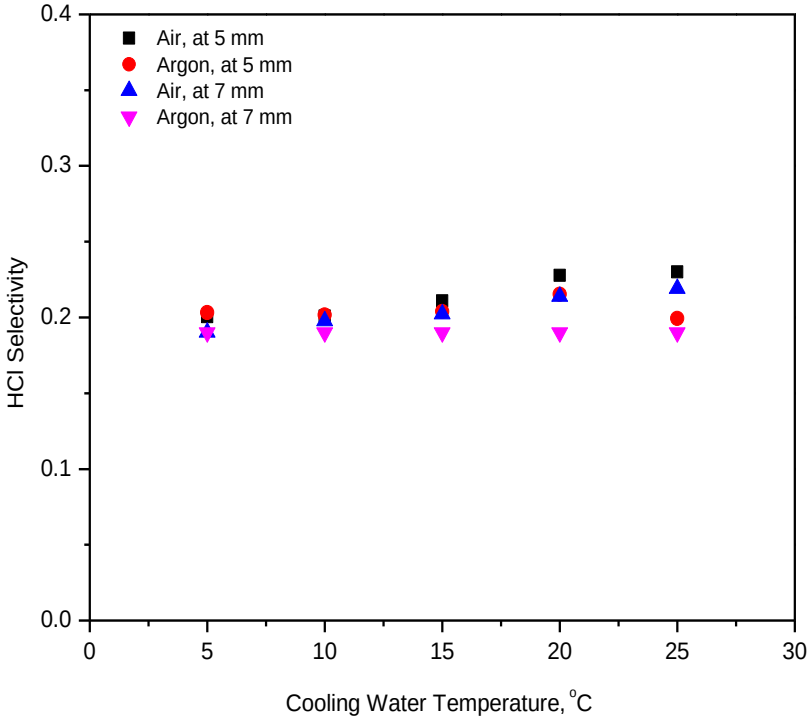

Figure 5.53 : Effect of Cooling Water Temperature on HCl Selectivity for Different Inert Gases
(T_b = 50 °C, feed flow rate = 2 L/min, cooling water flow rate = 1 L/min)

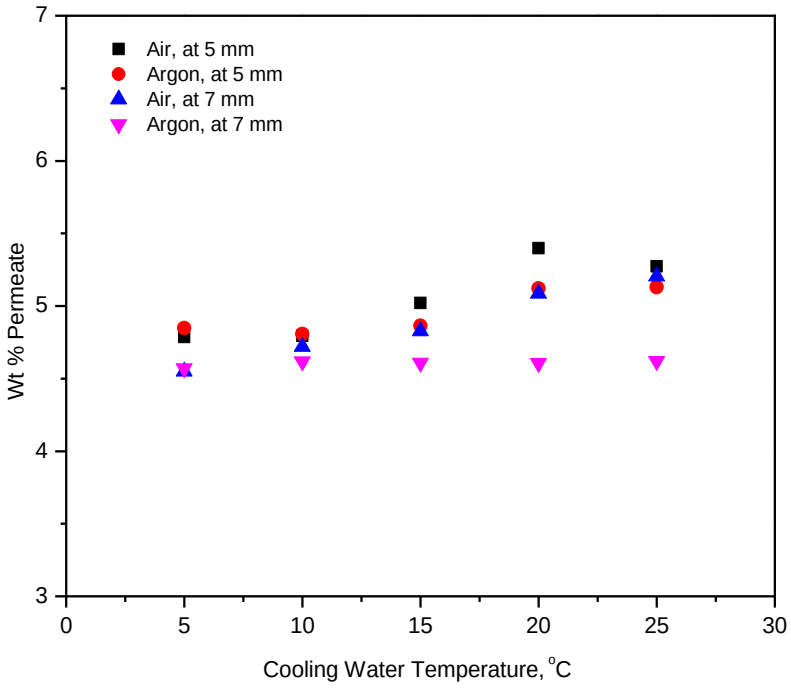

Figure 5.54 : Change in Permeate HCl Concentration for Different Inert Gases with Cooling Water Temperature
(T_b = 50 °C, feed flow rate = 2 L/min, cooling water flow rate = 1 L/min)

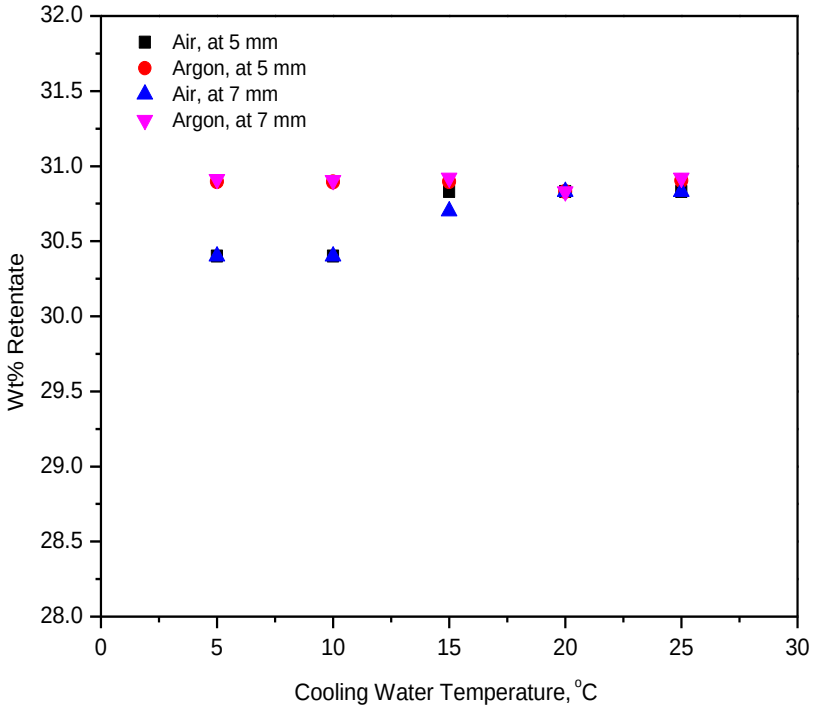

Figure 5.55 : Change in Retentate HCl Concentration for Different Inert Gases with Cooling Water Temperature
(T_b = 50 °C, feed flow rate = 2 L/min, cooling water flow rate = 1 L/min)

5.10 **Flux Calculation by ANN Model**

In the development of ANN model for AGMD process, 68 experiments were performed at different operating conditions. 5 input were selected that are corresponds to Bulk Feed Input Temperature (35-50 °C), Air Gap Thickness (3-11 mm), Feed Flow Rate (2-10 L/min), Cooling Water Temperature (5-25 °C) and Cooling Water Flow Rate (1-5 L/min). The other ANN model specifications are given in Table 5.9. Total permeate flux was selected as output target. Among the 68 AGMD experimental data sets, 75% of total data sets were used for the training purpose and remaining 25 % for testing and validation purpose. Thus, 51 AGMD data sets used for the training, 9 experimental data sets for the validation and 8 data sets for the testing of ANN model. The ANN topology used for the study can be presented as ANN (5:10:1), here 5 corresponds to the number of inputs and 10 shows the number of hidden layer neurons number and 1 represents the number of neuron in the output layer. The performance function used for the ANN modeling is Mean Squared Error (MSE). The feed-forward neural network was trained as shown in the Figure 5.56, and selects the one having minimum value of the performance function. The optimal values of network (5:10:1) parameters (i.e. weights and biases) , as shown in Table 5.10, gained after NN training using

Back-Propagation method based on Levenberg–Marquardt algorithm (LMA). The size of input weight matrix was found as (5×10).

Table 5.9: ANN Specifications

ANN Model	Specification
Inputs	5
Target	1 (Permeate Flux)
No. of Neurons	10 (In Hidden Layer)
Learning Function	TRAINLM
Adaptation Learning Algorithm	LEARNGDM
Performance Function	MSE
Transfer Function	TANSIG

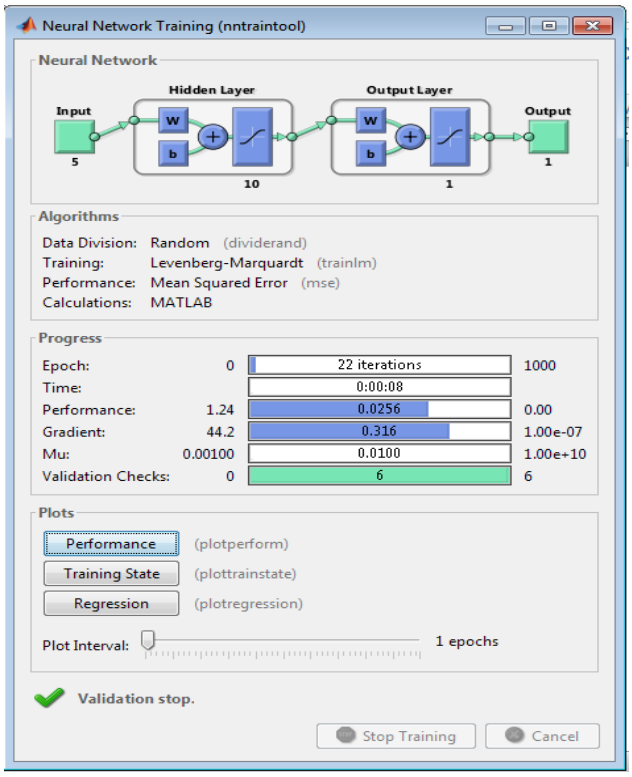

Figure 5.56 : Neural Network Model Training

Table 5.10 : Optimal Value of Network Weights and Biases Gained after NN training

Input Weight Matrix iw {1,1} (From Input layer to hidden layer)	- 2.0701	-1.9022	0.83952	-0.73637	0.86402
	- 0.51514	-1.1498	0.03047	1.0658	0.59096
	0.93402	-0.67564	-3.0758	-0.5984	1.3865
	0.9242	-0.18839	0.8057	-2.4215	0.90896
	3.4742	0.41218	-0.1281	0.05545	-0.0132
	0.22113	-0.71905	-0.72613	0.55333	-1.2286
	-0.89288	1.1446	0.41164	0.54595	0.98581
	1.0332	- 4.0763	0.84881	1.0291	1.473
	1.2023	-0.18927	-0.75473	-2.1229	0.47767
	0.13324	0.25542	0.02721	1.4128	-0.36144
Bias Vector b{1} to Hidden Layer	3.2209				
	1.1167				
	1.6319				
	2.6405				
	-0.19183				
	0.12229				
	-0.92608				
	1.4721				
	1.1362				
	-2.0214				
Layer Weight Vector lw{2,1} (From hidden layer to output layer)	[-0.057197 -1.7387 0.52395 -1.0742 -2.512 -5.47 1.4896 0.17111 -0.44075 -0.8567]				
Bias Scalar b{2} to Output Layer	[0.34717]				

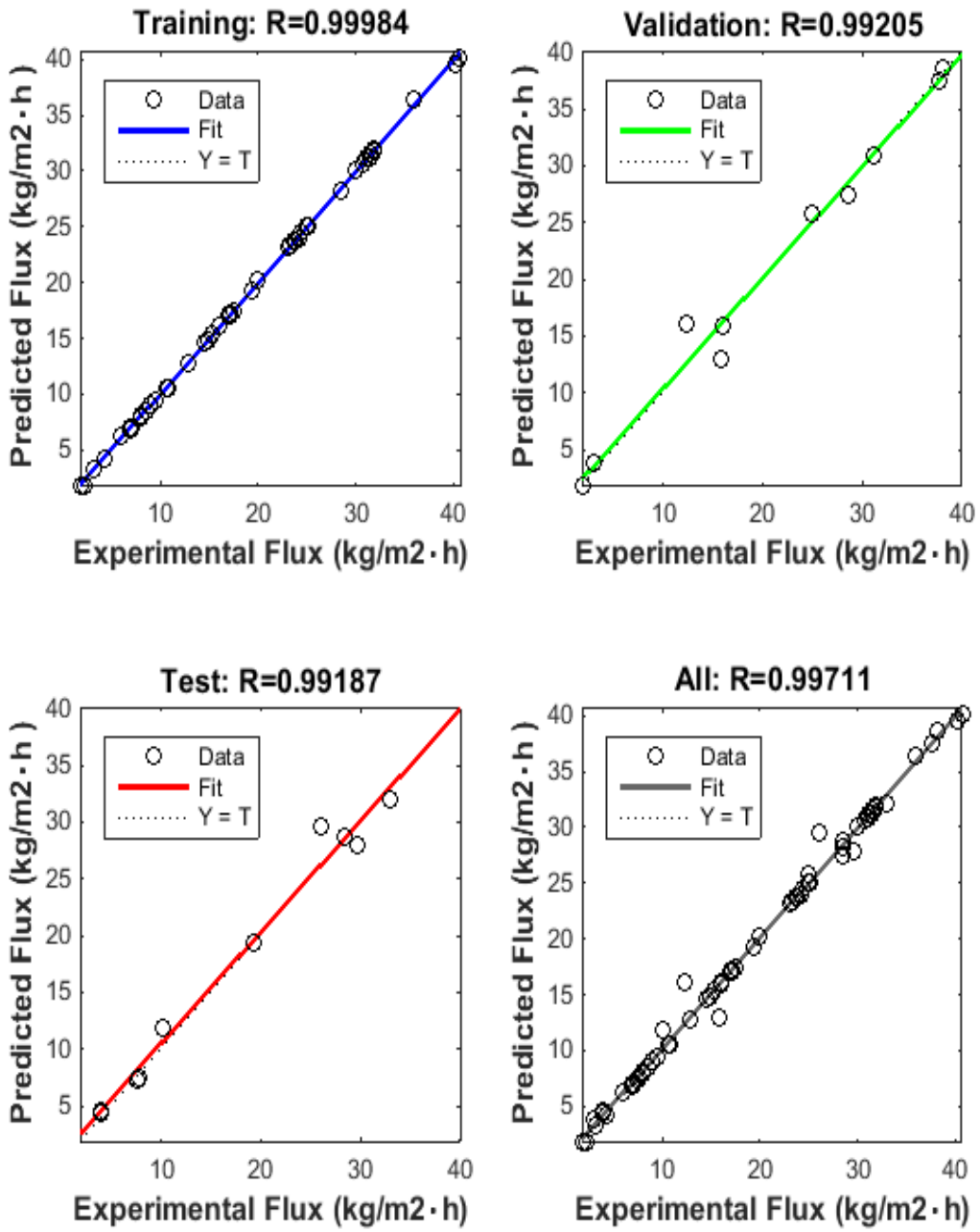

Figure 5.57 : Comparison of AGMD Experimental Data and ANN Predicted One for Independently Training, Validation and Testing Subsets and for Combined Data Set (Training + Validation + Testing)

Table 5.11 : Comparative Study of ANN Modeling and Mathematical Modeling

S. No.	Experimental Flux ($kg/m^2 \cdot h$)	Model (1) Flux	Model (2) Flux	MAPE for Model (1)	R^2 for Model (1)	MAPE for Model (2)	R^2 for Model (2)
1.	6.85	6.11	6.7692	3.261	0.997	2.971	0.994
2.	7.7	7.4	7.5517				
3.	10.8	10.14	10.6108				
4.	4	3.78	4.6037				
5.	31.9	32.31	32.0124				
6.	31.9	32.32	31.6974				
7.	31.8	32.32	31.8924				
8.	19.3	19.16	19.3371				
9.	17	16.58	16.9887				
10.	9	8.6	9.0685				
11.	15.8	15.62	12.943				
12.	24.2	25	24.0403				
13.	12.8	12.2	12.7837				
14.	20	19.2	20.1709				
15.	19.3	19.16	19.3371				
16.	17	16.58	16.9887				
17.	37.7	37.5	37.4797				
18.	38.2	38.04	38.6211				
19.	40.2	40.02	39.5088				
20.	40.7	40.2	40.0624				
21.	36	37	36.4661				
22.	28.5	28.4	28.7606				
23.	23.3	22.89	23.3027				
24.	7	7.11	7.0663				
25.	7.5	7.11	7.3561				
26.	7.15	7.11	7.0977				
27.	4.25	4.05	4.1365				
28.	3.85	4.05	4.4465				
29.	4.25	4.05	4.2474				
30.	1.8	1.81	1.8184				
31.	1.85	1.81	1.8118				
32.	2.25	1.81	1.8085				
33.	8	8.33	8.017				
34.	8.55	8.33	8.4493				
35.	8.1	8.33	8.2047				
36.	10.1	10.24	11.9235				
37.	10.55	10.24	10.5902				
38.	9.5	10.24	9.4415				
39.	14.9	16.39	14.8994				
40.	15.95	16.39	15.9378				
41.	15.35	16.39	15.3522				

S. No.	Experimental Flux ($kg/m^2 \cdot h$)	Model (1) Flux	Model (2) Flux	MAPE for Model (1)	R^2 for Model (1)	MAPE for Model (2)	R^2 for Model (2)
42.	17.15	17.81	17.1222	3.261	0.997	2.971	0.994
43.	17.45	17.81	17.4747				
44.	17.15	17.81	17.1716				
45.	23.7	24.08	23.6939				
46.	23.2	24.08	23.2112				
47.	23.8	24.08	23.8176				
48.	24.45	24.77	24.4412				
49.	24.9	24.77	25.7197				
50.	25.1	24.77	25.1379				
51.	3	2.82	3.8173				
52.	6	5.73	6.2251				
53.	28.6	28.7	27.4394				
54.	29.7	28.9	27.9044				
55.	30	29.56	30.0703				
56.	33	32.32	32.0817				
57.	30.7	30.59	30.669				
58.	26	25.84	29.5811				
59.	25	24.53	24.9815				
60.	28.5	28.4	28.3003				
61.	31.1	30.59	31.2332				
62.	31.2	30.59	30.8398				
63.	31.4	30.6	31.1243				
64.	31.4	30.6	31.6077				
65.	3.15	3.18	3.2077				
66.	12.35	11.62	16.0769				
67.	16.1	15.71	16.0877				
68.	14.62	13.32	14.6453				

Model (1): Mathematical Model

Model (2): ANN Model

The effect of feed inlet temperature on the permeate flux was studied for both the mathematical model and ANN model as shown in Figure 5.58. During the study all other parameters kept constant viz. Air Gap Width at 5 mm, Feed Flow Rate at 2 L/min, Cooling Water Temperature at 20 ^oC and Cooling Water Flow Rate at 1 L/min. The R^2 and MAPE values show the ANN model superiority over the mathematical model as shown in Table 5.12.

Table 5.12: Comparison of ANN and Mathematical Model in terms of Effect of Bulk Feed Input Temperature

Feed Input Temperature	Experimental Flux ($kg/m^2 \cdot h$)	Model (1) Flux	Model (2) Flux	MAPE for Model (1)	R^2 for Model (1)	MAPE for Model (2)	R^2 for Model (2)
30	4	3.78	4.6037	3.862	0.999	3.391	0.999
35	7.7	7.4	7.5517				
40	12.8	12.2	12.7837				
45	20	19.2	20.1709				
50	28.5	28.4	28.7606				

Model (1): Mathematical Model

Model (2): ANN Model

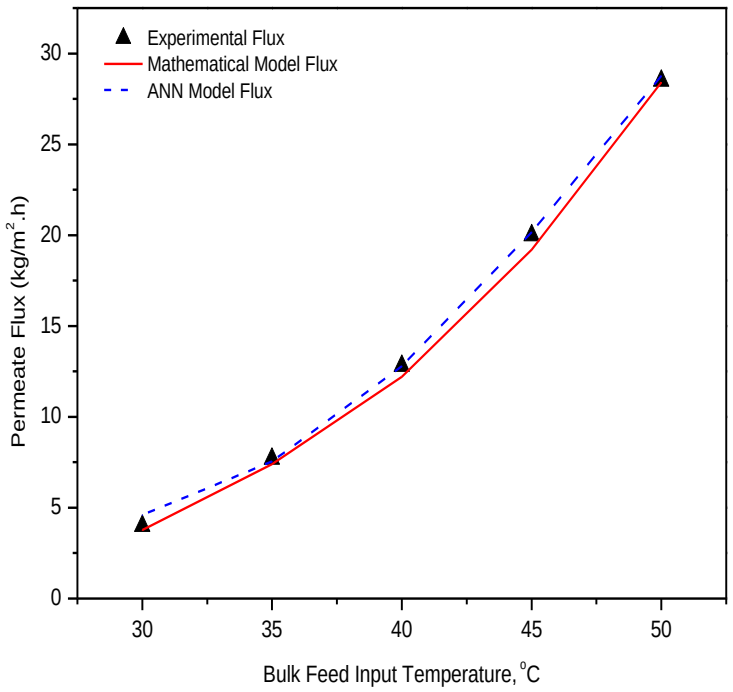

Figure 5.58 : Effect of Feed Input Temperature on Total Permeate Flux

Similarly, ANN model and mathematical model compares in terms of effect of air gap width on permeate flux at different operating conditions as shown in Figure 5.59. The R^2 and MAPE value for ANN model found better than the mathematical model as depicted in the Table 5.13.

Table 5.13 : Comparison of ANN and Mathematical Model in terms of Effect of Air Gap Width

(Feed inlet temperature at 50 ^{o}C, Feed Flow Rate at 2 L/min, Cooling Water Temperature at 20 ^{o}C and Cooling Water Flow Rate at 1 L/min)

Air Gap Width (mm)	Experimental Flux (kg/m^2·h)	Model (1) Flux	Model (2) Flux	MAPE for Model (1)	R^2 for Model (1)	MAPE for Model (2)	R^2 for Model (2)
3	36	37	36.4661	1.622	0.998	0.491	0.999
5	28.5	28.4	28.7606				
7	23.3	22.89	23.3027				
9	19.3	19.16	19.3371				
11	17	16.58	16.9887				

Model (1): Mathematical Model

Model (2): ANN Model

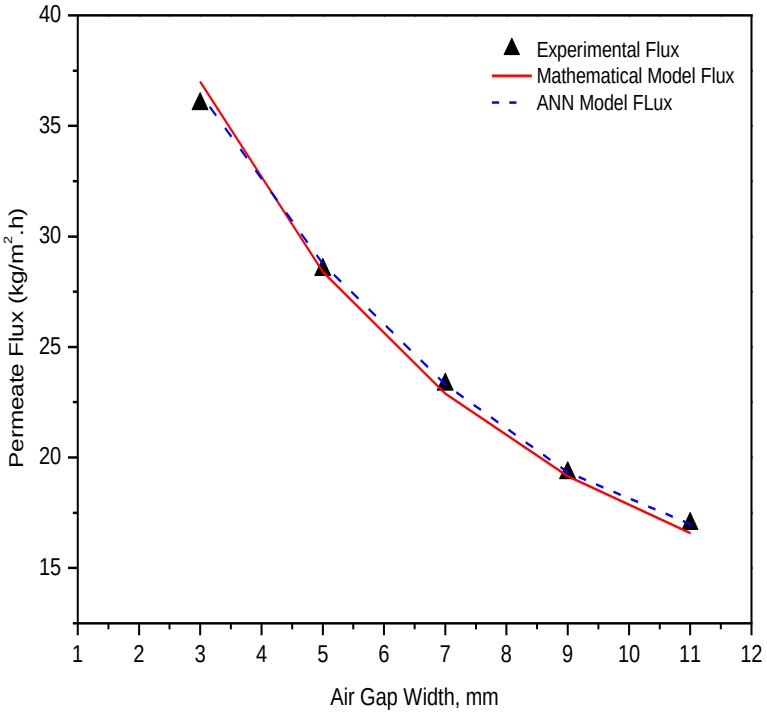

Figure 5.59: Effect of Air Gap Width on Total Permeate Flux

CHAPTER 6

ECONOMIC EVALUATION

Any developed process or technique cannot be successful until it is cost effective. Therefore the separation of HCl/Water azeotrope using AGMD process has been compared with the conventional extractive distillation process, in terms of specific energy consumption and unit product cost, to find out the effectiveness and profitability of the above developed AGMD process. The objective of this part of study is to simulate the HCl/water distillation process to compare the extractive distillation process with the AGMD process. The simulation software used for the study is AspenOne version 10.1 under licence from AspenTech.

6.1 **Cost Model Development for AGMD**

The process cost for the separation of HCl/Water azeotrope by AGMD is mainly depends on the plant capacity, plant life, energy charge and investment amortization. The total cost in AGMD primarily divided into two parts capital cost and annual operating cost. The main components of capital cost are cost of membrane module, purchasing cost of main and auxiliary equipment's, installation charges and land cost. The annual operating cost mainly covers the amortization or fixed Cost, operating & maintenance (O & M) Cost and membrane replacement cost. The O & M Costs are mainly consisting of; fixed operating & maintenance cost (FO & M) and variable operating & maintenance (VO & M) Cost. FO & M cost includes maintenance and staff salary while VO & M includes grid energy cost and pretreatment cost (Banat and Jwaied, 2008).

The common economic parameters used for the calculation are enumerated below:

Plant life – 10 year

Annual Interest Rate – 5%

Annual Membrane Replacement Rate – 1%

Chemical Pre-treatment Cost – Zero

Plant Availability – 90%

6.1.1 Capital Cost

The total capital cost includes cost of all the components which are one time investment. The purchased equipment cost is the beginning for calculating the capital investment. Thus,

it can be considered as the start point for calculation. Table 6.1 lists the capital investment cost for different purchased equipment's.

The plant considered for the cost calculation is on the laboratory scale; therefore the land cost can be neglected.

Table 6.1 : Different Equipment's Investment Cost

S. No.	Equipment	Cost (Rs.)
1.	Membrane	24043
2.	Membrane Module	30000
3.	Feed Tank	15000
4.	Chiller	40120
5.	Heater	1000
6.	Cooling Pump	2500
7.	Receiver	2000
8.	Acid Pump	21785
9.	Rotameter	10000
10.	Thermocouples	2500
11.	Piping Cost	3000
	Total	**151948**

- Total Equipment Cost (*Rs.*) = = 1,51,948 /-
- Installation Cost (*Rs.*) = 37,987/- (25% of the purchased Equipment Costs)
- Instrumentation & Control Cost (*Rs.*) = 37,987/- (25% of purchased equipment cost)
- Land Cost = zero

$$\text{Total Capital Cost } (Rs.) = \text{Total Equipment Cost} + \text{Installation Cost} + \text{Instrumentation \& Control Cost} \quad (6.1)$$

$$= 2{,}27{,}922 \text{ /-}$$

6.1.2 Annual Operating Cost

The annual operating cost includes cost of all the components incurred after establishing the plant and during the plant operation.

Amortized Capital Cost (ACC) or Annual Fixed Charges consist of annual interest amount paid for the borrowed capital and is calculated by the following formula (Tavakkoli *et al.*, 2017):

$$ACC\ (Rs.) = a * Capital\ Cost\ (CC) \quad (6.2)$$
$$= 29515.90/-$$

Here, a = Amortization Factor and calculated as:

$$a = \frac{i\,(1+i)^n}{(1+i)^n - 1} \quad (6.3)$$

Here, i is annual interest rate (5%) and n is life time of plant in year (10 yr).

Fixed Operating & Maintenance Cost - In this study, the annual operator and administrator cost considered as the 20% of the annual fixed charges or annual payment of the plant (Banat and Jwaied, 2008).

Finally,

$$FO\ \&\ M\ Cost\ (Rs.) = 0.2*ACC \quad (6.4)$$
$$= (0.2)(29515.90)$$
$$= 5903.18/-$$

Variable Operating & Maintenance Cost – As already discussed, the VO & M cost includes the membrane replacement cost, grid energy cost, raw material cost and chemical pre-treatment cost.

Since there is no chemical treatment required for the HCl/Water separation, therefore no chemical pre-treatment cost involved.

Since in the present study the azeotrope taken from such sources, as mentioned in the section 1.7.1, from which it has been discharged as the waste stream, therefore cost of raw materials is not accounted in the economic evaluation.

In almost all the membrane separation process, the frequency of membrane replacement mainly depends on the feed quality. For MD desalination processes the membrane replacement cost varies from 5% to 20% depending on the feed quality (Ettouney H. & Dessouky H., 2002). It has been already discussed, in section 5.5 under the heading membrane morphology study before and after the use, that the minimal membrane fouling was observed for the separation of HCl/Water azeotrope due to the fact of the volatile nature of feed components. As a result of negligible fouling on the membrane surface, the membrane replacement cost (MRC) is considered only 1% of membrane module cost for the 1 year plant life period.

$$MRC\ (Rs.) = 1\%\ of\ Membrane\ Module\ Cost \quad (6.5)$$
$$= 300\ /-$$

Grid Energy Cost includes the electricity cost required to run the plant. Electric energy contribution in the total energy consumption is maximum for the electrically operated plant (Xie *et al.*, 2016). The grid energy cost depends on the units of energy consumed in *kWh* and electricity tariff in *Rs/kWh*. The energy cost was estimated by the following formula (Tavakkoli *et al.*, 2017) assuming the electricity tariff as 7.5 *Rs/kWh* according to prevailing electricity board charges:

$$Grid\ Energy\ Cost\ (GEC) = No.of\ units\ (kWh/Day) * 7.5\ Rs/kWh \quad (6.6)$$

Number of unit consuming depends on the specific energy consumption and amount of experimental flux producing if plant is operated for one year. The specific energy consumption has been estimated 0.94039 kWh to generate per kilogram of 30.8 mass% (≈31 mass%) of HCl by using equation no. (4.3) mention in section 4.4.
The experimental flux producing is 681.09 kg/yr. Therefore, the number of unit consuming has been calculated as:

No. of units consuming = Experimental flux producing * specific energy consumption

$$= 681.09\ kg/yr * 0.94039\ kWh/kg$$

$$= 640.49\ kWh/yr$$

GEC has been calculated as –

$$= 640.49\ kWh/yr * 7.5\ Rs/kWh$$

$$= 4803.68\ Rs/yr$$

Finally, VO & M cost has been estimated by –

$$VO\ \&\ M\ Cost\ (Rs.) = GEC + MRC \quad (6.7)$$

$$= 5103.67/-$$

6.1.3 Total Annual Cost

The total annual cost (TAC) to break the HCl/Water azeotrope and consequently producing hyperazeotropic HCl solution has been assessed by the given equation:

$$TAC\ (Rs.) = ACC + FO\ \&\ M\ Cost + VO\ \&\ M\ Cost \quad (6.8)$$

$$= 29515.90 + 5903.18 + 5103.67$$

$$= 40522.75\ /-$$

6.1.4 Unit Product Cost

Unit Product Cost (UPC) means the cost required to produce per liter or m^3 of HCl solution and it can be calculated by the following formula (Banat and Jwaied, 2008):

$$UPC\ (Rs.) = \frac{TAC}{Plant\ Availability(f) * Capacity(M) * 365} \tag{6.9}$$

The experimental flux produced at the laboratory scale from 0.00212 m^2 membrane area was found as 1.80 lit/day. For large membrane area i.e. 1 m^2, the experimental flux produced has been estimated as 780 lit/day.

Finally,

$$UPC = \frac{40522.75\ Rs}{0.9 * 0.0018\ \left(\frac{m^3}{Day}\right) * 365\ (Day)}$$

$$UPC = 68531.63\ Rs/m^3$$

Or

$$UPC = 68.53\ \ Rs/lit.$$

In this calculation we assumed that the salvage value of the experimental unit at the end of the amortization time will be zero.

6.2 Cost Model Development for Extractive Distillation

In extractive distillation an entrainer is used to separate the azeotropic mixture by creating the volatility difference between the components of the azeotropic mixture. The entrainer and the less volatile component are collected from the bottom of distillation column and high volatile component is collected from the top. The extractive distillation column was simulated using AspenOne version 10.1 simulation software. The feed conditions (20.2 mass% HCl) and operating parameters like feed flow rate, feed temperature and feed pressure were kept same as used in AGMD process. In the simulation, 50 mass% Calcium chloride ($CaCl_2$) used as the entrainer (De Dietrich Process Systems). The entrainer is separated as bottom product and approx. 30 mass% HCl collected from the top. Sizing of column was performed to obtain the column diameter and height using flow rate, pressure, temperature and number of trays along the column. Then, area of heat exchangers (Reboiler and Condenser) was identified and the relevant column cost was calculated.

Redfrac model was used for the distillation column as shown in Figure 6.1. Column design parameters and simulation operating parameters are mentioned in the Table 6.2 and Table 6.3, respectively.

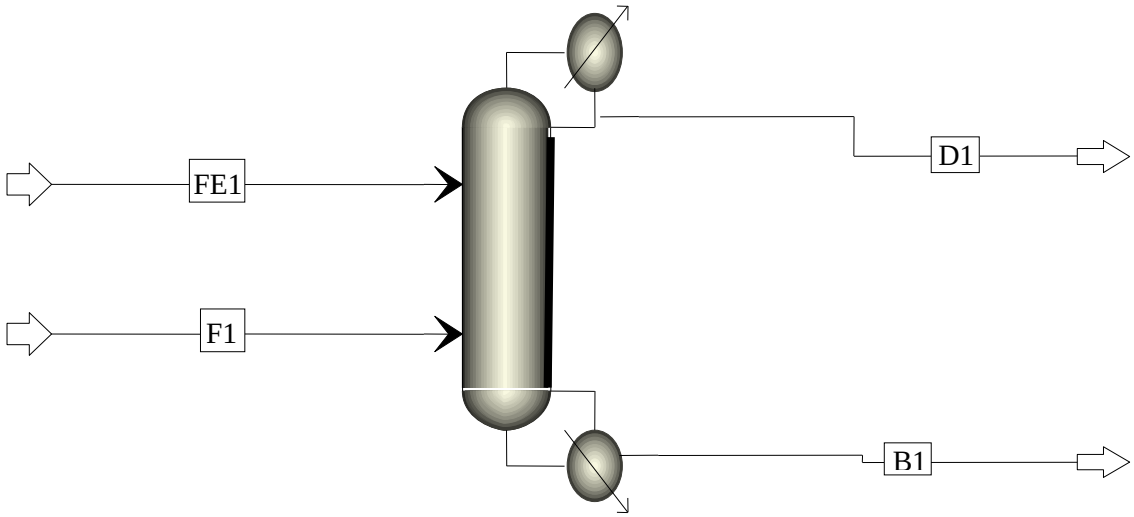

Figure 6.1 : Redfrac Column

Table 6.2 : Column Design Parameters

Specification	Type
Feed	HCl/Water
Entrainer	$CaCl_2$
Column	REDFRAC
Tray Type	Sieve
Reboiler	Kettle
Condenser	Total

Table 6.3 : Simulation Operating Parameters

Operating Variable	Extractive Column
Feed Flow Rate (kmol/h)	5.896
Entrainer flow Rate (kmol/h)	1.078
Feed Temperature (^{O}C)	50
Feed Pressure (atm)	1
Entrainer Temperature (^{O}C)	50
Entrainer Pressure (atm)	0.19
Distillate Rate (kmol/h)	4
Molar Reflux Ratio	1.5
Number of theoretical Stages	30
Entrainer stage location	7
Feed stage location	25

Table 6.4 : Simulation Results

Measurement	Value
Top Product Composition (mole fraction)	HCl - 0.1745 Water - 0.8255 $CaCl_2$ - 0
Bottom Product Composition (mole fraction)	HCl - 3.519e-16 Water - 0.97 $CaCl_2$ - 0.035
Condenser Duty (kJ/h)	-461660
Reboiler Duty (kJ/h)	435440
Condenser/Top stage Temperature (K)	227.732
Reboiler/ Bottom stage Temperature (K)	374.175
Column Diameter (m)	0.221

The total cost of the distillation column is the sum of the column shell costs and column trays costs. The column diameter, number of stages and heat exchangers (condenser and reboiler) duty are required for the cost calculations which have been evaluated from the aspen simulation as mentioned in the Table 6.4 and employed in the different correlations (Errico *et al.*, 2009) used for the cost calculation of column shell, column trays, heat exchangers and operating cost.

6.2.1 Heat Exchanger Cost Estimation

The heat transfer area of condenser is estimated by –

$$A_c = \frac{Q_c}{U_c \Delta T_{lm,c}} \tag{6.10}$$

Where, Q_c is the condenser duty, U_c is the overall heat transfer coefficient and $\Delta T_{lm,c}$ is the log mean temperature driving force for the condenser.

The heat transfer area of reboiler is estimated by equation (6.11):

$$A_R = \frac{Q_c}{U_c \Delta T_{lm,R}} \tag{6.11}$$

Where, Q_R is the reboiler duty, U_R is the overall heat transfer coefficient and $\Delta T_{lm,R}$ is the log mean temperature driving force for the reboiler.

Assuming shell & tube heat exchanger and made up of carbon steel, the correlation used for the cost estimation is given as:

$$Cost\ of\ Heat\ Exchanger(\$) = \left(\frac{M\ \&\ S}{280}\right)(474.67)A^{0.65} \tag{6.12}$$

Here, $M\ \&\ S$ is Marshall and Swift cost index (CEPCI, 2017) and A is heat exchanger area represented by A_c for condenser and A_R for reboiler.

6.2.2 Column Shell Cost

The column height calculated by given formula:

$$H = (N-1) * 0.6 + 6 \tag{6.13}$$

Here, 0.6 m considered as tray spacing and 6 m as disengagement.

The column cost calculated by correlation given as:

$$Column\ Shell\ Cost\ (\$) = \left(\frac{M\ \&\ S}{280}\right)(937.61)D^{1.066}H^{0.802} \tag{6.14}$$

Here, D and H are the column diameter and column height, respectively.

6.2.3 Column Tray Cost

The column tray cost calculated by equation (6.15):

$$Tray\ Cost\ (\$) = \left(\frac{M\ \&\ S}{280}\right)(97.24)D^{1.55}h \tag{6.15}$$

Here h is the tray stack height.

6.2.4 Operating Cost

Electricity was used to run the column.

$$\text{Specific energy consumption} = \text{Total heat duty (kJ/h)/Flux Produced(kg/h)}$$

$$= 916772/84.024$$

$$= 2.965\ kWh/kg$$

$$\text{Cost of electricity consumption (\$/Day)}$$

$$= \text{No. of units consuming per day} * \text{Cost of each unit}$$

$$= 5979.15(kWh/Day) * 7.5\ (\text{Rs./kWh})$$

$$= 44843.725/74$$

$$= 605.99\ \$/Day$$

6.2.5 Unit Product Cost

$$UPC = \frac{TAC}{Plant\ Availability(f) * Capacity(M)} \tag{6.16}$$

$$TAC\ (\$) = Condenser\ Cost + Reboiler\ Cost + Tray\ Cost + Column\ Shell\ Cost + Operating\ Cost$$

$$TAC = 11656 + 4572.40 + 507.72 + 20675.42 + 605.99$$

$$TAC(\$) = 38017.53$$

Finally,

$$UPC = \frac{38107.53\ \$ * Day}{0.9 * 2.022 * m^3 * Day}$$

$$UPC = 1548066.11\ Rs/m^3$$

Or

$$UPC = 1548.07\ Rs/lit.$$

6.3 **Results and Discussion**

The unit product cost gained by the AGMD experimental setup has been compared with the product cost calculated by ED plant study.

Table 6.5: Comparison between AGMD and ED Processes

	AGMD	Extractive Distillation
Specific Energy Consumption (kWh/kg)	0.940	2.965
Cost (Rs/lit)	68.53	1548.07

From the economic analysis outcomes as shown in Table 6.5, the specific energy consumption and production cost for the production of 30.8 mass% (≈31 mass%) HCl solution using AGMD method found lower than the conventional ED method, which proves AGMD fitness for the azeotrope mixture separation.

CHAPTER 7

CONCLUSIONS AND FUTURE WORK

7.1 **Conclusions**

The conclusions of the study of the breaking of HCl/Water azeotrope using air gap membrane distillation are summarized as follows:

1. The permeate flux and selectivity estimated by the developed mathematical model by varying different operating parameters were well fitted with experimental results having R^2 and MAPE values in the range of 0.940-0.999 and 9.59-1.02, respectively.
2. With azeotropic feed, the maximum concentration of HCl in retentate was achieved to 30.8 mass% HCl, i.e., hyperazeotropic solution and maximum concentration of HCl in permeate was found to be 15.29 mass% HCl, i.e., hypoazeotropic solution. The above results indicate a strong possibility of using AGMD for azeotropic mixture separation.
3. Selectivity of HCl in permeate was found to be less than 1 indicating more water flux in permeate.
4. On increasing feed temperature and feed flow rate, the permeate flux increases whereas on increasing air gap width and cooling water temperature, permeate flux decreases.
5. There is no significant effect of the cooling water flow rate on permeate flux, permeate HCl concentration and retentate HCl concentration.
6. The favorable process conditions required for breaking azeotrope mixture are small air gap width, high feed temperature, and low cooling water temperature.
7. Using CFD modeling, the average temperature at the feed side membrane surface was computed to be 320.22 K while solving mathematical modeling equations in MATLAB at the same operating conditions, it was obtained to be 321.7 K. Similarly, temperature at membrane side cooling surface obtained from CFD modeling and mathematical modeling was 307.53 K and 309.34 K, respectively. The value of R^2 and MAPE values for comparison between CFD and experimental results were calculated to be 0.995 and 5.94%, and the same for mathematical model versus experimental results were computed to be 0.999 and 3.69%. R^2 and MAPE values indicate that model prediction by CFD is in good agreement with experimental results and therefore it can be applied for getting reliable and reasonable results.

8. It can be observed that there was no reduction in permeate flux and selectivity for the continuous run of 50 h at azeotropic feed concentration. The permeate flux was seen at 25.2 kg/m^2·h, and it remains nearly constant for 50 h of operation. The above result may be due to the volatile nature of feed components, and that causes no deposition on the membrane surface. No membrane wetting was observed due to hydrophobic nature of PTFE membrane.
9. From the SEM and EDS, it was found that there was no deposition of any component on the membrane surface after 50 h of operation that was also confirmed by the pore size distribution curve.
10. Experimentally, 42% recovery has been achieved at 45 ^{o}C temperature to achieved 31 mass% HCl in feed tank. Theoretically, 31 mass% feed concentration in feed tank was achieved in 88.7 h with 26.6 % recovery at 40 ^{o}C. From recovery analysis, it can be concluded that HCl concentration in feed tank increases with increasing the temperature when operating at the fixed time.
11. Heat transfer correlation for the feed side membrane surface temperature at different feed flow rate and different feed inlet temperature was attained as-

    $Nu = 4.67\, Re^{0.75} Pr^{0.33}$.
12. Similarly, mass transfer correlation for the feed side membrane surface temperature at different feed flow rate and different feed inlet temperature was obtained as-

    $Sh = 10.13\, Re^{0.62} Sc^{0.33}$.
13. From the study of the effect of inert gases, it can be concluded that the total mass flux obtained using the light gas such as air was higher than the mass flux obtained using the heavy gas such as argon. Also in both the cases the permeate flux increases by increasing the bulk feed input temperature and feed flow rate while permeating flux decreases with the air gap width and cooling water temperature. Simultaneously, It can be observed that selectivity for heavy argon gas is shifted more from unity as compared to light gas air.
14. The experimental data were trained and validated by ANN model successfully. ANN predicted the data in agreement with experimental data; however, the MAPE values for ANN are slightly better.
15. From the economic analysis, the specific energy consumption and production cost for the production of 31 mass% HCl solution using AGMD method found lower than the conventional ED method, that proves AGMD suitability for the azeotrope separation.

7.2 **Contribution to Knowledge**

1. The effects of different operating parameters on the total permeate flux, selectivity and permeate and retentate concentrations have been studied by mathematical modeling and by experimental study, which was not explored earlier.
2. To the best of our knowledge, this present work is the first attempt to experimentally study the effect of argon (inert gas) on the breaking of HCl/Water azeotrope mixture in terms of permeate flux, selectivity, permeate and retentate concentrations.
3. Heat and Mass transfer correlation was developed for HCl/Water azeotrope system.
4. The comparison of AGMD process with the ED process in terms of unit product cost and specific energy consumption have been carried out to check the AGMD suitability for azeotrope mixture separation.

7.3 **Scope for Future Work**

1. It could be interesting to evaluate the feasibility and efficacy of AGMD process for different aqueous azeotropic mixtures separation (like Benzyl Alcohol /Water, Phenol/water etc.) and analyse the effect of different operating and membrane parameters on their azeotrope breaking point and selectivity.
2. The more detailed study of the effect of different inert gases like helium, SF_6 on breaking the azeotrope mixture can also be explored in future.
3. Since in the AGMD processes the condensing plate need to be located inside the membrane module and also maintaining the small air gap thickness is a complicated work therefore, designing and fabrication of AGMD module is a challenging task and thereby AGMD module designing requires dedicated research efforts by the membrane distillation community.
4. Yet another area for future research would be to analyse and understand the effect of pore size, membrane material and pore size distributions on the AGMD permeate.
5. Another challenge associated with the AGMD process is with air gap thickness that floods easily, so techniques for reducing flooding (more rapidly removing permeate from the gap) could be an important area of research.

REFERENCES

A.M. Alklaibi, N. and Lior (2007) 'Comparative Study of direct contact and air gap membrane distillation processes', *Ind. Eng. Chem. Res*, 2(46), pp. 584–590.

Abu, A.-R. F. *et al.* (2012) 'Theoretical assessment of dilute acetone removal from aqueous streams by membrane distillation', *Separation Science and Technology*, 34(14), pp. 2817–2836. doi: 10.1081/SS-100100807.

Abu AlRub, F. A., Banat, F. and Bani Melhem, K. (2003) 'Sensitivity Analysis of Air Gap Membrane Distillation', *Separation Science and Technology*, 38(15), pp. 3645–3667. doi: 10.1081/SS-120024222.

Al-Obaidani, S. *et al.* (2008) 'Potential of membrane distillation in seawater desalination: Thermal efficiency, sensitivity study and cost estimation', *Journal of Membrane Science*, 323(1), pp. 85–98. doi: 10.1016/j.memsci.2008.06.006.

Ali, A. *et al.* (2018) 'Membrane technology in renewable-energy-driven desalination', *Renewable and Sustainable Energy Reviews*. Elsevier Ltd, 81(April 2017), pp. 1–21. doi: 10.1016/j.rser.2017.07.047.

Alkhudhiri, A., Darwish, N. and Hilal, N. (2012a) 'Membrane distillation: A comprehensive review', *Desalination*. Elsevier B.V., 287, pp. 2–18. doi: 10.1016/j.desal.2011.08.027.

Alkhudhiri, A., Darwish, N. and Hilal, N. (2012b) 'Treatment of high salinity solutions: Application of air gap membrane distillation', *Desalination*. Elsevier B.V., 287, pp. 55–60. doi: 10.1016/j.desal.2011.08.056.

Alkhudhiri, A., Darwish, N. and Hilal, N. (2013a) 'Produced water treatment : Application of Air Gap Membrane Distillation', *Des*. Elsevier B.V., 309, pp. 46–51. doi: 10.1016/j.desal.2012.09.017.

Alkhudhiri, A., Darwish, N. and Hilal, N. (2013b) 'Treatment of saline solutions using Air Gap Membrane Distillation: Experimental study', *Desalination*. Elsevier B.V., 323, pp. 2–7. doi: 10.1016/j.desal.2012.09.010.

Alklaibi, A. M. and Lior, N. (2005) 'Transport analysis of air-gap membrane distillation', *Journal of Membrane Science*, 255(1–2), pp. 239–253.

Alsaadi, A. S. *et al.* (2013) 'Modeling of air-gap membrane distillation process : A theoretical and experimental study', *Journal of Membrane Science*, 445, pp. 53–65. doi: 10.1016/j.memsci.2013.05.049.

Alsehli, M., Choi, J. and Aljuhan, M. (2017) 'A novel design for a solar powered multistage flash desalination', *Solar Energy*. Elsevier Ltd, 153, pp. 348–359. doi:

10.1016/j.solener.2017.05.082.

Alves, V. D. and Coelhoso, I. M. (2006) 'Orange juice concentration by osmotic evaporation and membrane distillation: A comparative study', *Journal of Food Engineering*, 74(1), pp. 125–133. doi: 10.1016/j.jfoodeng.2005.02.019.

El Amali, A., Bouguecha, S. and Maalej, M. (2004) 'Experimental study of air gap and direct contact membrane distillation configurations: Application to geothermal and seawater desalination', *Desalination*, 168(1–3), p. 357. doi: 10.1016/j.desal.2004.07.020.

Anezi, A. A. Al *et al.* (2013) 'Potential of membrane distillation - a comprehensive review', *International Journal of Water*, 7(4), p. 317. doi: 10.1504/IJW.2013.056674.

Bagger-Jørgensen, R. *et al.* (2011) 'Recovery of volatile fruit juice aroma compounds by membrane technology: Sweeping gas versus vacuum membrane distillation', *Innovative Food Science and Emerging Technologies*. Elsevier Ltd, 12(3), pp. 388–397. doi: 10.1016/j.ifset.2011.02.005.

Baghel, Rakesh,U Sushant, S. K. (2017) 'A review on membrane applications and transport mechanisms in vacuum membrane distillation', *Rev Chem Eng*. doi: 10.1515/revce-2016-0050.

Baghel, R. *et al.* (2017) 'Treatment of Sudan III Dye from wastewater using Vacuum Membrane Distillation', *Journal of Basic and Applied Engineering Research*, 4(3), pp. 237–241.

Banat, F. *et al.* (2007a) 'Desalination by a "compact SMADES" autonomous solarpowered membrane distillation unit', *Desalination*, 217(1–3), pp. 29–37. doi: 10.1016/j.desal.2006.11.028.

Banat, F. *et al.* (2007b) 'Performance evaluation of the "large SMADES" autonomous desalination solar-driven membrane distillation plant in Aqaba, Jordan', *Desalination*, 217(1–3), pp. 17–28. doi: 10.1016/j.desal.2006.11.027.

Banat, F. A. *et al.* (1999) 'Application of Stefan ± Maxwell approach to azeotropic separation by membrane distillation', *Chemical Engineering Journal*, 73(1), pp. 71–75.

Banat, F. A., Abu Al-Rub, F., *et al.* (1999) 'On the effect of inert gases in breaking the formic acid-water azeotrope by gas-gap membrane distillation', *Chemical Engineering Journal*, 73(1), pp. 37–42. doi: 10.1016/S1385-8947(99)00014-5.

Banat, F. A., Al-Rub, F. A., *et al.* (1999) 'Theoretical investigation of membrane distillation role in breaking the formic acid-water azeotropic point: Comparison between Fickian and Stefan-Maxwell-based models', *International Communications in Heat and Mass Transfer*, 26(6), pp. 879–888.

Banat, F. a., Abu Al-Rub, F. and Shannag, M. (1999) 'Modeling of dilute ethanol–water

mixture separation by membrane distillation', *Separation and Purification Technology*, 16(2), pp. 119–131. doi: 10.1016/S1383-5866(98)00117-8.

Banat, F. A., Al-Rub, F. A. and Shannag, M. (1999) 'Simultaneous removal of acetone and ethanol from aqueous solutions by membrane distillation: prediction using the Fick's and the exact and approximate Stefan-Maxwell relations', *Heat and Mass Transfer*, 35(5), pp. 423–431. doi: 10.1007/s002310050344.

Banat, F. A. and Al-Shannag, M. (2000) 'Recovery of dilute acetone-butanol-ethanol (ABE) solvents from aqueous solutions via membrane distillation', *Bioprocess Engineering*, 23(6), pp. 643–649. doi: 10.1007/s004490000214.

Banat, F. A. and Simandl, J. (1994) 'Theoretical and experimental study in membrane distillation', *Desalination*, 95(1), pp. 39–52. doi: 10.1016/0011-9164(94)00005-0.

Banat, F. A. and Simandl, J. (1996) 'Removal of benzene traces from contaminated water by vacuum membrane distillation', *Chemical Engineering Science*, 51(8), pp. 1257–1265. doi: 10.1016/0009-2509(95)00365-7.

Banat, F. A. and Simandl, J. (1998) 'Desalination by Membrane Distillation: A Parametric Study', *Separation Science and Technology*, 33(2), pp. 201–226. doi: 10.1080/01496399808544764.

Banat, F. A. and Simandl, J. (1999) 'Membrane distillation for dilute ethanol: Separation from aqueous streams', *Journal of Membrane Science*, 163(2), pp. 333–348. doi: 10.1016/S0376-7388(99)00178-7.

Banat, F. A. and Simandl, J. (2000) 'Membrane distillation for propanone removal from aqueous streams', *Journal of Chemical Technology and Biotechnology*, 75(2), pp. 168–178. doi: 10.1002/(SICI)1097-4660(200002)75:2<168::AID-JCTB192>3.0.CO;2-X.

Banat, F. and Jwaied, N. (2008) 'Economic evaluation of desalination by small-scale autonomous solar-powered membrane distillation units', *Desalination*, 220(1–3), pp. 566–573. doi: 10.1016/j.desal.2007.01.057.

Bodell, B. R. (1965) 'United States Patent'.

Boi, C., Bandini, S. and Sarti, G. C. (2005) 'Pollutants removal from wastewaters through membrane distillation', *Desalination*, 183(1–3), pp. 383–394. doi: 10.1016/j.desal.2005.03.041.

Bonner, W. D., & Wallace, R. E. (1930) 'The Boiling Points of Constant Boiling Hydrochloric Acids', 52, pp. 1747–1750.

Bonyadi, S. and Chung, T. S. (2007) 'Flux enhancement in membrane distillation by fabrication of dual layer hydrophilic-hydrophobic hollow fiber membranes', *Journal of Membrane Science*, 306(1–2), pp. 134–146. doi: 10.1016/j.memsci.2007.08.034.

Bougecha, S., Chouikh, R. and Dhahbi, M. (2002) 'Numerical Study of the Coupled Heat and Mass Transfer in Membrane Distillation', *Desalination*, 152, pp. 245–252.

Bouguecha, S., Hamrouni, B. and Dhahbi, M. (2005) 'Small scale desalination pilots powered by renewable energy sources: Case studies', *Desalination*, 183(1–3), pp. 151–165. doi: 10.1016/j.desal.2005.03.032.

Brignole, E. and Pereda, S. (2013) 'Separation of azeotropic mixtures', *Supercritical Fluid Science and Technology*, 3, pp. 179–213. doi: 10.1016/B978-0-444-56364-4.00008-X.

Burgone, A. Vahdati, M. . (2000) 'Direct Contact Membrane Distillation', *Separation Science and Technology*, 35(8), pp. 1257–1284. doi: 10.1081/SS-100100224.

Cai, J. and Guo, F. (2017) 'Study of mass transfer coefficient in membrane desalination', *Desalination*. Elsevier B.V., 407, pp. 46–51. doi: 10.1016/j.desal.2016.12.013.

Calabrb, V. and Drioli, E. (1994) 'Theoretical and Experimental Study on Membrane Distillation in the Concentration of Orange Juice', *Ind. Eng. Chem. Res.*, 33, pp. 1803–1808. doi: 10.1021/ie00031a020.

Cath, T. Y., Adams, V. D. and Childress, A. E. (2004) 'Experimental study of desalination using direct contact membrane distillation: A new approach to flux enhancement', *Journal of Membrane Science*, 228(1), pp. 5–16. doi: 10.1016/j.memsci.2003.09.006.

CEPCI (2017) 'Economic Indicators 2008-2017: Chemical Engineering Plant Cost Index', *Chemical Engineering*, (February). Available at: www.chemengonline.com/pci.

Cerneaux, S. *et al.* (2009) 'Comparison of various membrane distillation methods for desalination using hydrophobic ceramic membranes', *Journal of Membrane Science*, 337(1–2), pp. 55–60. doi: 10.1016/j.memsci.2009.03.025.

Chan, M. T. *et al.* (2005) 'Membrane distillation crystallization of concentrated salts - Flux and crystal formation', *Journal of Membrane Science*, 257(1–2), pp. 144–155. doi: 10.1016/j.memsci.2004.09.051.

Chang, H. *et al.* (2012) 'Experimental and simulation study of a solar thermal driven membrane distillation desalination process', *Desalination*. Elsevier B.V., 286, pp. 400–411. doi: 10.1016/j.desal.2011.11.057.

Charfi, K., Khayet, M. and Safi, M. J. (2010) 'Numerical simulation and experimental studies on heat and mass transfer using sweeping gas membrane distillation', *Desalination*, 259(1–3), pp. 84–96. doi: 10.1016/j.desal.2010.04.028.

Chen, C.-C. *et al.* (1982) 'A local composition model for the excess Gibbs energy of aqueous electrolyte systems Part I: Single solvent, single completely dissociated electrolyte systems', *AIChE Journal*, 28(4), pp. 588–596. doi: 10.1002/aic.690320311.

Chen, K. *et al.* (2015) 'Study on vacuum membrane distillation (VMD) using FEP hollow

fiber membrane', *Desalination*. Elsevier B.V., 375, pp. 24–32. doi: 10.1016/j.desal.2015.07.021.

Cojocaru, C. and Khayet, M. (2011) 'Sweeping gas membrane distillation of sucrose aqueous solutions: Response surface modeling and optimization', *Separation and Purification Technology*. Elsevier B.V., 81(1), pp. 12–24. doi: 10.1016/j.seppur.2011.06.031.

Couffin, N., Cabassud, C. and Lahoussine-Turcaud, V. (1998) 'A new process to remove halogenated VOCs for drinking water production: vacuum membrane distillation', *Desalination*, 117(1–3), pp. 233–245. doi: 10.1016/S0011-9164(98)00103-9.

Curcio, E. and Drioli, E. (2005) 'Membrane Distillation and Related Operations - A Review', *Separation & Purification Reviews*, 34, pp. 35–86. doi: 10.1081/SPM-200054951.

De Dietrich Process Systems (no date) *Concentration of HCl acid above the azeotropic point*. Available at: https://www.dedietrich.com/en/solutions-and-products/mineral-acid-treatment/hydrochloric-acid-treatment/concentration-hcl-acid.

Ding, Z. *et al.* (2006) 'Experimental study of ammonia removal from water by membrane distillation (MD): The comparison of three configurations', *Journal of Membrane Science*, 286(1–2), pp. 93–103. doi: 10.1016/j.memsci.2006.09.015.

Dotremont, C. *et al.* (2010) 'Seawater desalination with memstill technology - a sustainable solution for the industry', *Water Practice and Technology*, 5(2). doi: 10.2166/wpt.2010.026.

Duong, H. C. *et al.* (2016) 'Evaluating energy consumption of air gap membrane distillation for seawater desalination at pilot scale level', *Separation and Purification Technology*. Elsevier B.V., 166, pp. 55–62. doi: 10.1016/j.seppur.2016.04.014.

El-Bourawi, M. S. *et al.* (2006) 'A framework for better understanding membrane distillation separation process, Journal of Membrane Science', *Journal of Membrane Science*, 285, pp. 4–29. doi: 10.1016/j.memsci.2006.08.002.

Errico, M. *et al.* (2009) 'A method for systematic synthesis of multicomponent distillation systems with less than N-1 columns', *Chemical Engineering and Processing: Process Intensification*, 48(4), pp. 907–920. doi: 10.1016/j.cep.2008.12.005.

Essalhi, M. and Khayet, M. (2012) 'Surface segregation of fluorinated modifying macromolecule for hydrophobic/hydrophilic membrane preparation and application in air gap and direct contact membrane distillation', *Journal of Membrane Science*. Elsevier, 417–418, pp. 163–173. doi: 10.1016/j.memsci.2012.06.028.

Ettouney, H. Dessouky, H. (2002) *Fundamentals of salt-water desalination*. Amesterdam: Elsevier.

Eykens, L. *et al.* (2017) 'Coating techniques for membrane distillation: An experimental

assessment', *Separation and Purification Technology*. Elsevier, 193(August 2017), pp. 38–48. doi: 10.1016/j.seppur.2017.10.070.

Eziyi, I. *et al.* (2013) 'Effects of salinity and feed temperature on permeate flux of an air gap membrane distillation unit for sea water desalination', in *2013 1st IEEE Conference on Technologies for Sustainability, SusTech 2013*, pp. 142–145. doi: 10.1109/SusTech.2013.6617311.

Fang, H. *et al.* (2012) 'Hydrophobic porous alumina hollow fiber for water desalination via membrane distillation process', *Journal of Membrane Science*. Elsevier B.V., 403–404, pp. 41–46. doi: 10.1016/j.memsci.2012.02.011.

Feng, C. *et al.* (2008) 'Production of drinking water from saline water by air-gap membrane distillation using polyvinylidene fluoride nanofiber membrane', *Journal of Membrane Science*, 311(1–2), pp. 1–6. doi: 10.1016/j.memsci.2007.12.026.

Findley, M. E. (1967) 'Vaporization through Porous Membranes', *Industrial & Engineering Chemistry Process Design and Development*, 6(2), pp. 226–230. doi: 10.1021/i260022a013.

Francis, L. *et al.* (2013) 'Material gap membrane distillation: A new design for water vapor flux enhancement', *Journal of Membrane Science*, 448, pp. 240–247. doi: 10.1016/j.memsci.2013.08.013.

Franken, A. C. M. *et al.* (1987) 'Wetting criteria for the applicability of membrane distillation', *Journal of Membrane Science*, 33(3), pp. 315–328. doi: 10.1016/S0376-7388(00)80288-4.

Fritz, J. J. and Fuget, C. R. (1956) 'Vapor Pressure of Aqueous Hydrogen Chloride Solutions, 0° to 50° C.', *Industrial & Engineering Chemistry Chemical & Engineering Data Series*, 1(1), pp. 10–12. doi: 10.1021/i460001a002.

Fritzmann, C. *et al.* (2007) 'State-of-the-art of reverse osmosis desalination', *Desalination*, 216(1–3), pp. 1–76. doi: 10.1016/j.desal.2006.12.009.

Fuller, E. and N.; Schettler, Paul D.; Glddlngs, J. C. (1966) 'A New Method for Prediction of Binary Gas - Phase Diffusion', *Industrial and Engineering Chemistry*, 58, pp. 18–27.

García-fernández, L. *et al.* (2017) 'Morphological design of alumina hollow fi ber membranes for desalination by air gap membrane distillation', *Desalination*, 420(July), pp. 226–240. doi: 10.1016/j.desal.2017.07.021.

García-Fernández, L., García-Payo, C. and Khayet, M. (2017) 'Hollow fiber membranes with different external corrugated surfaces for desalination by membrane distillation', *Applied Surface Science*. Elsevier B.V., 416, pp. 932–946. doi: https://doi.org/10.1016/j.apsusc.2017.04.232.

García-Payo, M. C. *et al.* (2002) 'Separation of binary mixtures by thermostatic sweeping

gas membrane distillation II. Experimental results with aqueous formic acid solutions', *Journal of Membrane Science*, 198(2), pp. 197–210. doi: 10.1016/S0376-7388(01)00649-4.

Garcia-Payo, M. C., Izquierdo-Gil, M. A. and Fernndez-Pineda, C. (2000) 'Air gap membrane distillation of aqueous alcohol solutions', *Journal of Membrane Science*, 169(1), pp. 61–80.

Gazagnes, L. *et al.* (2007) 'Desalination of sodium chloride solutions and seawater with hydrophobic ceramic membranes', *Desalination*, 217(1–3), pp. 260–266. doi: 10.1016/j.desal.2007.01.017.

Geng, H. *et al.* (2014) 'Study on a new air-gap membrane distillation module for desalination', *Desalination*. Elsevier B.V., 334(1), pp. 29–38. doi: 10.1016/j.desal.2013.11.037.

Gerbaud, V. and Rodriguez-Donis, I. (2014) 'Extractive Distillation', in *Distillation Equipment and Processes*. Academic Press, pp. 201–245.

Godino, M. P. *et al.* (1997) 'Water production from brines by membrane distillation', *Desalination*, 108(1–3), pp. 91–97. doi: 10.1016/S0011-9164(97)00013-1.

Gostoli, C. and Sarti, G. C. (1989) 'Separation of liquid mixtures by membrane distillation', *Journal of Membrane Science*, 41(C), pp. 211–224. doi: 10.1016/S0376-7388(00)82403-5.

Gostoli, C., Sarti, G. C. and Matulli, S. (1987) 'Low Temperature Distillation Through Hydrophobic Membranes', *Separation Science and Technology*, (November 2014), pp. 37–41. doi: 10.1080/01496398708068986.

Gryta, M. (2007a) 'Effect of iron oxides scaling on the MD process performance', *Desalination*, 216(1–3), pp. 88–102. doi: 10.1016/j.desal.2007.01.002.

Gryta, M. (2007b) 'Influence of polypropylene membrane surface porosity on the performance of membrane distillation process', *Journal of Membrane Science*, 287(1), pp. 67–78. doi: 10.1016/j.memsci.2006.10.011.

Gryta, M. (2016) 'The study of performance of polyethylene chlorinetrifluoroethylene membranes used for brine desalination by membrane distillation', *Desalination*. Elsevier B.V., 398, pp. 52–63. doi: 10.1016/j.desal.2016.07.021.

Guijt, C. M. *et al.* (2005a) 'Air gap membrane distillation: 1. Modelling and mass transport properties for hollow fibre membranes', *Separation and Purification Technology*, 43(3), pp. 233–244. doi: 10.1016/j.seppur.2004.09.015.

Guijt, C. M. *et al.* (2005b) 'Air gap membrane distillation: 2. Model validation and hollow fibre module performance analysis', *Separation and Purification Technology*, 43(3), pp. 245–255. doi: 10.1016/j.seppur.2004.09.016.

Guillen-Burrieza, E. *et al.* (2014) 'Membrane fouling and cleaning in long term plant-scale

membrane distillation operations', *Journal of Membrane Science*. Elsevier, 468, pp. 360–372. doi: 10.1016/j.memsci.2014.05.064.

Guillen-Burrieza, E. *et al.* (2016) 'Understanding wetting phenomena in membrane distillation and how operational parameters can affect it', *Journal of Membrane Science*. Elsevier, 515, pp. 163–174. doi: 10.1016/j.memsci.2016.05.051.

Guillén-Burrieza, E. *et al.* (2011) 'Experimental analysis of an air gap membrane distillation solar desalination pilot system', *Journal of Membrane Science*, 379(1–2), pp. 386–396. doi: 10.1016/j.memsci.2011.06.009.

Guillén-Burrieza, E. *et al.* (2012) 'Experimental evaluation of two pilot-scale membrane distillation modules used for solar desalination', *Journal of Membrane Science*. Elsevier B.V., 409–410, pp. 264–275. doi: 10.1016/j.memsci.2012.03.063.

Gunko, S. *et al.* (2006) 'Concentration of apple juice using direct contact membrane distillation', *Desalination*, 190(1–3), pp. 117–124. doi: 10.1016/j.desal.2005.09.001.

H.L.Horsley (1973) *Azeotropic Data III*. American Chemical Society, Washington,D.C.

Hamed, O. A. *et al.* (2000) 'Thermal performance of multi-stage flash distillation plants in Saudi Arabia', *Desalination*, 128, pp. 281–292.

Hanemaaijer, J. H. (2004) 'Memstill- Low cost membrane distillation technology for seawater desalination', *Desalination*, 168(1–3), p. 355. doi: 10.1016/j.desal.2004.07.019.

Harianto, R. A. *et al.* (2014) 'Surface Treatment of Air Gap Membrane Distillation (AGMD) Condensation Plates', *Applied Science and Convergence Technology*, 23(5), pp. 248–253. doi: 10.5757/ASCT.2014.23.5.248.

He, K., Hwang, H. J. and Moon, I. S. (2011) 'Air gap membrane distillation on the different types of membrane', *Korean Journal of Chemical Engineering*, 28(3), pp. 770–777. doi: 10.1007/s11814-010-0415-0.

He, Q. *et al.* (2014) 'Modeling and optimization of air gap membrane distillation system for desalination', *Desalination*. Elsevier B.V., 354, pp. 68–75. doi: 10.1016/j.desal.2014.09.022.

Himmelblau, D. M. (2000) 'Applications of artificial neural networks in chemical engineering', *Korean J. Chem. Eng.*, 17, pp. 373–392.

Hitsov, I. *et al.* (2017) 'Full-scale validated Air Gap Membrane Distillation (AGMD) model without calibration parameters', *Journal of Membrane Science*. Elsevier B.V., 533(April), pp. 309–320. doi: 10.1016/j.memsci.2017.04.002.

Huang, Q.-L. *et al.* (2017) 'Electrospun ultrafine fibrous PTFE-supported ZnO porous membrane with self-cleaning function for vacuum membrane distillation', *Journal of Membrane Science*. Elsevier B.V., 534(399), pp. 73–82. doi:

10.1016/j.memsci.2017.04.015.

Izquierdo-Gil, M. A., García-Payo, M. C. and Fernández-Pineda, C. (1999) 'Air gap membrane distillation of sucrose aqueous solutions', *Journal of Membrane Science*, 155(2), pp. 291–307. doi: 10.1016/S0376-7388(98)00323-8.

J. A. Wesselingh and R. Krishna (1990) *Mass Transfer*. Chichester, England: Ellis Horwood.

Jaafar, S. and Sarbatly, R. (2012) 'Geothermal Water Desalination by using Nanofiber Membrane', *International Conference on Chemical, Environmental and Biological Sciences (ICCEBS'2012) Penang, Malaysia*, (Md), pp. 46–50.

Jande, Y. A. C. and Kim, W. S. (2013) 'Desalination using capacitive deionization at constant current', *Desalination*. Elsevier B.V., 329, pp. 29–34. doi: 10.1016/j.desal.2013.08.023.

Jansen, A. E. *et al.* (2013) 'Development and pilot testing of full-scale membrane distillation modules for deployment of waste heat', *Desalination*. Elsevier B.V., 323, pp. 55–65. doi: 10.1016/j.desal.2012.11.030.

Jin, Z. *et al.* (2007) 'Removal of 2,4-dichlorophenol from wasterwater by vacuum membrane distillation using hydrophobic PPESK hollow hiber membrane', *Chinese Chemical Letters*, 18(12), pp. 1543–1547. doi: 10.1016/j.cclet.2007.10.007.

Jonsson, A. S. and R. Wimmerstedt and A.C.Harrysson (1985) 'Membrane Distillation-A Theoretical Study of Evaporation through Microporous Membrane', *Desalination*, 56, pp. 237--249. doi: 10.1016/0011-9164(85)85028-1.

K.A. Sharp (2001) 'Water: Structure and Properties', *Encyclopedia of Life Sciences*. John Wiley & Sons, Ltd. doi: 10.3139/9783446437197.003.

Kalla, S. *et al.* (2018) 'Experimental and Mathematical Study of Air Gap Membrane Distillation for Aqueous HCl Azeotropic Separation', *Journal of Chemical Technology & Biotechnology*, (July). doi: 10.1002/jctb.5766.

Karanikola, V. *et al.* (2015) 'Sweeping gas membrane distillation: Numerical simulation of mass and heat transfer in a hollow fiber membrane module', *Journal of Membrane Science*. Elsevier, 483, pp. 15–24. doi: 10.1016/j.memsci.2015.02.010.

Khalifa, Atia E, Dahiru U. Lawal, M. A. A. (2014) 'Performance Of Air Gap Membrane Distillation Unit For Water Desalination', in *International Mechanical Engineering Congress and Exposition, Proceedings of the ASME 2014*, pp. 1–6.

Khalifa, A. *et al.* (2015) 'Experimental and theoretical investigation on water desalination using air gap membrane distillation', *Desalination*. Elsevier B.V., 376, pp. 94–108.

Khalifa, A. *et al.* (2017) 'Experimental and theoretical investigations on water desalination

using direct contact membrane distillation', *Desalination*. Elsevier B.V., 404, pp. 22–34. doi: 10.1016/j.desal.2016.10.009.

Khalifa, A. E. (2015) 'Water and air gap membrane distillation for water desalination - An experimental comparative study', *Separation and Purification Technology*, 141, pp. 276–284. doi: 10.1016/j.seppur.2014.12.007.

Khalifa, A. E. and Lawal, D. U. (2015) 'Performance and Optimization of Air Gap Membrane Distillation System for Water Desalination', *Arabian Journal for Science and Engineering*, 40(12), pp. 3627–3639.

Khan, E. U. and Martin, A. R. (2014) 'Water purification of arsenic-contaminated drinking water via air gap membrane distillation (AGMD)', *Periodica Polytechnica, Mechanical Engineering*, 58(1), pp. 47–53. doi: 10.3311/PPme.7422.

Khayet, M. and Cojocaru, C. (2012a) 'Air gap membrane distillation: Desalination, modeling and optimization', *Desalination*. Elsevier B.V., 287, pp. 138–145. doi: 10.1016/j.desal.2011.09.017.

Khayet, M. and Cojocaru, C. (2012b) 'Artificial neural network modeling and optimization of desalination by air gap membrane distillation', *Separation and Purification Technology*. Elsevier B.V., 86, pp. 171–182. doi: 10.1016/j.seppur.2011.11.001.

Khayet, M. and Cojocaru, C. (2013) 'Artificial neural network model for desalination by sweeping gas membrane distillation', *Desalination*. Elsevier B.V., 308, pp. 102–110. doi: 10.1016/j.desal.2012.06.023.

Khayet, M., Godino, M. P. and Mengual, J. I. (2003) 'Possibility of nuclear desalination through various membrane distillation configurations : a comparative study', *Int. J. of Nuclear Desalination*, 1(1), pp. 1998–2002. doi: 10.1504/IJND.2003.003441.

Khayet, M., Godino, P. and Mengual, J. I. (2000) 'Theory and experiments on sweeping gas membrane distillation', *Journal of Membrane Science*, 165(July 1999), pp. 261–272. doi: 10.1016/S0376-7388(99)00236-7.

Khayet, M., Khulbe, K. C. and Matsuura, T. (2004) 'Characterization of membranes for membrane distillation by atomic force microscopy and estimation of their water vapor transfer coefficients in vacuum membrane distillation process', *Journal of Membrane Science*, 238(1–2), pp. 199–211. doi: 10.1016/j.memsci.2004.03.036.

Khayet, M. and Matsuura, T. (2003) 'Application of surface modifying macromolecules for the preparation of membranes for membrane distillation', *Desalination*, 158(1–3), pp. 51–56. doi: 10.1016/S0011-9164(03)00432-6.

Khayet, M. S. and Matsuura, T. (2011) *Membrane Distillation: Principles and Applications*. Elsevier Publication, Great Britain.

Kim, J. *et al.* (2004) 'Isotopic water separation using AGMD and VEMD', *Nukleonika*, 49(4), pp. 137–142.

Kim, Y. J. and Choi, J. H. (2010) 'Enhanced desalination efficiency in capacitive deionization with an ion-selective membrane', *Separation and Purification Technology*, 71(1), pp. 70–75. doi: 10.1016/j.seppur.2009.10.026.

Kimura, S., Nakao, S. and Shimatani, S. (1987) 'Transport phenomena in membrane distillation', *Journal of Membrane Science*, 33(3), pp. 285–298. doi: 10.1016/S0376-7388(00)80286-0.

Komgold, E., Korin, E. and Ladizhensky, I. (1996) 'Water desalination by pervaporation with hollow fiber membranes', *Desalination*, 107, pp. 121–129. doi: 10.1016/S0011-9164(96)00157-9.

Korin, E., Ladizhensky, I. and Korngold, E. (1996) 'Hydrophilic hollow fiber membranes for water desalination by the pervaporation method', *Chemical Engineering and Processing: Process Intensification*. Elsevier Science S.A., 35(6), pp. 451–457. doi: 10.1016/S0255-2701(96)04157-8.

Koschikowski, J. *et al.* (2009) 'Experimental investigations on solar driven stand-alone membrane distillation systems for remote areas', *Desalination*, 248(1–3), pp. 125–131. doi: 10.1016/j.desal.2008.05.047.

Koschikowski, J., Wieghaus, M. and Rommel, M. (2003) 'Solar thermal driven desalination plants based on membrane distillation', *Desalination*, 156(May), pp. 295–304. doi: 10.1016/S0011-9164(03)00360-6.

Krajewski, S. R. *et al.* (2006) 'Application of fluoroalkylsilanes (FAS) grafted ceramic membranes in membrane distillation process of NaCl solutions', *Journal of Membrane Science*, 281(1–2), pp. 253–259. doi: 10.1016/j.memsci.2006.03.039.

Krenker, A., Bester, J. and Kos, A. (2009) 'Introduction to the Backpropagation Artificial Neural Networks', *Artificial Neural Networks - Methodological Advances and Biomedical Applications*, pp. 0–19. doi: 10.1097/MEG.0b013e3282f198a0.

Krishna, R. and Standart, G. L. (1976) 'A multicomponent film model incorporating a general matrix method of solution to the Stefan-Maxwell equations', *AIChE J.*, 22(2), pp. 383–389.

Krivorot, M. *et al.* (2011) 'Factors affecting biofilm formation and biofouling in membrane distillation of seawater', *Journal of Membrane Science*. Elsevier B.V., 376(1–2), pp. 15–24. doi: 10.1016/j.memsci.2011.01.061.

Kujawska, A. *et al.* (2016) 'Removal of volatile organic compounds from aqueous solutions applying thermally driven membrane processes. 2. Air gap membrane distillation', *Journal*

of Membrane Science. Elsevier, 499, pp. 245–256. doi: 10.1016/j.cep.2015.02.010.

Kullab, A. and Martin, A. (2011) 'Membrane distillation and applications for water purification in thermal cogeneration plants', *Separation and Purification Technology*. Elsevier B.V., 76(3), pp. 231–237. doi: 10.1016/j.seppur.2010.09.028.

Kurokawa, H. *et al.* (1990) 'Vapor Permeate Characteristics of Membrane Distillation', *Separation Science and Technology*, 25(13–15), pp. 1349–1359. doi: 10.1080/01496399008050396.

de la Calle, A. *et al.* (2015) 'Dynamic modeling and simulation of a solar-assisted multi-effect distillation plant', *Desalination*. Elsevier B.V., 357, pp. 65–76. doi: 10.1016/j.desal.2014.11.008.

Lawal, D. U. and Khalifa, A. E. (2015) 'Experimental investigation of an air gap membrane distillation unit with double-sided cooling channel', *Desalination and Water Treatment*, (may), pp. 1–15. doi: 10.1080/19443994.2015.1042065.

Lawson, K. W. and Lloyd, D. R. (1996) 'Membrane distillation. II. Direct contact MD', *Journal of Membrane Science*, 120(1), pp. 123–133. doi: 10.1016/0376-7388(96)00141-X.

Lawson, K. W. and Lloyd, D. R. (1997) 'Membrane distillation', *Journal of Membrane Science*, 124(1), pp. 1–25. doi: 10.1016/S0376-7388(96)00236-0.

Lee, C. H. and Hong, W. H. (2001) 'Effect of operating variables on the flux and selectivity in sweep gas membrane distillation for dilute aqueous isopropanol', *Journal of Membrane Science*, 188(1), pp. 79–86. doi: 10.1016/S0376-7388(01)00373-8.

Lei, Z., Chen, B. and Ding, Z. (2005) *Special Distillation Processes*. First. Elsevier B.V.

Li, L. *et al.* (2004) 'Desalination by reverse osmosis using MFI zeolite membranes', *Journal of Membrane Science*, 243(1–2), pp. 401–404. doi: 10.1016/j.memsci.2004.06.045.

Li, Z. Y. *et al.* (2012) 'Flux patterns and membrane fouling propensity during desalination of seawater by forward osmosis', *Water Research*. Elsevier Ltd, 46(1), pp. 195–204. doi: 10.1016/j.watres.2011.10.051.

Lies, E. *et al.* (2017) 'Direct contact and air gap membrane distillation: Differences and similarities between lab and pilot scale', *Desalination*, 422(August), pp. 91–100. doi: 10.1016/j.desal.2017.08.018.

Liu, G. L. *et al.* (1998) 'Theoretical and experimental studies on air gap membrane distillation', *Heat and Mass Transfer*, 34(4), pp. 329–335. doi: 10.1007/s002310050267.

Liu, R. *et al.* (2012) 'Concentrating aqueous hydrochloric acid by multiple-effect membrane distillation', *Frontiers of Chemical Science and Engineering*, 6(3), pp. 311–321. doi: 10.1007/s11705-012-1207-3.

Liu, Z. *et al.* (2017) 'Experimental study of the optimal vacuum pressure in vacuum assisted

air gap membrane distillation process', *Desalination*. Elsevier B.V., 414, pp. 63–72. doi: 10.1016/j.desal.2017.03.031.

M.A., J. C. M. (1860) 'Illustrations of the dynamical theory of gases.Part II. On the process of difussion of two or more kinds of moving particles among another', *Philosophical Magazine*, 4(20), pp. 21–37. doi: 10.1080/14786446008642902.

MacGregor, R. K., and Emery, A. F. (1969) 'Free Convection Through Vertical Plane Layers—Moderate and High Prandtl Number Fluids', *ASME J. Heat Transfer*, 91, pp. 391–401. doi: 10.1115/1.3580194.

Mahdi, T. *et al.* (2014) 'State-of-the-Art Technologies for Separation of Azeotropic Mixtures', *Separation & Purification Reviews*, 44(4), pp. 308–330. doi: 10.1080/15422119.2014.963607.

Manolakos, D. *et al.* (2007) 'Experimental evaluation of an autonomous low-temperature solar Rankine cycle system for reverse osmosis desalination', *Desalination*, 203(1–3), pp. 366–374. doi: 10.1016/j.desal.2006.04.018.

Marini, F. *et al.* (2008) 'Artificial neural networks in chemometrics: History, examples and perspectives', *Microchemical Journal*, 88(2), pp. 178–185. doi: 10.1016/j.microc.2007.11.008.

Martinez-Diaz, L., F. J. F. D. (2001) 'Desalination of brines by membrane distillation', *Desalination*, 137, pp. 267–273. doi: 10.1016/S0011-9164(01)00228-4.

Masin, J., Lewis, M. and Vilim, R. (2006) 'Development of the low temperature hybrid Cu-Cl thermochemical cycle', *AIChE annual meeting, conference*, 2(l).

Matheswaran, M. and Kwon, T. (2007) 'Factors affecting flux and water separation performance in air gap membrane distillation', *Journal of Ind. Eng. Chem*, 13(6), pp. 965–970.

McCutcheon, J. R., McGinnis, R. L. and Elimelech, M. (2006) 'Desalination by ammonia-carbon dioxide forward osmosis: Influence of draw and feed solution concentrations on process performance', *Journal of Membrane Science*, 278(1–2), pp. 114–123. doi: 10.1016/j.memsci.2005.10.048.

McGinnis, R. L. *et al.* (2013) 'Pilot demonstration of the NH3/CO2 forward osmosis desalination process on high salinity brines', *Desalination*. Elsevier B.V., 312, pp. 67–74. doi: 10.1016/j.desal.2012.11.032.

Meindersma, G. W., Guijt, C. M. and de Haan, A. B. (2006) 'Desalination and water recycling by air gap membrane distillation', *Desalination*, 187(1–3), pp. 291–301. doi: 10.1016/j.desal.2005.04.088.

Mohammadi, T. and Safavi, M. A. (2009) 'Application of Taguchi method in optimization

of desalination by vacuum membrane distillation', *Desalination*. Elsevier B.V., 249(1), pp. 83–89. doi: 10.1016/j.desal.2009.01.017.

Mulder, M. (1991) 'Basic Principles of Membrane Technology', p. 363. doi: 10.1007/978-94-017-0835-7.

N. Miljkovic, R. Enright, Y. Nam, N. Lopez, Ken an Dou, J. Sack, E. N. W. (2012) 'Jumping-droplet-enhanced condensation on scalable superhydrophobic nanostructured surfaces', *Nanoletters*, 13, pp. 179–187. doi: 10.1021/nl303835d.

Nigiz, F. U. (2017) 'Preparation of high-performance graphene nanoplate incorporated polyether block amide membrane and application for seawater desalination', *Desalination*. Elsevier, (June), pp. 0–1. doi: 10.1016/j.desal.2017.08.025.

Pangarkar, B. L., Sane, M. G. and Parjane, S. B. (2011) 'Flux enhancement of air gap membrane distillation for desalination of groundwater by surface modification of membrane', *International Journal of ChemTech Research*, 3(4), pp. 1816–1820.

Perves Bappy, M. J. *et al.* (2017) 'Enhanced Freshwater Production Using Finned-Plate Air Gap Membrane Distillation (AGMD)', *MATEC Web of Conferences*, 103, p. 6014. doi: 10.1051/matecconf/201710306014.

Phattaranawik, J. *et al.* (2008) 'A novel membrane bioreactor based on membrane distillation', *Desalination*, 223(1–3), pp. 386–395. doi: 10.1016/j.desal.2007.02.075.

Phattaranawik, J., Jiraratananon, R. and Fane, A. G. (2003) 'Effect of pore size distribution and air flux on mass transport in direct contact membrane distillation', *Journal of Membrane Science*, 215(1–2), pp. 75–85. doi: 10.1016/S0376-7388(02)00603-8.

Poling, B. E. and Prausnitz, John M, J. P. O. (1987) *The Properties of Gases and Liquids*. Fifth Edit. McGRAW-HILL. doi: 10.1021/ja0048634.

Porada, S. *et al.* (2012) 'Water desalination using capacitive deionization with microporous carbon electrodes', *ACS Applied Materials and Interfaces*, 4(3), pp. 1194–1199. doi: 10.1021/am201683j.

R. Chouikh, S. Bouguecha, M. D. (2005) 'Modelling of a modified air gap distillation membrane for the desalination of seawater', *Desalination*, 181, pp. 257–265. doi: 10.1016/j.camwa.2003.05.010.

Raach, H. and Mitrovic, J. (2007) 'Simulation of heat and mass transfer in a multi-effect distillation plant for seawater desalination', *Desalination*, 204(1–3 SPEC. ISS.), pp. 416–422. doi: 10.1016/j.desal.2006.04.037.

Rivier, C. A. *et al.* (2002) 'Separation of binary mixtures by thermostatic sweeping gas membrane distillation - I. Theory and simulations', *Journal of Membrane Science*, 201(1–2), pp. 1–16. doi: 10.1016/S0376-7388(01)00648-2.

Rosalam, S., Chiam, C. K. and , S Widyaparamitha, Y W Chang, C. A. L. (2016) 'Water desalination by air-gap membrane distillation using meltblown polypropylene nanofiber membrane', *Earth and Environmental Science*, 36(12032). doi: 10.1088/1755-1315/36/1/012032.

Sarti, G. C., Gostoli, C. and Bandini, S. (1993) 'Extraction of organic components from aqueous streams by vacuum membrane distillation', *Journal of Membrane Science*, 80(1), pp. 21–33. doi: 10.1016/0376-7388(93)85129-K.

Schneider, C. A., Rasband, W. S. and Eliceiri, K. W. (2012) 'NIH Image to ImageJ: 25 years of image analysis', *Nature Methods*. Nature Publishing Group, 9(7), pp. 671–675. doi: 10.1038/nmeth.2089.

Schofield, R. W., Fane, a. G. and Fell, C. J. D. (1987) 'Heat and mass transfer in membrane distillation', *Journal of Membrane Science*, 33(3), pp. 299–313. doi: 10.1016/S0376-7388(00)80287-2.

Seader, Junior D & Henley, E. J. (2006) *Separation process principles*. Second Edi. John Wiley & Sons, Inc.

Sharaf, M. A., Nafey, A. S. and García-Rodríguez, L. (2011) 'Exergy and thermo-economic analyses of a combined solar organic cycle with multi effect distillation (MED) desalination process', *Desalination*. Elsevier B.V., 272(1–3), pp. 135–147. doi: 10.1016/j.desal.2011.01.006.

Shiklomanov, I. (1993) 'World fresh water resources', in *Water in crisis a guide to the world's fresh water resources*, pp. 13–24.

Shirazi, M. M. A. *et al.* (2014) 'Concentration of glycerol from dilute glycerol wastewater using sweeping gas membrane distillation', *Chemical Engineering and Processing: Process Intensification*. Elsevier B.V., 78, pp. 58–66. doi: 10.1016/j.cep.2014.02.002.

Shreve, R. N. (1956) *The Chemical Process Industries*. Second Edi. McGRAW-HILL. doi: 10.1038/158251a0.

Singh, D. and Sirkar, K. K. (2012) 'Desalination by air gap membrane distillation using a two hollow-fiber-set membrane module', *Journal of Membrane Science*. Elsevier, 421–422, pp. 172–179. doi: 10.1016/j.memsci.2012.07.007.

Sismanoglu, B. N. *et al.* (2013) *Argon: Production, Characteristics and Applications*. Nova Publisher, New York.

Smolders, K. and Franken, A. C. M. (1989) 'Terminology for Membrane Distillation', *Desalination*, 72(3), pp. 249–262.

Srisurichan, S., Jiraratananon, R. and Fane, A. G. (2005) 'Humic acid fouling in the membrane distillation process', *Desalination*, 174(1), pp. 63–72. doi:

10.1016/j.desal.2004.09.003.

Suk, D. E. *et al.* (2010) 'Development of novel surface modified phase inversion membranes having hydrophobic surface-modifying macromolecule (nSMM) for vacuum membrane distillations', *Desalination*. Elsevier B.V., 261(3), pp. 300–312. doi: 10.1016/j.desal.2010.06.058.

Swaminathan, J. *et al.* (2015) 'Experimental Investigation of High Efficiency Single-Stage membrane distillation configurations', in *The International Desalination Association World Congress on Desalination and Water Reuse 2015/San Diego, CA, USA*.

Swaminathan, J. *et al.* (2016) 'Membrane distillation model based on heat exchanger theory and configuration comparison', *Applied Energy*. Elsevier Ltd, 184, pp. 491–505. doi: 10.1016/j.apenergy.2016.09.090.

Swaminathan, J. *et al.* (2018) 'Energy efficiency of membrane distillation up to high salinity: Evaluating critical system size and optimal membrane thickness', *Applied Energy*. Elsevier, 211(November 2017), pp. 715–734. doi: 10.1016/j.apenergy.2017.11.043.

Swietoslawski, W. (1963) *Azeotropy and Polyazeotropy*. New York: Pergamon Press.

T, U. K. N. and Martin, A. (2014) 'Co-generation of Drinking Water and Domestic Hot Water Using Solar Thermal Integrated Membrane Distillation System', *Energy Procedia*. Elsevier B.V., 61, pp. 2666–2669. doi: 10.1016/j.egypro.2014.12.271.

Tan, Y. Z. *et al.* (2017) 'Influence of module orientation and geometry in the membrane distillation of oily seawater', *Desalination*. Elsevier, 423(September), pp. 111–123. doi: 10.1016/j.desal.2017.09.019.

Tavakkoli, S. *et al.* (2017) 'A techno-economic assessment of membrane distillation for treatment of Marcellus shale produced water', *Desalination*. Elsevier, 416(April), pp. 24–34. doi: 10.1016/j.desal.2017.04.014.

Tedesco, M. *et al.* (2015) 'Reverse electrodialysis with saline waters and concentrated brines: A laboratory investigation towards technology scale-up', *Journal of Membrane Science*, 492(May), pp. 9–20. doi: 10.1016/j.memsci.2015.05.020.

Thiel, G. P. *et al.* (2015) 'Energy consumption in desalinating produced water from shale oil and gas extraction', *Desalination*. Elsevier B.V., 366, pp. 94–112. doi: 10.1016/j.desal.2014.12.038.

Thiruvenkatachari, R. *et al.* (2006a) 'Separation of water and nitric acid with porous hydrophobic membrane by air gap membrane distillation (AGMD)', *Separation Science and Technology*, 41(14), pp. 3187–3199. doi: 10.1080/01496390600854651.

Thiruvenkatachari, R. *et al.* (2006b) 'Separation of Water and Nitric Acid with Porous Hydrophobic Membrane by Air Gap Membrane Distillation (AGMD)', *Separation Science*

and Technology, 41(February 2015), pp. 3187–3199. doi: 10.1080/01496390600854651.

Tian, R. *et al.* (2014) 'A new enhancement technique on air gap membrane distillation', *Desalination*, 332, pp. 52–59. doi: 10.1016/j.desal.2013.10.016.

Tijing, L. D. *et al.* (2015) 'Fouling and its control in membrane distillation-A review', *Journal of Membrane Science*. Elsevier, 475, pp. 215–244. doi: 10.1016/j.memsci.2014.09.042.

Tomabechi, K. (2010) 'Energy resources in the future', *Energies*, 3(4), pp. 686–695. doi: 10.3390/en3040686.

Tomaszewska, M., Gryta, M. and Morawski, A. W. (1998) 'The influence of salt in solutions on hydrochloric acid recovery by membrane distillation', *Separation and Purification Technology*, 14(1–3), pp. 183–188. doi: 10.1016/S1383-5866(98)00073-2.

Tomaszewska, M., Gryta, M. and Morawski, A. W. (2000) 'Mass transfer of HCl and H 2 O across the hydrophobic membrane during membrane distillation', 166, pp. 149–157.

Tomaszewska, M., Gryta, M. and Morawski, A. W. (2001) 'Recovery of hydrochloric acid from metal pickling solutions by membrane distillation', 23, pp. 591–600.

Udriot, H., Araque, A. and von Stockar, U. (1994) 'Azeotropic mixtures may be broken by membrane distillation', *The Chemical Engineering Journal and The Biochemical Engineering Journal*, 54(2), pp. 87–93. doi: 10.1016/0923-0467(93)02814-D.

Upadhyaya, S. *et al.* (2011) 'Parametric Sensitivity Analysis of Vacuum Membrane Distillation for Desalination Process', *Chemeca 2011, September 18 to 21, 2011 at the Hilton Hotel, Sydney, New South Wales*, p. 9.

Upadhyaya, S., Singh, K., Chaurasia, S. P., *et al.* (2016) 'Mathematical and CFD modeling of vacuum membrane distillation for desalination', *Desalination and Water Treatment*, (57), pp. 11956–11971. doi: 10.1080/19443994.2015.1048306.

Upadhyaya, S., Singh, K., Chaurasia, S. P., *et al.* (2016) 'Recovery and development of correlations for heat and mass transfer in vacuum membrane distillation for desalination', *Desalination and Water Treatment*, 57(55), pp. 26886–26898. doi: 10.1080/19443994.2016.1189245.

Upadhyaya, S., Singh, K., Chaurasia, S. P., *et al.* (2016) 'Recovery and development of correlations for heat and mass transfer in vacuum membrane distillation for desalination', *Desalination and Water Treatment*, 57(55), pp. 26886–26898. doi: 10.1080/19443994.2016.1189245.

Urtiaga, A. M. *et al.* (2001) 'Parallelism and differences of pervaporation and vacuum membrane distillation in the removal of VOCs from aqueous streams', *Separation and Purification Technology*, 22–23(September 1999), pp. 327–337. doi: 10.1016/S1383-

5866(00)00116-7.

Urtiaga, A. M., Ruiz, G. and Ortiz, I. (2000) 'Kinetic analysis of the vacuum membrane distillation of chloroform from aqueous solutions', *Journal of Membrane Science*, 165(1), pp. 99–110. doi: 10.1016/S0376-7388(99)00220-3.

Vazirnejad, T. *et al.* (2016) 'Application of Salt Additives and Response Surface Methodology for Optimization of PVDF Hollow Fiber Membrane in DCMD and AGMD Processes', *Journal of Membrane Science and Research*, 2, pp. 169–178. doi: 10.22079/jmsr.2016.21947.

Veerman, J. *et al.* (2008) 'Reducing power losses caused by ionic shortcut currents in reverse electrodialysis stacks by a validated model', *Journal of Membrane Science*, 310(1–2), pp. 418–430. doi: 10.1016/j.memsci.2007.11.032.

Veerman, J. *et al.* (2010) 'Electrical power from sea and river water by reverse electrodialysis: A first step from the laboratory to a real power plant', *Environmental Science and Technology*, 44(23), pp. 9207–9212. doi: 10.1021/es1009345.

Vega, R. and Vera, J. H. (1976) 'Phase equilibria of concentrated aqueous solutions containing volatile strong electrolytes', *The Canadian Journal of Chemical Engineering*, pp. 245–248. doi: 10.1002/cjce.5450540323.

Vinícius Gonçalves Maltarollo, K. M. H. and A. B. F. da S. (2013) 'Applications of Artificial Neural Networks in Chemical Problems', in *Artificial Neural Networks Kenji Suzuki, IntechOpen*. doi: 10.5772/51275.

Wang, J. *et al.* (2008) 'Effect of coagulation pretreatment on membrane distillation process for desalination of recirculating cooling water', *Separation and Purification Technology*, 64(1), pp. 108–115. doi: 10.1016/j.seppur.2008.07.022.

Wang, Q. *et al.* (2016) 'Desalination by pervaporation : A review', 387, pp. 46–60. doi: 10.1016/j.desal.2016.02.036.

Warsinger, D. E. M. *et al.* (2014) 'EFFECT OF MODULE I N CLI N ATIO N A N GLE O N AIR GAP MEMBRA N E IHTC15-9351', (Dcmd), pp. 1–14.

Warsinger, D. E. M. *et al.* (2015) 'Superhydrophobic condenser surfaces for air gap membrane distillation', *Journal of Membrane Science*. Elsevier, 492, pp. 578–587. doi: 10.1016/j.memsci.2015.05.067.

Wei, X. *et al.* (2012) 'CF4plasma surface modification of asymmetric hydrophilic polyethersulfone membranes for direct contact membrane distillation', *Journal of Membrane Science*. Elsevier B.V., 407–408, pp. 164–175. doi: 10.1016/j.memsci.2012.03.031.

Winter, D., Koschikowski, J. and Wieghaus, M. (2011) 'Desalination using membrane

distillation: Experimental studies on full scale spiral wound modules', *Journal of Membrane Science*. Elsevier B.V., 375(1–2), pp. 104–112. doi: 10.1016/j.memsci.2011.03.030.

Woldemariam, D. *et al.* (2017) 'Recovery of ethanol from scrubber-water by district heat-driven membrane distillation : Industrial-scale technoeconomic study', *Renewable Energy*. Elsevier Ltd, pp. 1–11. doi: 10.1016/j.renene.2017.06.009.

Woldemariam, D. M., Kullab, A. and Martin, A. R. (2017) 'District heat-driven water purification via membrane distillation: New possibilities for applications in Pharmaceutical Industries', *Industrial & Engineering Chemistry Research*, p. acs.iecr.6b04740. doi: 10.1021/acs.iecr.6b04740.

Xie, M. *et al.* (2016) 'Membrane-based processes for wastewater nutrient recovery: Technology, challenges, and future direction', *Water Research*. Elsevier Ltd, 89, pp. 210–221. doi: 10.1016/j.watres.2015.11.045.

Xie, Z. *et al.* (2009) 'Ammonia removal by sweep gas membrane distillation', *Water Research*. Elsevier Ltd, 43(6), pp. 1693–1699. doi: 10.1016/j.watres.2008.12.052.

Xie, Z. *et al.* (2011) 'Separation of aqueous salt solution by pervaporation through hybrid organic – inorganic membrane : Effect of operating conditions', *Desalination*. Elsevier B.V., 273(1), pp. 220–225. doi: 10.1016/j.desal.2010.10.026.

Xu, J. *et al.* (2016) 'Effect of operating parameters and membrane characteristics on air gap membrane distillation performance for the treatment of highly saline water', *Journal of Membrane Science*. Elsevier, 512, pp. 73–82. doi: 10.1016/j.memsci.2016.04.010.

Yang, X. H. *et al.* (2011) 'Study on Membrane Fouling Experiment of Stacked AGMD Module in Low Temperature', *Advanced Materials Research*, 396–398, pp. 458–462. doi: 10.4028/www.scientific.net/AMR.396-398.458.

Zaragoza, G., Ruiz-Aguirre, A. and Guillén-Burrieza, E. (2014) 'Efficiency in the use of solar thermal energy of small membrane desalination systems for decentralized water production', *Applied Energy*. Elsevier Ltd, 130, pp. 491–499. doi: 10.1016/j.apenergy.2014.02.024.

Zhao, D. *et al.* (2011) 'Theoretical analyses of thermal and economical aspects of multi-effect distillation desalination dealing with high-salinity wastewater', *Desalination*. Elsevier B.V., 273(2–3), pp. 292–298. doi: 10.1016/j.desal.2011.01.048.

Zheng, L. *et al.* (2016) 'Preparation of PVDF-CTFE hydrophobic membranes for MD application: Effect of LiCl-based mixed additives', *Journal of Membrane Science*. Elsevier, 506, pp. 71–85. doi: 10.1016/j.memsci.2016.01.044.

Zhu, B. *et al.* (2015) 'Application of robust MFI-type zeolite membrane for desalination of saline wastewater', *Journal of Membrane Science*. Elsevier, 475, pp. 167–174. doi:

10.1016/j.memsci.2014.09.058.

Zhu, C. *et al.* (1999) 'Ultrasonic stimulation on enhancement of air gap membrane distillation', *Journal of Membrane Science*, 161(1–2), pp. 85–93. doi: 10.1016/S0376-7388(99)00105-2.

Zwijnenberg, H. J., Koops, G. H. and Wessling, M. (2005) 'Solar driven membrane pervaporation for desalination processes', 250, pp. 235–246. doi: 10.1016/j.memsci.2004.10.029.

APPENDICES

Appendix A

MAPE Analysis between Theoretical and Experimental Flux

Mean Absolute Percentage Error (MAPE) is an important tool used to forecast the accuracy. MAPE is generally used to measure the error between actual and predicted value. MAPE is measured in terms of percentage and given by the following formula –

$$MAPE = \frac{100}{n}\left(\sum \frac{|Actual - Predicted|}{|Actual|}\right) \ldots\ldots\ldots\ldots\ldots (A.1)$$

In this study, flux calculated by the experiments considered as actual value and flux estimated by the mathematical model taken as the predicted value.

Table A.1: Actual and predicted flux measured at feed flow rate 2 L/min, air gap width 5 mm, cooling water temperature 20 ^{o}C, cooling water flow rate 1 L/min

Feed Temperature (^{o}C)	Experimental Flux (kg/m^2 ·h)	Mathematical Model Flux (kg/m^2 ·h)
30	4	3.78
35	7.7	7.4
40	12.8	12.2
45	20	19.2
50	28.5	28.4

By using equation$(A.1)$, MAPE value has been calculated as-

$$MAPE = \frac{100}{5}\left(\frac{|4-3.78|}{|4|} + \frac{|7.7-7.4|}{|7.7|} + \frac{|12.8-12.2|}{|12.8|} + \frac{|20-19.2|}{|20|} + \frac{|28.5-28.4|}{|28.5|}\right)$$
$$= 3.69\ \%$$

In the same way, the MAPE values at other conditions have been computed.

Appendix B

AGMD Experimental Data used for ANN Modeling

S. No	Feed Temperature (^oC)	Air Gap Width (mm)	Cooling Water Temperature (^oC)	Feed Flow Rate (L/min)	Cooling Water Flow Rate (L/min)	Exp-erimental Flux ($kg/m^2 \cdot h$)	Model Flux ($kg/m^2 \cdot h$)
1.	30	3	20	2	1	6.85	6.11
2.	35	5	20	2	1	7.7	7.4
3.	40	7	20	2	1	10.8	10.14
4.	30	5	20	2	1	4	3.78
5.	50	5	10	2	3	31.9	32.31
6.	50	5	10	2	4	31.9	32.32
7.	50	5	10	2	5	31.8	32.32
8.	50	9	20	2	1	19.3	19.16
9.	50	11	20	2	1	17	16.58
10.	35	3	20	2	1	9	8.6
11.	40	3	20	2	1	15.8	15.62
12.	45	3	20	2	1	24.2	25
13.	40	5	20	2	1	12.8	12.2
14.	45	5	20	2	1	20	19.2
15.	50	9	20	2	1	19.3	19.16
16.	50	11	20	2	1	17	16.58
17.	50	3	20	3	1	37.7	37.5
18.	50	3	20	4	1	38.2	38.04
19.	50	3	20	5	1	40.2	40.02
20.	50	3	20	6	1	40.7	40.2
21.	50	3	20	2	1	36	37
22.	50	5	20	2	1	28.5	28.4
23.	50	7	20	2	1	23.3	22.89
24.	30	3	5	2	1	7	7.11
25.	30	3	5	2	3	7.5	7.11
26.	30	3	5	2	5	7.15	7.11
27.	30	7	15	6	1	4.25	4.05
28.	30	7	15	6	3	3.85	4.05
29.	30	7	15	6	5	4.25	4.05
30.	30	11	25	10	1	1.8	1.81
31.	30	11	25	10	3	1.85	1.81
32.	30	11	25	10	5	2.25	1.81
33.	40	7	25	2	1	8	8.33

S. No	Feed Temperature (^oC)	Air Gap Width (mm)	Cooling Water Temperature (^oC)	Feed Flow Rate (L/min)	Cooling Water Flow Rate (L/min)	Exp-erimental Flux ($kg/m^2 \cdot h$)	Model Flux ($kg/m^2 \cdot h$)
34.	40	7	25	2	3	8.55	8.33
35.	40	7	25	2	5	8.1	8.33
36.	40	11	5	6	1	10.1	10.24
37.	40	11	5	6	3	10.55	10.24
38.	40	11	5	6	5	9.5	10.24
39.	40	3	15	10	1	14.9	16.39
40.	40	3	15	10	3	15.95	16.39
41.	40	3	15	10	5	15.35	16.39
42.	50	11	15	2	1	17.15	17.81
43.	50	11	15	2	3	17.45	17.81
44.	50	11	15	2	5	17.15	17.81
45.	50	3	25	6	1	23.7	24.08
46.	50	3	25	6	3	23.2	24.08
47.	50	3	25	6	5	23.8	24.08
48.	50	7	5	10	1	24.45	24.77
49.	50	7	5	10	3	24.9	24.77
50.	50	7	5	10	5	25.1	24.77
51.	30	7	20	2	1	3	2.82
52.	35	7	20	2	1	6	5.73
53.	50	5	20	3	1	28.6	28.7
54.	50	5	20	4	1	29.7	28.9
55.	50	5	20	5	1	30	29.56
56.	50	5	10	2	1	33	32.32
57.	50	5	15	2	1	30.7	30.59
58.	50	7	10	2	1	26	25.84
59.	50	7	15	2	1	25	24.53
60.	50	5	20	2	2	28.5	28.4
61.	50	5	15	2	2	31.1	30.59
62.	50	5	15	2	3	31.2	30.59
63.	50	5	15	2	4	31.4	30.6
64.	50	5	15	2	5	31.4	30.6
65.	30	9	2	20	1	3.15	3.18
66.	45	11	2	20	1	12.35	11.62
67.	45	7	2	20	1	16.1	15.71
68.	45	9	2	20	1	14.62	13.32

Brief Bio-Data

Sarita Kalla, *Married*
Father's Name: Mr. Satish Kumar Mishra
Mother's Name: Mrs. Manju Mishra
Husband's Name: Dr. Anshuman Kalla

Current Profile

Currently working as *Lecturer and in-charge Head*, Department of Chemical Engineering, Govt. Polytechnic College, Barmer, Rajasthan. (Technical Education Department, Govt. of Rajasthan)

Academic Qualifications

- **2015-Present: Ph.D. - Chemical Engineering**
  Malaviya National Institute of Technology, Jaipur, **CGPA – 9.33**
- **2015 : Master of Technology (M. Tech.) -** Process Modeling and Simulation
  University - Aligarh Muslim University, Aligarh, **Aggregate – 81.42 (Honours)**
- **2004 - 2008: Bachelor of Engineering (B.E.) - Chemical Engineering**
  University - University of Rajasthan, Jaipur, India, **Aggregate – 80.02% (Honours)**

Achievements

- **All India First Rank** in the exam for the post of Lecturer - Chemical Engineering, Technical Education Department conducted by Rajasthan Public Service Commission **(RPSC),** Ajmer.
- Qualified **GATE 2014** and **GATE 2011** with **87.59 percentile** and **87.76 percentile** in Chemical Engineering Branch.
- ***First rank*** holder in M.Tech. Entrance Exam (Chemical Engineering) conducted by Aligarh Muslim University (AMU), Aligarh. **(66 marks out of 100)**
- ***First rank*** holder in M.Tech course (Specialization in Process Modeling and Simulation) with aggregate 81.42 % in consecutive three semesters.

Membership of Professional Societies

- Associate Member of Indian Institute of Chemical Engineers (IIChE), LAM- 46237.
- Life Member of Indian Desalination Association (InDA), LM-401

Publications

- SCI(Scopus)/International Journal Papers: **04 (**03 - SCI, 01 - International)
- International/National Conferences: **04**
- Allied SCI(Scopus)/International Journal Papers: **02** (01 - SCI, 01 - International)
- Allied International/National Conferences: **02**
- Book Chapter : **01**

Short Term Courses/ FDP/Workshop/National Symposium Attended: 07